SYNTHESIS OF TOUGH HYDROGEL AND ITS APPLICATION IN SOFT ELECTRONIC FABRICATION

Thesis submitted in partial fulfilment

for the award of the degree

Doctor of Philosophy

By

SHRINKHALA ANAND

RAJIV GANDHI INSTITUTE OF PETROLEUM TECHNOLOGY

JAIS, INDIA – 229304

21BS0010 **2026**

CERTIFICATE

It is certified that the work contained in the thesis titled "***Synthesis of Tough Hydrogel and Its Application in Soft Electronic Fabrication***" by "***Shrinkhala Anand***" has been carried out under our supervision and this work has not been submitted elsewhere for a degree.

It is further certified that the student has fulfilled all the requirements of the Comprehensive, Candidacy, SOTA, and Open Seminar.

(Supervisor)	(Co-Supervisor)
Dr. Omvir Singh	**Prof. Umaprasana Ojha**

DECLARATION BY THE CANDIDATE

I, "***Shrinkhala Anand***", certify that the work embodied in this thesis is my own bonafide work and was carried out by me under the supervision of "***Dr. Omvir Singh***" and co-supervision of "***Prof. Umaprasana Ojha***" from "*August 2021*" to "*Dec 2025*", at Rajiv Gandhi Institute of Petroleum Technology, Jais, India. The matter embodied in this thesis has not been submitted for the award of any other degree. I further declare that I have faithfully acknowledged and given credit to the researchers and research community wherever their works have been cited in my work in this thesis. I further declare that I have not willfully copied any other's work, paragraphs, text, data, results, etc., reported in journals, books, magazines, reports, dissertations, theses, etc., or available at websites and have not included them in this thesis and have not cited as my own work.

Date:	**Shrinkhala Anand**
Place: RGIPT Jais	Roll No.: 21BS0010

CERTIFICATE BY THE SUPERVISOR (S)

It is certified that the above statement made by the student is correct to the best of our knowledge.

(Supervisor)	(Co-Supervisor)
Dr. Omvir Singh	**Prof. Umaprasana Ojha**

Signature & Seal of Head of Department

CERTIFICATE

CERTIFIED that the work contained in the thesis titled "***Synthesis of Tough Hydrogel and Its Application in Soft Electronic Fabrication***" by ***Ms. Shrinkhala Anand*** has been carried out under our supervision. It is also certified that she fulfilled the mandatory requirement of TWO quality publications arose out of his thesis work.

It is further certified that the two publications (copies enclosed) of the aforesaid ***Ms. Shrinkhala Anand*** have been published in the Journals indexed by –

a) SCI
b) SCI Extended
c) SCOPUS
d) *Non-indexed Journals-(only in special cases)(*Please enclose DPGC resolution in this regard)

Dr. Omvir Singh	**Prof. Umaprasana Ojha**	**Dr. Omvir Singh**
(Supervisor)	(Co-Supervisor)	(Convener, DPGC)

N.B.: Please strike out the category (a, b, c, d) that is not applicable.

COPYRIGHT TRANSFER CERTIFICATE

Title of the thesis: *Synthesis of Tough Hydrogel and Its Application in Soft Electronic Fabrication*

Name of the student: *Shrinkhala Anand*

Copyright Transfer

The undersigned hereby assigns to the Rajiv Gandhi Institute of Petroleum Technology, Jais all rights under copyright that may exist in and for the above thesis submitted for the award of the "Doctor of Philosophy".

Date:

Place: RGIPT Jais

Shrinkhala Anand

Roll No.: 21BS0010

Note: However, the author may reproduce or authorise others to reproduce material extracted verbatim from the thesis or a derivative of the thesis for the author's personal use, provided that the source and the Institute's copyright notice are indicated.

Dedicated to my beloved parents.....

Acknowledgement

First and foremost, I am expressing my sincere thanks to almighty god for his boundless grace, strength and guidance throughout my PhD journey. Their blessings provide me with the perseverance, clarity, and resilience needed to overcome challenges and successfully complete this research work.

I would like to express my profound gratitude to my thesis supervisor, Dr Omvir Singh, for his unwavering support, insightful suggestions, and critical discussions, which significantly contributed to improving the quality and depth of this work. I am thankful to my co-supervisor, Prof. U.Ojha, for his invaluable guidance, constant encouragement, and scholarly insight throughout the course of this research. His patience, technical expertise, constructive criticism, and continuous motivation played an important role in shaping this thesis and enhancing my research capabilities.

I sincerely acknowledge RGIPT, Jais, for providing me with the opportunity to carry out this research and for offering an excellent academic and research environment. I extend my heartfelt thanks to the Department of Energy and Human Sciences for providing the necessary laboratory facilities, infrastructure, and academic support required for the successful completion of this work. I am grateful to the faculty members and administrative staff of the department for their cooperation and support throughout my tenure.

I want to extend my sincere thanks to my friends (Amit and Navdeep), my senior, Dr Shubhankar Mandal, for teaching me about the small details of my material, instrumentation, data analysis and data plotting. He also guided me on time management and pressure management. Also, I want to thank my other lab seniors, Dr Niharika, Dr Chandan and Dr Arpan for their guidance and support in critical situations. I would like to thank my labmates, Dr Santosh Semwal and Yukti Setia, for their constant and unconditional support and love for me. Their assistance during experimental work, data analysis,

troubleshooting, and their valuable discussions created a motivating and collaborative research environment, making the research journey both productive and enjoyable.

I owe my deepest gratitude to my mother, my brother and my father for their unconditional love, sacrifices, patience, and unwavering support throughout my academic journey. Their belief in my abilities and continuous encouragement provided me with the strength and determination to pursue my goals with confidence.

Finally, I would like to express my heartfelt and special thanks to Arpit, Hema and Prerna for being a constant source of motivation, emotional support, and encouragement. Their patience, understanding, and faith in me played a significant role in helping me remain focused, confident, and resilient during the completion of this work.

I sincerely acknowledge everyone who has contributed directly or indirectly to the successful completion of this thesis and apologise if I have inadvertently omitted anyone.

Table of Contents

Acknowledgement…….....8

Table of Contents…….10

Preface …….....13

List of Figures…….. 194

List of Tables……..203

List of Scheme……205

List of Abbreviations……206

Chapter 1: Introduction and Literature Survey

Part 1: Introduction of Tough Hydrogel and Its Application In Soft Electronic Fabrication

1.1 Statement of the problems……..18

1.2. Background & History of Hydrogel..…….....18

1.3 Classification of Hydrogels……20

1.4 Research Motivation……...32

1.5 Research Objective……..33

1.6 Importance and Selection of Tough Hydrogels for Soft Electronic Applications……34

1.7 Strategies For The Synthesis of Tough Hydrogel……34

1.8 Key Problems Associated With Hydrogel Synthesis……....36

1.9 Application Of Tough Hydrogel In Different Sectors……...37

1.10 Tough Hydrogel as a Functional Material in Flexible, Wearable Bioelectronic Devices……..38

1.11 Challenges in Utilising Tough Hydrogels for Flexible Electronic Devices……41

1.12 Key Challenges And Future Prospects……42

1.13 Conclusion……...44

Part II: Literature Survey of Tough Hydrogel and Its Application In Soft Electronic Fabrication

1.14 Literature Survey…….45

Chapter 2 Materials & Methods

2.1 Experimental Section…….55

2.2 Methods Used For Mechanical Study……58

2.3 Physicochemical Characterisation Technique Used……...61

2.4 Electrochemical Study……70

Chapter 3 Polyelectrolyte Complexation Approach to Devise PEDOT: PSS-Based Printable, Self-Healable and Ultra-Stretchable Solid Electrolytes for Under-Water Electronics

3.1 Summary……74

3.2 Introduction……74

3.3 Synthesis Procedure of PEDOT-PSS-PAHT (PDTPS-PAHT-n) Ink……..78

3.4 Results & Discussion……..78

3.5 Conclusion……..101

Chapter 4 A Facile Media Polarity Control (MPC) Strategy to Tailor the Toughness & Adhesive Strength of Dual Monomer Single Network Hydrogels and Integrated Machine Learning Approach

4.1 Summary…….105

4.2 Introduction…….105

4.3 Synthesis Procedure of PAMSAAm-IP0.n Hydrogel……..109

4.4 Results & Discussion……...109

4.5 Conclusion……...136

Chapter 5 CNT Incorporated PAMPS/PAAm-Based Single Network Hydrogel for Strain Sensing Application

5.1 Summary…….139

5.2 Introduction…….139

5.3 Synthetic Procedure of AAmCNH-n hydrogel film……....144

5.4 Results & Discussion……...144

5.5 Conclusion……...155

Chapter 6 Summary & Future Recommendations

6.1 Summary and conclusion of the present work…….159

6.2 Recommendations……163

6.3 Future Perspectives……..164

References…….166

Preface

Hydrogels are 3-dimensional polymer networks made up of covalent or physical bonds, depending on their composition. It can absorb about 50-90% of water inside its matrix compared to the weight of monomer in the hydrogel. They show higher mechanical strength and stretchability in the range of 1200-2000% of the original length of hydrogels. Conventional hydrogels are brittle and have lower mechanical strength. By changing the strategy of preparation and incorporation of certain metals and nanoparticles, we can improve the mechanical properties and conductivity of hydrogels. Due to their higher mechanical and electrochemical properties, modern hydrogels can be used for the fabrication of electrochemical flexible energy storage devices, sensors for motion, temperature, and pressure detection based on the changes in the resistance of hydrogels under these stimuli.

Chapter 1: Introduction & Literature Survey

This chapter discussed the fundamental understanding of tough hydrogels, including their types, synthetic approaches, and diverse areas of application. Furthermore, we elaborated on the utilisation of hydrogels in energy-storage devices, highlighting their integration with metal-based hydrogels and carbon-based materials within the hydrogel matrix. Finally, we outlined the future scope of hydrogel-based systems in advancing next-generation energy technologies.

Chapter 2: Materials and methodology

This chapter discussed about the instrument and procedure used for the synthesis of tough hydrogel and materials characterisation. Here we discussed in detail about dimensions and methods of characterisation of materials. The major characteristic techniques discussed here are Fourier transform infrared spectroscopy (FT-IR), field-emission scanning electron microscope (FE-SEM), X-ray diffraction (XRD), X-ray photoelectron spectroscopy (XPS), Raman spectroscopy, UV-Vis

(ultraviolet-visible spectroscopy), Small Angle X-ray (SAXS), and High- resolution transmission electron microscope (HR-TEM).

Chapter 3: Polyelectrolyte Complexation Approach to Devise PEDOT: PSS-Based Moldable, Self-Healable and Ultra-Stretchable Solid Electrolytes for Under-Water Electronics.

This chapter discussed about the approach to synthesise a conducting ink with tunable viscosity through polyelectrolyte complexation between polyacryloyl hydrazide triflate (PAHT) and polystyrene sulfonate (PSS), enabling high Poly(3,4-ethylenedioxythiophene) (PEDOT) loading for fabricating stretchable, self-healable, and conductive solid electrolytes. While PEDOT: PSS systems are promising for metal- free flexible electronics, they often lack sufficient stretchability, mechanical strength, and stability in aqueous environments. The introduction of ionic linkages ($CONHNH_3^+\cdots SO_3^-$ and $SO_3^-\cdots CS^+$) between polymer chains provided strong film integrity in both organic and aqueous media, yielding high tensile strength, exceptional stretchability, and good ionic conductivity. The films also exhibited stable electrical performance, with an excellent $\Delta R/R_0$ value. As a proof of concept, the solid electrolyte functioned effectively as a strain sensor, showing repeatable $\Delta R/R_0$ responses to various body movements, even underwater. The system demonstrated suitable gauge factors of 4.4 (air) and 0.20 (submerged), confirming its potential for flexible and submersible strain-sensing applications.

Chapter 4: Media Polarity Control Strategy to Tailor the Mechanical Behaviour of Dual monomer Single Network Hydrogels and Integrated Machine Learning Approach.

This chapter addresses the challenge that very few simple and scalable strategies exist to simultaneously enhance hydrogel toughness and tailor their material properties. Conventional one-pot gelation of dual or multi-monomer systems often suffers from macrophase separation, which weakens

mechanical performance. To overcome this, a Media Polarity Control (MPC) technique was used to control solvent polarity to promote uniform phase mixing during gelation. As a proof of concept, a dual-monomer single-network hydrogel composed of acrylamide (AAm) and acrylamidomethyl-propanesulfonic acid (AMPS) was synthesised. The presence of IPA in the matrix also enables reliable performance at low temperatures, expanding its practical applicability. Finally, machine learning models were developed to predict tensile behaviour based on composition and crosslinking parameters across a wide range of hydrogel formulations, demonstrating the broader potential of the MPC strategy.

Chapter 5: Ultra-stretchable and Adhesive Hydrogel Synthesis and Incorporation of Carbon Nanotube to Fabricate Highly Conductive Electrolytes for Sensors

This chapter focuses on developing a new class of hydrogels that are highly stretchable, strongly adhesive, and electrically conductive, making them ideal for next-generation flexible and wearable sensors. To achieve this, carbon nanotubes (CNTs) are incorporated into the hydrogel network. CNTs introduce continuous conductive pathways, significantly improving the electrical conductivity of the hydrogel without compromising flexibility. Simultaneously, the polymer matrix is engineered to enhance mechanical strength, stretchability, and adhesion to various surfaces. These properties of ultra-stretchability, adhesive nature, mechanical strength, and high ionic/electronic conductivity enable the hydrogel to function as an efficient solid electrolyte for sensors. Such hydrogels can detect strain, motion, or pressure and are suitable for wearable, biomedical, and soft-robotic applications. This approach offers a simple yet powerful strategy to fabricate multifunctional, high-performance hydrogels for modern sensing technologies.

Chapter 6: Conclusion and future scope

This chapter summarises the work discussed above in all the chapters and outlines the future scope of this research work.

Chapter-I

Introduction and Literature Review

Part I: Introduction of Tough Hydrogel and Its Application In Soft Electronic Fabrication

Introduction

1.1 Statement of the problems:

Growing concerns about fossil fuel impacts have intensified research into green, sustainable materials for energy storage. Polymers, due to their abundance, low cost, biodegradability, and tunable properties, are increasingly used as gel electrolytes in energy storage systems. Their unique hierarchical matrix structures facilitate both mechanical stability and efficient ionic transport, making them promising candidates for next-generation flexible devices, which are in high demand for wearable and portable electronics. Most systems use polysaccharide (cellulose, alginate, chitosan) or protein-based (gelatin, silk) polymers as either the primary matrix, additives, or 3D scaffolds for hydrogel-based electrolytes. Polymers and hydrogels are deeply interrelated in energy storage systems, with polymers serving as the structural and functional backbone of hydrogels, and hydrogels acting as transformative materials that address key challenges in modern batteries, supercapacitors, and flexible/ wearable energy devices.

1.2 Background and History of Hydrogel

A three-dimensional hydrogel was first discovered in the late nineteenth century to advanced tough and conductive hydrogel. They are capable of absorbing a large quantity of water while maintaining structural integrity 1894[1]. Their advanced properties and multifunctional polymeric systems have positioned them as key materials in advanced energy storage and wearable technologies[2]. The first hydrogel was introduced in 1894, having only inorganic systems by Van Bemmelen[3], followed by synthetic hydrogels commercially prepared by Ivalon in 1949[4]. Further, poly(2-hydroxyethyl methacrylate) (pHEMA) were synthesised by Wichterle and Lim in 1960[5]. Such hydrogels demonstrated extensive swelling properties without dissolving, ensuring their application in soft contact lenses[6]. From the 1970s to the 1990s, hydrogel technology expanded rapidly in many fields,

including biomedical, drug delivery, wound healing and tissue engineering[7,8,9,10,11,12,13,14,15] Incorporation of natural polymers like gelatin, cellulose derivatives, alginate, and chitosan enhances biocompatibility but has weaker mechanical strength, and develops tougher hydrogel[16,17]. In the early 2000s, a major invention of tough hydrogels based on double-network (DN) hydrogel, interpenetrating (IPN) hydrogel, and topological design with improved elasticity, fracture resistance and fatigue durability was developed. The higher dissipating energy in sacrificial bonds and a hierarchical network is brittle in nature[18]. Advances in nanotechnology strengthen hydrogel via the incorporation of nanofillers. Incorporation of such nanofillers reinforced the hydrogel matrix and also imparted electrical conductivity[19], which enables their use in flexible electronics and energy device fabrication. Recently, the development of conductive hydrogel[20], ionic network[21] and electrolyte-rich[22] matrix led to the emergence of tough[23], conductive and anti-swelling hydrogels[24], making them suitable for functioning as solid-state electrolytes for batteries[25], supercapacitors[26], wearable flexible devices[27], ion thermoelectric systems and maintaining high ionic conductivity, mechanical flexibility and stability under repeated deformations[28]. Several challenges include a narrow range of electrochemical stability window, compatibility between conductivity and mechanical robustness and degradation in performance under extreme environmental conditions was observed[29]. Researchers have optimised some crosslinking strategies[30], nanocomposite designs and polymer-ion interactions strategies to synthesise a critical material which can act as a bridge between synthetic polymers and biological tissues and play an important role in the future development of sustainable, bio-integrated, and flexible energy storage technologies[31].

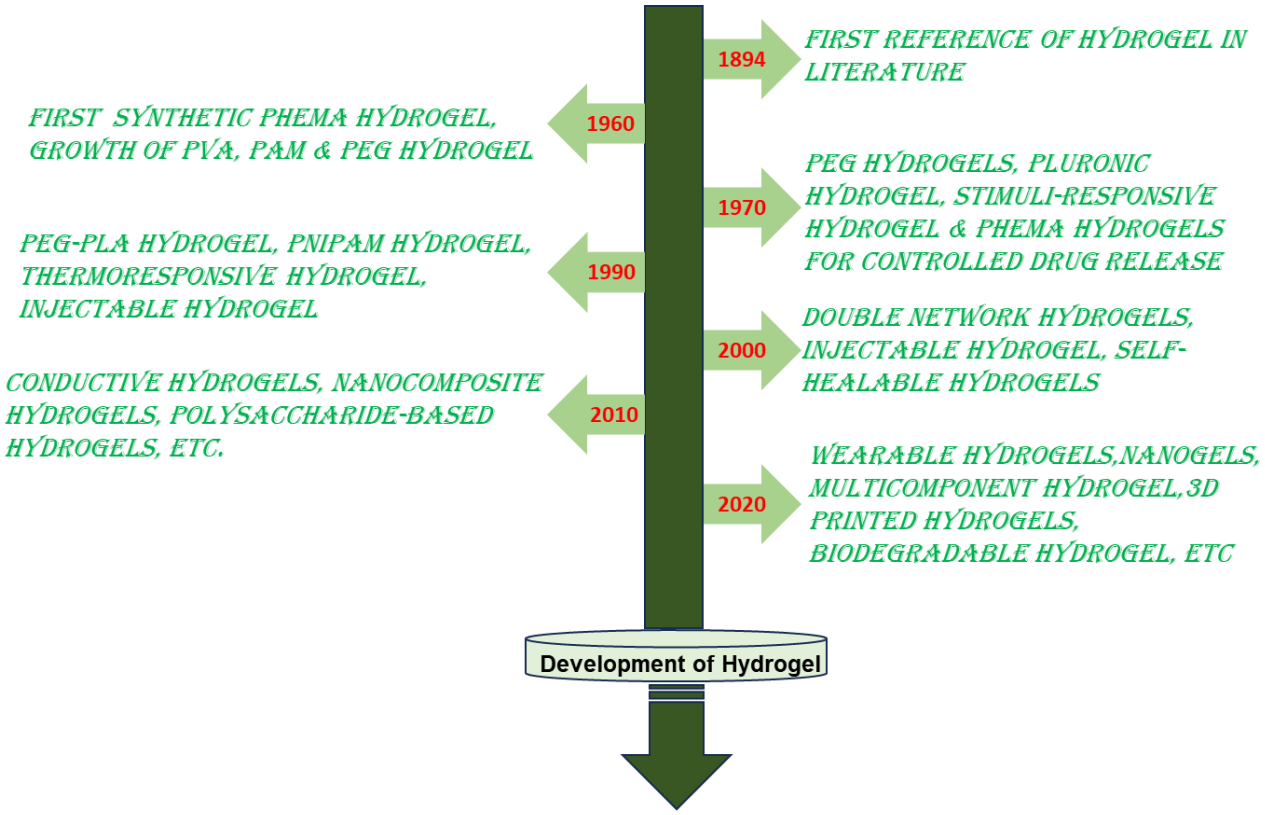

Figure 1.1: Development of hydrogels over the years

1.3 Classification of Hydrogels

1.3.1 Single Network (SN) Hydrogels: Single Network (SN) hydrogels are classified based on the origin of the polymer. Natural hydrogels like alginate, gelatin, and hyaluronic acid exhibit excellent biodegradability and biocompatibility[32]. They are weaker in mechanical strength and limited tunability[33]. Synthetic hydrogels, on the other hand, have precise control over structure, mechanical strength and their stability, enabling their application in flexible electronics, wearable sensors and biomedical devices[34]. SN hydrogels based on polymer composition are classified as homopolymer hydrogels with uniform polymer arrangement, controlled swelling behaviour and copolymeric

hydrogels, which have improved mechanical strength and adjustable tunability and lastly interpenetrating polymer network (IPN) hydrogels, which include double-network systems, showed enhanced toughness, stretching and energy dissipation. Crosslinking methods can create physically crosslinked hydrogels with reversible non-covalent interactions. These are flexible and self-healing, but have very limited mechanical strength. Other types include responsive hydrogel that can undergo changes when exposed to external stimuli such as temperature, pH, light, or electric fields.

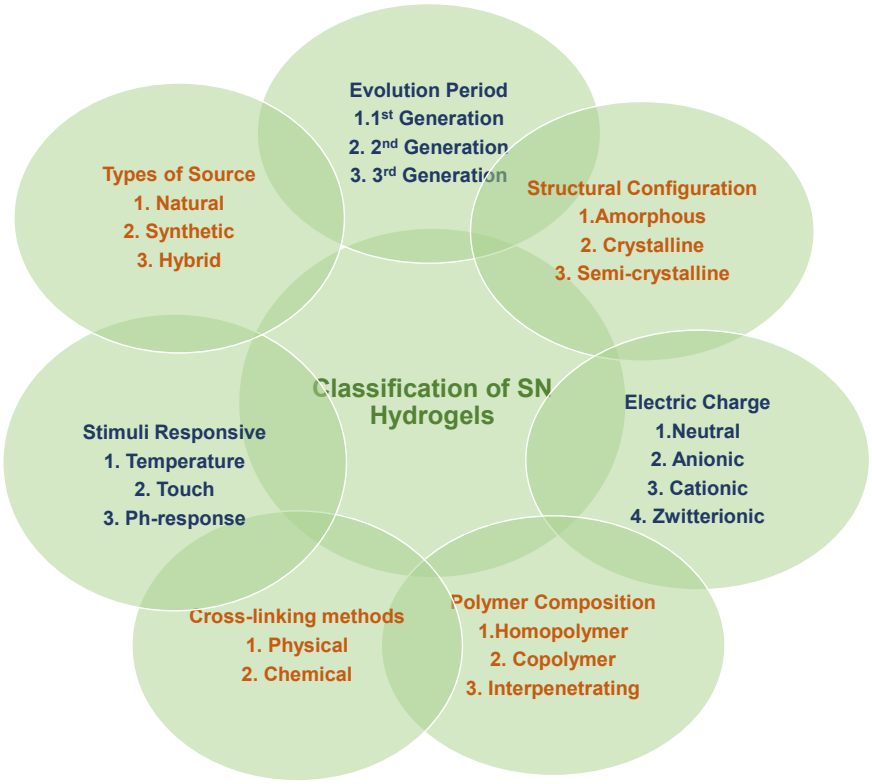

Figure 1.2: Schematic of the classification of Single Network (SN) Hydrogel

A) Based on the evolution period:

Hydrogels are commonly classified by generations based on the evolution of their chemistry and functionality. The first generation, starting in the 1960s, consists of chemically crosslinked hydrophilic polymers such as pHEMA, polyacrylamide (PAM), polyvinyl alcohol (PVA), and cellulose-based

hydrogels. The second generation arose in the 1970s and introduced stimuli-responsive hydrogels, which are capable of reacting to environmental conditions like pH, temperature, or specific biomolecules, and found widespread use in smart drug delivery systems and sensors. The third generation, beginning in the late 1990s and continuing through today, features "smart" or "tunable" hydrogels[35]. These are formed through advanced physical interactions, such as stereo-complexed networks and cyclodextrin crosslinking, with properties engineered for precise responsiveness in biomedical applications.

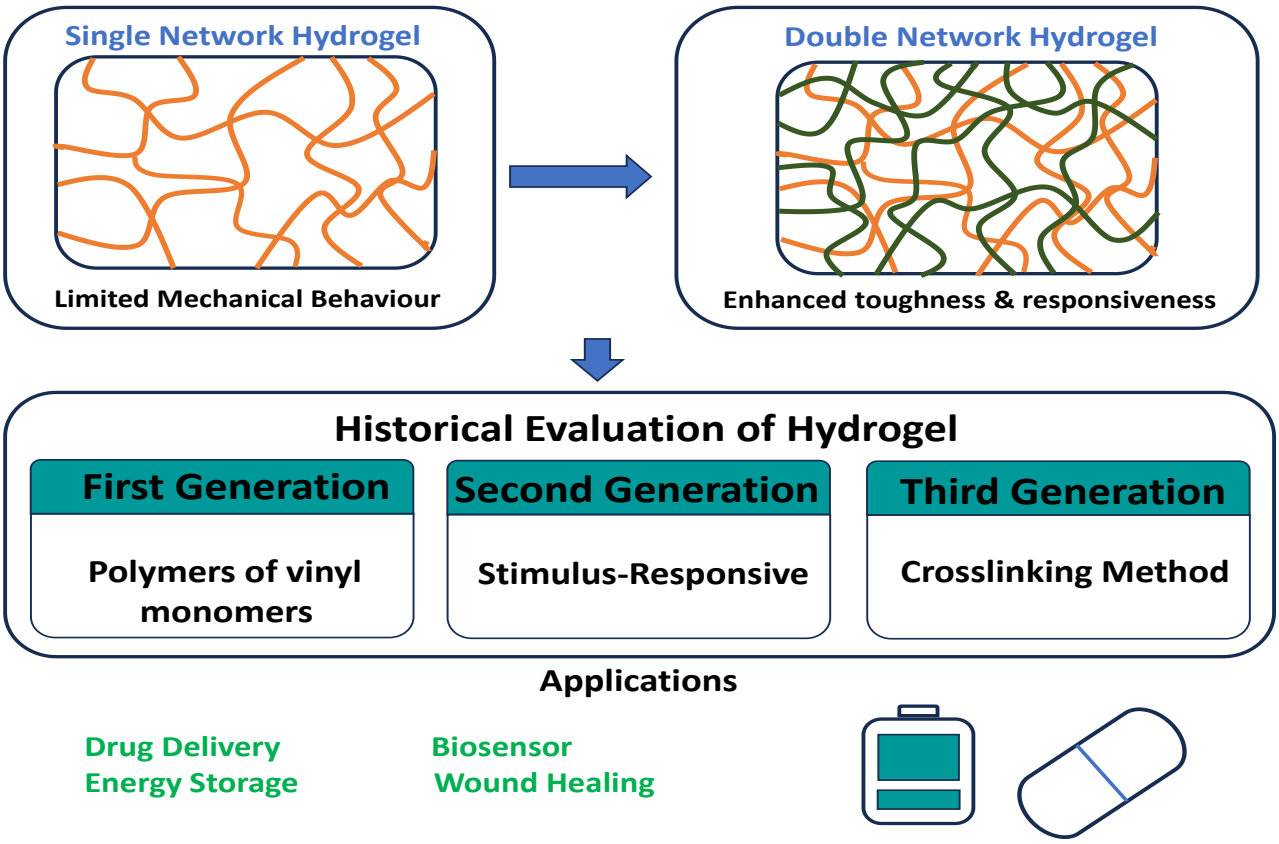

Figure 1.3: Schematics of the development of Hydrogel and its application

At present, hydrogel research remains a highly active field, serving as the foundation for novel biomedical, industrial, and environmental technologies. Current innovation trends focus on multi-

responsive hydrogels, biocompatible delivery systems, advanced sensor materials, and regenerative medicine scaffolds.

Table 1.1: Generational Development of hydrogel throughout the years

Generation	Period	Properties	Limitations	Material
1st	1960s-1980s	Chemically crosslinked	Brittle in nature	pHEMA, PVA, PAM
2nd	1990s-2000s	Stimuli responsive	Moderate strength	PNIPAM, PAA, polyaniline
3rd	2010s---continue	Multifunctional, self-healing, bioactive	Complex synthesis	DN hydrogels, supramolecular hydrogels, nanocomposite hydrogels

B) Based on the source: Based on the source, the hydrogels are broadly classified as natural, synthetic, and hybrid hydrogels depending on the origin of polymers used.

- **Natural Hydrogels:** Derived from naturally occurring polymers like polysaccharides and proteins. Some common examples include alginate, collagen, gelatin, chitosan, dextran, agarose, and hyaluronic acid. These hydrogels have excellent biodegradability and biocompatibility as they closely resemble the natural extracellular matrix (ECM) of biological tissues[36]. They also support cell adhesion and proliferation and help with tissue regeneration, making them suitable for biomedical applications. Natural hydrogels, although they exhibit poor mechanical strength and limited stability, are widely used in wound healing, drug delivery, cell encapsulation, and cartilage tissue engineering.
- **Synthetic Hydrogels:** Derived from chemically synthesised polymers like poly (vinyl alcohol) (PVA), poly (N-isopropylacrylamide) (PNIPAm), poly (acrylamide) (PAAm). These hydrogels have tunable degradation, controlled mechanical properties and high reproducibility. They have superior structural stability compared to natural hydrogels and can easily be modified according to specific applications. They generally lack biological activity and other required

functionalities for biomedical applications. These hydrogels are useful in biosensor fabrication, flexible electronics, soft robotics and drug delivery.

- **Hybrid Hydrogels:** These are a combination of natural and synthetic polymers that have both improved mechanical performance and biological functionality. PEG-collagen hydrogels, HA-PVA systems, and Gelatin Methacryloyl (GeIMA-based) hydrogels are such examples. These hydrogels have some enhanced biocompatibility, better structural stability, and tunability than natural or synthetic hydrogels. Their balanced properties enable them to be used as 3D bioprinting and injectable scaffolds for cartilage tissue engineering.

C) Based on Polymer Composition: Based on polymer composition, hydrogels are of the following types:

- Homopolymeric Hydrogels: formed from a single type of monomer, result in a uniform polymer network. A hydrogel based on polyacrylamide is an example. These are simple to synthesise and have consistent structural properties.
- Copolymeric Hydrogels: These hydrogels have two or more different types of monomers. The integration of multiple monomers improves the swelling behavior, mechanical properties, and degradation rate. One of the examples is the PEG-co-PCL-based hydrogels.
- Interpenetrating Polymer Network (IPN) Hydrogels: Such hydrogels have physically crosslinked polymeric networks entangled within each other's matrix. Hydrogels have better mechanical stretchability, toughness, and stability as compared to single network systems. Commonly used in load-bearing for tissue engineering applications.
- There is one more category of IPN, semi-IPN hydrogels. These contain crosslinked network and linear network chains dispersed within the structure. Hydrogels have improved mechanical properties and easy fabrication steps with better mechanical performance.

D) Based On The Type of Crosslinking

- Physically Crosslinked Hydrogels: Formed via non-covalent interactions such as ionic interactions, chain entanglement, and hydrogen bonding. Generally are biocompatible and injectable as they do not need chemical crosslinking. They usually have poor mechanical strength. Alginate-Ca^{2+} based hydrogels and freeze-thaw PVA-based hydrogels are some examples.
- Chemically Crosslinked Hydrogels: These hydrogels involve covalent bonds and techniques such as photo crosslinking, free radical polymerisation and enzymatic crosslinking, etc. They have better mechanical strength, controlled degradation and long-term stability. GeIMA and Poly(ethylene glycol) diacrylate (PEGDA-based) hydrogels are some of the examples.

E) Based on Electric Charge:

- Neutral Hydrogel: Composed of neutral hydrophilic polymers with non-ionisable properties in aqueous media. Their swelling nature is majorly dependent on the number of hydrogen bonds and water-polymer interactions rather than the electrostatic force of interactions. Such hydrogels have lower protein adsorption, good biocompatibility and minimal ionic interaction. Some of the examples include Poly(ethylene glycol) (PEG) based hydrogels useful in the medical field.
- Anionic Hydrogel: These hydrogels have negatively charged polymers with functional groups such as sulfate, carboxylate or phosphate groups that get ionised in aqueous media. Their polymeric chain repulsion increases water absorption and swelling capacity. A few examples include poly(acrylic acid), alginate, and hyaluronic-based hydrogels. These are pH-responsive and applicable in drug delivery systems, wound healing, tissue engineering and bioseparation due to their high ionic conductivity, excellent hydration and good biological compatibility.

- Cationic Hydrogel: These hydrogels possess positively charged polymers such as amino or quaternary ammonium group-containing polymers. They interact strongly with the negatively charged proteins, nucleic acids and biological membranes. Typical examples include chitosan and polylysine-based hydrogels. Due to the presence of electrostatic interactions, these hydrogels show antibacterial activity, improve cellular interaction and mucoadhesion. Widely used for controlled drug delivery, wound healing, antimicrobial coating, and gene delivery applications. They are also useful in stimuli-responsive biomedical applications due to their charge-dependent swelling properties.
- Zwitterionic Hydrogels: Such hydrogels contain positive and negative functional units in the same polymeric matrix, being electrically neutral. They have strong hydration layers resulting in better water retention. Some of the common examples include carboxybetaine and sulfobetaine-based hydrogels. Their biocompatibility and poor protein adsorption make them suitable for biosensors, drug delivery, biomedical implants and tissue engineering applications.

F) Based on Responsiveness: Stimuli-responsive hydrogels are capable of changing their physical and chemical properties in response to external stimuli like light, temperature, pH, electric & magnetic fields. A few examples include poly(N-isopropylacrylamide) (PNIPAm) as a thermoresponsive hydrogel used for injectable drug delivery and smart biomaterials. Poly(acrylic acid)- and chitosan-based hydrogels as pH-responsive materials for controlled and targeted drug delivery. Some other types include light-responsive hydrogels for soft actuators, electric- and magnetic-responsive hydrogels for biosensors, artificial muscles, flexible bioelectronics, and soft robotics.

G) Based on Structural Configuration: Hydrogels based on polymeric chain arrangement inside the matrix are classified as amorphous, crystalline and semi-crystalline. In an amorphous hydrogel, the chains are irregularly arranged responsible for its higher flexibility, swelling capacity and elastic

nature. On the other hand, in crystalline hydrogel, there is a highly ordered arrangement of chains inside the hydrogel matrix. Due to this, the hydrogel has rigidity, better mechanical strength and lesser swellability. Semi-crystalline hydrogels possess both phases in the same hydrogel matrix. Therefore, they have combined the flexibility and swelling property of the amorphous region and the mechanical stability of crystalline domains. One of the examples is poly(vinyl alcohol) (PVA) based hydrogel useful in biomedical applications.

1.3.2 Double Network (DN) Hydrogels

Double Network (DN) hydrogels are composed of two interpenetrating polymer networks, a rigid and highly crosslinked brittle first network and a soft, loosely crosslinked stretchable second network[37]. On applied stress the first brittle network fractures and dissipates energy, while the second hydrogel network is elastic and can maintain integrity. There is some synergistic mechanism that provides DN hydrogels an exceptional toughness, higher fracture resistance and high stretchability, allowing the hydrogel film to mimic the mechanical behaviour of living tissues such as cartilage and ligaments[38]. Some common examples include PAM/alginate[39], PAM/chitosan[40] and chitosan/poly(2-acrylamido-2-methylpropanesulfonic acid)[41] DN hydrogel. DN hydrogels can be widely applied in tissue engineering[42], flexible soft electronics[43], sensors[44], artificial cartilage, and load-bearing biomedical implants[45] due to their superior mechanical performance.

1.3.3 Synthetic Approach of Double Network Hydrogel

DN hydrogels are typically used two step polymerisation process. A rigid and brittle polymer network was formed using a highly crosslinked polymer network. This network was then swollen in a precursor solution of second monomer, crosslinker and initiator, which gets diffused inside the first network. After polymerisation forms a soft and flexible second network interpenetrating inside the first network matrix. These polymeric arrangements result in a tough and resilient hydrogel[46]. Another approach

involves microgel-based DN formation[47], nano-material incorporation as strengthening agents[48], photo-initiated polymerisation and chemical coupling methods[49] to improve mechanical performance and maintain shape.

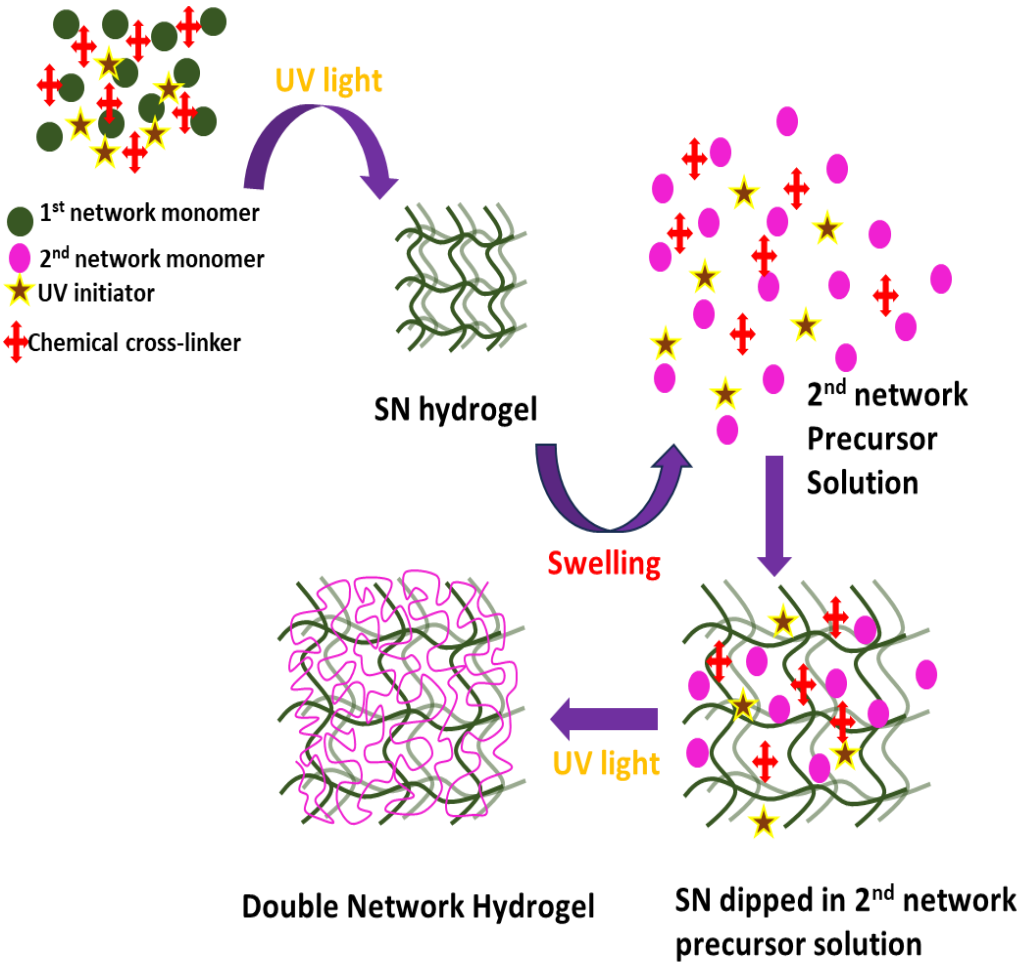

Figure 1.4: Schematic of the synthetic approach of Double Network (DN) Hydrogels

1.3.4 Classification of Double Network (DN) Hydrogels

DN hydrogels are classified based on polymer composition, crosslinking methods and application. The classification allows better understanding of their structural design, suitability for advanced applications and mechanical performances.

A) Based on Polymer composition: The DN hydrogel can be categorised into synthetic-synthetic, natural-synthetic, and natural-natural systems based on polymer composition.

- Synthetic-synthetic DN hydrogels have two synthetic networks of polymers, perform excellent toughness, tunability and mechanical properties. Few of the examples are polyacrylamide (PAAm), polyvinyl alcohol (PVA) based hydrogels. They may have poor biodegradability and biocompatibility based on the polymer used.
- Natural-synthetic DN hydrogel includes some natural polymer (gelatin, cellulose, chitosan, etc) along with a synthetic one in a single hydrogel system. Such a hydrogel shows better biodegradability and compatibility, along with cell integration, mechanical robustness and stability. These DN hydrogels have wide application in wearable electronics, wound dressing and tissue engineering.
- Natural-natural DN hydrogels contain all naturally derived polymers. They have low toxicity, biodegradability and are biocompatible. Therefore, such DN hydrogels are suitable for biomedical applications. However, they have lower mechanical strength and flexibility than synthetic DN hydrogels.

B) Based on Crosslinking strategies: Based on their network synthesis strategies, the DN hydrogels can be classified as physically crosslinked and chemically crosslinked DN hydrogels.

- For physical crosslinking, the non-covalent interactions, hydrogen bonding, crystallisation, chain entanglement and hydrophobic interactions are responsible. Such hydrogels have reversible arrangements of networks, show self-healing behaviour, can be injectable, and are stimuli-responsive in nature. However, their durability and mechanical stability are relatively lower.

- For chemical crosslinking, there is a presence of covalent bonds within the hydrogel matrix formed via a chemical crosslinker or some polymerisation reactions. This type of DN hydrogel has better mechanical strength, long-term durability and superior structural stability. All these properties make them a suitable material for load-bearing applications. Also, the permanent nature of the covalent bond might reduce the self-healing ability of these DN hydrogels.

C) Based on Functional Applications: DN hydrogels depending on their performance in different sectors, can be classified as self-healing, tough hydrogel and conductive hydrogel systems.

- The self-healable DN hydrogels can heal or repair any damage in their matrix using reversible dynamic interactions. Such a property in hydrogel significantly enhances the durability and reliable application in wearable sensors and other electronic devices.
- Tough DN hydrogels are a special kind of hydrogel system with high stress-bearing ability, an excellent range of stretchability of ~ 1000%.-2000%, and lower hysteresis loops representing their excellent repeating ability without any structural failure. This overall mechanical toughness arise from an effective energy dissipation in between two interpenetrating networks, which makes them a suitable material for soft robotics, flexible electronics.
- Conductive DN hydrogels have integrated metal nanoparticles, ionic salts, carbon nanotubes or conductive polymers inside their matrix, which provide them with electrical conductivity. Such hydrogels, due to their flexible, conductive and biocompatible nature, are well suited for strain sensing applications, material for bioelectrode, human-machine interface, and as electrolyte for flexible batteries and supercapacitors.

1.3.5 Key Challenges of Double Network (DN) Hydrogels

Despite its exceptional toughness, DN hydrogels suffer from irreversible damage due to permanent bond breakage, limiting self-recovery under repeated loading[50]. Physically crosslinked hydrogels have partial recovery but exhibit mechanical instability and stress relaxation over time[51]. The synthetic procedure is complex and requires precise control over the polymer composition, crosslinking density and network balance. Toughness, self-healing ability, biocompatibility and higher stability remain a key challenge in DN synthesis for advanced biomedical engineering[52] applications.

Table 1.2: Comparison table for Single Network and Double Network Hydrogel

Feature	**Single Network Hydrogel**	**Double Network Hydrogel**
Structure of Hydrogel	One polymer network is usually homogeneous	Two interpenetrating networks with contrasting crosslinking densities
Mechanical Strength	Moderate strength, elasticity, often brittle under high stress	Very high toughness and strength, highly resistant to fracture,
Toughness	High chain entanglement, high crosslink density, need modification to improve performance	The first network acts as a sacrificial network, and the second network maintains integrity
Elasticity/Recoverability	Highly elastic in some designs, but limited durability under heavy load	Some designs can achieve high energy dissipation some designs offer rapid self-recovery
Fabrication Complexity	Usually simple, single-step synthesis	More complex, multi-step process (sequential or combined polymerisation)
Swelling Behaviour	Typically high, it can weaken the mechanical strength in the swollen state	Balanced by the differing swellabilities of each network

1.4 Research Motivation: The research motivation focused on designing conductive inks and hydrogels that have significant stretchability, self-healing ability, and mechanical resilience, which remains a significant challenge in the field of flexible and wearable electronics. Although PEDOT: PSS-based materials offer good electrical conductivity, they typically suffer from limited stretchability and mechanical robustness. To overcome these limitations, polyelectrolyte complexation with polyacryloyl hydrazide triflate (PAHT) is explored as a strategy to develop conductive inks with tunable viscosity, improved stretchability, and self-healing properties. Achieving a careful balance between conductivity and mechanical characteristics through dynamic ionic linkages is essential for the inks' practical use in underwater and wearable electronics devices. The primary motivation is to create a polymeric conductive ink system that is compatible with flow-based fabrication methods, such as 3D printing, and can maintain stable function under both environmental and underwater conditions[53]. Developing a simple and scalable method to enhance both the toughness and adhesive strength of dual monomer single network hydrogels by mediating the polarity of the gelation medium. Most of the strategies for tough hydrogels rely on complex multi-network design, such as double networks, alignment techniques, or post-gelation treatments. However, these approaches are not always practical for large-scale or application-specific formulations, and one-pot methods involving multiple monomers often suffer from issues like macrophase separation, which reduces mechanical performance[54].

There is a pressing need for simple and scalable methods that can improve both toughness and adhesive strength in hydrogels at the same time. Many existing approaches rely on complex multi-network designs or require multi-step fabrication processes, which can be impractical for real-world applications. One challenge in one-pot polymerisation of dual monomer hydrogels in water is phase separation during gelation[55], which weakens their mechanical properties. To address this, controlling

the polarity of the gelation medium by using mixed solvents has been proposed as a way to promote better phase mixing and polymer chain entanglement, resulting in improved mechanical toughness and adhesive performance. Additionally, the approach aims to create hydrogels capable of functioning well at low temperatures, a condition where most conventional hydrogels fail. To further aid hydrogel design, machine learning methods are applied to predict mechanical properties from formulation parameters, enabling more rational and efficient material development. The synthetic approach provides a stretchable and self-healing hydrogel with a conductive nature are suitable candidate for flexible, soft material to be used in flexible, wearable electronic devices.

1.5 Research Objective

- ✓ To achieve a balance between conductivity and mechanical resilience in conductive polymer systems via dynamic ionic linkages, making them suitable for flow-based fabrication methods such as 3D printing and stable operation under environmental and underwater conditions.
- ✓ To produce hydrogels that maintain functional performance at low temperature conditions, expanding their practical applicability.
- ✓ To develop a simple and scalable strategy to simultaneously enhance the toughness and adhesive strength of dual monomer single network hydrogels by promoting phase mixing and chain entanglement during one-pot polymerisation.
- ✓ To design and formulate conductive hydrogels with tunable viscosity, enhanced stretchability, and self-healing properties through polyelectrolyte complexation aimed at flexible and wearable electronics.
- ✓ The objective revolves around innovating hydrogels and conductive ink formulations to realise multifunctional materials with improved mechanical, adhesive, and electrical properties for advanced applications in flexible electronics and biomedical devices.

1.6 Importance of Tough Hydrogels for Soft Electronics

From the various hydrogel categories, tough hydrogels were the most suitable material for soft electronic applications as they have an exceptional combination of stretchability, functional adaptability, mechanical robustness, and flexibility. The conventional hydrogels are soft materials, biocompatible and contain high water content, but they have poor mechanical strength, structural stability, and suffer from lower fracture resistance when undergoing repeated mechanical loading-unloading. However, the traditional elastomers show better elasticity and durability but suffer from dehydration, poor ionic conductivity, unable to execute tissue-like properties necessary for biointegrated electronic systems. The tough hydrogel, however, can effectively solve these problems by introducing advanced network architectures. Such hydrogels have improved fatigue resistance, toughness and high energy dissipating property with better intrinsic flexibility and better hydration. These properties are required in soft electronics, as the material undergoes continuous stretching, compression, twisting, bending, and cyclic deformation during usage. Additionally, due to its tunable nature, tough hydrogels can also incorporate some other necessary functionalities, such as self-healability, transparency, conductivity, adhesiveness, stimuli-responsive and reprocessability. These properties of tough hydrogel make it a suitable material for electronic skins, soft actuators, wearable sensors, and flexible energy storage devices. Hence, tough hydrogel selection over other conventional hydrogels and elastomers is a better choice as they have the necessary properties of mechanical stability, biological compatibility, and functional stability needed for long-term durability and reliable performance of the device.

1.7 Strategies for The Synthesis of Tough Hydrogel

Hydrogels possess valuable mechanical and physicochemical properties, but conventional types are brittle, limiting their use in flexible electronics and load-bearing applications. Enhancing toughness

involves introducing energy dissipation mechanisms[56], reversible physical bonds for self-healing[57], and adopting specific design principles such as low crosslink density for extensibility and stress dissipation to prevent crack propagation[58]. Tough hydrogels can be classified into three main types: (i) homogeneous tough hydrogels, which reduce structural heterogeneities to improve load distribution and stretchability[59], (ii) energy-dissipating hydrogels, which incorporate mechanisms to absorb mechanical energy and limit crack growth[60], and (iii) multifunctional crosslinker-based hydrogels, which use nanocomposites or particles to dissipate energy through polymer particle bond fracture[61]. Some of the examples include Slide-Ring DN hydrogel,[62] Nanocomposite DN hydrogel,[63] 3D printed DN hydrogel[64], etc.

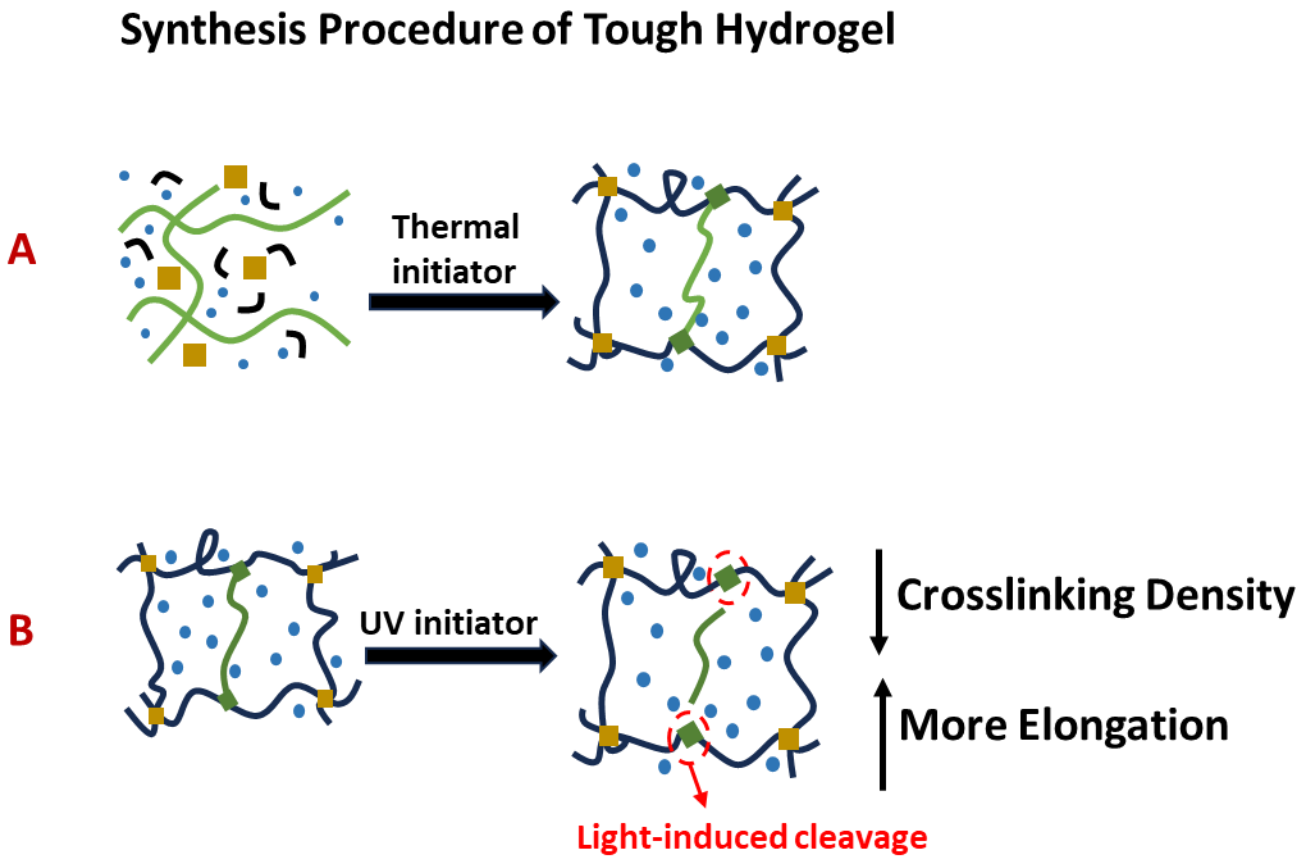

Figure 1.5: Schematic showing the synthetic strategy of tough hydrogel.

1.8 Key Problems Associated with Tough Hydrogel Synthesis

There are various factors that affect the hydrogel synthesis which including controlling crosslinking density, to difficult to precisely control the degree of crosslinking, affecting swelling, mechanical strength, porosity, and drug release profile. The second problem in the Macrophase separation results in a heterogeneous structure with poor mechanical integrity or performance inconsistency[65]. Some remaining initiator residue during the incomplete polymerisation leads to weaker hydrogel linkages and mechanical strength, which results in toxicity in biomedical applications and instability in sensors or batteries[66]. The next parameter is pH, and temperature can cause incomplete gelation, network collapse, or side reaction.

In the Ultra-violet (UV) or thermal-initiated radical polymerisation, the interference of oxygen with the free radical causes collapse of the network formation or surface defects[67]. Many hydrogels, especially single-network ones, are mechanically weak and prone to cracking during or after the synthesis. Some hydrogels undergo syneresis (expelling water after gelation), especially during storage or curing. This phenomenon results in structure alternation and ionic conductivity, especially critical in energy devices[68].

These challenges can be easily overcome by the use of inert gas (N_2) during free radical polymerisation[69], one-pot synthesis, use of biocompatible initiators[70], synthesis of composite hydrogels[71] (e.g., nanofillers) to enhance mechanical properties, and designing of self-cross-linkable systems[72] (e.g., catechol-modified hydrogels). The obtained hydrogels have evolved in terms of composition, structure, and functionalities to meet the biomedical[73], pharmaceutical[74], environmental, and industrial[75] applications.

1.9 Application of Tough Hydrogels in Different Sectors:

Tough hydrogels are a versatile material for modern-day technological, environmental and medical challenges, as they have higher water content, biocompatibility, stimuli responsiveness and tunable mechanics. Hydrogels have wide applications in wound dressings, tissue engineering scaffolds[76], biosensors for health monitoring[77], ophthalmic devices[78], and controlled drug delivery in healthcare and biomedical applications[79]. The tunable chemistry and higher swelling rate of hydrogels enabled their application in pollutant removal[80], soil moisture retention in agriculture[81], smart sensing of environmental toxins[82], and water purification. Hydrogels also function as flexible gel electrolytes for batteries and supercapacitors, active materials for soft robotics[83], electronic skin and actuators[84]. Hydrogels also served as bioink for 3D-printing[85], stimuli-responsive[86] and self-healing materials[87] applicable for advanced research and smart systems.

Table 1.3: Application of Single Network and Double Network Hydrogel

Single Network	**Double Network**
Wound Dressing	Tissue Engineering
Tissue Engineering	Drug Delivery
Drug Delivery	Wound Healing
Biosensing	Bio adhesive
Cell and tissue scaffolds	Wearable sensors, soft robotics
Flexible electronics	Food packaging, an advanced load-bearing biomaterial

1.10 Tough Hydrogel as a Functional Material in Flexible, Wearable Bioelectronic Devices

Hydrogels are a potential material for functional and flexible bioelectronic devices due to their various properties, such as a high range of mechanical stretchability, high-water content, tunable behavior and ionic conductivity. Single-network (SN) and double-network (DN) hydrogels have distinct advantages to offer in strain-sensing, wearable, and bioelectronic systems. Due to their soft and hydrating network, the hydrogels can form a close interface with the skin surface while maintaining the biocompatibility and flexibility. Additionally, single-network hydrogels and double-network hydrogels can be incorporated with some conductive or responsive material for signal transmission, mechanical adaptability and deformation sensing.

1.10.1 Single Network (SN) Tough Hydrogel in Flexible Electronic Devices

Single-network (SN) tough hydrogels are useful in flexible and wearable electronics due to their tunable, hydrated polymeric structure. Also, they can exhibit high ionic conductivity through acid and salt loading and the addition of conductive fillers (e.g., CNTs, MXene, Graphene). They are often eco-friendly and biocompatible. Therefore, suitable for wearable sensors, tissue interfacing platforms and soft electronic devices where they can be used as soft substrate, ion-transport media, and conductive matrices. Hydrogels made up of PAM, PVA, PEG, gelatin, and chitosan have been explored in biomedical and soft electronic applications. Some single network (SN) hydrogels have dynamic linkages (ionic bonding, hydrogen bonding, reversible covalent bonding, etc) in the matrix. Therefore, enable their autonomous crack repair and improved durability under mechanical strain. Hence, a single network (SN) hydrogel can be a safer, softer, and hydrated alternative to the conventional rigid materials.

Table 1.4: Common Single Network (SN) Hydrogel Systems used for Different Applications

SN hydrogel Polymer	Function	Application
PVA	Flexible gel matrix	Wearable sensors
PAM	Ion transport medium	Soft bioelectronics
PEG	Hydrogel host matrix	Biomedical devices
Chitosan	Bio-based polymer	Green biomedical systems
Gelatin	Biopolymer matrix	Biodegradable wearable platforms

These hydrogels are easy to fabricate, cost-effective, and have tunable mechanical and electrical properties. SN hydrogels are compatible with flexible and bio-integrated electronics. Although they have lower mechanical toughness and a quick drying out over time (due to loss of water content). Also, their medium conductivity and mechanical instability need an enhancement via the incorporation of suitable nanomaterials or by applying secondary reinforcement strategies.

1.10.2 Double Network (DN) Tough Hydrogels in Flexible Electronic Devices

Double-network (DN) hydrogels are a suitable material for advanced flexible electronic devices as they replace the poor mechanical properties of single-network (SN) hydrogels by merging the rigid energy-dissipating network with a flexible, soft network, resulting in high strength, toughness, and fatigue resistance under repeated deformation. The ion-rich and hydrated matrix of the double network (DN) hydrogel improved its ionic transport property, resulting in a stable functional performance[88]. These mechanical and conductive properties of DN hydrogel allowed their effective use as flexible sensors and wearable bioelectronics, and self-healing wearable soft devices and tissue interfacing systems.

Table 1.5: Common Double Network (DN) Hydrogel Systems in Flexible Electronic Devices

1st Network	**2nd Network**	**Role**
Alginate	PAAm	Tough,ion-conductive matrix
PVA	PAM	Stretchable wearable platform
Chitosan	PAM/PEG	Biocompatible, self-healing matrix
Gelatin	PAA	Transparent, self-repairing hydrogel

Double-network (DN) hydrogels exhibit several desirable properties for next-generation flexible and wearable electronic systems. They provide high mechanical strength, enhanced ionic transport capability, and excellent fatigue resistance under repeated loading/unloading cycles. Many DN hydrogels are also self-healing, adhesive[89], and biocompatible[90], making them highly suitable for transportable and wearable energy platforms[91]. Despite these advantages, DN hydrogels present certain challenges. Their synthesis is relatively complex, involving multiple preparation steps, and they may suffer from **w**ater loss over time, which can adversely affect long-term stability[92].

Table 1.6: Summary Comparing Single Network (SN) and Double Network (DN) Hydrogel Properties

Property	**SN hydrogel**	**DN hydrogel**
Strength	Low	High
Toughness	Low	Excellent
Conductivity	Moderate	High (if doped)
Self-Healing	Rare	Common
Energy Storage Suitability	Basic	Advanced and wearable

1.11 Challenges in Utilizing Tough Hydrogels for Flexible Electronic Devices

Tough Hydrogels act as promising functional materials for the next-generation flexible devices, including wearable sensors and flexible electronics. Their high ionic conductivity, flexibility, environmental friendliness, biocompatibility, and adaptability make them suitable for use as wearable and implantable systems. One of the major challenges linked with the dryness in hydrogel due to water evaporation causes a lowering of ion transport, mechanical shrinkage, cracking in harsh environmental conditions, and poor functional stability during prolonged environmental exposure. Additionally, the random swelling property can also adversely affect the matrix stability and integrity of hydrogel systems. This severely restricts the long-term durability of the hydrogel. Single-network (SN) hydrogels have a weak mechanical nature and poor fatigue resistance, restricting their performance during continuous mechanical deformation. Scalability issues, uncontrolled swelling and layer delamination can cause the biodegradation and shortening of device lifetimes[93]. Also, maintenance of structural integrity along with flexibility and hydration remains a major challenge in hydrogel design. Incorporation of nanomaterials and conductive polymers has been explored to enhance the mechanical stability and physicochemical performance of the hydrogel. Therefore, a homogeneous dispersion of such fillers inside the hydrogel matrix and proper phase mixing remain significant concerns. Another challenge includes the fabrication complexity of advanced hydrogel systems, especially double network (DN) hydrogels and nanocomposite hydrogels. Their multistep synthesis process, long-term degradation properties, and interfacial instability affect the reproducibility and larger-scale fabrication. Additionally, it is difficult to opt for multiple characteristic useful properties such as flexibility, toughness, hydration stability, biocompatibility, self-healing and conductivity in a single hydrogel system. To overcome the above limitations, various strategies have been adapted. Those include double networking, nanomaterial reinforcement, the introduction of humectants, the development of

hybrid polymer systems, and surface modification. These approaches enhance the structural stability and mechanical strength, durability and hydration retention of hydrogel systems.

1.12 Key Challenges and Future Prospects

Hydrogels have emerged as an important advanced soft material due to their flexibility, tunable network structure and multifunctional property, especially wearable, flexible and sustainable devices. SN hydrogels have a simple network structure, low cost, and easy scalability. DN hydrogels have superior mechanical strength, self-healing ability, and fatigue resistance as they have dynamic bonding, stretchability, longer shelf life, and good energy storage ability. Introduction of DN hydrogels with MXenes, graphene, CNTs and conductive polymers improves conductivity and toughness, useful for advanced wearable, 3D printable and implantable electronic devices. In future endeavours, the research will be focused on developing multifunctional hydrogel systems with improved mechanical stability, self-healing ability, injectability, anti-drying and anti-freezing properties, and better structural adaptability. Also, with the advancement in stimuli-responsive hydrogels, nanocomposite hydrogels and 3D printable hydrogel systems, there is a potential for hydrogels for advanced material applications. Furthermore, the structurally stable and multifunctional hydrogels with long-term performance can be an important direction for future research.

Table 1.7: Future Potential of SN vs DN Hydrogels

Feature	**SN- Hydrogels**	**DN hydrogels**
Fabrication	Simple, low-cost	Complex but tunable
Mechanical Strength	Moderate	High (tough, durable)
Best Use	Scalable, low-cost devices	Wearables, flexible/stretchable devices

Smart Features	Basic	Self-healing, multi-responsive
Future Role	Biodegradable and large-scale systems	Advanced multifunctional hydrogels

Hydrogels are increasingly used as solid or quasi-solid electrolytes, binders, electrode matrices and separators in energy storage and conversion systems as they combine high ionic conductivity with mechanical safety and flexibility. Hydrogels replaced liquid electrolytes and separators in batteries, offering stable ion transport, lowering dendrite growth[94] and improving cycle stability[95] while reducing leakage and fire hazards. Their flexible, self-healing network[96] enables flexible and wearable device applications, maintaining the rapid charge-discharge capability[97] under repeated mechanical deformation. Their properties can be tuned through nanoparticles[98], ionic liquids[99], redox additives[100], and multifunctional polymer[101] to enhance safety and performance in a wider range of temperatures[102]. The dynamic nature of bonds[103] and self-healing behaviour extended the device's shelf-life, and conductive fillers[104] simultaneously improve its ionic and electronic transport with higher energy storage. DN and composite architecture supplied with nanomaterials such as CNTs, MXene, graphene, cellulose nanofibers and clay nanosheets make them suitable for soft electronic applications[105]. The interconnected polymer framework has higher elasticity, toughness, and fatigue resistance, enabling the hydrogel for bending, stretching (~1000%), and compression with good electrochemical performance. Hydrogels have enhanced electrode-electrolyte interface contact, low interfacial resistance, and effective charge transfer. The water-rich ability and permeable structure represent rapid ion diffusion and stable interfacial reactions. This synergistic ionic, higher mechanical and interfacial nature enabled safe, durable, and flexible energy storage devices useful for wearable and deformable applications[106].

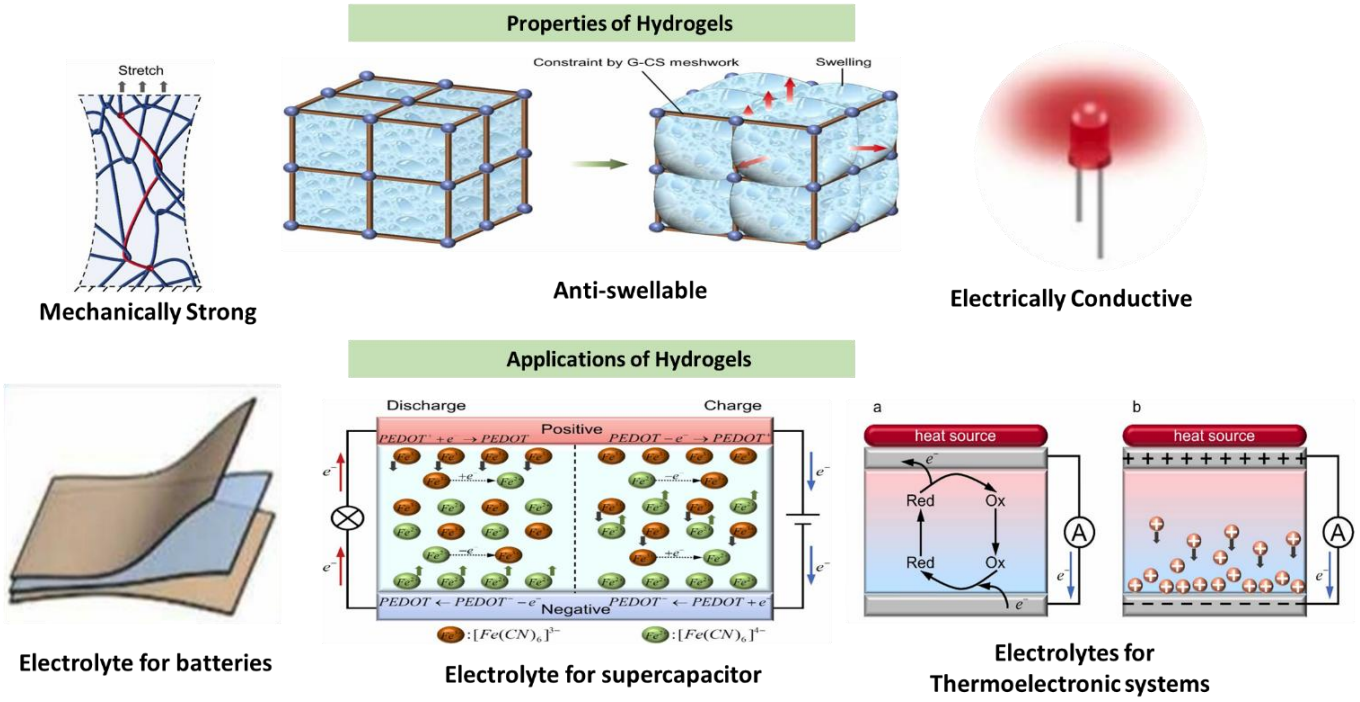

Figure 1.6: Schematic of properties and applications of hydrogel in energy storage and conversion

1.13 Conclusion

Tough hydrogels proved to be a suitable material for wearable soft electronics. Strategies such as double networking, IPN and nanoparticle incorporation have simultaneously improved the functional behavior and mechanical stability of hydrogel systems. But their application is limited to device fabrication as they suffer from fast dehydration, structural instability, poor fatigue resistance and poor long-term stability. Multifunctionality such as self-healing, transparency, stretchability and biocompatibility further complicated the material design as only very few strategies are known currently for tough hydrogel with such combined properties. Future aspects include next-generation flexible and wearable electronic devices. We are focusing on the development of advanced hydrogel systems with enhanced structural stability, multifunctionality, adaptability, and injectability. The

progress in hydrogel research highlights their significance as a versatile advanced soft material useful to the next-generation multifunctional applications.

Part II: Literature Survey of Tough Hydrogel And Its Application In Soft Electronic Fabrication

1.14 Literature Survey

Tough Hydrogels are an important class of material used for flexible and wearable electronic devices as they are rich in water content, have tunable physicochemical properties[107],[108], tissue-like softness and have brilliant deformability. Their three-dimensional matrix can absorb and sustain a huge amount of water with higher structural integrity via physical and chemical crosslinking[109]. Hydrogels have achieved extreme importance in wearable sensors, soft actuators, bioelectronic devices, flexible electronic devices and tissue engineering applications as they are flexible and biocompatible in nature[110],[111]. However, conventional hydrogels have very poor mechanical properties, limited stretchability, and their degradation performance is influenced by dehydration. Their poor durability affects the application in flexible electronics[112]. Therefore, efforts have been taken to develop multifunctional and mechanically stable systems with enhanced mechanical and electrochemical performance, and they should be reprocessable and environmentally stable.

1.14.1 Subclassification of Tough Hydrogels

A) Homogeneous tough hydrogels: Homogeneous tough hydrogels are a class of hydrogels that achieve both high mechanical strength and toughness through a uniform, well-organized polymer

network structure. Unlike many conventional mechanically weak hydrogels, due to inhomogeneous, uneven crosslinking, homogenous tough hydrogels are engineered to have an even distribution of network crosslinks and polymer chain entanglements at the microscopic level. This homogeneity allows the applied mechanical load to be distributed evenly throughout the material, which minimizes stress concentration and reduces the risk of crack initiation and propagation[113]. Toughness in these hydrogels primarily arises from effective energy dissipation mechanisms such as viscoelasticity and physical chain entanglements rather than relying on heterogeneous domains or multiple networks[114]. These homogenous tough hydrogels were prepared using free radical polymerisation with a high concentration of monomer and a low amount of chemical crosslinker[115]. These methods result in a densely entangled polymer network with few imperfections and many mobile physical cross-links, which facilitates efficient dissipation when the hydrogel is stretched or compressed. As a result, these hydrogels can sustain large deformations, recover their shape after stress release, and resist fracture, even at higher degrees of swelling[116]. Homogenous tough hydrogels are soft, water-rich materials with a structurally uniform network, exhibiting exceptional strength and stretchability due to optimised energy dissipation and minimised structural defects[117].

B) Energy-dissipating tough hydrogels: Energy-dissipating hydrogels are a class of soft materials specially engineered to absorb and dissipate mechanical energy when subjected to stress or deformation[118]. This property is crucial for improving hydrogel toughness and durability. The key principle behind energy-dissipating hydrogels is the incorporation of structures or bonds within the polymer network that can reversibly break and reform, or rearrange, during mechanical loading.

The main energy dissipation mechanisms include:

- **Sacrificial Bonds and Networks**: These are physical or chemical bonds (such as hydrogen bonds, ionic interactions, hydrophobic associations, or metal-ligand coordination) that break

under stress, absorbing energy in the process. After the stress is removed, these bonds can partially or fully reform, allowing the hydrogel to recover its structure[119].

- **Non-covalent Interactions:** The use of reversible cross-links, such as host-guest interactions or supermolecular chemistry, enables hydrogels to dissipate energy over a wide range of timescales[120]. Fast and slow relaxing bonds can work together to increase toughness by spreading energy dissipation across different molecular motions.
- **Polymer Chain Entanglements and Sliding:** In some hydrogels, physically entangled or slide-ring structures allow polymer chains to slide past each other under stress. This sliding action dissipates energy and enables the hydrogel to stretch and deform without fracturing[121],[122].
- **Viscoelasticity and hysteresis:** Hydrogels exhibit viscoelastic behaviour[123], where deformation results in hysteresis, i.e., energy loss due to internal friction and rearrangement, further contributing to energy dissipation[124].

By combining these design principles, energy-dissipating hydrogels can withstand repeated mechanical impacts or stretches, making them ideal for applications such as shock-absorbing materials[125], tissue engineering, soft robotics, and artificial cartilage[126]. The challenge in developing these materials lies in balancing rapid recovery (so the hydrogel can return to its original shape quickly) and strong energy dissipation for robust mechanical resilience.

C) Multifunctional crosslinker-based tough hydrogels: Multifunctional crosslinker-based hydrogels are hydrogels synthesised using crosslinking agents that possess multiple reactive sites, enabling the formation of complex, robust, and often dynamic three-dimensional polymer networks[127]. These multifunctional crosslinkers allow simultaneous bonding at several points of the polymer chains, thereby enhancing the mechanical strength, stability, and functionality of the resulting

hydrogels. The use of multifunctional crosslinkers enables precise control over the hydrogel's network architecture, including crosslink density and spatial distribution, which in turn influences the hydrogel's swelling behaviour, elasticity, and responsiveness to environmental stimuli[128]. Multifunctional crosslinkers can also introduce dynamic or reversible bonding features such as light responsiveness, pH sensitivity, or self-healing capabilities when designed appropriately. Synthesis methods typically involve free radical polymerisation, where multifunctional monomers or crosslinkers polymerise simultaneously, forming a highly interconnected network in a single-step process[129]. Alternatively, sequential physical and chemical crosslinking processes may be combined to form hydrogels with multifunctional properties, such as enhanced mechanical performance and targeted bioactivity[130]. These hydrogels find applications in areas like biomedical engineering (e.g., drug delivery, tissue scaffolds), environmental remediation[131], and soft robotics due to their multifunctional nature, mechanical robustness, combined with tailored stimuli-responsive behaviours. The multifunctional crosslinkers contribute significantly to the versatility[132] and adaptability[133] of the hydrogels in diverse conditions and applications.

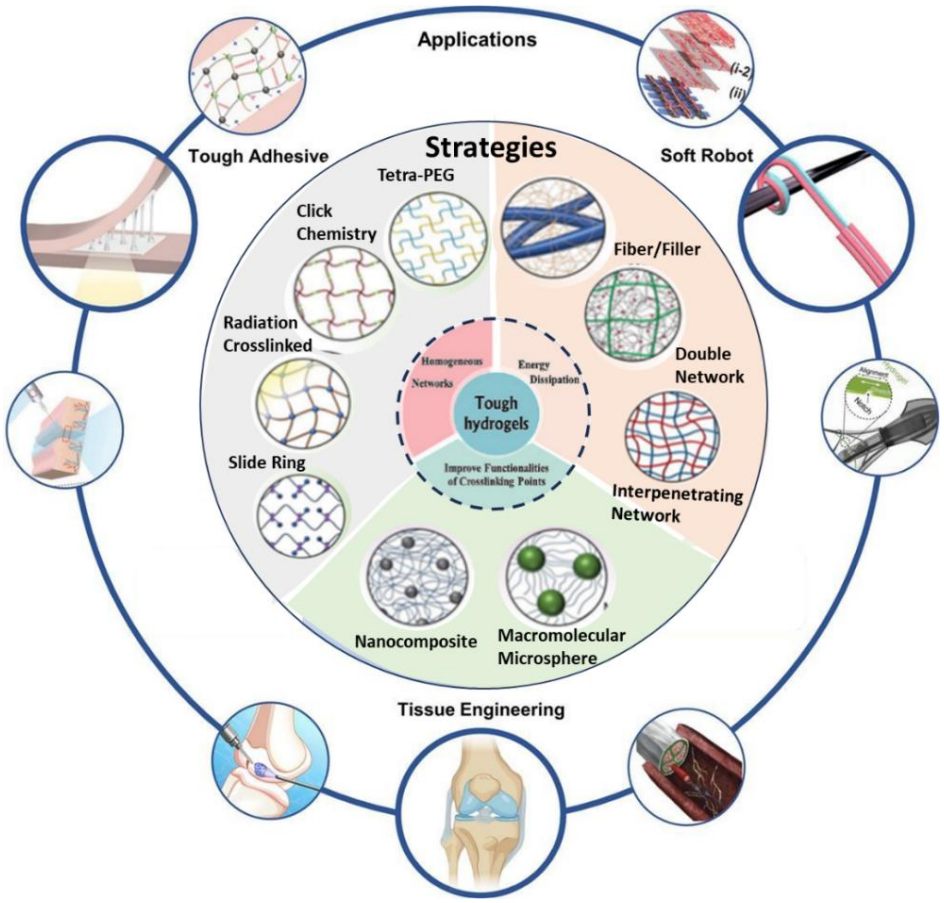

Figure 1.7: Schematics showing the synthetic approach & application of tough hydrogel

1.14.2 Tough Hydrogels in Flexible Electronic Devices

The tough hydrogel systems have become a major interest in flexible electronics fabrication, as the conventional hydrogels are not stable under repeated mechanical loading-unloading and deformation[134],. Tough hydrogels are designed for dissipating mechanical energy via reversible interactions, interpenetrating networks[135], and efficient sacrificial bonds. Double network hydrogels are one of the most widely applicable strategies for enhancing hydrogel toughness. These include a rigid and brittle network and a second soft network responsible for the structural integrity[136]. Several studies have reported a double-network hydrogel with remarkable mechanical properties. A highly stretchable hydrogel system was reported by Sun et al., synthesised by using an ionic-covalent

crosslinking method, resulting in a mechanically resilient and transparent hydrogel system[137]. Also, the supramolecular hydrogels with mixed host-guest interactions, incorporating hydrogen bonding and metal-ligand coordination complex, improve their fatigue resistance[138] and self-recovery. Tough hydrogels are suitable for flexible electronic device fabrication as they have the high mechanical durability required for interfacial tissue interaction, and they are ionically conductive in nature[139]. Tough hydrogels have a stable hydrated matrix that can facilitate the ion transport and are interfacially compatible with tissues[140]. These properties make the tough hydrogel a suitable material for wearable sensors, implantable bioelectronics and electronic skins.

Table 1.8 Tough Hydrogel Applications In Flexible Electronics

Application	**Required Properties**	**Common Hydrogels Systems**
Strain sensors	Stretchability, sensitivity	CNT/PAM hydrogels
Electronic skin	Self-healing, softness	Supramolecular hydrogels
Supercapacitors	Ionic conductivity	PVA-based conductive gels
Bioelectronics	Biocompatibility	GelMA and HA hydrogels

1.14.3 Conductive Tough Hydrogels and Conductivity Mechanisms

Conductive hydrogels, due to their mechanical flexibility and electrically conductive nature[141], have attracted attention. The conductivity may be ionic, electronic, or via hybrid conductive pathways. Ionic conductivity hydrogels contain dissolved salts, ionic liquids, and acids inside their matrix to facilitate the migration of ions. Electronically conductive hydrogels have incorporated conductive fillers like carbon nanotubes (CNTs), MXenes, intrinsically conductive polymers, and metallic nanoparticles into the matrix[142]. CNTs are generally used as nanomaterials for conductivity enhancement due to their

high electrical conductivity, superior mechanical strength and higher aspect ratio. The preparation of a uniform CNT dispersion with a polymer matrix is a challenging task as they have strong van der Waals interactions and phase aggregation tendency[143]. Techniques such as polymer-assisted dispersion and surface modification helped to overcome these problems.

Hydrogels based on Graphene and MXene materials have excellent electrochemical properties useful for flexible electronic devices and sensing applications[144]. To enhance the electronic conductivity and electrochemical performance[145], several conductive polymers are being used. However, their excessive loading can affect the flexibility and mechanical strength of the hydrogel system[146]. Therefore, to synthesise a hydrogel system with balanced mechanical and electrochemical performance is a challenge for the scientific community.

Table 1.9 : Comparison of Conductive Fillers in Tough Hydrogels

Conductive Fillers	**Conductivity Mechanics**	**Advantages**	**Limitations**
CNTs	Electronic conduction	High conductivity and flexibility	Dispersion difficulty
Graphene	Percolation network	Excellent mechanical strength	Aggregation tendency
MXenes	Metallic conductivity	High capacitance	Oxidation sensitivity
Conductive Polymers	Intrinsic conductivity	Good processability	Brittleness

1.14. 4 Tough Hydrogel Optimisation Strategies

Several strategies are being explored to improve the performance of hydrogels for flexible electronic devices. Nanocomposite reinforcement with graphene, cellulose nanofillers, MXenes, nanoclays, and

CNTs has been used to improve the structural stability[147], mechanical strength, and conductivity of the materials. Use of dynamic covalent and supramolecular interactions to fabricate a self-healing hydrogel has also been explored[148]. The hydrogels with hydrogen bond interaction have significantly higher toughness and energy dissipation in their matrix[149]. Other approaches include the dual crosslinking have both chemical and physical interactions, resulting in an effective enhancement of the hydrogel's elasticity, toughness and structural stability[150]. Solvent engineering and cryogelation are a few other strategies to improve the water retention, anti-freezing ability and environmental stability[151]. Recent development of deep eutectic solvents (DES) based hydrogels is a promising material for flexible electronic devices with their excellent ionic conductivity, anti-freezing nature, lower volatility and eco-friendly nature[152]. Such hydrogels have better electrochemical performance and moisture retention than other water-based systems[153]. Hence, these multifunctional hydrogels have been explored for future generation flexible electronics and interfacial bioelectronic device fabrication.

Materials & Methods

CHAPTER-II

2.1 Experimental Section

This section includes the experimental part related to the synthesis of tough hydrogels using different monomer or polymer units along with crosslinkers and photo/thermal initiators. After the synthesis of these hydrogels, their application were studied in the field of energy storage devices fabrication based on their mechanical and electrochemical properties. All the chemicals utilised for synthesis, and the techniques used to characterise the synthesis of hydrogels, have also been briefly described.

2.1.1. Chemicals

All the chemicals used for the synthesis of materials are of laboratory reagent grade and used without further purification.

Poly(sodium 4-styrenesulfonate) (PSS), average Mw~ 70 000g/mol (Sigma-Aldrich), 3,4-ethylene dioxythiophene (EDOT) (Sigma-Aldrich), potassium persulfate (KPS) (Sigma-Aldrich~ 99%), triflic acid (Thermo fisher Scientific India Pvt. Ltd.), hydrazine hydrate (Ranchem, 99%), methyl acrylate (SD Fine Chemicals 99%), Tetrabutylammonium bromide (TBAB) (SD Fine Chemicals), and tetrahydrofuran (Finar Ltd. (99%) were utilized as purchased unless specified. PAHz (Intrinsic viscosity ~ 0.27 dL/g) was synthesised. Acrylamidomethyl propane sulfonic acid (AMPS, Sigma-Aldrich,99%), Acrylamide (Sisco Research Lab. Pvt., 99%), Acrylic acid (AA, Thermo-fisher Scientific India Pvt. Ltd.), PEGDA (Avg. Mn= 250, Sigma-Aldrich, 99%), oxoglutaric acid (Sigma-Aldrich,99%), Isopropyl alcohol (IPA, Rankem, 99%), ethanol (EtOH, C.H. Fine Chemical, 99.9%), Tetrahydrofuran (THF, Finar, 99.0%), rice straw, ferrocene, methanol (MeOH, SD Fine Chem., 99.0%) as received. (Sisco Research Lab. Pvt., 99%), CNT. Milipore ELGA water purifiers were used to obtain DI water.

2.1.2. PEDOT-PSS-PAHT (PDTPS-PAHT-n) Ink synthesis

a) PEDOT: PSS Dispersion Preparation

A dispersion of PEDOT: PSS was prepared by mixing 0.027 mol (3.9 g) EDOT with 3.1 g of PSSNa powder in 10 ml DI water for 15 min at 25 ℃. To the solution, 0.65 g of KPS was added, and the solution was stirred for 2 h at 60 °C on a hot plate cum stirrer. A dispersion of dark blue colour was obtained.

b) PEDOT-PSS-PAHT (PDTPS-PAHT-n) Ink Preparation

A representative synthesis of PDTPS-PAHT-1.0 is described as follows: 3 ml of 30 wt% PAHz was mixed with 0.0013 mol (0.195 g) of triflic acid, and the mixture was stirred in a vortex mixture for 5 min. The viscous solution of PAHT was then added to 7 ml of PEDOT: PSS dispersion under continuous stirring on a hot plate cum stirrer at 60 °C. After 1 h of mixing, a viscous mass was obtained. The above mass was utilised as the conductive ink to fabricate different shapes via printing, drop-casting and spin coating procedures.

c) Synthesis of Thin Films

To create a thin, Consistent layer, the PDTPS-PAHT-n conducting ink was drop cast on a Teflon surface and allowed to air dry for the whole night.

2.1.3. Synthesis of PAMSAAm-IP-n based hydrogel

Hydrogel samples were synthesised in a one-pot procedure. For synthesis of a typical hydrogel PAMSAAm-IP0.1, 0.45 g AMPS, 0.45 g AAm, 2 μL PEGDA were mixed in a glass vial containing 1.5 mL of solvent (H_2O: IPA 90:10 v/v). Then 1 mol% of oxoglutaric acid was added and the resulting solution was purged with N_2 for 10 min. Then the solution was syringed out and injected

into glass molds, and the gelation was carried out under UV light (365 nm) for 5 h. Similarly, various PAMSAAm-IP-n samples were synthesised by varying monomer content, crosslinker and solvents. A total of 75 samples were prepared, and the formulation data along with their mechanical properties were utilised to train and test the machine learning model.

2.1.4. Synthesis of PAAm-CNH hydrogel

a) Synthesis Procedure of Carbon Nanotube: For the synthesis of CNT material, 2.5 g extracted lignin (from rice straw) and 0.5 g of ferrocene were dissolved in 150 mL of ethanol and stirred magnetically for 2 h. Then, the mixture was sonicated for 90 min and subsequently transferred into a 250 mL Teflon-lined autoclave tube inside a stainless steel reactor, then heated in an electrical muffle at 180 °C for 120 min. A pale yellow powder of the pretreated lignin mixture was obtained. The obtained solid was carbonised for 6 hours at 600°C under an inert gas atmosphere. The carbonised material was then dried in a vacuum oven at 100 °C. This CNT material was then used for further synthesis and characterisation procedures[154].

b) Synthesis of CNT Solution: For the preparation of CNT, we took the pre-characterised CNT particle in a 10 mL mixture of DI water and DMF (9:1) (vol: vol) and mixed it via stirring at 1000rpm on a mechanical stirrer for 1 hr. A uniform solution of CNT in H_2O: DMF was obtained. We vary the CNT amount according to our requirement, including 0.5wt%, 1wt% and 2wt%, respectively.

c) Synthesis of Hydrogel: A one-pot synthetic method was used to synthesise the hydrogel using a photoinitiator. The precursor solution of hydrogel was prepared by mixing the AAm (0.45g), AMPS (0.45g) monomers, PEGDA (2µL), Oxoglutaric acid (initiator) (130µL) in 1.5ml of CNT solution. Poured the above form precursor solution in a glass mold and put it under UV light for 5

hrs for gelation. The obtained hydrogel film was used for further mechanical testing and other characterisation processes.

2.2 Methods used for Mechanical Study

2.2.1 Universal tensile machine (UTM): Mechanical test and adhesive test of hydrogel samples were performed by using Tinius Olsen H5KL universal tensile machine (UTM) at 10mm/min machine speed. Sample dimensions were ($15x8x1mm^3$). Young's modulus E values were derived from the Hookean slope. It has a Force Capacity - 25KN, having a Minimum Test Speed – 0.001mm/min.

Figure 2.2.1: Schematic diagram of the Universal tensile machine for mechanical performance testing

2.2.2 Dynamic Mechanical Analyser (DMA): It is used to measure a material's viscoelastic properties (stiffness, damping) by applying oscillating forces and analysing its response, revealing changes with temperature, time, and frequency, crucial for understanding polymers, composites.

Dynamic Magnetic Analyser: Frequency sweep data of PDTPS-PAHT-n were recorded by a DMA Q800 TA Instruments.

Figure 2.2.2: Schematic diagram of the Dynamic Mechanical Analyser for testing the strength of the hydrogel

2.2.3 Thermal Gravimetric Analyser (TGA): TGA was used to determine the thermal stability of hydrogel samples. TGA model Linseis STA 1100 has been employed to determine the difference in the weight of the polymer in the thermal working condition in the presence of airflow/N_2 100 ml/min. The TGA data were recorded on an instrument at a heating rate of 10°C/min.

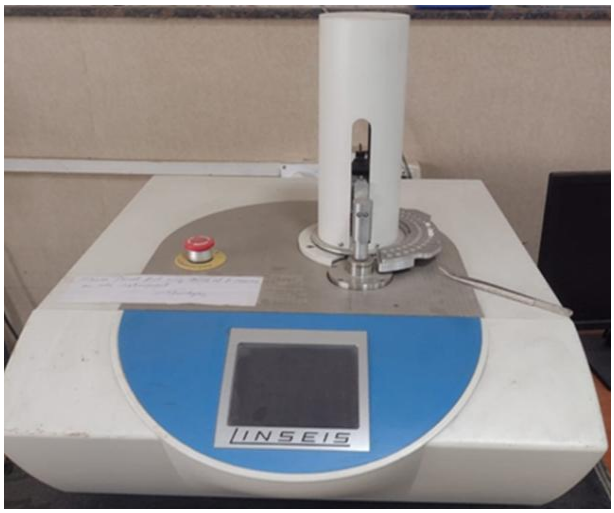

Figure 2.2.3: Schematic diagram of the Thermal Gravimetric Analyser to test the thermal stability of the hydrogel

2.2.4 Rheometer: The viscosity versus shear rate of the conductive ink was recorded on a Modular Compact Rheometer MCR302e under room-temperature conditions using parallel plate geometry. For testing the viscosity, 2 g of PDTPS-PAHT-n conducting inks was dropped over the platform of a rheometer, and the viscosity versus shear rate plots were extracted under room-temperature conditions.

Figure 2.2.4: Schematic diagram of the Rheometer instrument for viscosity analysis of conductive ink.

2.2.5 Lyophiliser: It was used primarily to remove water from sensitive hydrogel materials, extending shelf life, preserving structure, and making products lightweight for transport, by freezing them and then sublimating the ice under vacuum. Also, freeze-drying of a hydrogel sample in an equilibrium state was performed by using a lyophiliser.

Figure 2.2.5: Schematic diagram of a Lyophiliser for freeze-drying the hydrogel

2.3 Physicochemical Characterisation Technique Used:

The synthesised hydrogels have been thoroughly characterised by using different analytical techniques as mentioned below.

2.3.1 X-Ray Powder Diffraction (XRD): X-ray diffraction (D8 Advance,Malvern Panalytical's instrument) with CuKα radiation ($\boldsymbol{\lambda}$= 1.5418 Å) was used to characterise the crystal phases of hydrogel samples. The accelerating voltage and applied currents were 40kV and 30mA, respectively. The diffraction data at angle $2\boldsymbol{\theta}$ from 5^{o} to 60^{o} were collected at a step size of 0.02^{o} accumulating data for 60 sec per step. XRD is a useful technique to identify the crystal phases that exist in a sample. Freeze-dried hydrogel samples were put on the XRD stand, then analysed.

Figure 2.3.1: Schematic diagram of X-ray Powder Diffraction instrument to check crystallinity of hydrogel.

2.3.2 Small-Angle X-ray Diffraction Spectroscopy (SAXS): Small-angle X-ray spectroscopic images were recorded by a XENOCS, Xuess 3.0 HR instrument at SD 1000mm for an exposure time of 1h under uniaxial stretching mode. It was a non-destructive analytical technique that probes the structure, shape, and size (nanometer to micron scale) of polymeric materials in solution by measuring X-ray diffraction at very small angles, revealing large-scale features like shapes, internal structures (pores, domains). The SAXS plots were derived under environment mode to maintain an adequate water content in the samples. The as-synthesised hydrogel sheet was mounted on a tensile stage (Modular force stage, Linkam) and kept in the sample chamber of a SAXS instrument. Acquisitions were taken for 1 h at different stretches of the samples controlled by the programmed macro at a sample to detector distance of 1.5 m.

Figure 2.3.2: Schematic diagram of the Small-angle X-ray Spectroscopy instrument for insight study of the hydrogel matrix

2.3.3 X-ray Photoelectron Spectrometer: it was used to identify the surface to the subsurface composition of the hydrogel present on the surface. It enables an evaluation of all the possible chemical states of any element present on the surface to the subsurface of a polymer. it was used to identify the surface-to-subsurface composition of the hydrogel present on a surface. It enables an evaluation of all the possible chemical states of any element present on the surface to the subsurface of a polymer. The XPS analysis was conducted in an ultra-high vacuum (UHV) set-up with a monochromatic AlKα X-ray source (h = 1486.6eV), working at 14.5kV and 35mA, and a high-resolution gamma Thermo Fisher Scientific Model: Nexsa base Inc. The pressure in the chamber was retained at about 7 x 10^{-10} mbar. The measurements were conducted in the fixed transmission mode with a fixed energy of 200 eV, resulting in an improved energy resolution of 0.25 eV. The charging effect was minimised by the flood gum. The binding energy scales were standardised by the sp^2 hybridised C1S line of graphitic carbon at 284.8 eV. For XPS depth analysis, the sample surface was etched with argon ions for 30 s, and then data was collected after

multiple rounds of etching from the surface to the bulk. Avantage 5.922 software was used for XPS mapping and data analysis.

Figure 2.3.3: Schematic diagram of X-ray Photoelectron Spectrometer for elemental analysis of hydrogel

2.3.4 Field emission Scanning electron microscopy(FE-SEM): It was a very powerful technique for the morphological study of polymer samples. Scanning electron microscopy images were taken on FEI Quanta 200F utilising a tungsten filament fixed with lanthanum hexaboride (LaB6) as an X-ray source equipped with an ETD (Everhart-Thornley detector). Scanning electron microscopic images of gold-coated dried hydrogel films were recorded in JEOL (JSM 7900).JSM-7900F (Jeol Ltd.) equipped with an energy dispersive X-ray spectroscope (EDAX) was used to record the FESEM images and elemental mapping of the freeze-dried, synthesised and swelled hydrogel samples, and images were recorded. The EDS elemental mapping in SEM was performed along a line scan, and subsequently, the elemental intensity data were plotted.

Figure 2.3.4: Schematic diagram of FE-SEM instrument for morphological study of hydrogel surface

2.3.5 Atomic force microscopy (AFM): It is a very-high-resolution type of scanning probe microscopy. The AFM data of a dried spin-coated film was recorded by AFM Bruker Fastscan. The tip details for the AFM study are as follows: Si tip with a cantilever-T-650 nm.The Atomic force microscopic (AFM) data of freeze-dried hydrogel films were recorded by AFM Bruker Fastscan using a Si-tip with a cantilever T:650nm. For confocal Raman mapping and spectra JASCO NRS-5500 instrument was used.

Figure 2.3.5: Schematic diagram of AFM instrument for phase study of hydrogel surface

2.3.6 Fourier transform infrared spectroscopy (FTIR): FTIR spectroscopy is one of the powerful analytical tools for compound identification and functional group analysis using PerkinElmer Spectrum. It is based on the principle that a molecule can exist in a variety of vibrational and rotational levels depending upon the release or absorption of energies in a particular range of the electromagnetic spectrum. This characteristic adsorption and emission form the basis of IR spectroscopy. The normal range of the infrared spectrum employed is between 4000 cm^{-1} to 400 cm^{-1}. The range from 4000 to 1200 cm^{-1} is generally considered the functional group region was corresponding to specific adsorption or emission bands of the various functional groups. Frequencies below 1200 cm^{-1} are considered characteristic of the fingerprint region and are important in identifying the complete structure of a pure compound. The advantage of FTIR lies in its versatility in that the analysis can be carried out in any state of matter. However, compounds in which there is no change of dipole moment in any mode of vibration are IR inactive as selection rules for emission/absorption of IR radiation mandate that there should be a shift in dipole moment between the states during emission of absorption. Further, predominantly ionic compounds are also IR inactive. The FTIR spectra of synthesized samples were collected using a Nicolet 8700 research spectrometer at a resolution of 4 cm^{-1}. The solid samples were pelletized with KBr in order to take the FTIR scans. FTIR bands were analysed in a Nicolet 8700 FT-IR spectrometer, along with beam slitter XT-KBr and utilizing a DTGS TEC detector in the region of 4000-400 cm^{-1}. The operating conditions were as follows: 2 cm^{-1} spectral resolution and 36 kHz scan speed.It was used to record the FTIR data of different hydrogel films.

Figure 2.3.6: Schematic diagram of a Fourier Transform Infra-red spectrometer for functional group analysis

2.3.7 Confocal Raman Spectrometer: It was merges a Raman spectrometer with an optical microscope, using a pinhole (confocal setup) to filter out-of-focus light, enabling high-resolution 2D/3D chemical imaging and analysis of hydrogel sample volumes with exceptional depth selectivity, identifying molecular structures, compositions, and distributions non-destructively.Raman spectra of conductive films were recorded on a JASCO NRS-5500 instrument using laser beams of 785nm and 532nm, and 20X resolution was used to capture all the spectra and images of hydrogel samples. Freshly prepared hydrogel were attached over glass slide and Raman spectra at 532 nm laser beam, 20X resolution,10 accumulation, using JASCO NRS-5500 instrument were recorded.

Figure 2.3.7: Schematic diagram of a Confocal Raman Spectrometer for surface analysis

2.3.8 Microscope: Self-healing images of hydrogel samples were recorded on a Mag Cam DC series microscope. Self-healing involves repairing of cut or damaged region via several reversible interactions like ionic interactions, hydrogen bonding, host-guest interaction, physical chain entanglement, or dynamic covalent bonds. To observe the mechanics behind the healing, MagCam microscopes were used with high-resolution optical magnification cameras due to its ability to capture the self-healing process in real time.

A sharp cut was made in the hydrogel and placed gently in contact with a glass slide. A transmitted light of 50x-200x is ideal for observing the healing interface.

Figure 2.3.8: Schematic diagram of a Microscope for insight image capturing

2.3.9 UV-Vis spectroscopy: Agilent Technologies, Carry 5000 with DRS 2500 was used to record the UV-visible spectroscopic data of diluted commercial PEDOT: PSS dispersion and synthesised PEDOT: PSS dispersion. It is a powerful analytical technique to study light absorption by hydrogels, concentration of solutes, and optical property analysis in dispersions. It also monitors the conversion of photoinitiator during curing and explains the interaction of these hydrogels with dyes and incorporated nanoparticles. For dispersion analysis, UV-Vis becomes a quantitative tool to measure the concentration of particles. To perform UV-Vis of the hydrogel film, the hydrogel was placed in a solid sample holder and scanned across the 200-800nm range to record its absorption or transmission spectrum.

Figure 2.3.9: Schematic diagram of a UV-Vis spectrometer to check the transparency of the hydrogel

2.4 Electrochemical Study:

The electrochemical study was performed using an Autolab Electrochemical workstation (M204 PGSTAT).

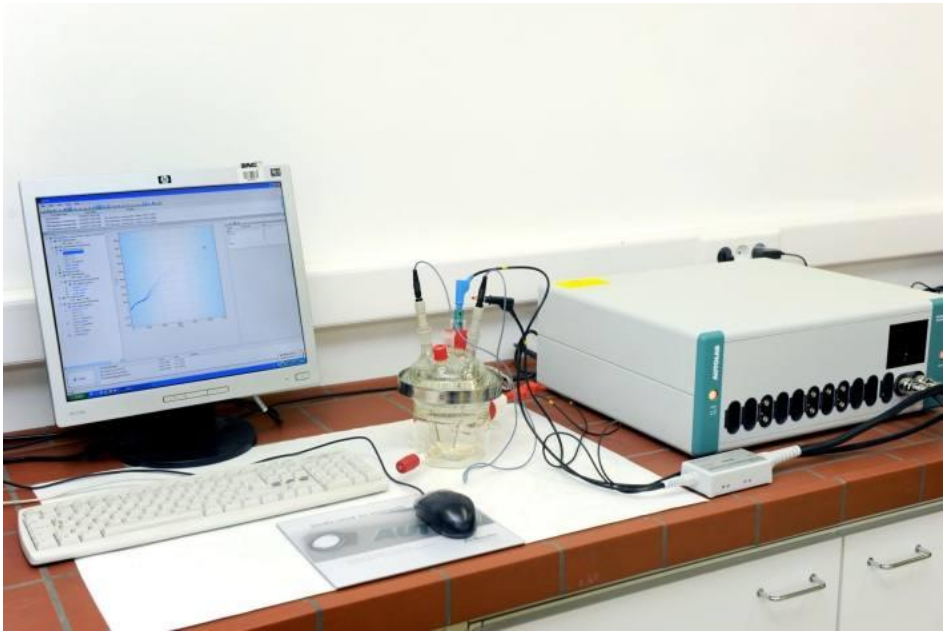

Figure 2.4.1: Schematic diagram of Autolab potentiostat for electrochemical study of hydrogel

Electrochemical characterisation is a method for analysing electrical, ionic and redox behaviour of hydrogel, understanding their ability to be used in flexible electronics, sensors, solid-state

electrolytes, and energy storage devices. Techniques such as electrochemical impedance spectroscopy (EIS), linear sweep voltammetry (LSV), Cyclic voltammetry (CV) and chronoamperometry, the conductivity and electrochemical behaviour of hydrogel can be studied. The Autolab instrument PGSTAT M204 workstation is an essential tool for studying the electrochemical performances of hydrogels. Through a combination of above above-discussed techniques, researchers are able to get a detailed insight into the hydrogels' ionic behaviour, redox nature, and electrochemical stability. These detailed characterisations focus on the hydrogel formulations and explain their practical application in advanced energy storage and conversion techniques.

Polyelectrolyte Complexation Approach to Devise PEDOT: PSS-Based Printable, Self-Healable and Ultra-Stretchable Solid Electrolytes for Under-Water Electronics

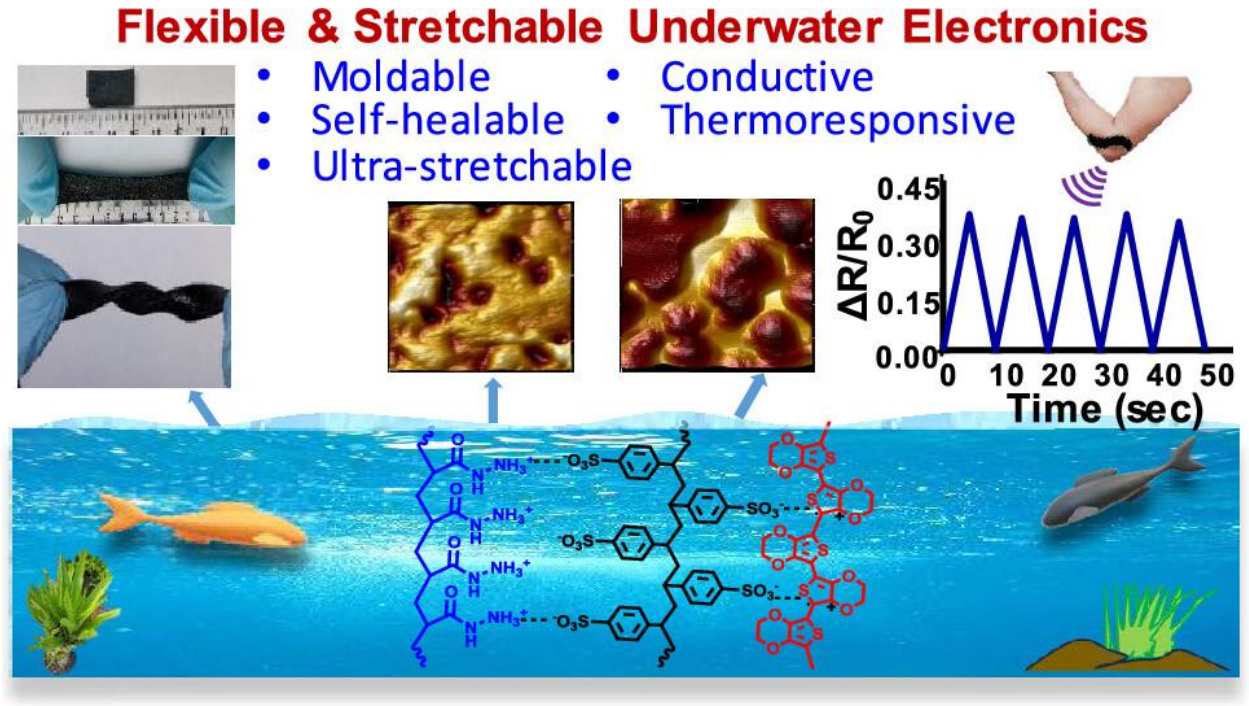

CHAPTER-III

3.1 Summary

PEDOT: PSS-based systems possessing effective opto-electronic behavior are promising for metal particle free flexible electronics applications. However, these systems currently suffer from low stretchability, mechanical resilience and performance in aqueous media. In this article, polyelectrolyte complexation between polyacryloyl hydrazide triflate (PAHT) and polystyrene sulfonate (PSS) is utilized to devise conducting ink with tunable viscosity at high PEDOT loading for printing stretchable, self-healable and conductive solid electrolytes for flexible electronics applications. The possible ionic linkages ($CONHNH_3^+$---SO_3^- and SO_3^----CS^+) between the polymeric segments enabled film integrity in various organic and aqueous media and imparted effective tensile strength (0.14 MPa) & stretchability (~1120%), while maintaining effective ionic conductivity (18 S/m). The film displayed an effective $\Delta R/R_0$ value of ~26.2 at 600% stretching. As a proof of concept, the ability of these solid electrolytes towards strain sensing application was studied. The system was able to display repeatable change in $\Delta R/R_0$ values in response to various bodily movement under submersible conditions and an adequate Gauge factor value of 4.4 and 0.20 under environmental and under-water conditions supporting its viability towards strain sensing applications.

3.2 Introduction

Currently, a notable attention is imparted to the development of flexible and stretchable electronic devices as a possible substitute to the conventional rigid electronics systems especially for applications in the area of bioelectronics,[155] wearable and health monitoring devices.[156,157] Especially to print these flexible electronics utilizing conductive inks have gained popularity owing to the ease of complex shape attainability, low fabrication cost and sustainability.[158] The

conductivity, viscosity and surface tension of the conductive inks and the tensile behavior of the resulting printed device are some of the determining factors towards further utilization of the formulation. Metallic nanostructures owing to their high conductivity (~10^7 S/m) are widely utilized as conducting fillers in the ink nanocomposites currently. For example, densely loaded Ag nanoparticles in polycaprolactone and BC-Lipase matrix displayed superior conductivity value of 2.1 x 10^4 S/m and stretchability till 80%.[159] Similarly, recyclable polymer, multiple metal microparticles and liquid metal based composition was digitally printed and laser patterned to form stretchable and self-healable films for sensing applications.[160] However, metallic particles are known to form oxidative layer on the surface with exposure to environment under specific conditions, that compromises the conductivity and propensity of these systems towards agglomeration along with adverse toxicity.[161] Furthermore, a flexible matrix such as polydimethylsiloxane (PDMS) or Ecoflex is utilized in certain cases to impart adequate elasticity to the sample.[162]

Therefore, the development of metal nanoparticle free conductive inks possesses certain advantages from the prospective of superior stability, ease of synthesis and low sintering temperature. For example, single walled carbon nanotubes (SWCNT), carbon nanofibers, graphene sheets are utilized as conducting fillers owing to their high conductivity and large surface area for fabrication of flexible electronics.[163] Use of conducting polymers offers another exciting avenue to develop conductive ink compositions offering adequate conductivity. For example, aqueous dispersion of polyethylenedioxy thiophene (PEDOT): polystyrene sulfonate (PSS) displaying adequate conductivity and transparency is a suitable candidate to be utilized as a conducting matrix.[164] However, the films generated from the PEDOT:PSS dispersion tend to exhibit low stretchability owing to the rigidity of the backbone of the PEDOT segment. To

circumvent the above, PEDOT:PSS based hydrogel systems were developed those offered flexibility, healability and injectability.[165] Composites of the PEDOT:PSS based system with various hydrogels enabled the films to be stretchable, a property desirable for these systems to be utilized for strain sensing applications.[166] Similarly, blending of PEDOT:PSS with waterborne polyurethane improved the elongation at break from ~5 to 33% with a conductivity value of 77 S/cm.[167] However, the stretchability of such PEDOT:PSS based composite systems have remained below 300% in most of the cases to the best of our knowledge.[168,169]

Ability of these flexible electronics films to recover from damage and self-heal under autonomous conditions is anticipated to further promote their self-life and usability. Therefore, avenues to induce self-healing ability in flexible electronics systems is another important aspect studied currently.[170,171] For example, dynamic linkages, hydrogen bonded motifs,[172] coordination bond[173] and inclusion chemistry present in the polymeric matrix have been utilized to impart self-healing ability to the wearable electronics system.[174] For example, metal-ligand coordination was utilized as the dynamic linkage to induce autonomous self-healing ability to the semi-conducting film.[175] The percolation threshold was controlled in the bled to optimize gauze factor value of electronic skin. Ionic interaction is promising to induce autonomous self-healing behavior in these reconfigurable electronics systems due to their swift dynamic behavior.[176] For example, an ion cluster driven system displayed ultrafast self-healing kinetics along with high stretchability up to 1130%.[177] Similarly, a carboxylate anion and metal ion interaction based self-healable and stretchable hydrogel system displayed adequate adhesive behavior and high gauge factor value up to 12.2 and elongation till 1400%.[178]

Overall, the role of PEDOT:PSS as a conducting matrix for development of wearable sensors is well articulated in literature.[179,180] The challenge remains to formulate a suitable

conductive ink that can be utilized for ambient condition 3D printing application to fabricate ultra-stretchable films. Furthermore, uniform dispersibility of PEDOT component throughout the film along with adequate stretchability is desirable to utilize the same for strain sensing application. Most of the reported composite systems use the confinement of PEDOT:PSS in the hydrogel matrix in a non-interactive manner, which affect the uniformity of the distribution of the above conducting segment and control for further optimization. Therefore, necessary strategies to formulate PEDOT-PSS based inks capable of printing stretchable films with possibility of further optimization in segment distribution and adequate mechanical properties is desirable for utilization of the same for flexible electronics applications. PSS segment in the dispersion offers the possibility of utilizing polyelectrolyte complexation in the system with a suitable polycation to formulate conducting systems with desirable mechanical behavior and flexibility. Importantly, the salt content in these polyelectrolyte complexes may be controlled to alter the physical state to fluid or solid.[181] This allows the flexibility to optimize the viscosity of the resulting ink necessary for printing applications.

In this report, we have utilized polyacryloyl hydrazide triflate (PAHT) as a polycation to form the polyelectrolyte complex with PSS segment in PEDOT:PSS. Triflate is utilized as the salt content to control the viscosity of the resulting PEDOT:PSS-PAHT system and formulate a conductive ink for printing applications. The salt content is also useful in tailoring the ionic conductivity necessary for flexible electronics applications. The $–CONHNH_3^+$ functionality of PAHz is presumed to form the ionic linkage with the $–SO_3^-$ of the PSS segment and both PAHT and PSS segment are known to ionically coordinate with the PEDOT moiety, which has resulted in an interactive multipolymer ink.[182] The ink is utilized to fabricate different shapes to demonstrate its viability for the 3D printing application, which is important from the prospective

of device fabrication.[183,184] The interactive nature of the segments are anticipated to control the distribution of these segments in the matrix necessary for useful mechanical and electrochemical behavior. The phase distribution, tensile behavior and strain sensing ability of the resulting system is studied in detail. The strain sensing ability of the system is also assessed under environmental and under-water conditions to understand the viability of system for underwater electronics.

3.3 Synthesis of PEDOT-PSS-PAHT (PDTPS-PAHT-n) Ink:

The complete synthesis was included in Chapter 2, Section 2.1.2

3.4 Results & Discussion

The PEDOT: PSS aqueous dispersion was prepared from PSS and EDOT using the procedure reported in the literature.[185] The λ_{max} at 255 nm in the UV-Vis spectra supported the formation of a PEDOT: PSS dispersion (**Figure 3.1**).[186]

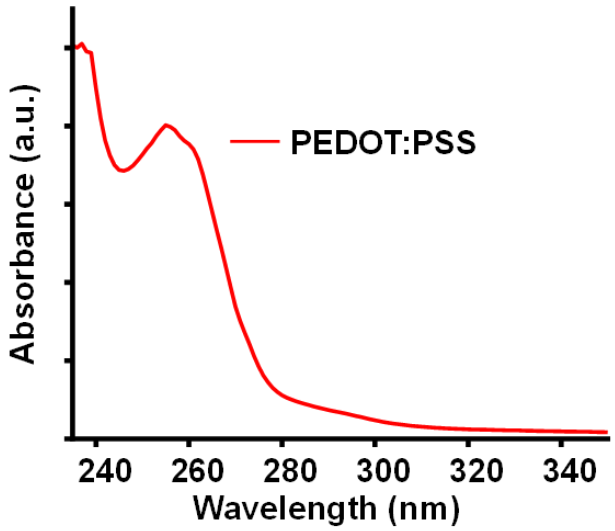

Figure 3.1: UV-Vis spectra of the synthesized PEDOT:PSS

The cyclic-voltametry (CV) traces displayed the oxidation and reduction peaks at 0.25 and -0.48 V, respectively, further supporting the PEDOT: PSS synthesis (**Figure 3.2**).[187]

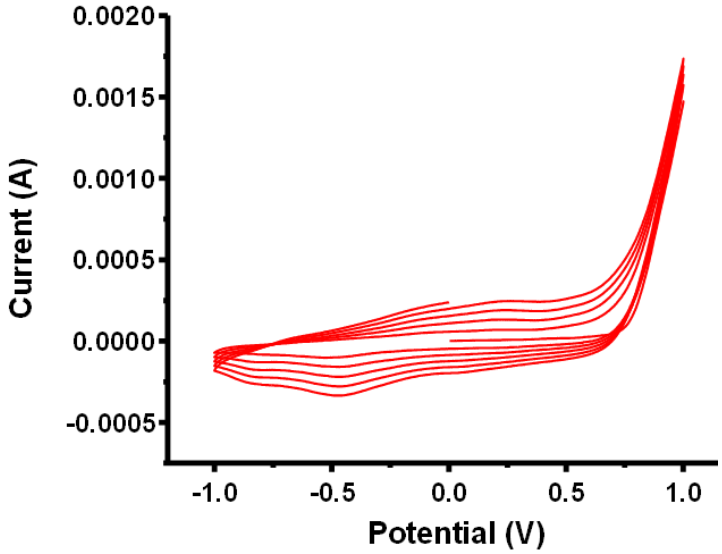

Figure 3.2: CV data of the synthesized PEDOT:PSS.

PAHz was ionized in aqueous solution using triflic acid to the corresponding PAHT. Generation of a positively charged –$CONHNH_3^+$ unit that will form dynamic ionic interactions with the –SO_3^- group of polystyrene (PSS) part of PEDOT: PSS. The triflate ($CF_3SO_3^-$) ion will improve the ionic conductivity, control the viscosity of ink, stabilise the dispersion and assist in the ink formation. Relative to the other conventional acids, the triflic acid has superior protonation ability, better ionic mobility, reversible ionic interactions responsible for self-healing ability, a high amount of non-coordinating triflate anions in the matrix and stable underwater performance. Other corresponding salts were not tested in the present work. But the choice of triflic acid was made due to its enhanced conductivity, better mechanical performance and processability. The PDTPS-PAHT-n were formulated by adding PAHT to the PEDOT: PSS dispersions and varying the molar ratio between PSS and PAHT in the ink (**Table 3.1**). The corresponding $CONHNH_3^+$---SO_3^- ionic linkages formed in the ink formulation aided the viscosity of the system (**Scheme 3.1**). The PEDOT chains

also formed corresponding ionic linkages with the PSS to constitute the overall PAHz-PEDOT-PSS network in which all the three different polymeric systems were ionically interlinked with each other.

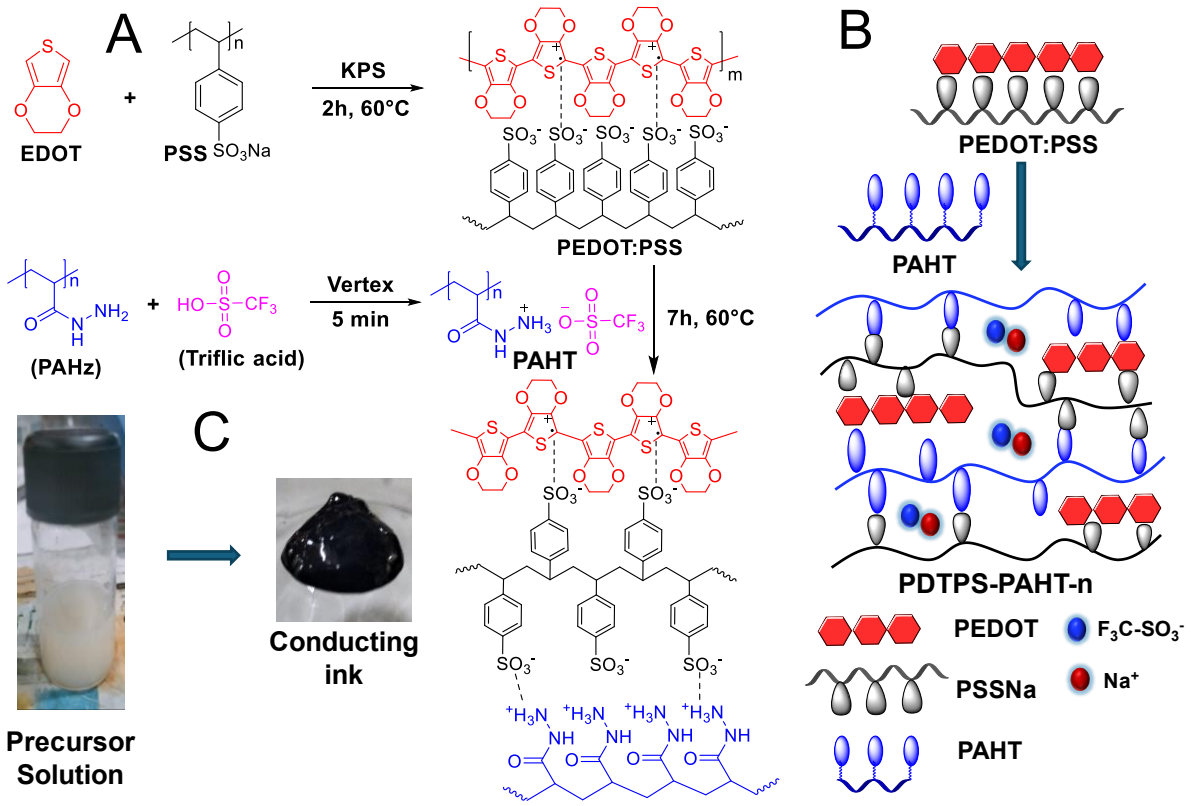

Scheme 3.1: The schematics showing the synthetic procedure of PDTPS-PAHT-n conductive ink and the possible ionic linkages present in the samples.

The FTIR band at 1174 cm^{-1} accountable to S=O of PSS shifted to ~1186 cm^{-1} in the PDTPS-PAHT-1.0 suggesting the possible formation of $CONHNH_3^+$---SO_3^- ionic linkage. Similarly, the band at 1036 cm^{-1} accountable to the C-S of PSS shifted to 1058 cm^{-1} supporting the above (**Figure 3.3A**). The FTIR data displayed bands at 1608 and 1639 cm^{-1} supporting the presence of PAHT and PEDOT components. Similarly, in Raman spectra the peak at 1441.5 cm^{-1} corresponding to C_α=C_β of PEDOT moiety in PEDOT-PSS shifted to 1415.2 cm^{-1} in the PDTPS-PAHT-1.0 film suggesting possible change in doping level via interaction with $CONHNH_2$ of

PAHT segment as reported in literature (**Figure 3.3B**).[188] The XRD data supported mainly the amorphous nature of the PDTPS-PAHT-n film. The broad peak at 24.4° 2θ value may be attributed to inter-chain π-stacking of aromatic moieties present in the system (**Figure 3.3C**).[189] The O 1s XPS peaks at 531.8 eV accountable to C=O moieties and N 1s peak at 400.4 eV supported the presence of PAHT segment on the surface (**Figure 3.3D-E**). Similarly, the S 2p peaks at 168.9 and 168.0 eV for the free (SO_3^-) and ionically coordinated ($-SO_3^-$---H_3N^+-) sulfate groups were observed on surface. The S 2p peaks at 163.8 and 165.6 eV accountable to C-S and C-S^+ supported the presence of PEDOT segment in the composition (**Figure 3.3F,**). Similarly, the C 1s spectra displayed peaks at 286.0 and 288.5 eV for the C-O and C=O supporting the presence of PAHT and PEDOT segments in the sample (**Figure 3.3G**). The swellability of a typical PDTPS-PAHT-1.0 film in water (74%) was maximum followed by ethanol (45%), whereas the swellability of the film in other organic solvents (~1-20%) were negligible (**Figure 3.3H**). The films were stretched up to ~5 times of it's original length and the initial shape was retrieved after release of the force (**Figure 3.3I1**). The film also underwent twisting, rolling, pressing and other deformations without undergoing any visible damage supporting mechanical resilience (**Figure 3.3I2-I4**).

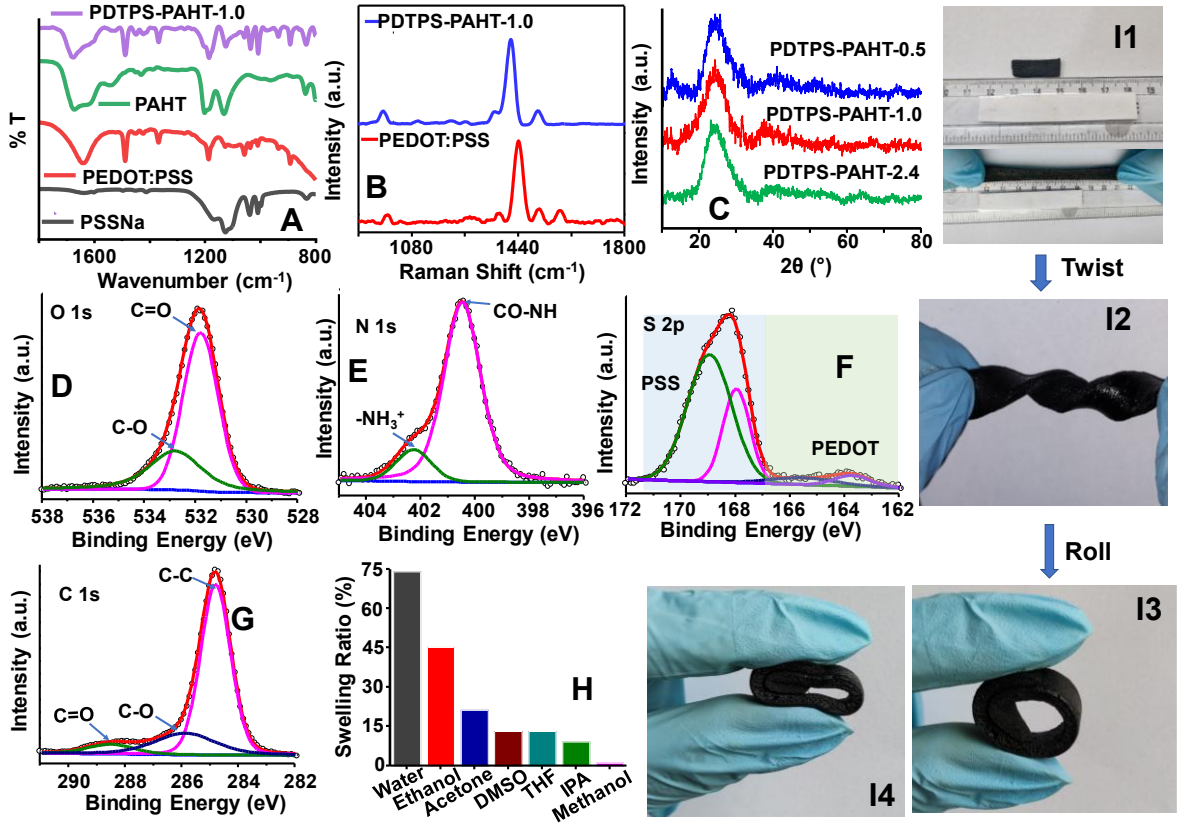

Figure 3.3: (A) The FTIR data of precursors and PDTPS-PAHT-1.0 films, (B) the Raman data of PEDOT:PSS and PDTPS-PAHT-1.0, (C) the XRD data of various PDTPS-PAHT-n compositions, (D) O 1s, (E) N 1s, (F) S 2p and (G) C 1s XPS traces of PDTPS-PAHT-1.0, (H) the solvent uptake ability of PDTPS-PAHT-1.0, demonstration of (I1) stretchability, (I2) twisting ability, (I3) rolling and (I4) foldability of the film and the folded film is pressed to show the mechanical resilience.

Table 3.1: Composition and mechanical property data of the PDTPS-PAHT-n compositions

Code	PSS (mol/l)*	PAHT (mol/l)*	PEDOT (mol/l)*	UTS$^{\Psi}$ (MPa)	ε (%)	*E* (MPa)	UCS$^{\chi}$ (MPa)
PDTPS-PAHT-2.4	0.7	1.7	1.4	0.14	343	0.42	0.83
PDTPS-PAHT-1.4	0.9	1.4	1.6	0.14	354	0.19	0.60
PDTPS-PAHT-1.0	1.0	1.0	1.9	0.10	1120	0.06	0.37

PDTPS-PAHT-0.5	1.2	0.7	2.2	0.12	507	0.12	0.73

*The molar ratios are with respect to the repeating unit, $^{\Psi}$UTS: Ultimate tensile strength, $^{\chi}$UCS: Ultimate compressive strength, ε denotes the elongation at break, *E* stands for Young's modulus.

The SAXS analysis of the PDTPS-PAHT-n thin films were carried out under tensile mode. The Guinier domain spacing (D) values were calculated using the following equation.[190]

$$D = 2\pi/q$$

The D value, which depicts the average distance between the aggregates, suggested that the amount of PAHT controlled the size and distribution of segregates in the film. The D value for PDTPS-PAHT-2.4 ($CONHNH_3^+:SO_3^-$ ≈ 2.4, mol:mol) was calculated to be 317.6 nm (**Figure 3.4A**). On gradually decreasing the $CONHNH_3^+:SO_3^-$ ratio, the D value exhibited an increasing trend. At $CONHNH_3^+:SO_3^-$ ≈ 0.5, the D value increased to 379.3 nm supporting the above. The broad peak in the Fourier-Porod region (q ≈ 0.005 to 0.05 $Å^{-1}$) also exhibited a gradual shift towards the lower q value suggesting a possible change in the shape of the segregates (**Figure 3.4A**). The AFM data reflected a similar trend in the morphology of PDTPS-PAHT-n. The AFM micrograph of PDTPS-PAHT-1.0 ([PAHT]/[PSS] ≈ 1.0) displayed the spherical soft domains possibly assigned to PAHT are well separated by the PEDOT:PSS hard domain (**Figure 3.4C-C1**). In PDTPS-PAHT-1.4 ([PAHT]/[PSS] ≈ 1.6), the population of soft segment increased and the spheres appeared to join together to form continuous layers (**Figure 3.4D-D1**). With further increase in PAHT content ([PAHT]/[PSS] ≈ 2.4), both the domain became continuous and formed a gyroid type segregation pattern in PDTPS-PAHT-2.4 (**Figure 3.4E-E1**). However, the surface appeared to be mostly covered by the hard segment domain at low PAHT content in PDTPS-PAHT-0.5 ([PAHT]/[PSS] ≈ 0.6) and no specific pattern was visible (**Figure 3.5**).

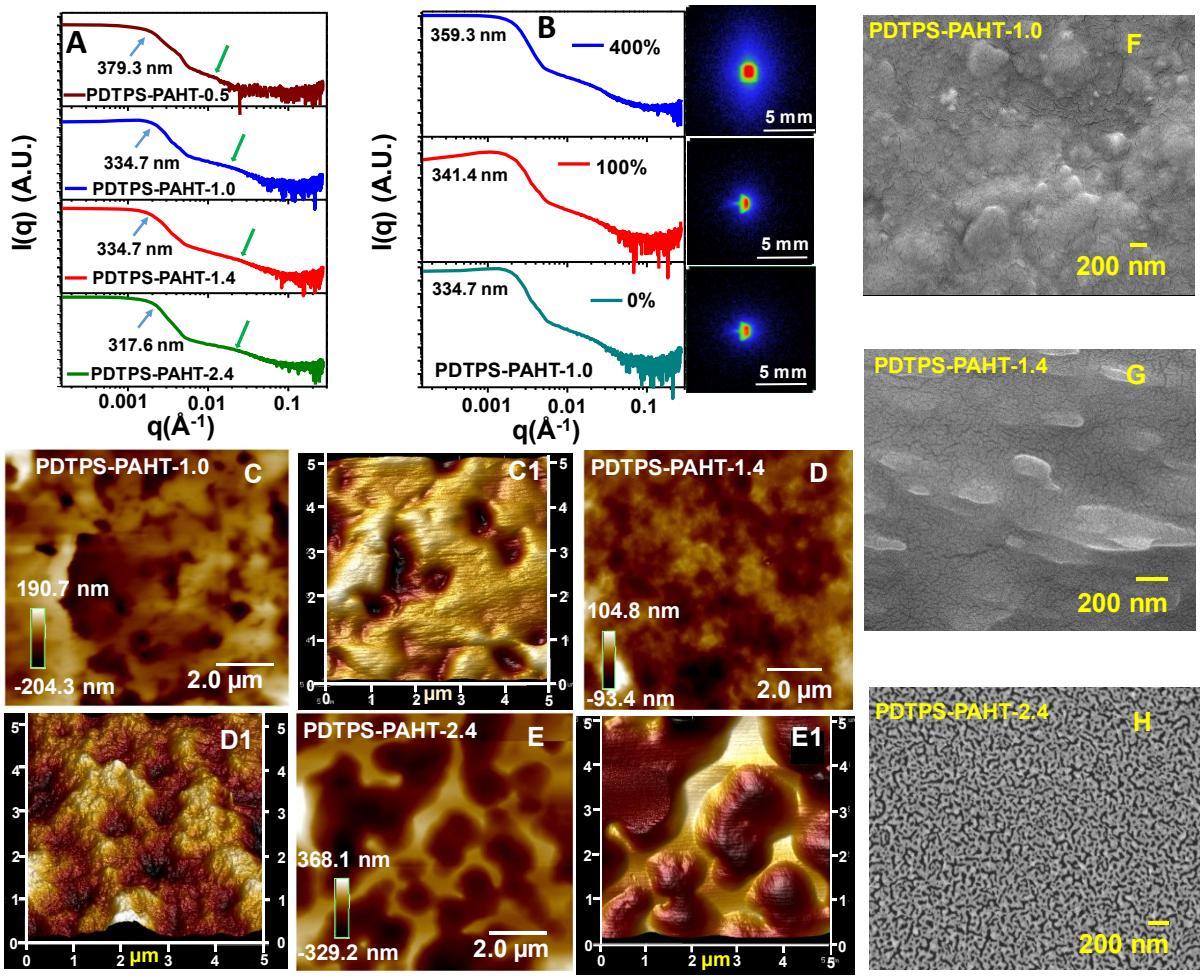

Figure 3.4: (A) The SAXS profile of PDTPS-PAHT-n films recorded under tensile mode, (B) the effect of stretching on the SAXS profile of PDTPS-PAHT-1.0, the AFM micrographs of (C & C1) PDTPS-PAHT-1.0, (D and D1) PDTPS-PAHT-1.4 and (E & E1) PDTPS-PAHT-2.4 at different magnification, the FESEM images of (F) PDTPS-PAHT-1.0, (G) PDTPS-PAHT-1.4 and (H) PDTPS-PAHT-2.4 films.

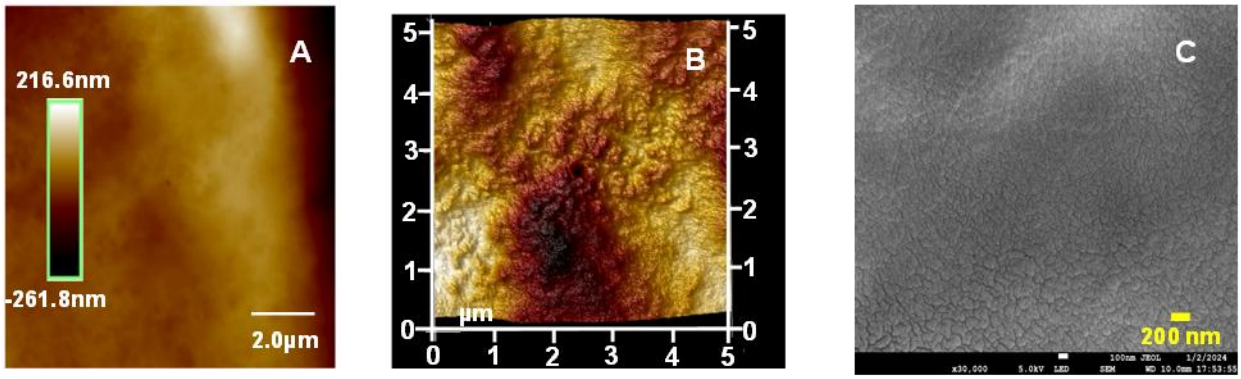

Figure 3.5: A, B) AFM and C) FE-SEM images of PDTPS-PAHT–0.5.

The SAXS data of the PDTPS-PAHT-1.0 was further collected at different stretching extent. The 100% stretched sample exhibited minor increase in D value (341.4 nm) suggesting no significant change in the distribution of segregates (**Figure 3.4B**). Interestingly, the value increase to 359.3 nm at 400% stretching suggesting a possible increase in the spacing between the segregates. Possibly, under stretching the uncoiling of soft segment domain contributed to the above increase in D value (**Figure 3.4B**). The SAXS 2D data also displayed a notable change in scattering profile to somewhat anisotropic nature supporting the above (**Figure 3.4B**). The FESEM data supported the segregation pattern observed from AFM data (**Figure 3.4F, G & H**). PDTPS-PAHT-1.0 displayed spherical domain on the surface of the film and flake like pattern with width between 100-200 nm was observed on the surface of PDTPS-PAHT-1.4 film (**Figure 3.4F-G**). Interestingly, the PDTPS-PAHT-2.4 film displayed fibrillar morphology supporting the SAXS and AFM observation (**Figure 3.4H**).

The as-synthesized PDTPS-PAHT-n films possessing water content value of 26-28% were utilized for mechanical property analysis (**Figure 3.6**).

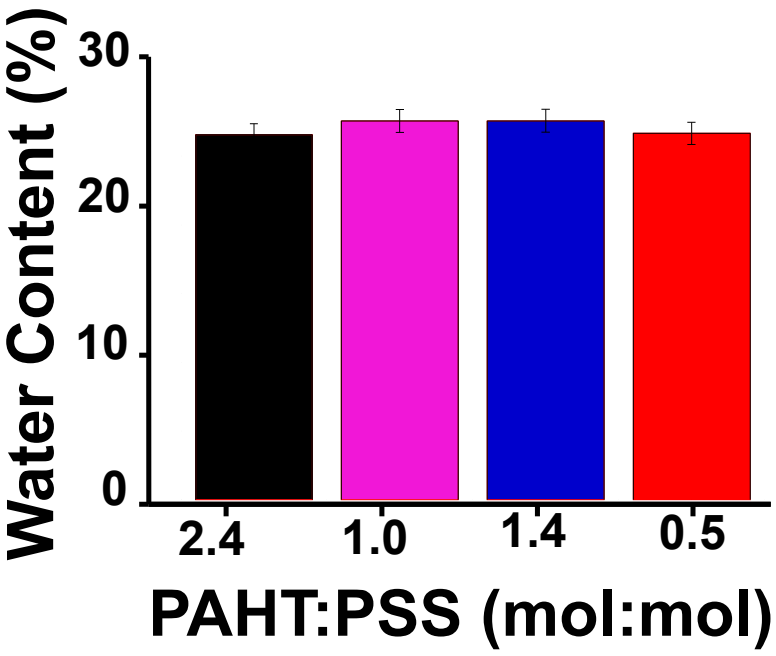

Figure 3.6: The water content in PDTPS-PAHT-n films repeated three times.

The tensile data of the PDTPS-PAHT-n uniform thin films were recorded under ambient conditions. The UTS and ε values were observed between 0.10 to 0.14 MPa and 343 to 1120% respectively (**Figure 3.7A, Table 3.1**). The PDTPS-PAHT-1.0 possessing equimolar ratio of PAHT and PSS segments displayed optimum ε value (1120%) possibly owing to the presence of the maximum number of $CONHNH_3^+$---SO_3^- ionic crosslinks in the system (**Table 3.1**, **Figure 3.7A**). Ionic linkage-based physical crosslinks are known to aid the extensibility of the hydrogel systems.[191] However, as the molar ratio between PAHT and PSS deviated from 1.0, the ε value notably decreased to 343-507% (**Table 3.1**). The stretchability of these samples are superior among the PEDOT: PSS systems reported in literature for strain sensing applications to the best of our knowledge (**Figure 3.7B, Table 3.2**).

Table 3.2: Table for the comparison of the Strain and Gauge factor values of the current material with the recent literature.

Sl. No.	Material Code	ε (%)*	GF	References
1	PEDOT:PSS@PVA	520	5.4	192
2	PEDOT:PSS/PVA	600	3.9	193
3	PEDOT:PSS/CNT	430	1.4	194
4	PVA-Mxene-PEDOT:PSS	890	2.5	195
5	Starch/NaCMC	180	2.71	196
6	PVA/PEDOT:PSS	180	0.41	197
7	VM-PS	990	3.46	198
8	$M_{20}S_{12}$PPH	890	4.21	199
9	**PDTPS-PAHT-1.0**	**1120**	**4.4**	**This Work**
*Maximum strain of the samples				

The samples also exhibited adequate compressibility up to 90% of the original height. The UCS values were observed in the range of 0.4 to 0.8 MPa (**Figures 3.7D , Table 3.1**). The PAHT:PSS ratio controlled the tensile behavior and the *E* value decreased with the decrease in PAHT content in the samples (**Figure 3.7C, Table 3.1**). However, the change in UTS values was marginal throughout the compositions (**Figure 3.7A & 3.7C**). The hysteresis studies were performed under both tensile and compression mode to understand the mechanical resilience of the PDTPS-PAHT-n films. The PDTPS-PAHT-1.0 displayed residual strain value of ~20% after the first cycle during tensile hysteresis studies. Importantly, the residual strain notably decreased below ~5% from second cycle onwards suggesting adequate recovery of the sample after release of stress. (**Figure 3.7E**). The relatively large residual strain at the end of the first cycle may be attributed to the memory associated with the film preparation procedure and is a known phenomenon with crosslinked samples.[200]

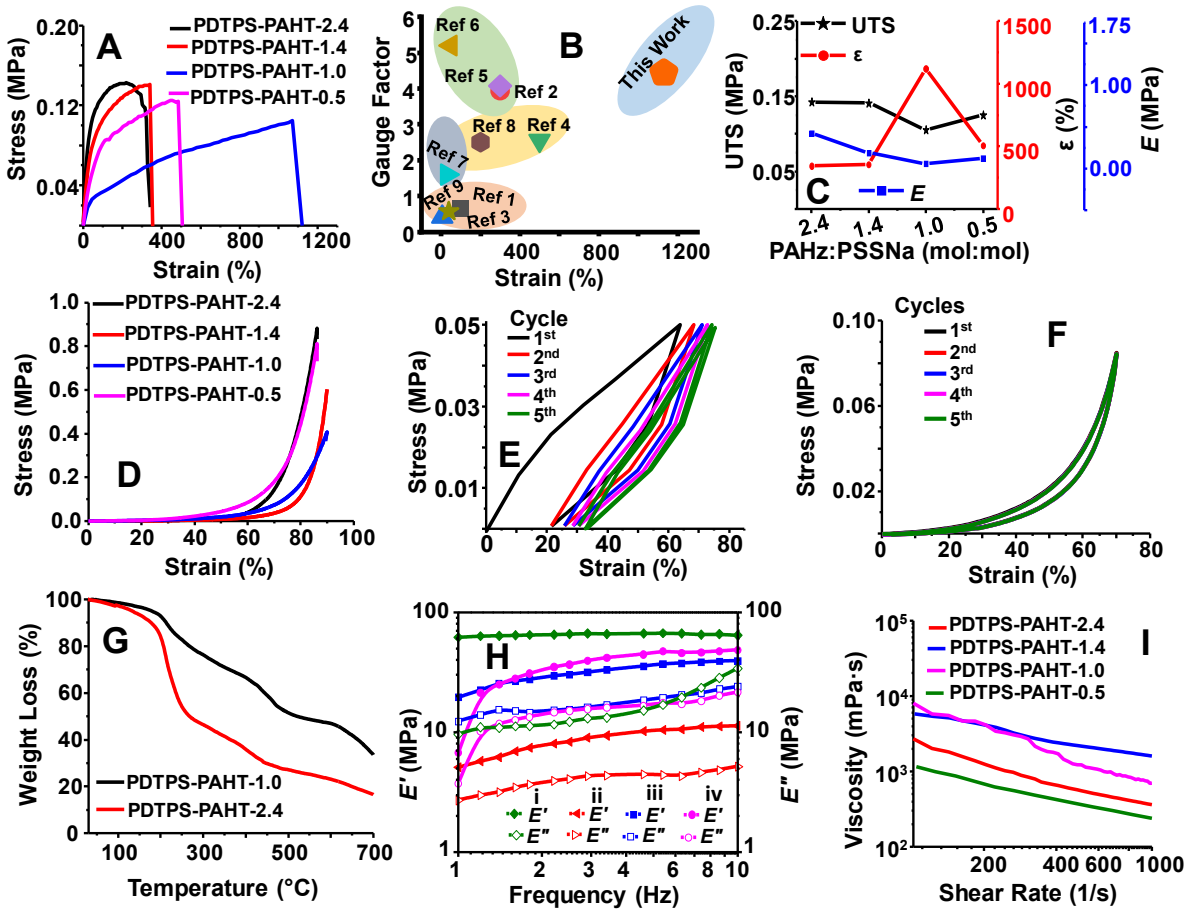

Figure 3.7: (A) The tensile and (D) compressive traces of the PDTPS-PAHT-n films recorded under ambient conditions, (B) the comparative chart showing the ε and Gauze factor values of reported PEDOT:PSS based composites and PDTPS-PAHT-1.0, Ref S1 to S10 are available in SI, (C) the effect of PAHT:PSSNa molar ratio on the tensile properties of the PDTPS-PAHT-n. (E) tensile and (F) compressive hysteresis cycles of PDTPS-PAHT-1.0 film, (G) the TGA thermograms of the PDTPS-PAHT-n samples, (H) the frequency sweep data of the PDTPS-PAHT-n films, i, ii, iii, iv represents PDTPS-PAHT- 0.5, 2.4, 1.4, & 1.0 respectively (I) the viscosity versus shear rate data of the PDTPS-PAHT-n samples.

The compressive cycles displayed effective recovery of the sample after each cycle, and the forward and reverse cycles were mostly superimposable, suggesting the samples have a superior resilience under compressive stress (**Figure 3.7F**).

The TGA analysis of the PDTPS-PAHT-n samples was carried out under N_2 atmosphere to understand the thermal stability of the samples (**Figure 3.7G**). The 10% weight loss of the samples occurred around 200 ºC, and the weight loss at 220 ºC increased with an increase in PAHT content, possibly owing to the degradation of the hydrazide linkage.[201] The frequency scans supported the crosslinked nature of the sample via the $CONHNH_3^+$---SO_3^- ionic linkages as the *E*' value was higher compared to that of the *E*" value over the measured frequency range for all the compositions (**Figure 3.7H**). Lastly, to assess the printability of the ink, the effect of shear rate on viscosity was measured. The samples exhibited shear thinning behaviour and the viscosity gradually decreased with an increase in shear rate (**Figure 3.7I**). Importantly, the shear thinning behaviour was prominent with composition possessing an equimolar amount of PAHT and PSS (PDTPS-PAHT-1.0). This is important from the perspective of uniformly passing the ink through orifice and utilizing the ink compositions for printing various shapes targeting the desired application.

The viscosity of the inks was tailorable by varying the water content of the system. The ink was suitable for flow printing, painting and drop-casting to generate uniform shapes. To demonstrate this, a curved rectangular mesh and honeycomb-type shapes were printed by releasing ink through a plastic nozzle under manual pressure (**Figure 3.8A-C**). The shapes were readily flexible and were bent by ~180º without experiencing any physical damage in the shapes. One of the sides of the honeycomb shape was able to lift 20 g weight supporting the adequate tensile strength of the films **(Figure 3.8D**). The FESEM image of the printed sample was mostly smooth in nature supporting the homogeneity of the ink (**Figure 3.8E**). Owing to presence of various ionic

linkages in the samples, the films were anticipated to exhibit self-healing behavior. To assess the self-healing ability of the films, a thin cut made on the PDTPS-PAHT-1.0 film was gently pressed to allow the connectivity between two edges. The sample was then left undisturbed to allow the self-healing process. The cut section gradually healed and became unrecognizable after 12 h (**Figure 3.8F0-F3**). The UTS and ε values of the healed sample recovered up to 39% and 71% respectively of the original value supporting the healing process (**Figure 3.8G**). Possibly, the $CONHNH_3^-$---SO_3^- ionic linkage reformed at the damaged site to promote the chain rearrangement of PAHT and PSS segments and healing process (**Figure 3.8H**).

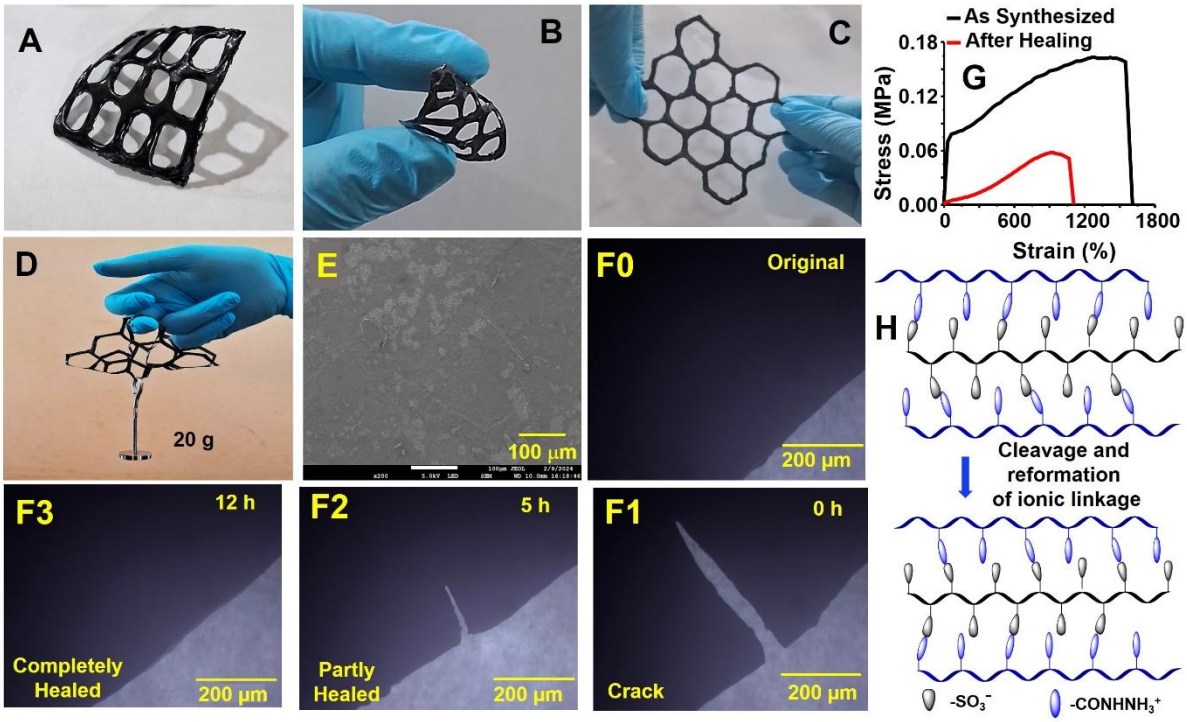

Figure 3.8: The (A) curved mesh and (C) honeycomb shape printed from the PDTPS-PAHT-1.0 conductive ink using a plastic nozzle, (B) the PDTPS-PAHT-1.0 mesh is folded manually, (D) 20 g weight is hanging from a folded honeycomb shape, (E) the FESEM image of the surface of 3D printed object, (F0) a thin rectangular film of PDTPS-PAHT-1.0, (F1) the film with a cut made using a blade, (F2) the partially healed F1, (F3) the healed F1 after 12 h, (G) the tensile traces of

original and self-healed film, (H) the proposed mechanism of self-healing via reformation of the $CONHNH_3^+$---SO_3^- ionic linkage.

Table 3.3:Comparative Analysis of Previously Reported Self-Healing Hydrogels with PDTPS-PAHT-1.0

S.No.	Hydrogel System	Self-Healing Mechanism	Self-Healing Efficiency	Reference
1.	Peptide Nanofibrillar Hydrogel	Dynamic noncovalent interactions	Rapid self-healing within minutes at room temperature	[202]
2.	Nanoconfined PAAm Hydrogel	Polymer chain entanglement	Up to 100% self-healing efficiency with modulus ~ 50 MPa	[203]
3.	HA-Fe-EDTA Hydrogel	Dynamic coordination bonding	Rapid self-healing with maintained strength after repeated healing	[204]
4.	O-CMC-g-poly(NVP-co-AAm) hydrogel	Dynamic Hydrogen Bonding	Complete healing within 15 s for optimised formulation	[205]
5.	Boc-Phe-Aib-OH peptide hydrogels	Supramolecular noncovalent interactions	Excellent thixotropic recovery and self-healing cycles were rheologically confirmed	[206]
6.	**This Work**	**PDTPS-PAHT-1.0 Hydrogel Film**	**Dynamic ionic interactions between $CONHNH_3^+\cdots SO_3^-$ and $SO_3^-\cdots CS^+$ groups within 12hrs**	-------

The ionic conductivity of the PDTPS-PAHT-n films were measured from the EIS spectra in 0.1 M NaCl solution. The values were obtained in the range of 13 to 16 S/m and seemed to minorly slightly increase with the amount of PEDOT component in the system (**Figure 3.9A , 3.9A(1))**. The values were similar to that of the ionic conductivity of PEDOT: PSS-based gels reported from EIS data in recent literature.[207]

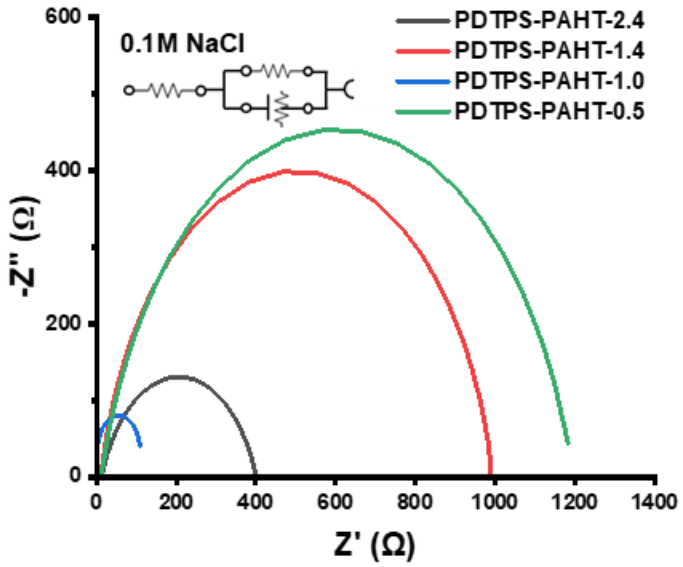

Figure 3.9A (1): EIS plots for the PDTPS-PAHT-n in 0.1 M NaCl electrolyte.

The data further suggested that addition of PAHT to the system is not compromising the conductivity of the system to a significant extent. Possibly, with addition of PAHT, the ionic content of the film in the form of $CONHNH_3^+$ and $CF_3SO_3^-$ increased in the matrix, which aided the ionic conductivity of the film. To support the above, the conductivity value of PDTPS-PAHT-1.0 at different triflic acid concentration was recorded. Presumably, the value increased from 16 to 22 S/m on increasing the triflic acid content from 5 to 20 mol% with respect to PAHz repeating unit supporting the above (**Figure 3.9B, 3.9B(1**).

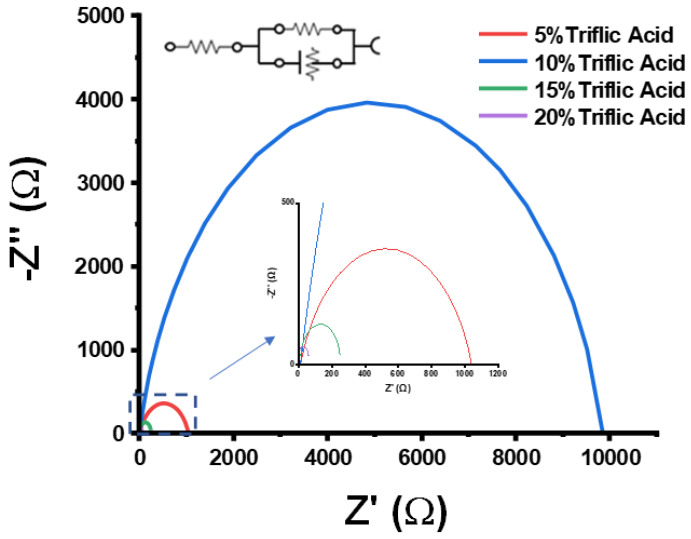

Figure 3.9B (1): EIS plots for the PDTPS-PAHT-1.0 with varying triflic acid (%) in 0.1 M NaCl + 6% Methanol electrolyte.

However, the films in presence of ≥20% triflic acid became less extensible. Therefore, the sample with 15% triflic acid was utilised for the strain sensing purposes. On addition of 6% methanol to the electrolyte, the conductivity value displayed minor improvement (**Figure 3.9A, 3.9A (2)**).

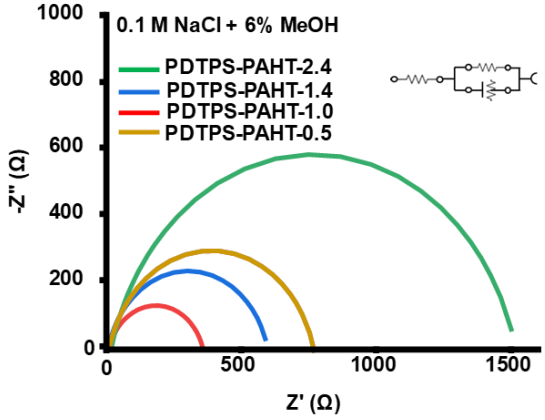

Figure 3.9A (2): EIS plots for the PDTPS-PAHT-n in 0.1 M NaCl + 6% Methanol electrolyte.

The presence of alcohols in solution is known to promote the conductivity value of PEDOT: PSS-based systems in the literature.[208] The effect of temperature on conductivity was then assessed by measuring the ionic conductivity values between 25 to 65 ºC (**Figure 3.9C, 3.9C(1)**).

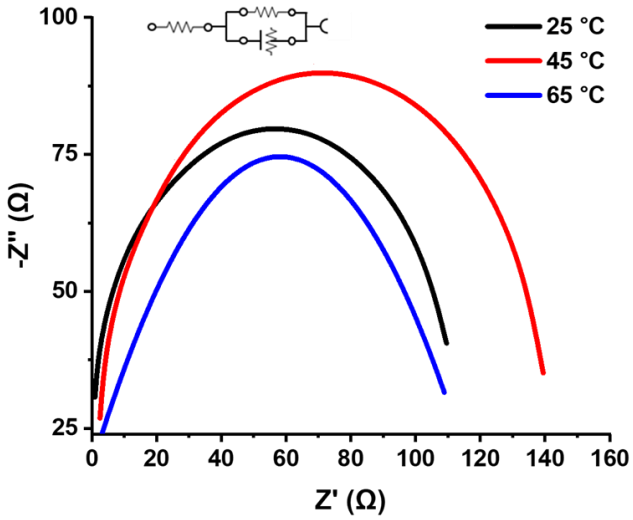

Figure 3.9C(1): EIS plots for the PDTPS-PAHT-1.0 in 0.1 M NaCl electrolyte with varying temperature.

Presumably, the value gradually increased from 16 to 29 S/m with increase in temperature till 65 ºC possibly owing to a faster transport of ions at higher temperature.

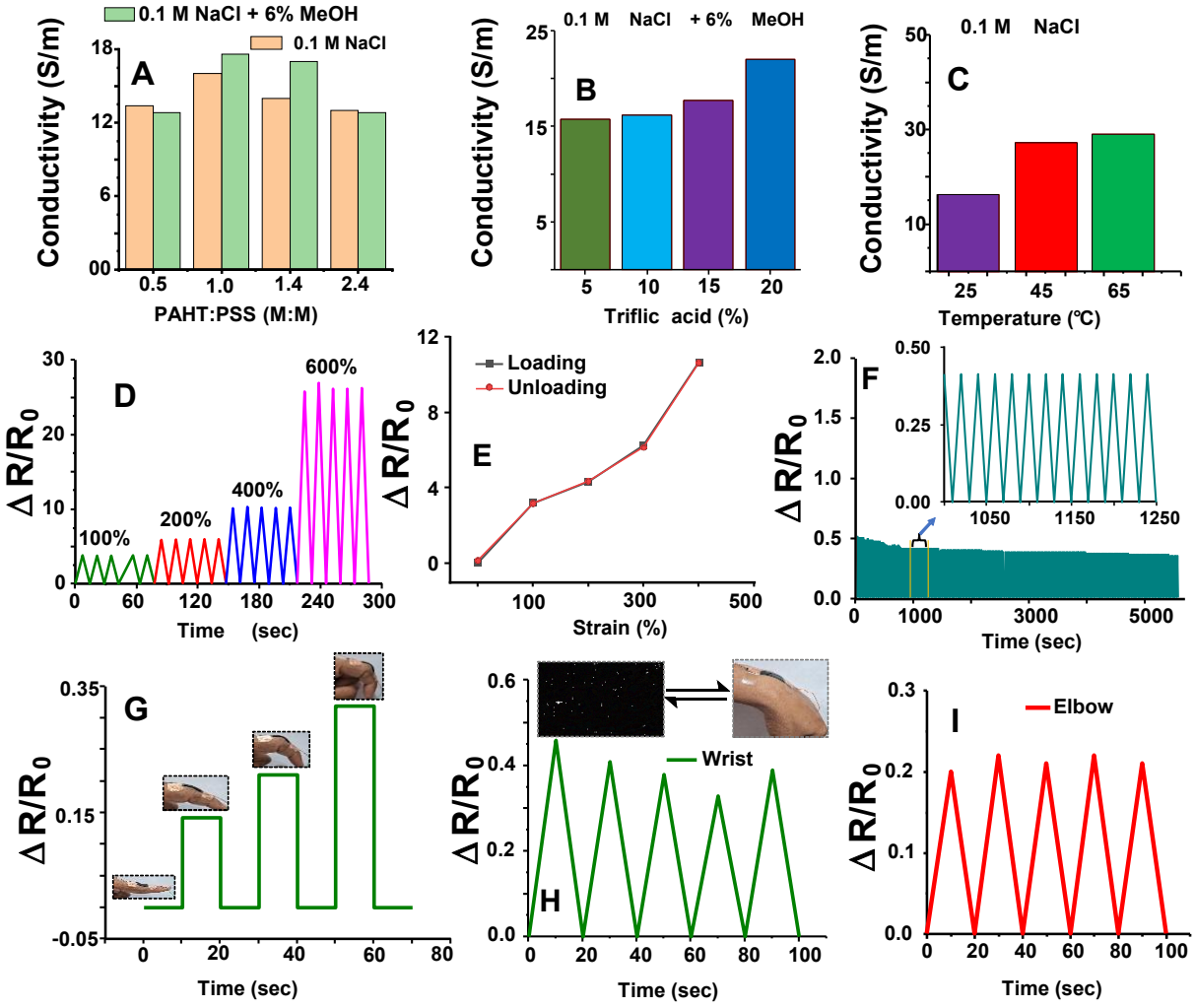

Figure 3.9: (A) The conductivity data of the PDTPS-PAHT-n films measured in 0.1 M NaCl and 0.1 M NaCl + 6% methanol solutions, (B) the effect of triflic acid on the conductivity of PDTPS-PAHT-1.0 film, (C) the effect of varying temperature on the conductivity of PDTPS-PAHT-1.0 film, in presence of 0.1M NaCl, (D) the $\Delta R/R_0$ data of PDTPS-PAHT-1.0 film measured for five continuous cycles at a particular extension, (E) the $\Delta R/R_0$ values obtained at each extension for forward and reverse extension cycle, (F) the $\Delta R/R_0$ values measured for 200 continuous extension (70 %) and release cycles, (G) denotes the change in $\Delta R/R_0$ values associated with the film of PDTPS-PAHT-1.0 for the bending of finger, $\Delta R/R_0$ values of five consecutive bending and relaxation cycles of a PDTPS-PAHT-1.0 film attached to (H) wrist and (I) elbow.

The strain-sensing ability of the PDTPS-PAHT-1.0 film was measured by recording the $\Delta R/R_0$ value at different stretching conditions. The $\Delta R/R_0$ value gradually increased with the stretching extent. At 600% elongation, the value reached ~26.2, suggesting the film may be a suitable candidate for various strain-sensing applications (**Figure 3.9D**). Continuous five cycles at each elongation step produced identical $\Delta R/R_0$ values supporting the reproducibility of the measurement and viability of the system for strain sensing applications (**Figure 3.9D**). The $\Delta R/R_0$ values for extension and relaxation cycles were also measured to further understand the accuracy of the measurement. The $\Delta R/R_0$ values observed during the relaxation cycle matched those of the extension step, supporting the above (**Figure 3.9E**). Subsequently, 200 continuous stretching and relaxation cycles of a PDTPS-PAHT-1.0 film were recorded to understand the performance for a long period. The cycles produced similar $\Delta R/R_0$ values (0.41 at 70%) at each stretching cycle up to the 200 cycles studied without experiencing notable deviation suggesting the reproducibility of the data (**Figure 3.9F**). Overall, the study supported that these PDTPS-PAHT-n films offer a viable platform to utilize these for strain sensing applications. A uniform film of PDTPS-PAHT-1.0 was installed on various body parts and the bodily motions were monitored. The film installed on an index finger displayed gradual increase in $\Delta R/R_0$ values from 0.14 to 0.32 for various bending motion of the finger suggesting the film may be utilized to monitor partial and full bending motion of the finger (**Figure 3.9G**). Similarly, the film attached to the elbow ($\Delta R/R_0 \approx 0.22$) and wrist ($\Delta R/R_0 \approx 0.46$) also effectively measured the bending motion of the part by displaying a specific and repetitive $\Delta R/R_0$ value supporting the viability of the system for possible skin electronics applications (**Figure 3.9H-I, Figure 3.9J**).

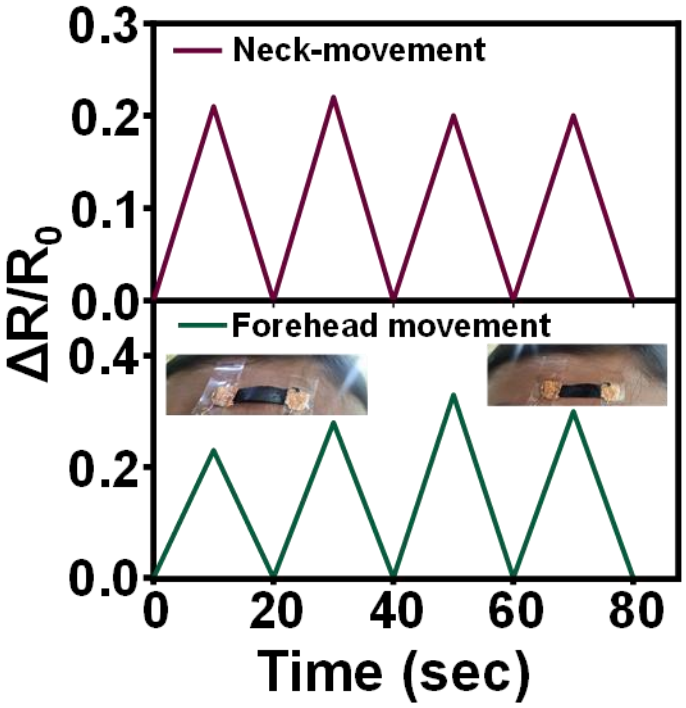

Figure 3.9J: $\Delta R/R_0$ values associated with the film of PDTPS-PAHT-1.0 for the neck and forehead movement.

Similarly, the sample with 0.40 mm ($\Delta R/R_0 \approx 5.9$ at 400%) and 0.15 mm thickness ($\Delta R/R_0 \approx 2.4$ at 400%) displayed lower $\Delta R/R_0$ values compared to that of the 0.75 mm thickness (11.6 at 400%) film (**Figure 3.9D, 3.9D(1)**).

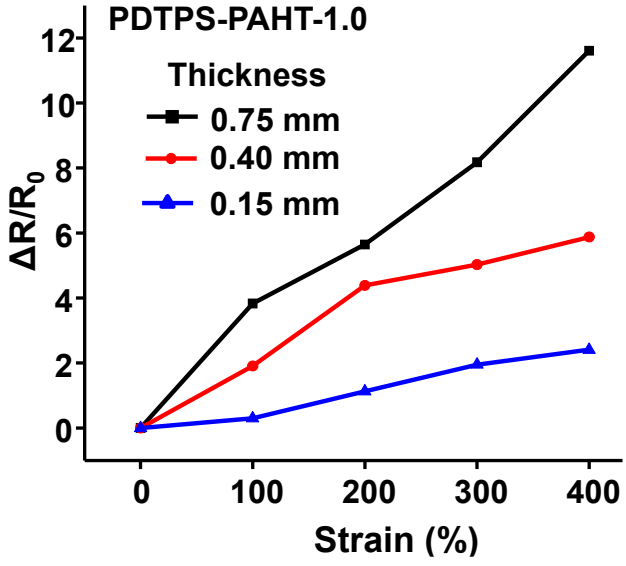

Figure 3.9D(1): The $\Delta R/R_0$ data of PDTPS-PAHT-1.0 films possessing different thickness.

The performance of the PDTPS-PAHT-1.0 as thin films was evaluated to understand the effect of thickness on tensile and strain sensing properties. On decreasing thickness till 0.15 mm, the UTS value gradually increased till 0.56 MPa and the ε value decreased till 650% (**Figure 3.10A**). This may possibly be attributed to the decrease in water content ability with decrease in thickness of the films (**Figure 3.10B**).

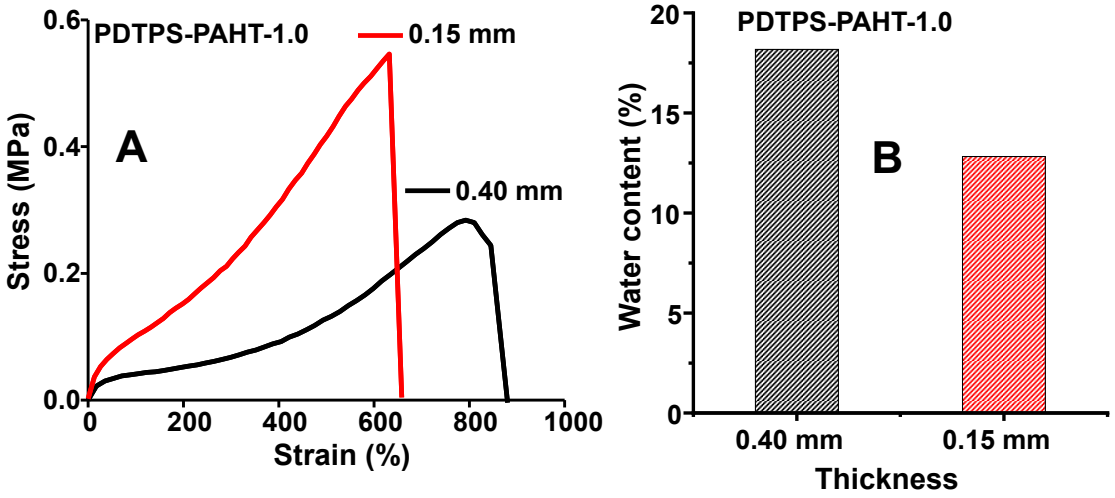

Figure 3.10: The (A) tensile traces and (B) water content of the PDTPS-PAHT-1.0 films possessing different thickness recorded under ambient conditions.

Possibly, the low water content of the thin films compromised the ion transport necessary for effective strain sensing behavior.

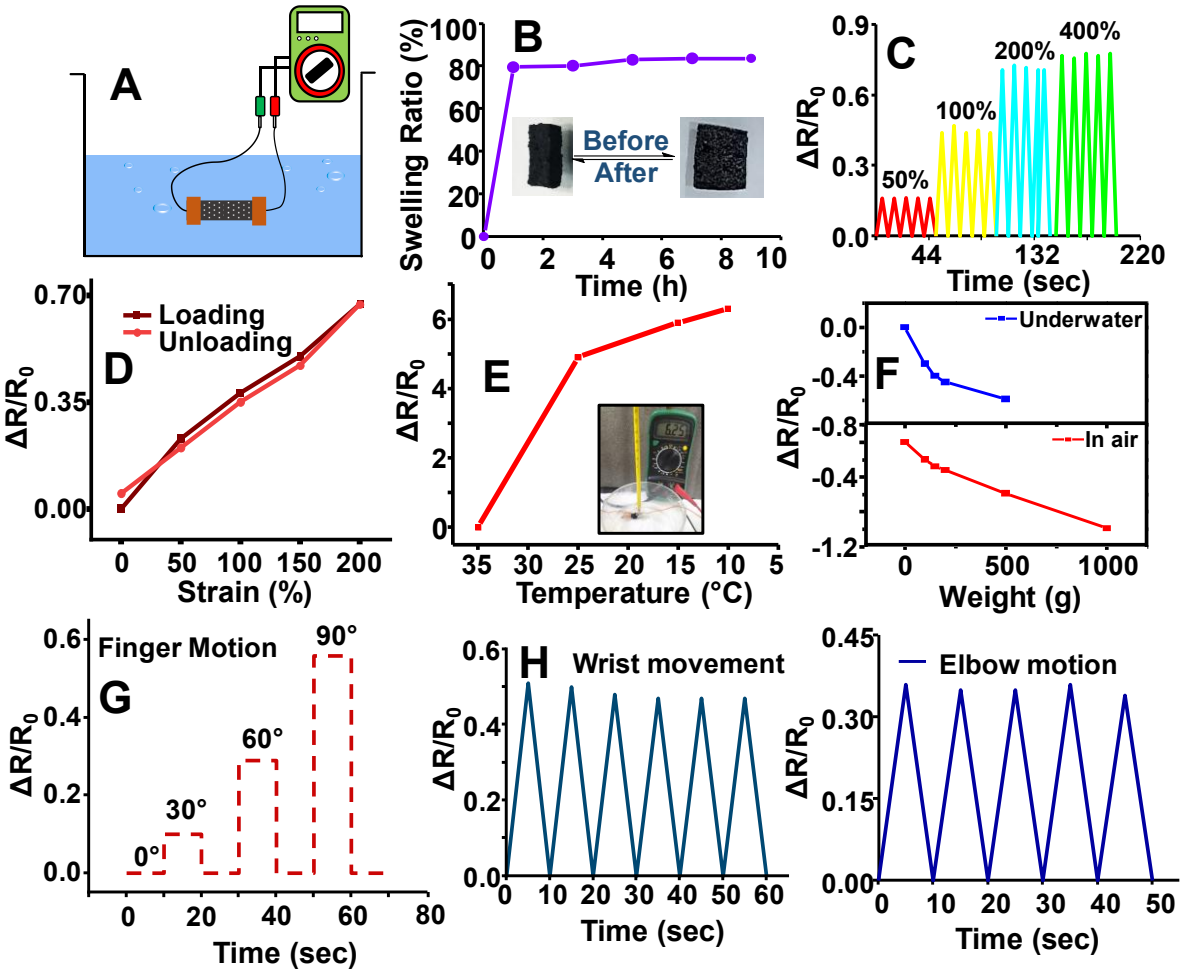

Figure 3.11: (A) The schematics showing the experimental set up utilized to monitor under-water strain sensing data, (B) the PDTPS-PAHT-1.0 film swellability under water, (C) the five repetitive cycles recorded at each elongation extent till 400%, (D) the $\Delta R/R_0$ values obtained at each extension for forward and reverse extension cycle, in under-water conditions, (E) the ΔR/R0 value associated with the varying temperature (F) the $\Delta R/R_0$ value associated with changing pressure

(G) finger, (H) wrist and (I) elbow motion under water, the change in $\Delta R/R_0$ value with temperature and pressure for under-water conditions.

Monitoring of devices installed beneath water body, divers and personals working in under-water conditions offers an important area for which strain sensors for monitoring of temperature, pressure, vibration and stretching is desirable.[209,210] To understand the mechanical integrity of PDTPS-PAHT-1.0 under water, a typical film was immersed in water for 15 min under ambient temperature conditions and the tensile data was recorded. The UTS value (0.16 MPa) of the resulting soaked sample was comparable to that of the original film. However, the ε value decreased from 1120 to 600%, which may be attributed to the increase in water content of the film (68%) (**Figure 3.12)**.

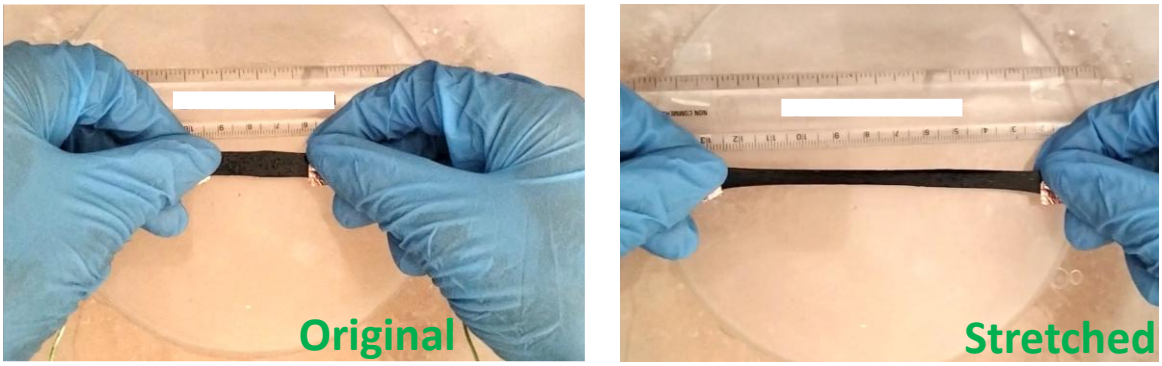

Figure 3.12: The demonstration of stretchability of PDTPS-PAHT-1.0 film recorded at 10 °C.

Subsequently, the effectiveness of the system for such application in under-water conditions were assessed. A typical PDTPS-PAHT-1.0 connected to multimeter via insulated wires was dipped in water and the $\Delta R/R_0$ value with stretching was monitored (**Figure 3.11A**). The PDTPS-PAHT-1.0 film swelled till 80% at equilibrium in water (**Figure 3.11B**). The swelled film was then stretched till 400% inside water and the $\Delta R/R_0$ value was measured. The value gradually increased with

stretching and reached 0.8 at 400% elongation suggesting the system may be useful for under-water strain monitoring applications (**Figure 3.11C**). Five consecutive cycles at different stretching extent also produced similar $\Delta R/R_0$ values suggesting the viability of the system (**Figure 3.11C**).

The $\Delta R/R_0$ values for an extension and release cycle was monitored under water (**Figure 3.11D**). The values obtained during the extension phase was comparable to that of the values measured during release cycle for a particular ε suggesting the values are reliable and the system may be suitable for under water strain sensing operation. Subsequently, the change in $\Delta R/R_0$ with temperature and pressure was monitored anticipating the conditions of various water bodies at higher depth. The $\Delta R/R_0$ value gradually increased till 6.3 with decrease in temperature from 35 to 10 ºC suggesting the PDTPS-PHT-1.0 may be utilized to measure the change in temperature under water (**Figure 3.11E**). Similarly, the $\Delta R/R_0$ value decreased till -0.99 in air under 1000 g load and -0.62 inside water under 500 g load supporting the pressure sensing ability of the system (**Figure 3.11F**). Subsequently, motion of finger ($\Delta R/R_0 \approx 0.56$), wrist ($\Delta R/R_0 \approx 0.51$) and elbow ($\Delta R/R_0 \approx 0.36$) under water was monitored using PDTPS-PAHT-1.0 film, which produced specific $\Delta R/R_0$ outputs for each different bodily deformation (**Figure 3.11G-I**). The study suggested that the PDTPS-PAHT-n films may be a suitable candidate for monitoring of various under water phenomena.

3.5. Conclusion

PAHT can be used as an interactive additive in PEDOT:PSS based system to produce uniform conductive ink for printing solid electrolytes suitable for flexible electronics applications. The resulting printed materials exhibit effective stretchability and flexibility along with self-healing

behavior owing to the presence of dynamic $CONHNH_3^+$---SO_3^- ionic linkages. The films exhibit adequate conductivity up to 18 S/m. The PDTPS-PAHT-n films possessing limited swellability in water may be utilized for under-water strain sensing applications. The study suggests that the film exhibit effective gauge factor value of 4.4 under environmental conditions and is able to detect specific motions of various body parts by displaying a specific $\Delta R/R_0$ value. The PDTPS-PAHT-1.0 film also exhibits adequate gauge factor value of 0.20 under-water and promises to be a potential candidate for sensing various under-water phenomena such as strain, temperature and pressure. The application of the samples may also be extended to other flexible electronics in future.

A Facile Media Polarity Control (MPC) Strategy to Tailor the Toughness & Adhesive Strength of Dual Monomer Single Network Hydrogels and Integrated Machine Learning Approach

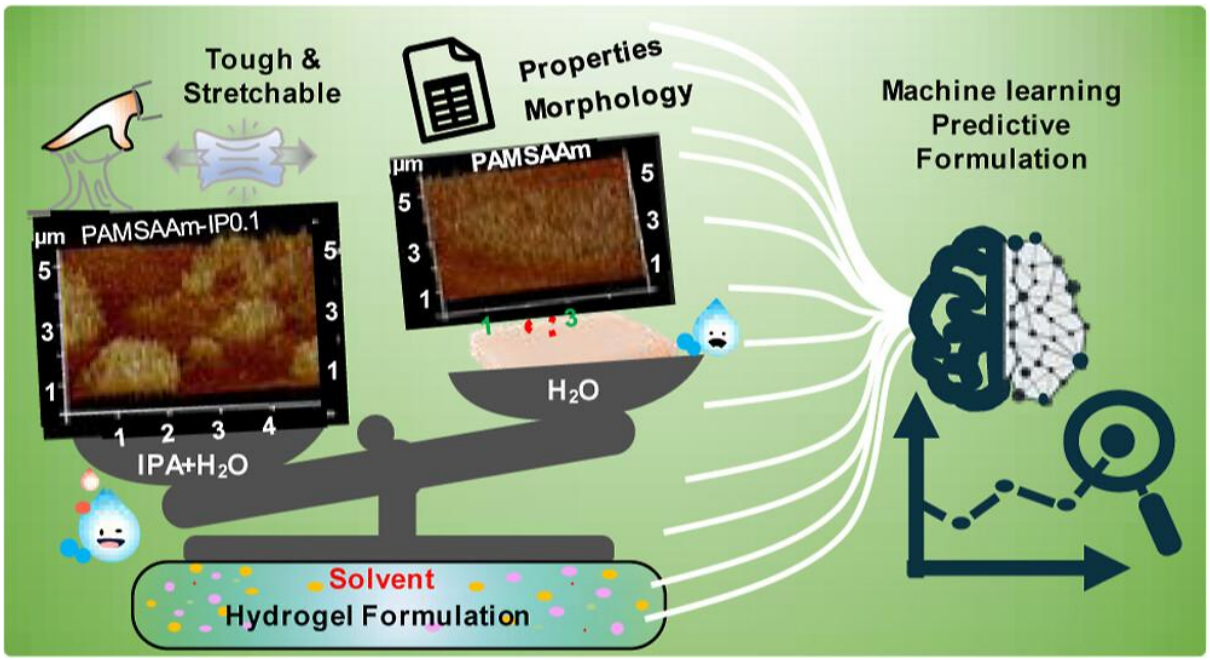

CHAPTER-IV

4.1 Summary

Facile and scalable procedures to enhance the toughness of hydrogels and tailor their material behaviors simultaneously are notably limited in the literature. Especially, one-pot gelation of dual/multi monomer systems suffers from the issue of macrophase separation, which compromises the mechanical behavior of the resulting hydrogels. In this article, a facile media polarity control (MPC) strategy is reported to enhance the stretchability and adhesive strength of dual monomer single network hydrogel by promoting phase mixing in a one-pot procedure. As a proof of concept, acrylamidomethyl-propanesulfonic acid (AMPS) and acrylamide (AAm) based dual monomer single network hydrogel is synthesised and evaluated. The resulting hydrogel (PAMPSAAm-IP0.1) exhibit superior extensibility (ε, 1050%), tensile strength (UTS, 110 kPa) and adhesive strength (0.25 MPa) compared to that of the control synthesised in H_2O (ε ≈ 230%, UTS ≈ 70 kPa and adhesive strength ≈ 0.03 MPa), supporting the viability of the strategy. Importantly, these compositions having isopropyl alcohol (IPA) in the matrix retain their functional behaviour at low temperature conditions, suggesting their viability under said conditions. Subsequently, a number of hydrogel compositions are derived using various solvent mixtures, and a machine learning approach is utilised to predict the tensile behaviour of the hydrogels based on the compositional ratios and crosslinking conditions.

4.2 Introduction

Hydrogels possessing adequate strength, stretchability and toughness promise to address key issues in healthcare,[211,212] flexible electronics,[213] energy storage,[214] adhesive,[215,216] coating,[217] photonic[218] and commodity domains.[219,220] Several successful strategies ranging from double networking,[221] network alignment,[222] salting out,[223] incorporation of energy dissipating physical

& ionic crosslinks,[224] incorporation of stress reinforcing domain,[225] and introduction of slide rings[226] have well attempted in the literature to enhance the toughness of the hydrogels in literature. Double network hydrogels possessing two independent networks of different crosslink densities entangled with each other offer a unique means to enhance the compressive strength of the hydrogels, where the fluidity of the loosely crosslinked second network dissipates energy and improves strength.[227] Similarly, directional freezing followed by the salting out strategy offered an effective means to improve the tensile strength and toughness of the polyvinyl alcohol based hydrogel system via formation and arrangement of anisotropic microstructures.[228] Use of slide-ring-based movable crosslinks composed of hydroxypropyl-α-cyclodextrin, enabled reversible crystallization and melting of PEG chains, leading to ultra-high toughness and fast recovery from stress.[229]

In most of the design criteria reported in literature, the orientation of the chains, number of crosslinks and presence of energy dissipating reversible linkages offer key advantages to enhance the toughness and strength of the resulting hydrogel systems. Typically, in single network hydrogels, the number of covalent crosslinks aided the strength and compromised the elongation and toughness of the system, whereas the entanglement and segregation of the chains possibly acted as physical crosslinks and supported the elongation and toughness of the hydrogels via dissipation of energy under stress.[230] In double network hydrogel systems several approaches are effectively reported to enhance the entanglement of the system and thereby improving the mechanical behavior of the hydrogel systems. For example, additional entanglement inducing polymeric agent such as hydroxypropyl cellulose was utilized to improve the tensile behavior of poly(N-iso-propylacrylamide) hydrogels.[231] Similarly, the chemical crosslinks of second network was strongly suppressed to synthesize a double network hydrogel system with strengthened

physical entanglement, which exhibited improved tensile strength and elongation.[232] Two networks with independent crosslink functionalities were entangled with each other to aid the physical entanglement, which exhibited improved mechanical properties and bi-axial folding behaviour.[233] Though several strategies to improve the entanglement are successful in multi-network systems, the approaches to realise the same in single network systems are desirable since single network hydrogels possibly ensure segment uniformity, functionality of the particular segment, repeated swelling and deswelling life cycle and ease of synthesis.[234] However, the number of approaches to enhance the tensile strength in single network hydrogel systems are fairly limited in the literature to the best of our knowledge. For example, a recent effective strategy showed that the presence of ionic liquid in the gel matrix promotes the formation of a homogeneous network with abundant non-covalent crosslinks between the polymer chains and notably improves the fracture strength, toughness and modulus of the system.[235]

Among several factors, the entanglement of polymeric chains in a gel system is subject to polarity of the medium. One-pot gelation of dual/multi monomer systems in water is likely to suffer from phase segregation during the gelation process, which possibly compromises the tensile behavior of resulting gel systems.[236,237] To overcome this, we have utilized a simple media polarity control (MPC) strategy to promote the phase mixing and chain entanglement in single network dual monomer hydrogel system by controlling the polarity of the medium through use of mixed solvents. Presence of mixed solvents (water and organic solvent) in hydrogel matrix is known to promote phase segregation leading to useful material behavior.[238] For example, equilibrating an as-synthesized polyacrylamide (PAAm) based hydrogel in water/ethanol mixture induced anisotropy and phase separation leading to modulation of tensile & adhesive behavior.[239,240] Similarly, replacing the DMSO-H_2O media with H_2O in a physically crosslinked hydrogel system

induced formation of hydrophobic domains that modulated the tensile behavior.[241] However, the number of reports are fairly limited and mostly utilizes post-gelation solvent exchange. Furthermore, developing a mechanistic understanding of the segment behavior in covalently crosslinked dual-monomer single network systems synthesized in polarity controlled media may not be available in literature to the best of our knowledge. This chapter aims to develop an in-depth understanding of the segmental arrangement by carrying out gelation of multiple monomers in mixed solvent media and assessing its effect on the resulting mechanical behavior. The resulting tensile properties and adhesive behavior is compared to that of the control to validate the efficacy of the strategy. Furthermore, to formulate hydrogel compositions with predictive tensile properties a machine learning approach is explored. In recent years, different machine learning approaches are introduced to study such complex dataset for protein hydrogels[242], bio-analytics[243], bio-3D printing[244], organic synthesis designs[245,246], prediction of hydrogel topology and polymer designs.[247,248,249,250] For example, a machine learning (ML) model was developed recently to predict the hydrogel forming capacity of nucleosides.[251] Similarly, a real-time material recognition system was developed to predict the potential of conductive hydrogels for wearable and bioelectronics applications.[252] However, ML models to correlate between precursor compositions and media polarity to that of the material behavior of conventional dual-monomer single network hydrogel systems may not be available in literature. Therefore, inspired by recent rises of artificial intelligence (AI) and ML, the authors intended to develop a predictive machine learning model, which result in formulations to synthesize hydrogels with adequate accuracy. A key parameter in the design of tough hydrogels is the relative ratio of chemical and physical crosslinks present in the system. Therefore, polarity of gelation media and compositional ratio of precursors are utilized as one of the key parameter for development of the model.

4.3 Synthesis Procedure of PAMSAAm-IP0.n Hydrogel:

The complete synthesis was included in Chapter 2, Section 2.1.3

4.4 Results & Discussion

To evaluate the MPC strategy, H_2O and H_2O-isopropyl alcohol (IPA) mixture were chosen as the gelation media in the first phase. 2-Acrylamido-2-methylpropane sulfonic acid (AMPS) and acrylamide (AAm) was utilized as the dual monomer system and poly(ethyleneglycol) diacrylate (PEGDA) was used as the covalent crosslinker for the one-pot hydrogel synthesis. The rationale for the monomer selection was based on their complementary physicochemical behavior and ability towards a mechanically stable and adhesive hydrogel system. AMPS being highly hydrophilic and ionic monomer, contains sulfonic acid ($–SO_3H$) that has a strong affinity for water, providing surface adhesiveness and ionic interaction to the hydrogel matrix. While the acrylamide unit contributes towards the hydrogen bonding via $–CONH_2$ groups, enhanced the mechanical toughness, flexibility and dissipating energy to the hydrogel. This combination of monomers forms a hydrogel that is highly stretchable and has strong adhesion. IPA, on the other hand regulate the solvent polarity and supports a uniform distribution of monomers inside the matrix. Compared with only water, the water-IPA mixture improves the phase mixing and generates interactive microdomains, which leads to better tensile strength, stretchability and adhesive property. Because of its optimised polarity and amphiphilic behavior, IPA was a superior choice over other alcohols. IPA can balance the mixing of both the hydrophilic and somewhat hydrophobic polymer segments. Other alcohols otherwise show either excessive polarity or poor miscibility of the monomers, which result in weak mechanical properties. Other conditions such as photo initiator amount and gelation time were kept constant for both the systems and the tensile behavior of both the

systems were assessed. The Fourier transform infrared (FTIR) spectra of both the hydrogels displayed characteristic peaks for -CONH and -SO_3H suggesting the presence of both PAMPS and PAAm segments in the hydrogels (**Figure 1**).

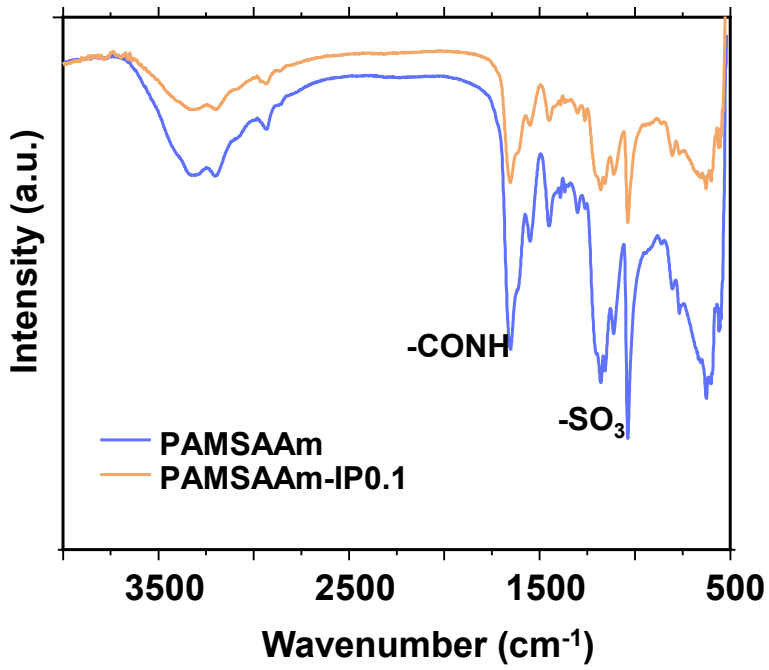

Figure 4.1: FTIR Spectra of PAMSAAm and PAMSAAm-IP0.1 samples

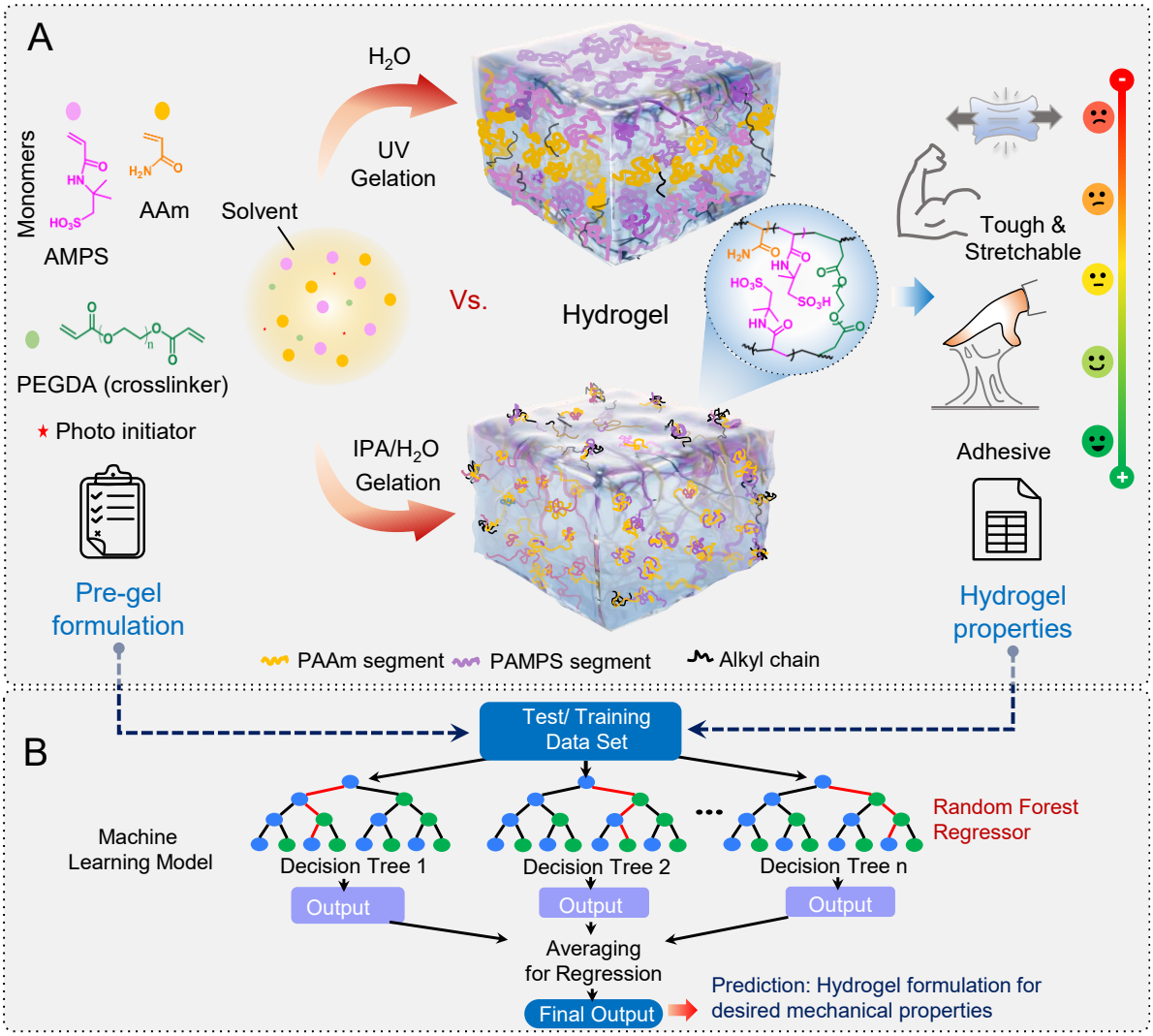

Scheme 4.1: A) Schematics of one-pot synthesis of the PAMSAAm-IP0.1 and PAMSAAm from the pre-gel solution containing monomers, crosslinker, photo initiator and solvent. Models demonstrating the unique morphology of PAMSAAm-IP0.1 and control along with enhanced physicochemical properties, such as adhesiveness and stretchability, B) Schematic illustration of machine learning tool to predict pre-gel formulation for a desired hydrogel with specific mechanical properties. The pre-gel formulations and hydrogel properties data are utilized in a machine learning model: random forest model (MTRFR) as test and training data to develop a predictive model for hydrogel formulations.

The hydrogel (PAMSAAm-IP0.1) synthesized in H_2O:IPA (90:10, v:v) displayed superior ultimate elongation (ε, 1050%) compared to that of the synthesized in pure H_2O (PAMSAAm, ε = 230%). The ultimate tensile stress (UTS) value (110 kPa) of the PAMSAAm-IP0.1 was notably higher compared to that of the PAMSAAm (70 kPa) (**Figure 4.2A**). The samples synthesized in higher amount of IPA (H_2O:IPA = 80:20, 70:30 & 60:40, v:v) also displayed superior ε value (650 – 940%) compared to that of the control (**Figure 4.2B & Figure 4.2B"**).

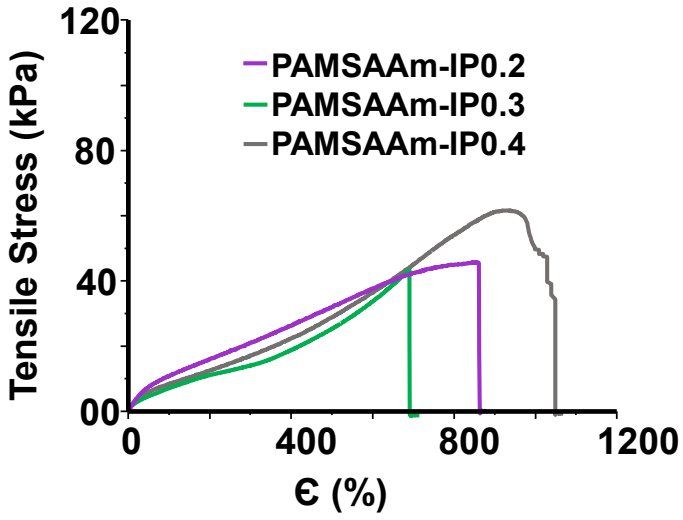

Figure 4.2B: Tensile traces of as-synthesized PAMSAAm-IP-n samples while varying IPA amounts in the pre-gel formulation.

The composition optimization exercise revealed that 10 vol% of IPA in H_2O and 2 mol% of PEGDA with respect to the monomers resulted in hydrogels with superior tensile behavior (**Figure 4.2C**). The solvent combination was then altered by using THF, DMF, ethanol and butanol in place of IPA in aqueous media. However, the hydrogels produced using the above solvent combinations failed to mimic the tensile behavior of PAMSAAm-IP0.1 (**Figure 4.2D**). Hydrogels are known to exhibit varying phase behaviors based on the characteristics of the solvent, such as dielectric properties and wettability. This variation is attributed to the differences in hydrophilicity among

the monomers and their distribution within the copolymer network, which ultimately influences the properties of the hydrogel.[253,254,255] The optimized PAMSAAm-IP0.1 hydrogel showed adequate mechanical performance when subjected to different mechanical deformations. The resulting hydrogel demonstrated high mechanical durability when twisted and stretched (**Figure 4.2 E1- E2**) or knotting followed by stretching (**Figure 4.2 F1- F2**) and showed low hysteresis and recoverability during five consecutive cyclic loading-unloading cycles when stretched up to 800% to its initial length (**Figure 4.2 G**).

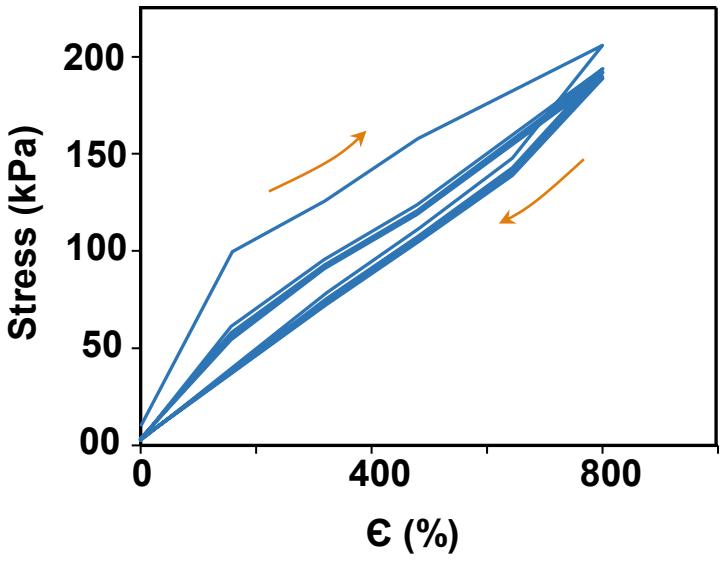

Figure 4.2 G: Hysteresis plot of PAMSAAm-IP0.1 recorded under fixed strain (800%) mode for five consecutive loading- unloading cycles.

The PAMSAAm-IP0.1 film also effectively withstood extensive and compressive forces (**Figure 4.2 H**).

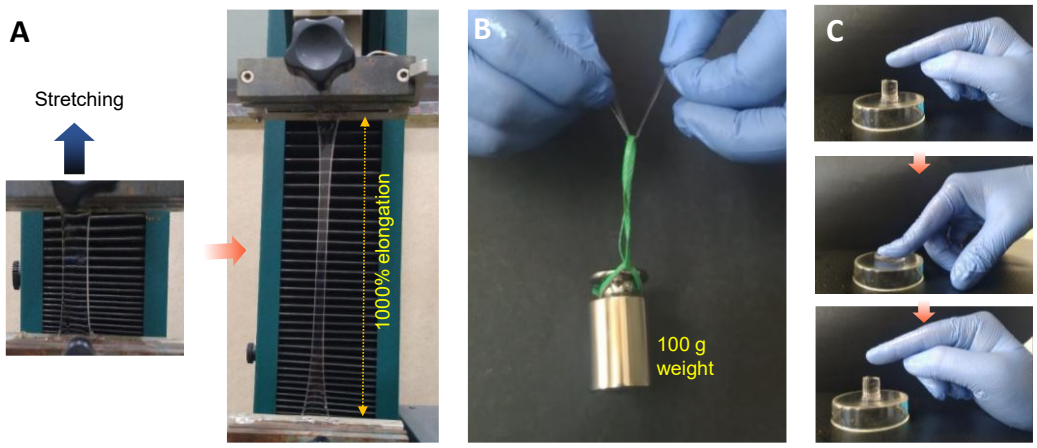

Figure 4.2 H: Demonstration of mechanical performance of a PAMSAAm-IP0.1 hydrogel film. Digital image of A) Tensile test of PAMSAAm-IP0.1 hydrogel on UTM machine stretched up to 1000%. B) The sample withstands mechanical deformation when a 100 g weight was hung on it. C) A cylindrical PAMSAAm-IP0.1 hydrogel resisting compressive failure when pressed by thumb.

To further assess the versatility of the approach, hydrogel compositions (PAMSAA-IPn & PAAAAm-IPn) based on other monomer combinations such as AMPS-acrylic acid (AA) and AA-AAm were synthesized in H_2O-IPA mixtures. The tensile data revealed that the extensibility of samples synthesized in H_2O-IPA mixture is readily controlled by the amount of IPA in water and an optimized amount of IPA in water is necessary to synthesize hydrogels with superior tensile behavior (**Figure 4.2 I**).

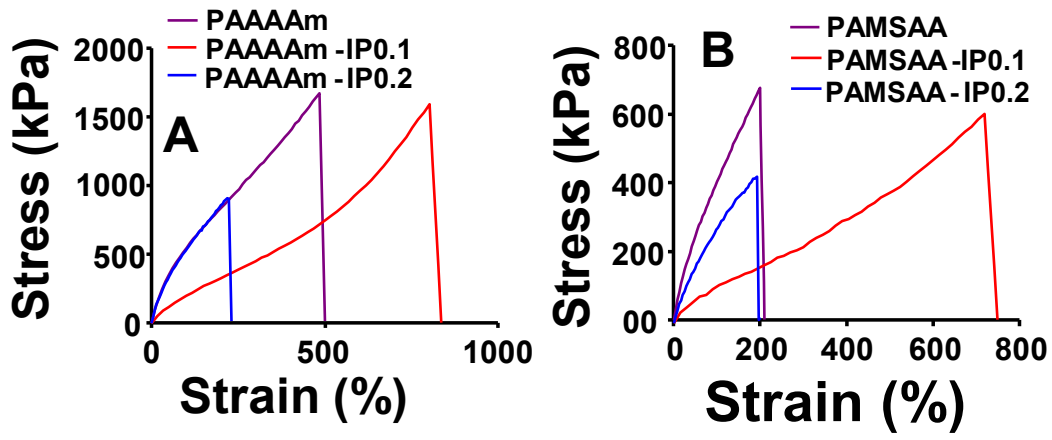

Figure 4.2 I: Tensile trace of different PAAAAm, PAAAAm-IPn, PAMSAA, PAMSAA-IPn compositions

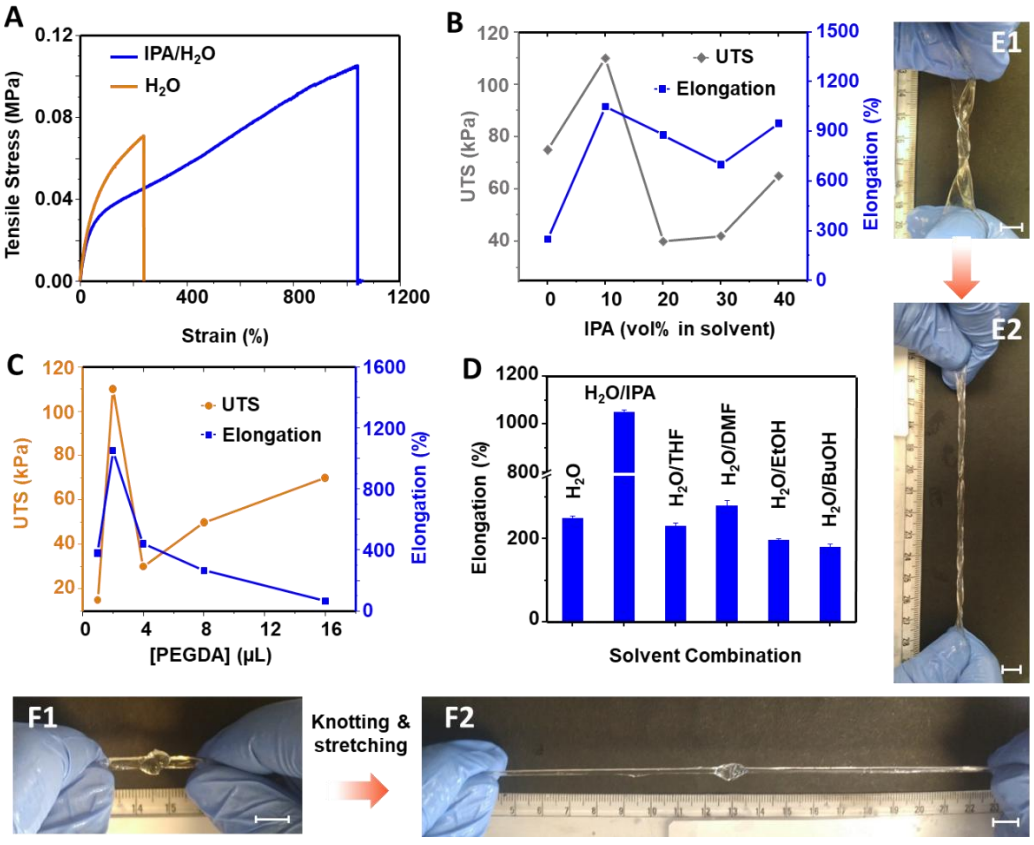

Figure 4.2: A) Tensile traces of PAMSAAm-IP0.1 (IPA:H_2O = 10:90, v:v), and PAMSAAm (IPA:H_2O = 00:100, v:v). B) Comparison of mechanical properties of PAMSAAm-IPn hydrogels

with varying IPA amount in the pre-gel solution. C) Effect of PEGDA amount on the mechanical properties of a PAMSAAm-IP0.1 hydrogel. D) Plot depicting variation in stretchability of the resulting hydrogels when different solvents are used in the pre-gel formulations in 10 vol% along with the water. Demonstration of mechanical properties of the optimized PAMSAAm-IP0.1 hydrogel. E1-E2) Digital images of a hydrogel being twisted and stretched and F1-F2) knotting followed by stretching. Silicone oil coating is used to avoid stickiness while samples are being deformed. The scale bar is 1 cm for digital images.

To understand the origin of superior tensile behavior of PAMSAAm-IP0.1 compared to that of the control, the structural distribution of the segments was investigated using various spectroscopic techniques. The S 2p and N 1s X-ray photoelectron spectroscopic (XPS) surface elemental mapping of the freeze-dried hydrogel samples revealed that the hydrogel synthesized in H_2O (PAMSAAm) displayed higher amount of S compared to that of the PAMSAAm-IP0.1 (**Figure 4.3A1-A2**). The amount of O was also somewhat higher in PAMSAAm compared to that of the PAMSAAm-IP0.1 suggesting the prevalence of PAMS segment on the surface of former (**Figure 4.3J**).

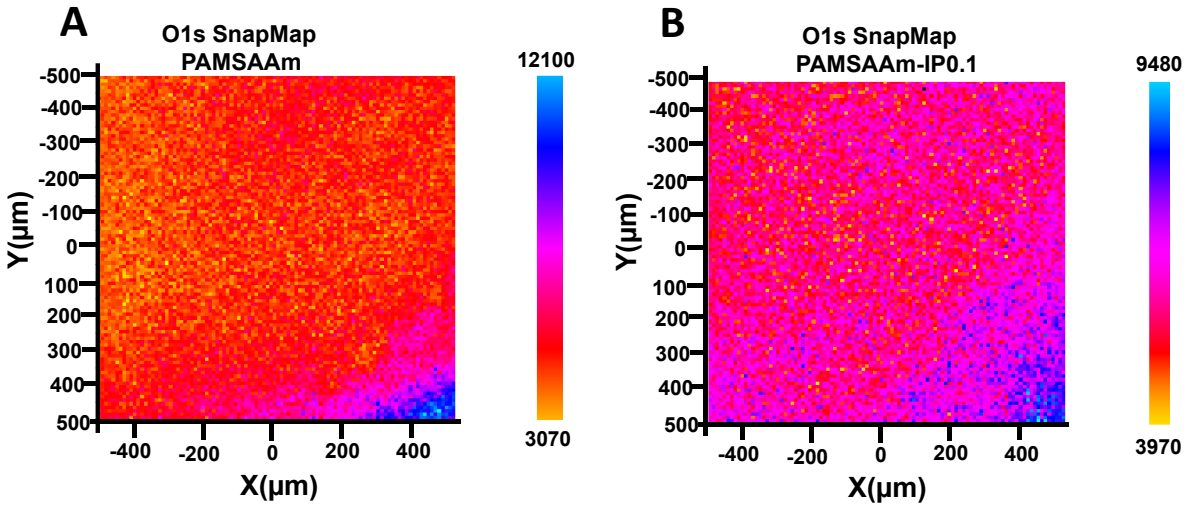

Figure 4.3J: XPS elemental mapping for the freeze-dried hydrogel samples A) PAMSAAm and B) PAMSAAm-IP0.1 depicting O1s Snap Map.

The notably higher amount of N on surface of PAMSAAm-IP0.1 suggested that in mixed solvent system, the resulting hydrogel possessed both PAMS and PAAm segments on the surface (Figure 4.3B1-B2 and 4.3K).

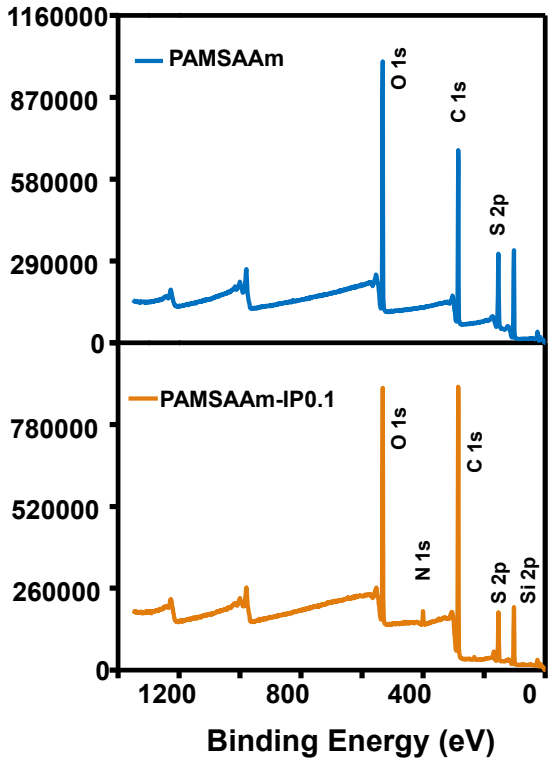

Figure 4.3K: XPS survey spectra of PAMSAAm and PAMSAAm-IP0.1 samples.

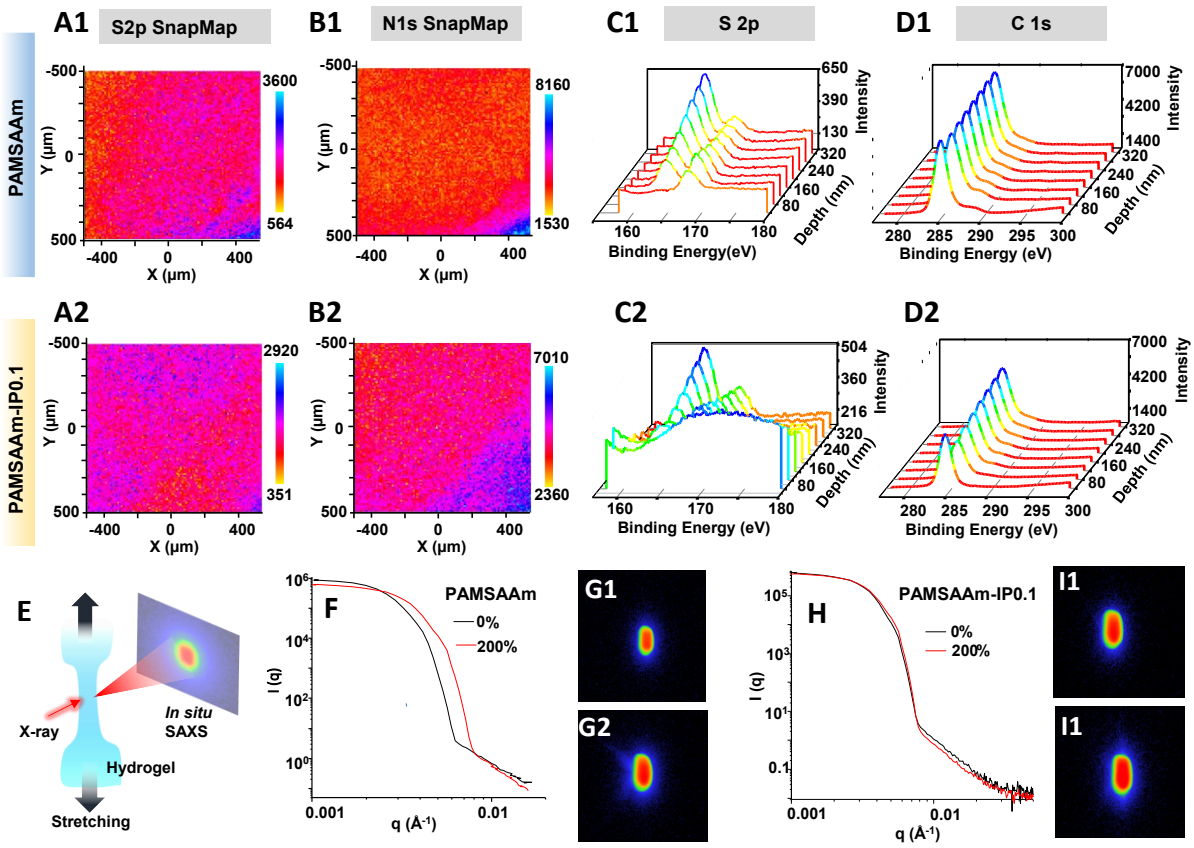

Figure 4.3: XPS mapping of hydrogel surface- (A1) S 2p mapping of PAMSAAm, (A2) S 2p mapping of PAMSAAm-IP0.1, B1) N 1s mapping of PAMSAAm, B2) N 1s mapping of PAMSAAm-IP0.1, S 2p XPS depth profile data of C1) PAMSAAm & C2) PAMSAAm-IP0.1, C 1s XPS depth profile data of D1) PAMSAAm & D2) PAMSAAm-IP0.1, E) Schematics depicting *in situ* SAXS while the hydrogel is being stretched uniaxially, F) *In situ* SAXS scattering profile data of original and uniaxially stretched (200%) PAMSAAm film, G1-G2) corresponding 2D scattering maps of original and stretched PAMSAAm, H) scattering profiles of original and stretched (200%) PAMSAAm-IP0.1 film and I1-I2) corresponding 2D scattering maps when PAMSAAm-IP0.1 sample stretched up to 0 and 200%, respectively.

The XPS depth profiling data revealed that PAMSAAm possessed notable amount of free SO_3H groups (168 eV) along with hydrogen bonded SO_3H groups (164 eV) (**Figure 4.3C**). With depth,

the amount of free SO_3H groups decreased and the hydrogen bonded SO_3H groups increased suggesting that the concentration of PAAm segment possibly increased with depth. Interestingly, the proportion between free and hydrogen bonded SO_3H moieties remained similar from surface till 320 nm depth in PAMSAAm-IP0.1 suggesting the PAAm segment is uniformly distributed from surface to bulk, whereas in PAMSAAm, the surface concentration of PAAm segments is notably limited.[256] Possibly, the presence of mixed solvent in PAMSAAm-IP0.1 promoted the solvation of both the segments facilitating their distribution throughout the sample matrix, whereas in only H_2O, the more hydrophilic PAMPS segment preferentially occupied the surface to minimize the surface energy enabling the PAAm to remain towards the core. The C 1s depth profiling revealed a notably higher amount of C on the surface of PAMSAAm compared to that of the PAMSAAm-IP0.1 further supporting the higher concentration of PAMS segment on surface of the former (**Figure 4.3D**). Importantly, the amount of C gradually increased with depth for PAMSAAm-IP0.1, whereas the C amount was similar throughout the studied depth till 320 nm for PAMSAAm suggesting the gradual increase in PAMS segment from surface towards the bulk in case of the former. The observation supported the surface mapping data. The overall XPS analysis revealed that in PAMSAAm, the PAMS segment mostly covered the surface, whereas in PAMSAAm-IP0.1 both PAMS and PAAm segments contributed to both surface and bulk compositions. To further investigate the segmentations, *insitu* small angle X-ray scattering (SAXS) experiment was performed while the samples are subjected to uniaxial strain (**Figure 4.3E**). The SAXS data of the PAMSAAm revealed a spacing of ~165 nm between the segregates, which decreased to 130 nm on stretching the film by 200% (**Figure 4.3F**). Interestingly, the domain spacing remained unchanged after stretching the sample for 200% in PAMSAAm-IP0.1. This suggested that possibly, the domains in PAMSAAm are isolated, whereas the domains in

PAMSAAm-IP0.1 are interactive in nature (**Figure 4.3H**). The 2D scattering map of as-prepared PAMSAAm broadened with stretching suggesting possible alternation in size & weak nature of the segregates, whereas the scattering map for PAMSAAm-IP0.1 remained largely unchanged till stretching the film up to 200% (**Figures 4.3G and I**).[257] This observation also favored phase mixing in the hydrogel promoted by the polarity control of the media.

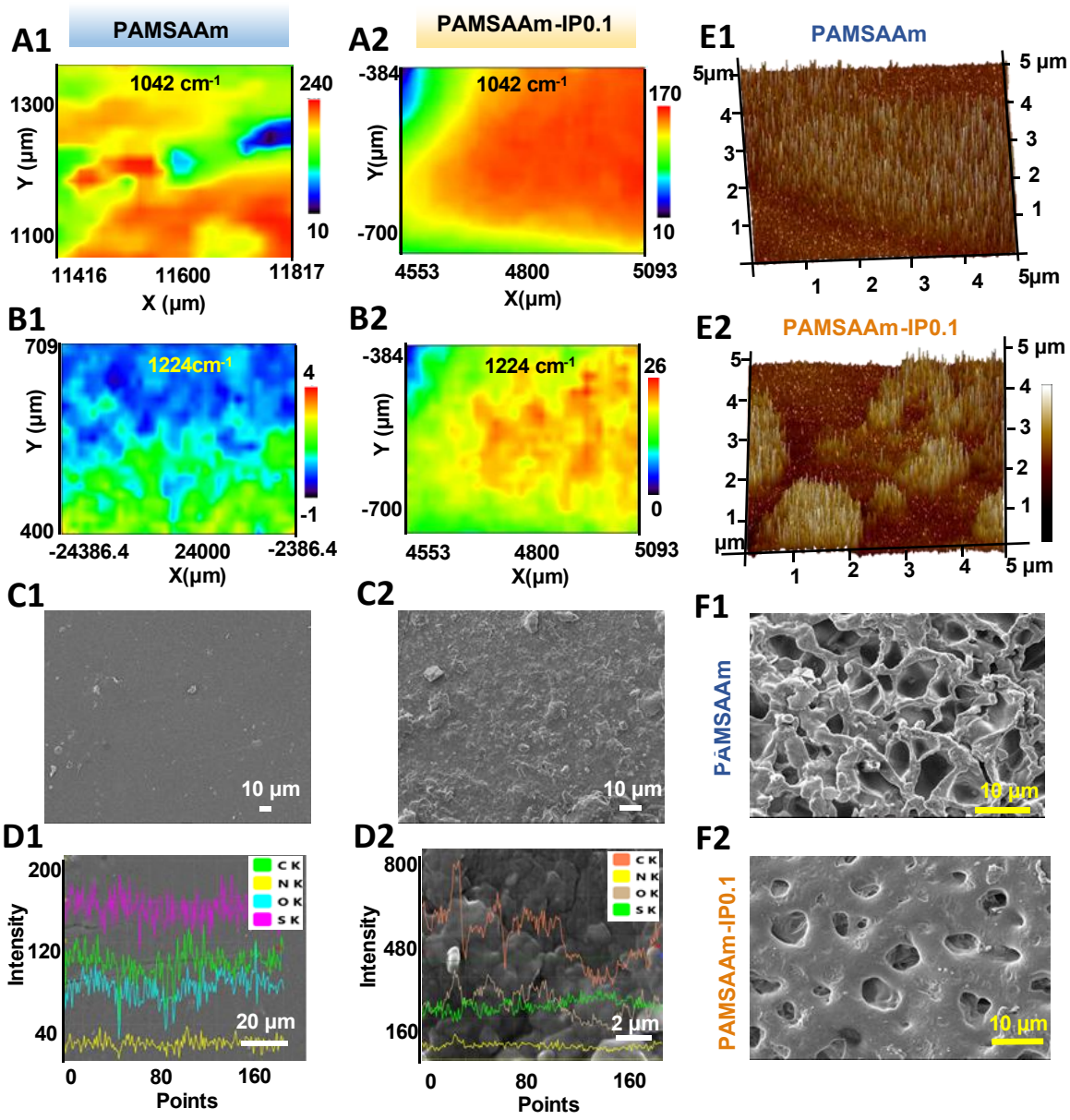

Figure 4.4: A1-B1) Confocal Raman mapping of the surfaces of PAMSAAm at 1042 and 1224 cm^{-1} respectively and A2-B2) Confocal Raman mapping of the surfaces of PAMSAAm-IP0.1 at 1042 and 1224 cm^{-1} respectively. C1-C2) FESEM images of as synthesized followed by freeze dried PAMSAAm and PAMSAAm-IP0.1 films respectively, D1-D2) EDS elemental line scan data of C1 and C2, the overlaid plots showing intensity of elements along the line scan, E1-E2) AFM height profile images of freeze dried PAMSAAm and PAMSAAm-IP0.1 showing distinctive segregated microdomains for the latter and FESEM images of fully swelled in aqueous media followed by freeze dried (F1) PAMSAAm and (F2) PAMSAAm-IP0.1.

The Raman confocal mapping of the films corresponding to SO_3H peak at 1042 cm^{-1} and $CONH_2$ peak at 1224 cm^{-1} were recorded to understand the distribution of above functionalities on surface. In PAMSAAm, moderate to high amount of SO_3H moieties were observed, whereas the amount of $CONH_2$ was negligible (**Figure 4.4A1, B1 and 4.4G**).

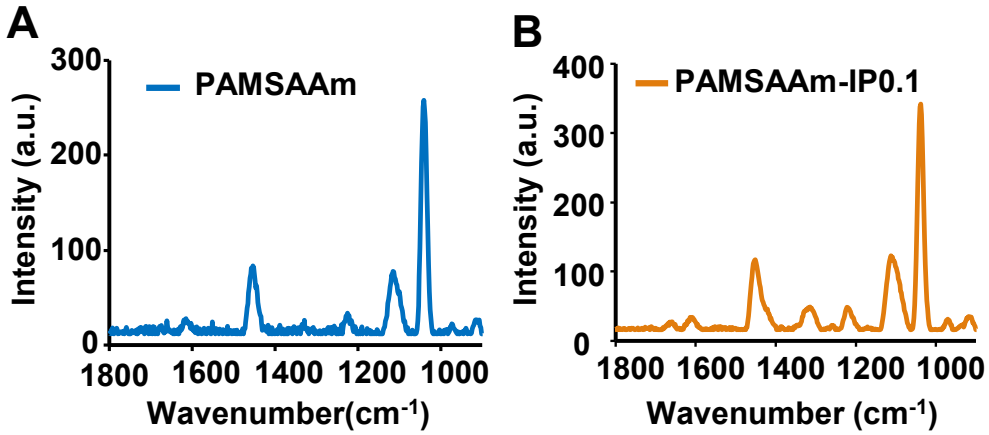

Figure 4.4G: Raman Spectra of A) PAMSAAm and B) PAMSAAm-IP0.1 hydrogels

Interestingly, on PAMSAAm-IP0.1 surface both SO_3H and $CONH_2$ moieties were observed in low to moderate amount (**Figure 4.4A2, B2**). The observation favored the presence of both the segments on the surface further supporting the XPS and SAXS data. The scanning electron

microscopy and energy dispersive X-ray spectroscopy (SEM-EDS) data of as-synthesized followed by freeze-dried PAMSAAm and PAMSAAm-IP0.1 films were recorded to assess the surface morphology (**Figure 4.4C1-D1**). The data for PAMSAAm revealed ultra-high amount of S and negligible amount of N uniformly distributed throughout the surface suggesting the prevalence of -SO_3H moieties on surface supporting the XPS data. Interestingly, the SEM-EDS data of PAMSAAm-IP0.1 revealed an un-even surface morphology with high amount of hydrocarbon content on surface along with SO_3H and $CONH_2$ functionalities suggesting the presence of both PAMS and PAAM segments and alkyl chains on surface (Figure 3C2-D2). Possibly, the presence of multiple segments promoted the formation of mixed microphase domains on surface. The AFM image of PAMSAAm-IP0.1 revealed presence of micro domain (~1-2 μm), whereas the size of segregate in PAMSAAm film was relatively broad (~6 μm) (**Figure 4.4E1-E2**). Finally, as-synthesized films of PAMSAAm-IP0.1 and PAMSAAm were fully swelled in aqueous media and freeze-dried to observe the internal structure after equilibrating the samples with water (**Figure 4.4F1-F2**). The PAMSAAm films were porous in nature with isolated pores and thin walls. The PAMSAAm-IP0.1 were relatively less porous with thick walls suggesting the crosslinking media notably contributes to the morphology of the hydrogels and in presence of mixed solvent the phase mixing possibly compromises the porosity.[258]

The PAMSAAm-IP0.1 possessing different polar and hydrophobic functionalities on the surface and an uneven microphase separated morphology was anticipated to interact with various surfaces and display effective adhesive characteristics.[259,260] To assess the above, the adhesiveness of the PAMSAAm-IP0.1 and PAMSAAm films were examined. The film swiftly glued to various surfaces such as glass, skin, wood, biopolymers, plastic, iron and rubber supporting the adhesive nature (**Figure 4.5A**). The PAMSAAm-IP0.1 displayed adhesive strength of 0.25 MPa on glass

surface, which is much superior to that of the PAMSAAm (0.03 MPa) (**Figure 4.5B**). The sample synthesized using 10 vol% IPA in H_2O displayed maximum adhesive strength and the value gradually decreased with further increase in IPA content in the solvent (**Figure 4.5C**). This suggested that an optimized ratio between IPA and H_2O is desirable to maximize the adhesive behavior. The cohesion of PAMSAAm-IP0.1 and its adhesive ability with other hydrogels revealed that the cohesive ability (0.08 MPa) of the sample is weaker compared to its adhesive behavior (0.10 to 0.25 MPa) (**Figure 4.5D**). The adhesive strength of PAMSAAm with other hydrogel compositions were limited to 0.12 MPa (**Figure 4.5H**).

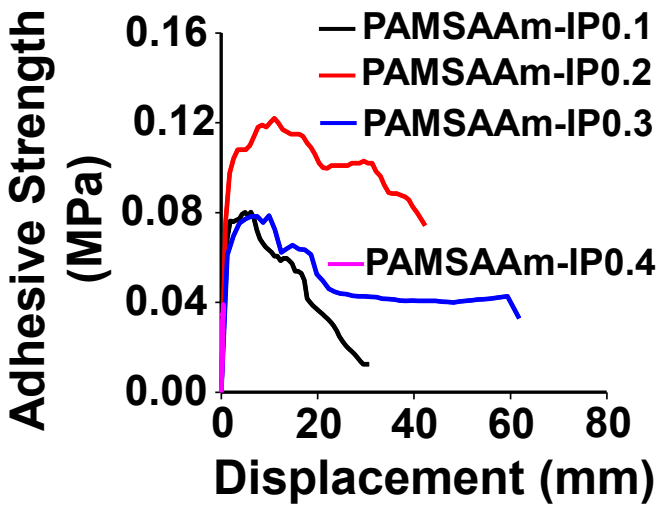

Figure 4.5H: Adhesive performance of different PAMSAAm-IP-n samples when adhered to PAMSAAm hydrogel in lap shear mode. PAMSAAm hydrogel was adhered to glass slide and different PAMSAAm-IP-n samples were varied on the other glass substrate and sandwiched.

A comparative Ashby plot was constructed to understand the adhesive strength of the current hydrogel system with that of the several recently reported systems (**Figure 4.5E and Table**

4.1).[261,262,263,264,265,266,267,268,269,270,271,272] The data revealed that PAMSAAm-IP0.1 demonstrates superior adhesive strength and stretchability simultaneously.

Table 4.1: Comparison table of adhesive strength (towards glass substrate) and elongation at break in a tensile test of PAMSAAm-IP0.1 hydrogel with reported hydrogel systems in literature.

S.No.	Material	Adhesive strength (MPa)	Strain (%)	Reference
1.	P16V4-THMA/CS	0.02	292.4	Ref S1
2.	MR/PAAc–PAM–PDA 0.5g	0.015	660	Ref S2
3.	PGA-GeIMA	0.005	160	Ref S3
4.	PAA/QCS	0.05	600	Ref S4
5.	GNT-M	0.02	200	Ref S5
6.	AIMA-e-AIBA	0.01	250	Ref S6
7.	30wt% GG	0.06	700	Ref S7
8.	OHAdop/GC+GC/borax/PDA	0.03	650	Ref S8
9.	PSA-DA/DES gel	0.093	1400	Ref S9
10.	BSA/Alg-Dopa-PAA	0.24	910	Ref S10
11.	AA/HEAA/Chitosan/MMA	0.011	1350	Ref S11
12.	CMC/CS/PAA	0.013	900	Ref S12
13.	**PAMSAAm-IP0.1**	**0.25**	**1050**	**This Work**

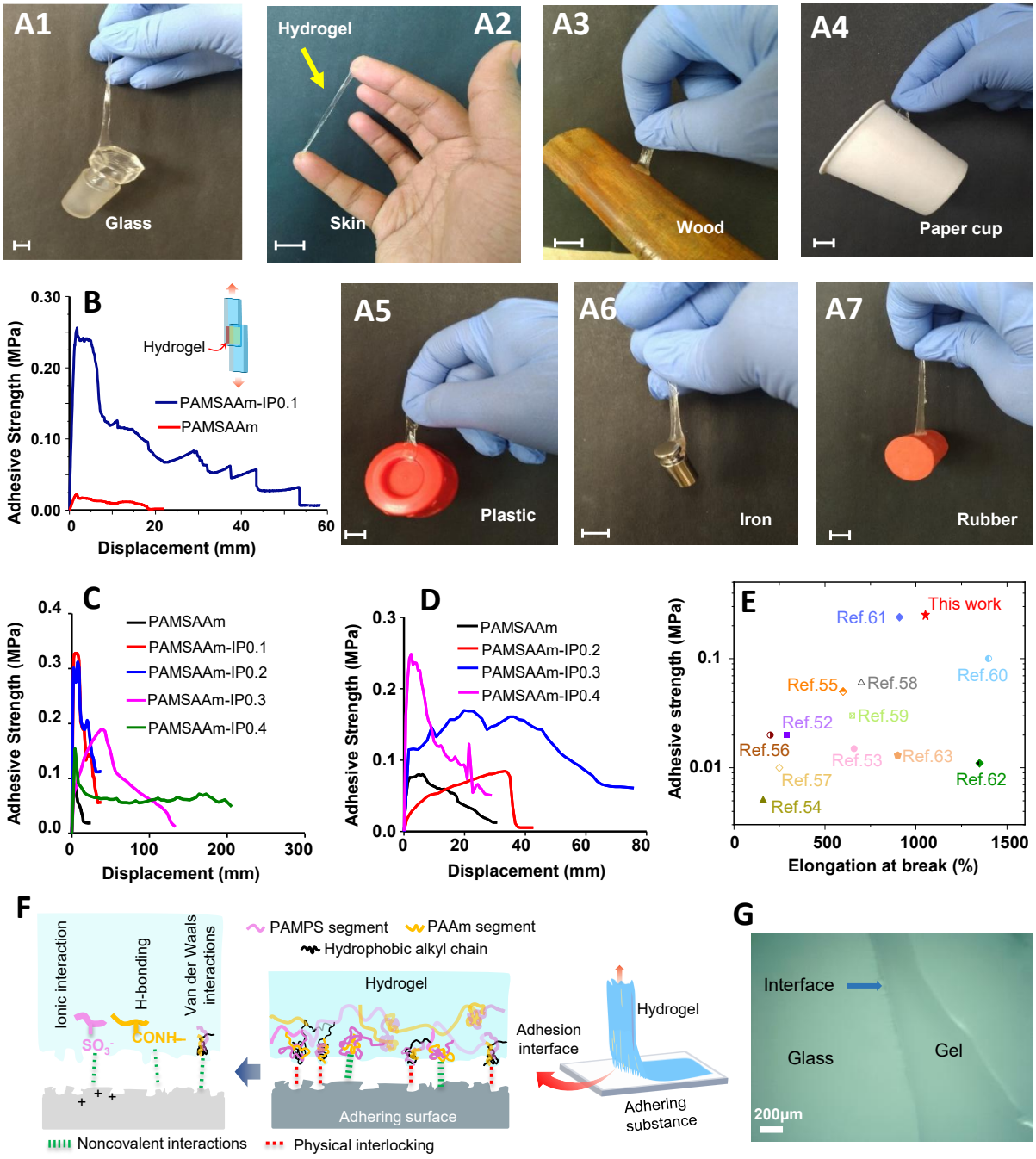

Figure 4.5: Demonstrations of adhesive properties of the PAMSAAm-IP0.1. Digital images of as-synthesized PAMSAAm-IP0.1 film adhered to different surfaces- A1) glass stopper, A2) human skin, A3) wood, A4) paper cup, A5) HDPE cap, A6) Stainless steel weight and A7) rubber stopper. B) Performance of PAMSAAm and PAMSAAm-IP0.1 under lap-shear adhesive test on glass surface. C) Self-adhesive performance of PAMSAAm film and other compositions

under lap-shear test, when both glass substrates having similar hydrogel samples attached to it. D) Performance of PAMSAAm-IP0.1 under lap-shear adhesive test on PAMSAAm and PAMSAAm-IP-n hydrogel surfaces, when PAMSAAm-IP0.1 is attached to one glass substrate and the other one is varied. E) Ashby plot of adhesive strength and elongation at break during tensile testing (in %) of PAMSAAM-IP0.1 with other reported hydrogel systems. F) Schematic illustration of the adhesion mechanism. G) Microscopic image of the interface between PAMSAAM-IP0.1 hydrogel and a glass substrate while the hydrogel is being peeled off. The scale bar for digital images is 1 cm.

The adhesion mechanism is anticipated to involve physical interlocking and various noncovalent interactions at the adhering interface between hydrogel and substrate surfaces. The AFM and FESEM data revealed an uneven surface for PAMSAAm-IP0.1 with phase segregated microdomains consisting of different polymeric segments distributed throughout the surface (**Figure 4.3**). These surface roughness and micro-features are known to increase effective surface area and enhance the adhesion ability with other surfaces through physical interlocking mechanisms.[273,274]Additionally, an abundance of ionic groups (from PAMPS segments) and polar functional groups (from both the PAMPS and PAAm segments) on the hydrogel surface further strengthen interaction with the adhering surface through various noncovalent interactions e.g.-ionic/hydrogen bonding, and Van der Waals interactions to induce adhesion (**Figure 4.5F**).[275,276] To further enhance the understanding of the adhesion mechanism, a microscopic image of the interface between the hydrogel and the adhering substrate was captured during the peeling process of the hydrogel from a glass substrate (**Figure 4.5G**). The appearance of stretched residual legs and associated micro-domain residues on the glass surface serves as evidence for the adhesion mechanism associated with microphase.

Subsequently, the low temperature viability of the hydrogel was evaluated in the temperature range of 0 to -15 °C **(Figure 4.6).** The samples retained adequate stretchability and flexibility in the studied temperature range. However, the extent of stretchability gradually decreased with a decrease in temperature (**Figure 4.6A**). A PAMSAAm-IP0.1 film folded, twisted and stretched without undergoing any visible damage supporting its ability to withstand different deformations necessary for further applications (**Figure 4.6B-D**). The film also adhered to various surfaces such as plastic, glass and polymers under low temperature conditions (**Figure 4.6E-G**). A PAMSAAm-IP0.1 thin film was installed to a knee joint anatomy model and the knee was folded and relaxed repeatedly at -15 ºC to observe the applicability of the sample for similar applications (**Figure 4.6H**). The operation was swiftly conducted without affecting the sample integrity. Overall, the above demonstrations supported that these hydrogel compositions may be effectively utilized under low temperature conditions. Further to understand the solvent retention ability of the hydrogel, a typical PAMSAAm-IP0.1 film with water content of ~50% was exposed to environment (temperature: 25 ºC, humidity: 40%) for several hours and the water content was monitored. The data revealed that over a period of 12 h, the loss in solvent content was limited to 12% only suggesting adequate water retaining ability (**Figure 4.6I**).

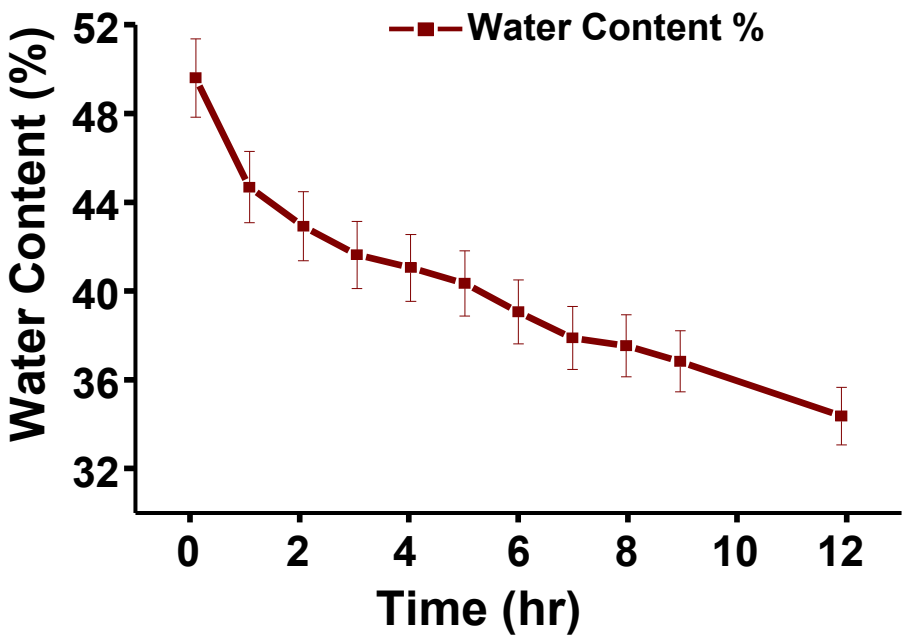

Figure 4.6I: Water content of PAMSAAm-IP0.1 hydrogel after 12 hr of air exposure, measured three times with different samples of the same composition.

Possibly, the evaporating tendency of IPA was subdued owing to the presence of water, as the boiling point of water-IPA mixture is known to be higher compared to that of the pure IPA.

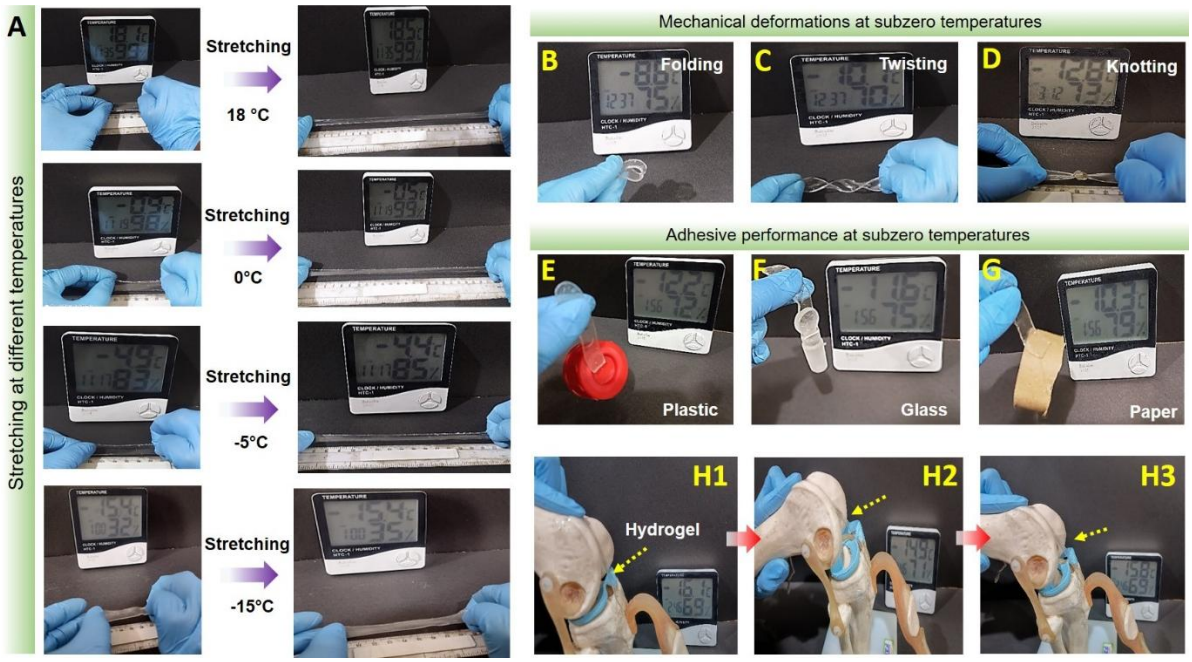

Figure 4.6: Performance of PAMSAAm-IP0.1 hydrogel under sub-zero temperatures, A) digital images of PAMSAAm-IP0.1 film demonstrating stretchability at different subzero temperatures, digital images of a PAMSAAm-IP0.1 film subjected to different mechanical deformations such as B) folding, C) twisting and D) knotting at sub-zero temperature, adhesive performance of PAMSAAm-IP0.1 sample at sub-zero temperature when adhered to E) plastic cap, F) glass stopper and G) paper, (H1-H3) digital images of a PAMSAAm-IP0.1 film attached to a knee joint model kept at -15 ºC and subjected to repeated bending and relaxing cycles, the temperatures are visible in the sensor screens behind the scenes.

Subsequently, machine learning approach was utilized to predict the hydrogel formulation with a desired tensile behavior. A total of 75 formulations and consequent mechanical properties were utilized for multi-target random forest regression (MTRFR) training and testing datasets (**Figure 4.7A-B, Scheme 4.1B, Table 4.2 and Figure 4.7I**).

Table 4.2: Table summarizing mechanical properties of different hydrogel formulations

	Pre-gel formulation					**Mechanical properties**	
Sl. No	**Solvent (mixed solvent in v/v ratio)**	**Solvent (mL)**	**AMPS (g)**	**AAm (g)**	**PEGDA (uL)**	**UTS (kPa)**	**Elong. at break (%)**
1	H_2O	1.5	0.45	0.45	2	75	250
2	H_2O: IPA 90:10	1.5	0.45	0.45	2	110	1050
3	H_2O:IPA 90:10	1.5	0.45	0.45	4	30	440
4	H_2O:IPA 90:10	1.5	0.45	0.45	8	50	265
5	H_2O:IPA 90:10	1.5	0.45	0.45	1	15	380
6	H_2O:IPA 80:20	1.5	0.45	0.45	4	35	450
7	H_2O:THF 90:10	1.5	0.45	0.45	2	40	230
8	H_2O:MeOH 90:10	1.5	0.45	0.45	2	70	185
9	H_2O:DMF 90:10	1.5	0.45	0.45	2	60	280
10	H_2O:EtOH 90:10	1.5	0.45	0.45	2	65	195
11	H_2O:BuOH 90:10	1.5	0.45	0.45	2	50	180
12	H_2O:IPA 95:5	1.5	0.45	0.45	2	55	430
13	H_2O:IPA 80:20	1.5	0.45	0.45	2	40	880

14	H_2O:IPA 70:30	1.5	0.45	0.45	2	42	700
15	H_2O:IPA 60:40	1.5	0.45	0.45	2	65	950
16	H_2O:IPA90:10	2	0.45	0.45	2	25	800
17	H_2O:IPA90:10	2.5	0.45	0.45	2	13	1150
18	H_2O:IPA90:10	1.5	0.45	0.308	2	12.5	580
19	H_2O:IPA90:10	1.5	0.45	0.154	2	6	910
20	H_2O:IPA 90:10	1.5	0.45	0.45	6	50	300
21	H_2O:IPA 85:15	1.5	0.45	0.45	1	20	270
22	H_2O:IPA 85:15	1.5	0.45	0.45	2	55	550
23	H_2O:IPA 85:15	1.5	0.45	0.45	4	80	450
24	H_2O:IPA 96:4	1.5	0.45	0.45	2	41	610
25	H_2O:IPA 96:4	1.5	0.45	0.45	4	40	215
26	H_2O:IPA 96:4	1.5	0.45	0.45	8	37	80
27	H_2O:IPA 94:6	1.5	0.45	0.45	2	40	640
28	H_2O:IPA 94:6	1.5	0.45	0.45	4	52	310
29	H_2O:IPA 94:6	1.5	0.45	0.45	6	45	155
30	H_2O:IPA 87:13	1.5	0.45	0.45	2	72	1030
31	H_2O:IPA 87:13	1.5	0.45	0.45	4	50	630
32	H_2O:IPA 87:13	1.5	0.45	0.45	6	48	230
33	H_2O:IPA 70:30	1.5	0.45	0.45	4	48	755
34	H_2O:IPA 70:30	1.5	0.45	0.45	6	35	600
35	H_2O:IPA 75:25	1.5	0.45	0.45	4	25	500
36	H_2O:IPA 80:20	1.5	0.45	0.45	4	48	800
37	H_2O:IPA 80:20	1.5	0.45	0.45	6	32	250
38	H_2O:IPA 92:8	1.5	0.45	0.45	2	42	1000
39	H_2O:IPA 92:8	1.5	0.45	0.45	4	44	420
40	H_2O:IPA 90:10	1.5	0.65	0.45	2	65	1000
41	H_2O:IPA 90:10	1.5	0.325	0.45	2	54	1150
42	H_2O:IPA 90:10	1.5	0.45	0.617	2	45	1110
43	H_2O:IPA 90:10	1.5	0.45	0.77	2	57	850
44	H_2O:IPA 90:10	1.5	0.131	0.45	2	40	790
45	H_2O:IPA 90:10	1.25	0.45	0.45	2	52	900
46	H_2O:IPA 90:10	1.75	0.45	0.45	2	32	1010
47	H_2O:IPA 65:35	1.5	0.45	0.45	2	16	270
48	H_2O:1PA 65:35	1.5	0.45	0.45	4	20	800
49	H_2O:IPA 65:35	1.5	0.45	0.45	6	22	350
50	H_2O:IPA 60:40	1.5	0.45	0.45	4	27	700
51	H_2O:IPA 60:40	1.5	0.45	0.45	6	26	600
52	H_2O:EtOH 80:20	1.5	0.45	0.45	2	74	325
53	H_2O:EtOH 70:30	1.5	0.45	0.45	2	39	382
54	H_2O:EtOH 60:40	1.5	0.45	0.45	2	26	430
55	H_2O:EtOH 80:20	1.5	0.45	0.45	4	59	105
56	H_2O:DMF 90:10	1.5	0.45	0.45	4	78	320
57	H_2O:DMF 80:20	1.5	0.45	0.45	2	48	410
58	H_2O:DMF 70:30	1.5	0.45	0.45	2	51	400
59	H_2O:THF 90:10	1.5	0.45	0.45	4	53	400
60	H_2O:THF 80:20	1.5	0.45	0.45	2	23	660
61	H_2O:THF 70:30	1.5	0.45	0.45	2	20	690
62	H_2O:IPA 90:10	3.5	0.45	0.45	2	5	30
63	H_2O:IPA 90:10	3.5	0.45	0.45	45	22	45
64	H_2O:IPA 90:10	4	0.45	0.45	4	6	700
65	H_2O:IPA 90:10	4	0.45	0.45	12	9	190
66	H_2O:MeOH 90:10	1.5	0.45	0.45	4	68	240
67	H_2O:MeOH 80:20	1.5	0.45	0.45	2	60	325
68	H_2O:MeOH 70:30	1.5	0.45	0.45	2	55	510
69	H_2O:BuOH 90:10	1.5	0.45	0.45	4	62	260

70	H_2O:BuOH 80:20	1.5	0.45	0.45	2	66	400
71	H_2O:BuOH 70:30	1.5	0.45	0.45	2	45	485
72	H_2O:BuOH 60:40	1.5	0.45	0.45	2	75	440
73	H_2O:MeOH 60:40	1.5	0.45	0.45	2	37	400
74	H_2O:DMF 60:40	1.5	0.45	0.45	2	53	440
75	H_2O:THF 60:40	1.5	0.45	0.45	2	22	1000

The strategy of machine learning training was to take a possible range of data points and split them into two parts: i.e. training set and test set. The training set was used to construct the model, where the MTRFR analyzes the data to establish a mathematical representation. A larger training set generally leads to a stronger and more reliable model, especially in regression tasks, where capturing the full range of data distribution is crucial to minimizing extrapolation errors and improving prediction accuracy.[277]

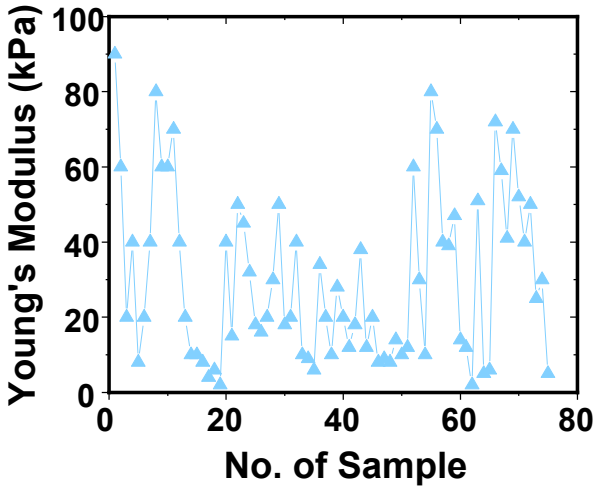

Figure 4.7I: Young's modulus of hydrogel samples utilized in the testing and training dataset.

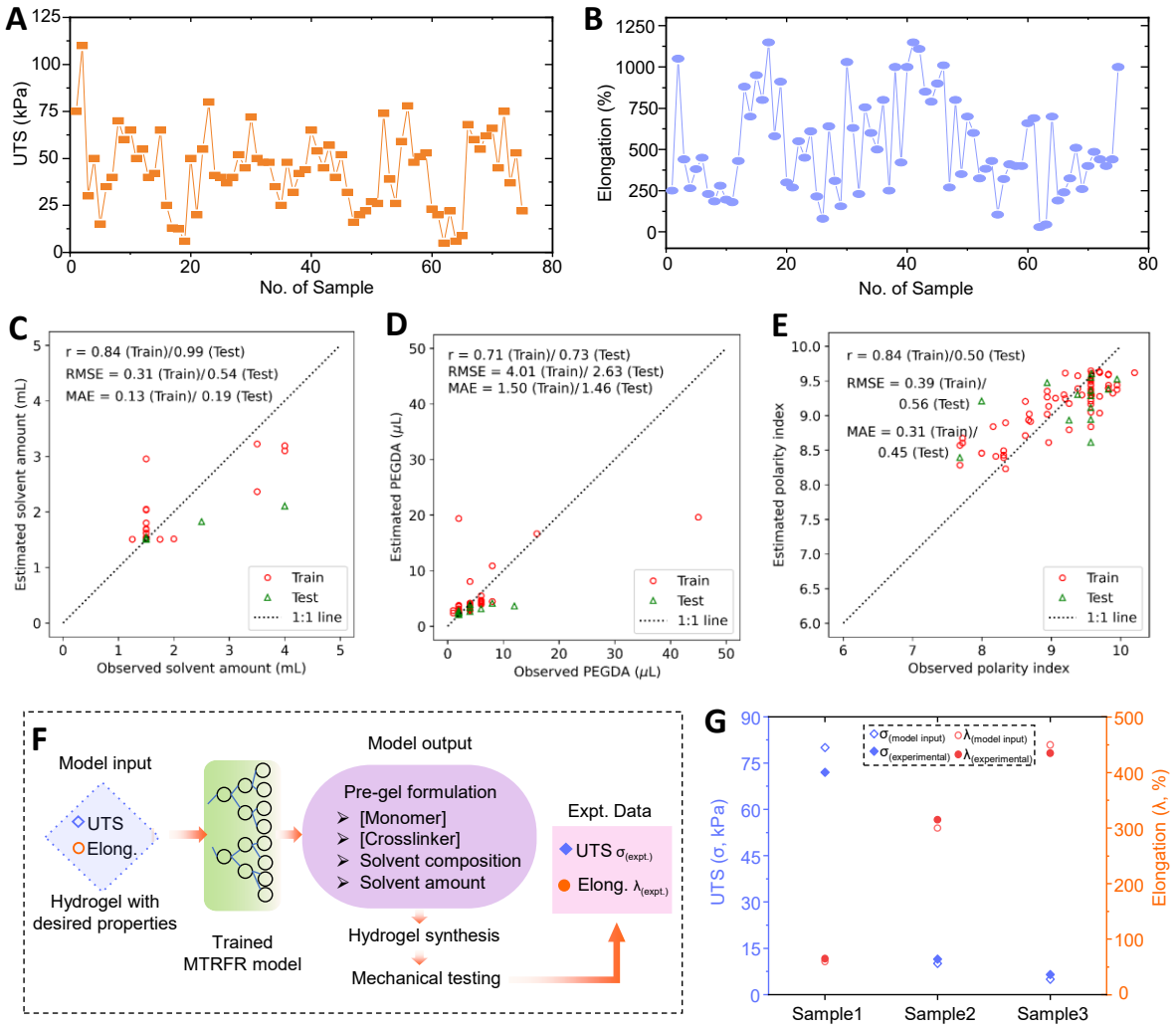

Figure 4.7: Machine learning (ML) tool to predict pre—gel composition for a hydrogel with desired physio-chemical properties. A-B) Plots illustrating UTS and elongation of the all hydrogel samples utilized as test and training data. The plots depicting ML model accuracy for different parameters C) Solvent amount, D) Crosslinker PEGDA concentration and E) Solvent polarity index. RMSE, MAE, r values and distribution of test and training data along the 1:1 line visualizes the accuracy of the ML model. F) Schematic illustration of a protocol to prepare a hydrogel with desired mechanical properties utilizing the prediction from the trained MTRFR model. G) Comparison of UTS and elongation values of the model input and the experimental data recorded on the resulting hydrogel.

Accuracies for predicting amount of PEGDA crosslinker (PEGDA), total solvent amount (Solvent_amount), and polarity of the solvent mixture (Polarity_Index) in both the training and testing datasets are illustrated in **Figure 4.7C-E** on a 1:1 plot. For the solvent amount in the pre-gel solution, the correlation was r = 0.84 (Train) and 0.99 (Test). Error estimates exhibited an RMSE of 0.3l mL (Train) and 0.24 mL (Test), along with an MAE of 0.13 mL (Train) and 0.19 mL (Test) (**Figure 4.7C**). However, it is important to note that at lower solvent amount (~1.5 mL) ranges, there were overestimations observed in the training results. At higher solvent amounts, underestimation of MTRFR is evident. Similarly, for the PEGDA crosslinker concentration in the pre-gel solution, the correlation was r = 0.71 (Train) and 0.73 (Test) (**Figure 4.7D**). Error estimates exhibited an RMSE of 4.01 µL (Train) and 2.71 µL (Test), along with an MAE of 1.50 µL (Train) and 1.46 µL (Test). The model also estimates one of the key parameters of the pre-gel formulation i.e. solvent polarity index. Solvent polarity index was theoretically calculated for different solvent mixtures including H_2O:IPA, H_2O:THF, H_2O:DMSO, H_2O:Ethanol etc. in various proportions. For this parameter, the correlation was r = 0.84 (Train) and 0.50 (Test) (**Figure 4.7E**). Whereas the RMSE of 0.39 (Train) and 0.56 (Test), along with an MAE of 0.31 (Train) and 0.45 (Test), estimate the error in model prediction. Although the distribution of the train and test data along the 1:1 line depicts a sound estimation by the used MTRFR model.

Finally, to verify the model accuracy and practical applicability, the authors intended to synthesise a hydrogel sample as per the model prediction and then compare the results **(Table 4.3).**

Table 4.3: Summary of the validation samples

Validation sample	Model input: desired hydrogel properties	Model Training data range	MTRFR predicted hydrogel formulation used for synthesis
Sample1	UTS: 80 kPa Elongation: 60%	UTS: 5-110 kPa Elongation: 30-1150 %	AMPS: 0.45 g AAm: 0.45 g PEGDA: 16 µL Solvent: 62.5 wt% H_2O:IPA: 90:10 (v/v)
Sample2	UTS: 10 kPa Elongation: 300%		AMPS: 0.45 g AAm: 0.45 g PEGDA: 2 µL Solvent:62.5 wt% H_2O:IPA: 75:25 (v/v)
Sample3	UTS: 5 kPa Elongation: 450%		AMPS: 0.45 g AAm: 0.45 g PEGDA: 8 µL Solvent: 81.6 wt% H_2O:IPA: 90:10 (v/v)

For a typical test, the input data set (with parameters UTS =10 kPa and elongation = 300%) was plugged into the above-trained MTRFR model, aiming for a stretchable hydrogel with such mechanical properties. Then a hydrogel (Sample 2) was synthesised as per the output parameters, having the predicted pre-gel formulation and the mechanical properties were analysed (**Figure 4.7F and 4.7J).**

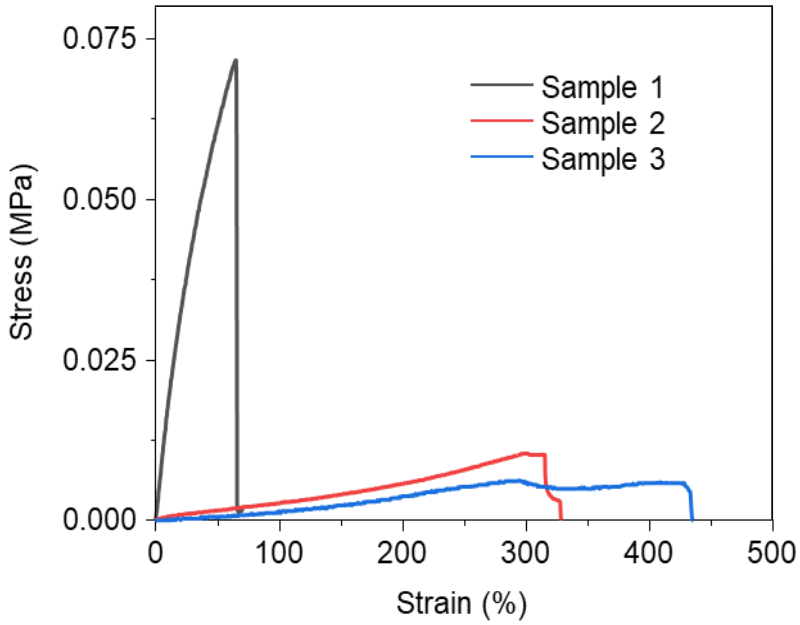

Figure 4.7J: Tensile traces of hydrogel samples prepared as per the machine learning predicted pre-gel formulation.

Figure 4.7G depicts the comparison of the UTS and elongation values of the resulting hydrogel (Sample 2) with the model input value. The result shows a comparable value even for the other two different instances (Sample 1 and 3), proving that model predictions are true. The selection of these validation samples (with specified range) was committed by ensuring comprehensive coverage of the variability in the predictor space of hydrogel formulations, which minimises the effects of covariate shift, improving the model's ability to generalise and produce reliable predictions across diverse test scenarios.[278] Although the model can further be improved with a big data set or by other predictive models like artificial neural networks to predict other physico-chemical properties like adhesion, polymer morphology. Thus, the work paves the way to integrate chemical and material science with today's data science and machine learning approaches.

4.5. Conclusion

Use of mixed solvents to tailor the polarity of the crosslinking medium offers a convenient and facile strategy to synthesise stretchable hydrogels based on dual monomer systems with adhesive and other functional behaviour. The solvent ratio may be controlled to vary the tensile behaviour and adhesive ability. A detailed surface mapping analysis reveals that the polarity of the medium governs the distribution of segments in the resulting hydrogel matrix and the morphology of the samples. The strategy is simple and may be extended to the synthesis of other dual/multi monomer single network hydrogel systems with tailored mechanical property behaviour. The samples are promising for low-temperature applications, unlike the conventional hydrogels based on pure H_2O. Machine learning may be utilised to predict the tensile behaviour of compositions based on their precursor ratio and other experimental parameters.

CNT Incorporated PAMPS/PAAm-Based Single Network Hydrogel for Strain Sensing Application

Table Of Content

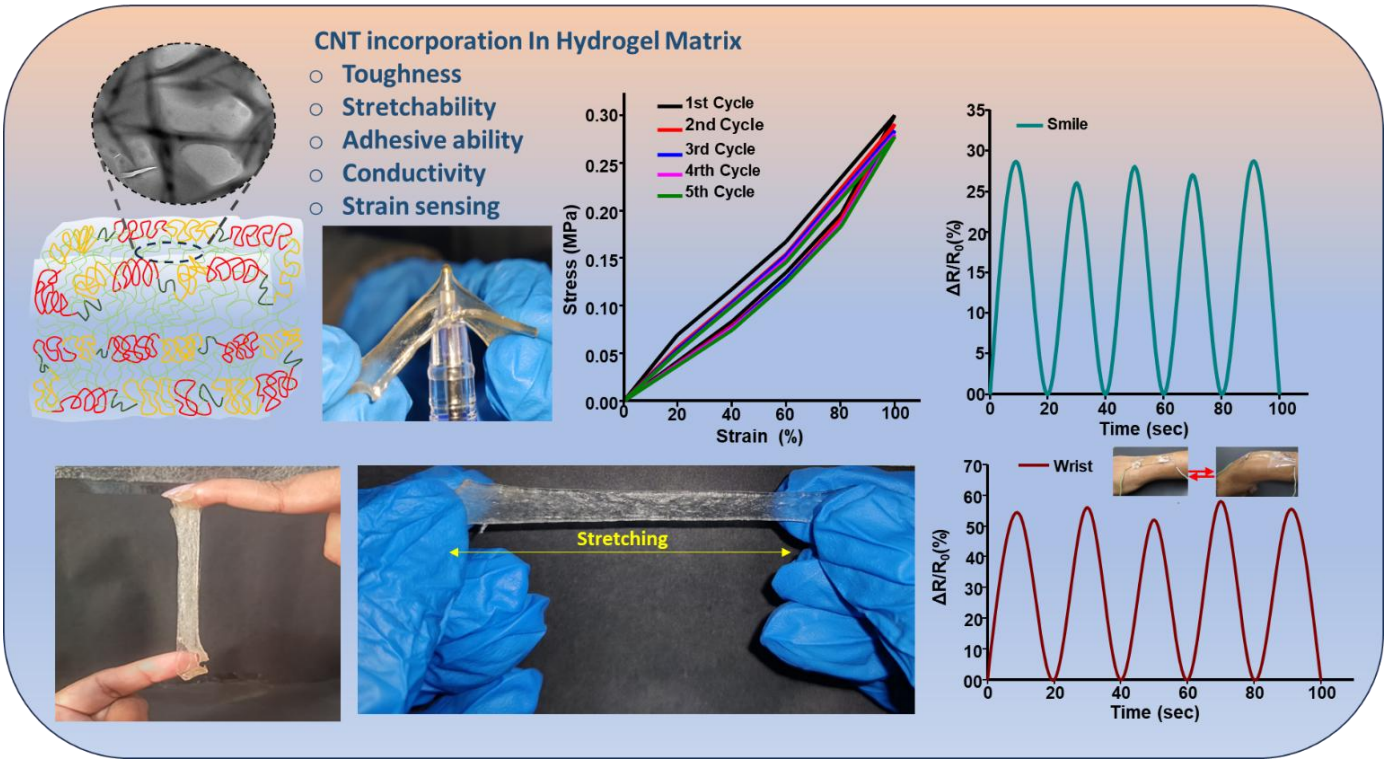

CHAPTER-V

5.1 Summary

A hydrogel matrix incorporated with carbon nanotube (CNTs) chains has modified microstructures observed via microscopic techniques. These changes in the structure of the hydrogel matrix lead to their tolerance ability in stress bearing and the strength of the hydrogels as compared to the CNT-free hydrogel. Tested for mechanical characterisation, CNT-reinforced hydrogels have prominent stretchability, toughness and tensile strength. With increasing the CNT amount, stress tolerance and energy dissipation also improved, indicating their dependence on CNT content. The formed hydrogel also shows excellent adhesive behaviour, conforming to some kind of interfacial bonding between CNT and polymer chains. This behaviour shows their possibilities towards flexible electronics applications. CNT in hydrogel make them conductive (~35S/m) with 2wt% CNT varying with CNT amount. This conductive nature of hydrogel enables them to monitor any change in resistance and sense the bodily movement, where any deformation induces a measurable change in resistance. The sensor exhibits repeatable change in signal output and supports its ability to be used as a strain sensor ($\Delta R/R_0$ (%) ~140). The combined effect of toughness, stretchability, strength, and adhesion, along with conductivity, enables the strain transduction with maintained integrity of structure on repeated loading-unloading cycles. From the above discussion, we concluded the CNT-incorporated hydrogel will be a suitable candidate for next-generation wearable sensors, flexible soft-robotics designs, and IoT interface applications as it represents a class of material with mechanical robustness, strong adhesion and strain-responsive behaviors.

5.2 Introduction

Incorporation of CNT in the hydrogel matrix enhances its mechanical strength, flexibility and conductivity all in one step and also provides some adhesive strength to the surface. Due to all

such reasons, the CNT incorporated hydrogel is the material used for wearable strain-sensing applications. CNT-reinforced conductive hydrogel is strain sensitive, can detect a large range of values (up to 1000%), and has a very low detection limit. It is also firm, can heal itself, sticks to things, and stays stable in a harsh environment. Using this technique to develop a wearable strain sensor that can track body motion even in harsh conditions.[279] One-pot synthesis approach made it easy and fast to synthesise a CNT-loaded conductive graphene-based hydrogel applicable for sensing, catalysis, energy, and environmental remediation, useful for soft actuation.[280] CNT dispersion can be used to develop a dual-crosslinked network design using TOCNs as dispersants for CNT and give mechanical support to the hydrogel system.[281] Porous CNT networks help ions transport and help membranes cling together, useful for flexible electrochemical sensors. CNT films can also be used as electrodes that can bend and stretch while still conducting electricity, suitable for soft wearable gadgets and bioelectronics that go on the skin[282]. When strain is applied to percolated CNT networks, their resistance changes. The way the network changes shape affects these changes. This is how CNTs are utilised in sensors for stretching and conducting[283]. There is a strong interaction between biopolymers and CNTs. This is why chitosan/CNT hydrogels are so robust and flexible, safe for living beings, and able to fight germs. This is why they are helpful for health care and wearables that can sense human motion[284]. A supercapacitor made from biomass with cellulose hydrogel electrolytes and lignosulfonate/SWCNT hydrogel electrodes is incredibly flexible, has high capacitance, and works well in repeated deformation, good for wearable gadgets[285]. Hyaluronic acid/single-walled carbon nanotube hybrid crosslinked microfibers are exceedingly robust, stable, and durable. These microfibers are very promising for biomedical devices that are implanted, artificial muscles, and bioactuators. CNTs provide it strength and the ability to hold electricity, which might be incredibly helpful for health-monitoring devices,

wearable electronics, and electronic skin[286]. Use of organohydrogels and conductive hydrogels to sense strain, gas, humidity, and temperature. Organohydrogels are more stable over time, dry and freeze better, and are more sensitive than normal hydrogels[287]. CNT-based conductive hydrogels and composites can be used in bioelectronics, soft robotics, and devices that can be worn or implanted. Adding CNTs makes things far better at carrying electricity, lasting longer, not breaking down, and being safe for the environment. These materials make it possible to have a dependable sensing, actuation, and biological interface. Because of this, CNT-hydrogel devices that can be bent and implanted within the body could be the next big thing in medical electronics[288]. Some studies discussed about the safety, chirality control, and scaling issues of carbon nanotubes (CNTs) as they become key materials for flexible electronics, wearable sensors, energy conversion, and multifunctional composites of the next generation[289]. The CNC-mediated A-MWCNT–reinforced double-network hydrogel has excellent stretchability, durability, and sensitivity since it has dynamic bonds, utilised in flexible electronics and wearable strain sensors. Introduction of a multifunctional PAAm/SA/CNT double-network hydrogel for remote actuation and low-temperature strain sensing. Freeze-thawing method is used to synthesise a PVA/SA hydrogel sensor with added bacterial cellulose. They can sense strain and pressure in two ways for a long time. The hydrogel reacts to both mechanical and electrical signals at the same time.[290],[291] The chitosan-CNT-based hydrogel was freeze-lyophilised, has a high porosity (>94%) and higher antibacterial activity that gets better as the CNT concentration goes up. For CNT-hydrogel strain sensors, the CNTs need to spread out evenly and form strong mechanical networks. One good choice is to use dual-crosslinked network designs that use nanomaterials like TEMPO-oxidised cellulose nanofibers (TOCNs) as both CNT dispersants and mechanical reinforcements[292].The main electromechanical sensing mechanism that makes CNT-based stretchable conductors operate

is based on variations in resistance that rely on strain and are regulated by changes in the network. Changes in resistance in percolated CNT networks are largely induced by strain. This is the basic arrangement for electromechanical sensing systems that let you keep track of strain in sensors and stretchable conductors[293] with great accuracy. Advanced conductive network topologies improve sensing even further. A dual-network hydrogel consisting of PAAM and SA, carbon nanotubes (CNTs) and polypyrrole (PPy) makes the material particularly sensitive to stress[294]. An exceptionally stretchable, conductive and strong material is synthesised by introducing sulphur-containing CNT useful in epidermal electrode ECG monitoring, EMG monitoring. Similarly, a laponite nanoclay and poly(N-isopropylacrylamide) (PNIPAM) based system has exceedingly robust behaviour, heals quickly, conducts electricity slowly, and is sensitive to changes in temperature and strain. The double-network hydrogel strain sensor works well at any temperature and uses SiO_2 nanoparticles[295]. Nanocellulose and chitosan have made the PVA/MXene/graphene (PMG) conductive hydrogel stronger. These hydrogel has potential for flexible strain sensors and smart sports apps[296]. Conductive hydrogels and composites created with CNTs have come a long way in bioelectronics, soft robotics, and wearable or implantable gadgets[297]. Biopolymers and CNTs perform well together, which makes it possible to develop sensors that are safe for living things. Chitosan/CNT hydrogels are particularly strong and elastic as they have a strong interaction between biopolymers and CNTs. The electrodeposited CNT-chitosan hydrogel anode has greater electrochemical activity, as it has more power and current density[298]. This demand for wearable and flexible electronic devices required soft material with high stretchability, mechanical strength, electrical conductivity, and durability under various conditions. Their three-dimensional network structure contains a large amount of water, has a tissue-like softness, biocompatibility and attaches to human skin easily. To increase the strength of the hydrogel, CNT-incorporated hydrogels have

attracted attention as CNTs provide better electrical conductivity, high aspect ratio, and mechanical strength. A key challenge is their strong interfacial interaction between CNTs and the polymer matrix and weak adhesive nature leads to CNT aggregation, mechanical failure and disturbance in signal output under repeated stretching.

In this work, we design a CNT-incorporated hydrogel system based on loosely bound polymer networks of PAMPS and PAAm segments. CNT chains are dispersed well in their matrix. By the interfacial engineering method, these hydrogels have enhanced toughness, adhesion to different surfaces (including glass, skin, metal, plastic and rubber), and excellent stretching and maintained electrical conductivity. CNT incorporation not only enhances the polymer network but also supports an effective pathway for strain-dependent resistance changes. This ability makes the system capable of reliable strain sensing over a wide deformation range. Mechanical testing and adhesive study reveal that hydrogel can survive at harsh conditions without getting deformed and without leaving any residue on the substrate surface, indicating their reusability and long shelf-life. Also, these hydrogels have practical applications in strain sensing and wearable electronics device fabrication. By combining both the mechanical and electrical properties, these hydrogels can be used to design soft, conductive, and adhesive hydrogel systems, highlighting their use for next-generation wearable sensors, artificial skin, and bioelectronic interfaces.

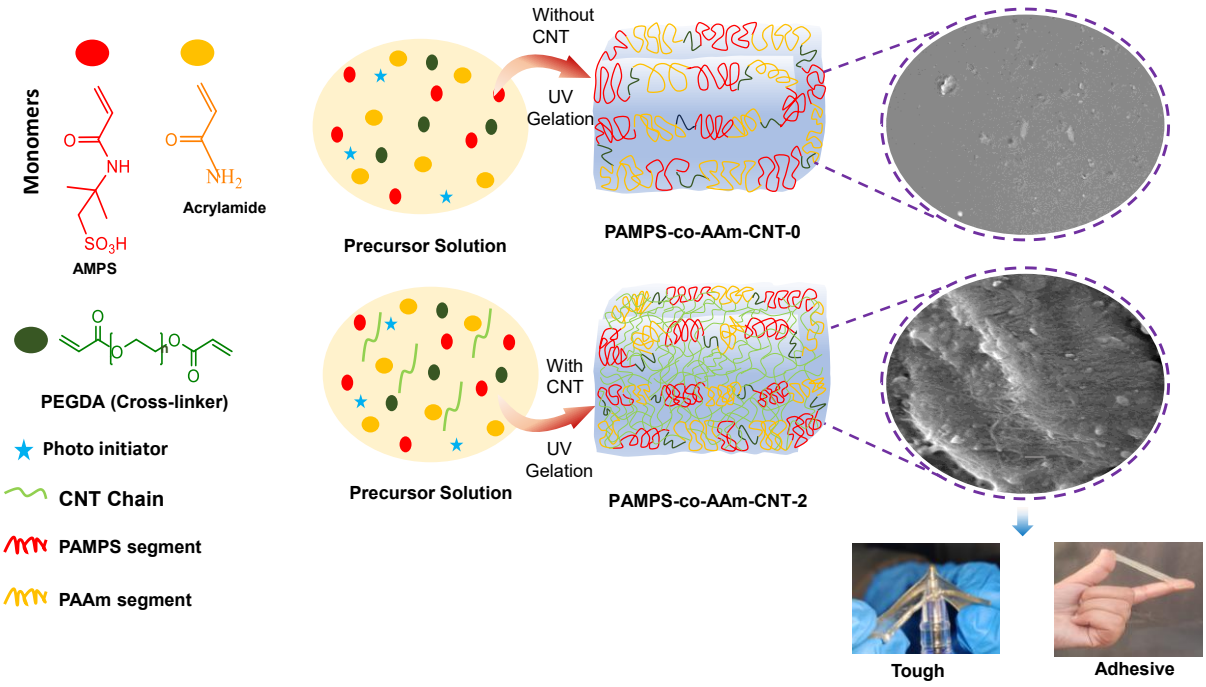

Schematic 5.1: The schematics showing the synthetic procedure of AAmCNH-0 and AAmCNH-n hydrogel film and possible morphological differences on CNT incorporation

5.3 Synthetic Procedure of AAmCNH0-n hydrogel film:

The complete synthetic procedure was explained in Chapter 2, Section 2.1.4.

5.4 Results & Discussion

To confirm the presence of CNT inside the hydrogel matrix and its proper mixing with other polymer components, several spectroscopic techniques were used. Raman spectroscopic data of AAmCNH-n appeared around D-band (~1350cm-1) and G-band (~1580cm-1), confirming the in-plane stretching of sp^2 carbon atoms and graphitic structure and crystallinity of CNTs[299], which is not present in the sample without CNT (AAmCNH-0) **(Figure 5.1A).** Also, a change in the intensity ratio indicates the proper CNT dispersion and interaction to the hydrogel matrix**.** The

XRD pattern of the hydrogel showed a broad spectrum, indicating a predominantly amorphous network. On CNT introduction certain change in the diffraction pattern appeared, displaying its partial alignment in the hydrogel matrix. Also, absence of any sharp peak confirmed proper distribution of CNT inside the hydrogel matrix rather than aggregation. This phenomenon supported a homogenous network and compact morphology. A peak at 2θ=20.23°, corresponding to the (002) plane was obtained . In case of the CNT-incorporated AAmCNH-2 film, the Bragg diffraction peak of PAMPS-PAAm-MWCNTs at 2θ=25.72° was retained[300] **(Figure 5.1 B).** To further verify XRD results, HR-TEM images of CNT dispersion were drop-cast on the grid of the instrument and dried overnight. Analysis showed the rod-like structure with rough surface and hollow centres of carbon nanotubes dispersed in precursor media. The scattering pattern displayed the appearance of a crystalline-like pattern, and the distance between them was calculated to be at 3.46A°, corresponding to the (002) plane[301] **(Figure 5.1 C1-C12).** There is a possibility of some additional interactions, like hydrogen bonding, ionic interactions and CNT-induced physical entanglement responsible for a denser and more interconnected network **(Schematic 1)**. FE-SEM image of completely swelled followed by freeze-dried AAmCNH-n hydrogel samples, shows morphological differences in the structures. The hydrogel sample with 2wt% CNT (AAmCNH-2) shows some uniform thread-like arrangement in the matrix, confirming the structural support of CNT in the mechanical strength, as it enhanced the interaction between polymer segments[302] **(Figure 5.1 F1).** The hydrogel sample with a lower concentration of CNT in the matrix shows slightly thick folding in the matrix, possibly due lesser amount of CNT **(Figure 5.1 E1).**

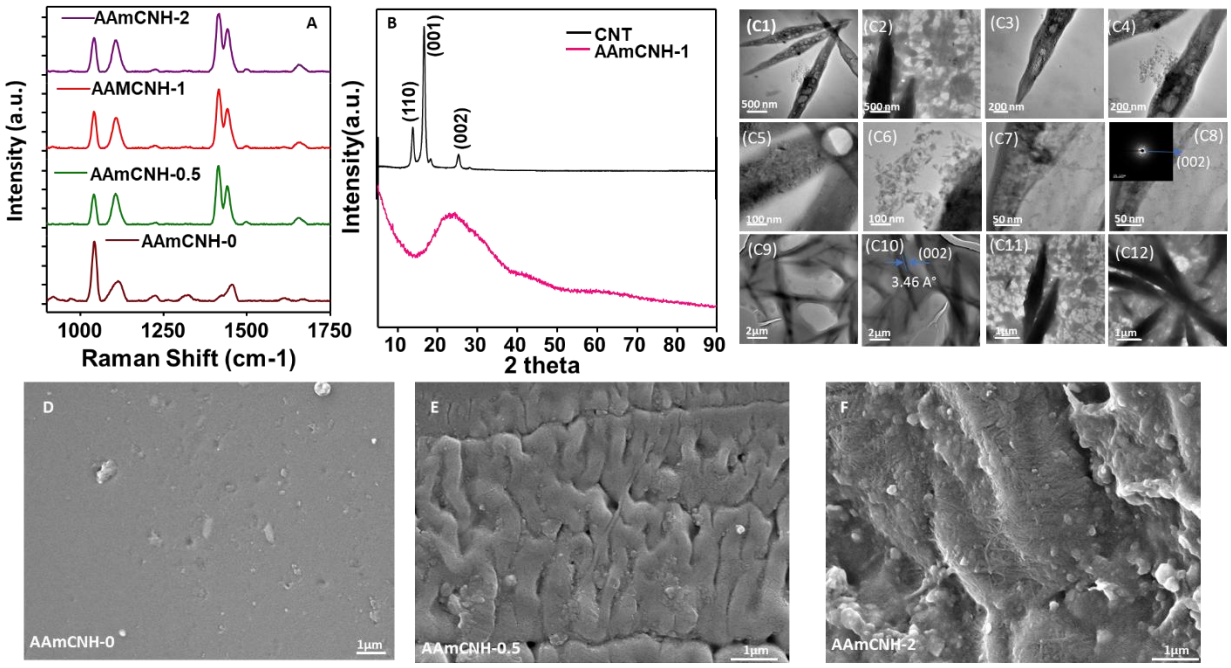

Figure 5. 1: (A) Raman data of AAmCNH-n and AAmCNH-0 hydrogel film, (B) XRD spectra of CNT dispersion and AAmCNH-2 film, (C) HR-TEM images of CNT dispersion to check the structure of CNT particles, FE-SEM image of freeze-dried (D) AAmCNH-0 film, (E) AAmCNH-0.5 film, (F) AAmCNH-2 film, based on the concentration of CNT in hydrogel matrix

On the other hand, hydrogels with only polymer segments do not have any such folding in the hydrogel matrix, concluding the effect of CNT in improving the physical property of the hydrogel **(Figure 5.1 D1).**The mechanical performance of as-synthesised AAmCNH-n hydrogel was studied. Hydrogel film with 2 wt% CNT (AAmCNH-2) displayed ultimate tensile strength (UTS) value of 0.76 MPa with stretchability (Є) up to ~388 % **(Figure 5.2A).** Similarly, films with a lower concentration of CNT in the matrix show lower values of mechanical strength and elongation %. Particularly, film with 1 wt% and, 0.5wt% CNT displayed UTS values of 0.88MPa at elongation % up to ~467 % and 0.47MPa at elongation up to ~387%, respectively. Also, the control sample

without any CNT incorporation showed a maximum strength (UTS) value of 0.62MPa at elongation % up to 156%. Suggesting the effect of CNT introduction on the mechanical strength and elongation % of hydrogel films. **(Figure 5.2A).** Hysterisis data was taken from a rectangular hydrogel film. The narrow nature of the hysteresis plot indicated the elastic behaviour of the film up to a maximum elongation % of 250% and the obtained UTS value was 0.30MPa. **(Figure 5.2B)** The rectangular hydrogel film was taken and stretched up to a certain limit **(Figure 5.2 C1 & C2).** A knot was put on the hydrogel film and stretched, showing the fatigue behaviour of the hydrogel **(Figures 5.2 D1 & D2).** Also, the film was twisted and stretched up to a certain extent **(Figures 5.2 E1 & E2).**

These deformations of the hydrogel film confirmed the toughness of the hydrogel film and opened a window for its capabilities to be used as wearable and flexible sensors.

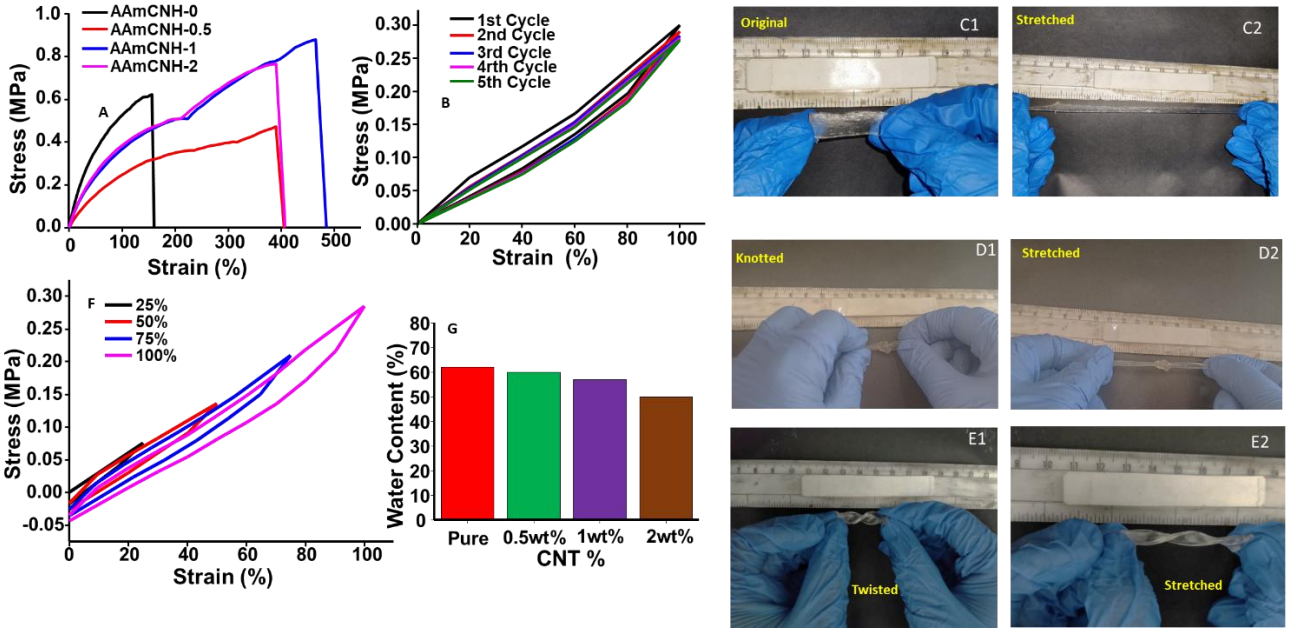

Figure 5.2: A) Tensile traces of AAmCNH-n hydrogel films . B) The cyclic tensile hysterisis plot of as-synthesised AAmCNH-2 hydrogel film C1) Digital images of unstretched AAmCNH-2

hydrogel film, C2) Digital images of stretched AAmCNH-2 hydrogel film, D1) Digital images of AAmCNH-2 hydrogel film having knott. D2) Digital image of knotted & stretched AAmCNH-2 hydrogel film. E1) Digital image of twisted AAmCNH-2 hydrogel film E2) Digital image of twisted-stretched AAmCNH-2 hydrogel film. F) Hysterisis plot of AAmCNH-2 hydrogel film at different limiting strains. G) Percentage water content plot of AAmCNH-n hydrogel films.

The film also tested for other deformations as pinching against the tip of the pen, and came out without any rupture in the hydrogel film **(Figure 5.3A).** The film showed transparency as it reflected the written letters **(Figure 5.3B).** The hydrogel film can also survive the load, as demonstrated when a load of 30g was hung on the hydrogel film **(Figure 5.3C).** Comparative data was plotted about the mechanical behaviour of the hydrogel film with 2wt% CNT (AAmCNH-2). The obtained UTS, elongation % and Young's modulus were 0.8MPa, ~500% and 0.99 MPa, respectively. The hydrogel film also showed the conductivity of around 100S/m **(Figure 5.3D)**. The mechanical properties of AAmCNH-2 hydrogel were compared with previously reported work, and it was superior to others **(Figure 5.3E).** The comparison of UTS, stretchability and Young's modulus was entirely an indication of its better achievement as a suitable material for strain sensing application **(Table 5.1)**.

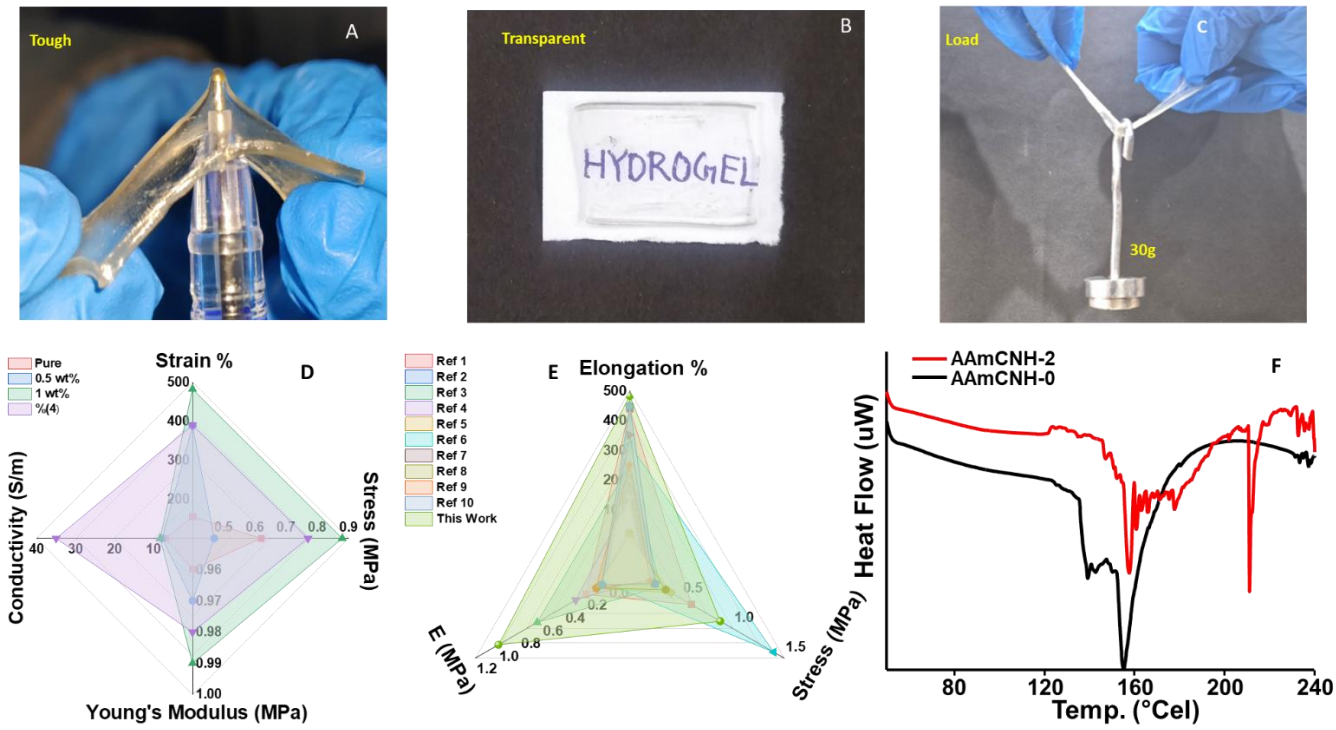

Figure 5.3:A) Digital image of AAmCNH-2 hydrogel film pinched against the tip of the pen to check the toughness, B) Digital image of AAmCNH-2 hydrogel film to check the transparency of film, C) Digital image of AAmCNH-2 hydrogel film showing its load bearing ability, D) Radar plot showing the mechanical strain, stress, young's modulus and conductivity of AAmCNH-2 film, E) Ashby plot comparing the mechanical performance of AAmCNH-2 hydrogel with previously reported literature, F) DSC plot to check the thermal stability of AAmCNH-n films.

DSC analysis is one of the most common methods for the determination of the network arrangement of polymer materials. The DSC profile of the AAmCNH-n samples showed a large melting peak at around 160°C for PAMPS/PAAm hydrogels and at around 155°C for CNT, indicating the significant influence of CNTs for the crystallisation of polymers **(Figure 5.3F).** The reason for this increased crystallinity of the nanocomposite hydrogels as CNT acts as a nucleation

site for the polymer-carbon nanotube interactions. The results show that the incorporation of CNT was successfully achieved.[303]

Table 5.1: Comparison table of UTS, Stretchability and Young's Modulus of AAmCNH-2 and previously reported hydrogel systems

S.No.	**Sample Code**	**% Ɛ**	**Stress (MPa)**	**E (MPa)**	**Adhesive Strength (MPa)**	**Reference**
1.	PMI-3	438	0.6	0.2	No	R[304]
2.	PAM/CS/PPy@PDA/TA-0	444	0.25	0.01	Yes	R[305]
3.	Gel-Alg-20-2.0-Ca^{2+}-EDC	250	0.3	0.64	Yes	R[306]
4.	MBBA-hydrogel	140	0.16	0.29	No	R[307]
5.	Rehydrated CNFs	12	0.4	0.10	No	R[308]
6.	PAAm	318	1.4	0.02	Yes	R[309]
7.	PA-T1.5	350	0.23	0.06	No	R[310]
8.	PEDOT: PSS hydrogel	20	0.35	0.1	No	R[311]
9.	Sensor hydrogel	250	0.20	0.11	No	R[312]
10.	C/P-0.4/N	450	0.25	0.05	Yes	R[313]
11.	**AAmCNH**	**482**	**0.88**	**0.99**	**Yes**	**This work**

The AAmCNH-2 has different conformal contact with irregular surf[314]aces, confronting high-aspect ratio of CNT networks that possibly created mechanical interlocking, load transfer, and

crack resistance across interfaces. Schematics showed the stretching of two hydrogel sticks together and separated while stretched in different directions **(Figure 5.4A).** The AAmCNH-2 displayed adhesive strength of 0.37 MPa on the glass surface, superior to that of the AAmCNH-0 (MPa). The remaining hydrogel films displayed the adhesive strength in the range of 0.06 to 0.31 MPa **(Figure 5.4B).** The sample synthesised using 2wt% of CNT displayed a maximum adhesive force of 0.56 N up to an elongation % of ~ 293.6%**.** The rest of the hydrogel film showed the adhesive force in the range of 0.087 to 0.46 N up to elongation % in the range of ~20 to 176 % **(Figure 5.4C)**. The hydrogel film was tested for adhesion to the human skin. It leaves no residue after peeling off from the skin **(Figure 5.4 D1-D4).** The digital photographs of adhesion of hydrogel were taken for different surfaces, including metal, skin, glass, plastic, wood, and cardboard **(Figure 5.4 E1- E6).**

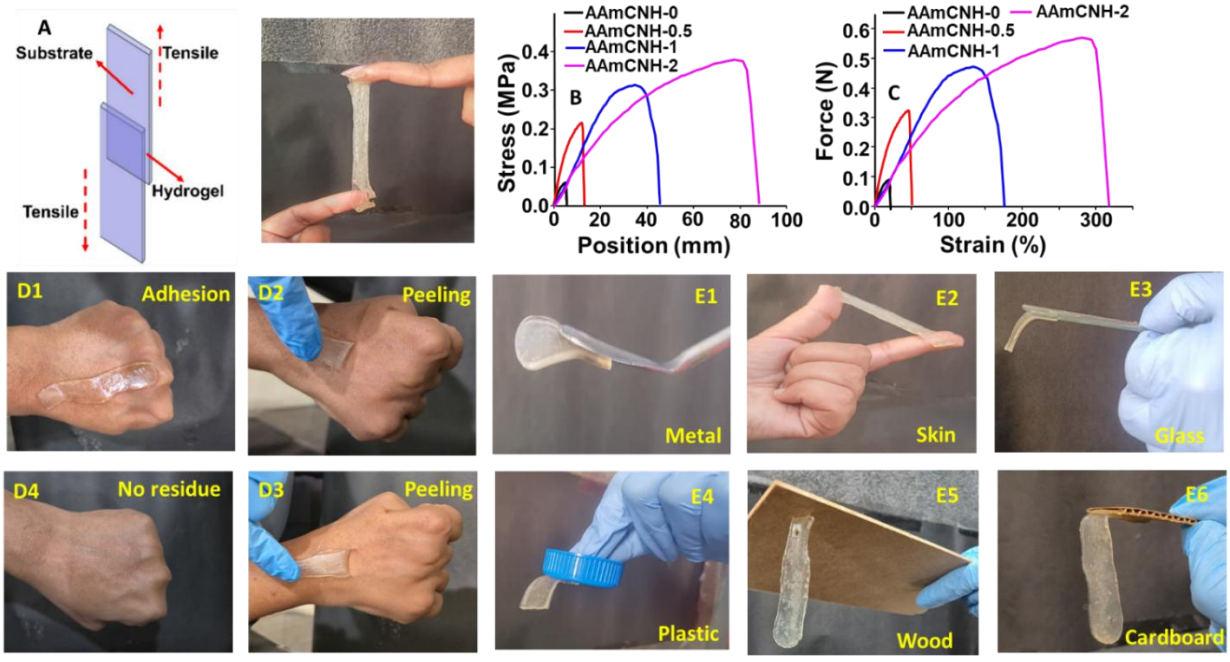

Figure 5.4: A) Schematic showing hydrogel tearing sandwiched between two glass slides & digital image of adhesion on human skin, B) Adhesion plot of the AAmCNH-n hydrogel film, C) Adhesion plot of the AAmCNH-n hydrogel film displaying the change of adhesive force with

strain change, The macroscopic peeling test for AAmCNH-n hydrogels on human skin, D1) Adhesion on the human skin, D2) Partial peeling on human skin, D3) complete peeling of human skin, D4) Human skin leaving no residue, Digital images of as-synthesized AAmCNH-2 film adhered to different surfaces- E1) metal, E2) human skin, E3) glass, E4) plastic cup, E5) wood, and E6) cardboard.

The mechanical stability of hydrogel film AAmCNH-n and adhesive behaviour were complemented by the conductivity, making it better suited for flexible strain sensing applications. The film was attached to a copper wire through copper tape and then connected to a multimeter **(Figure 5.5 A).** These arrangements were made for the measurement of the change of resistance at different deformations and to sense different bodily movements.

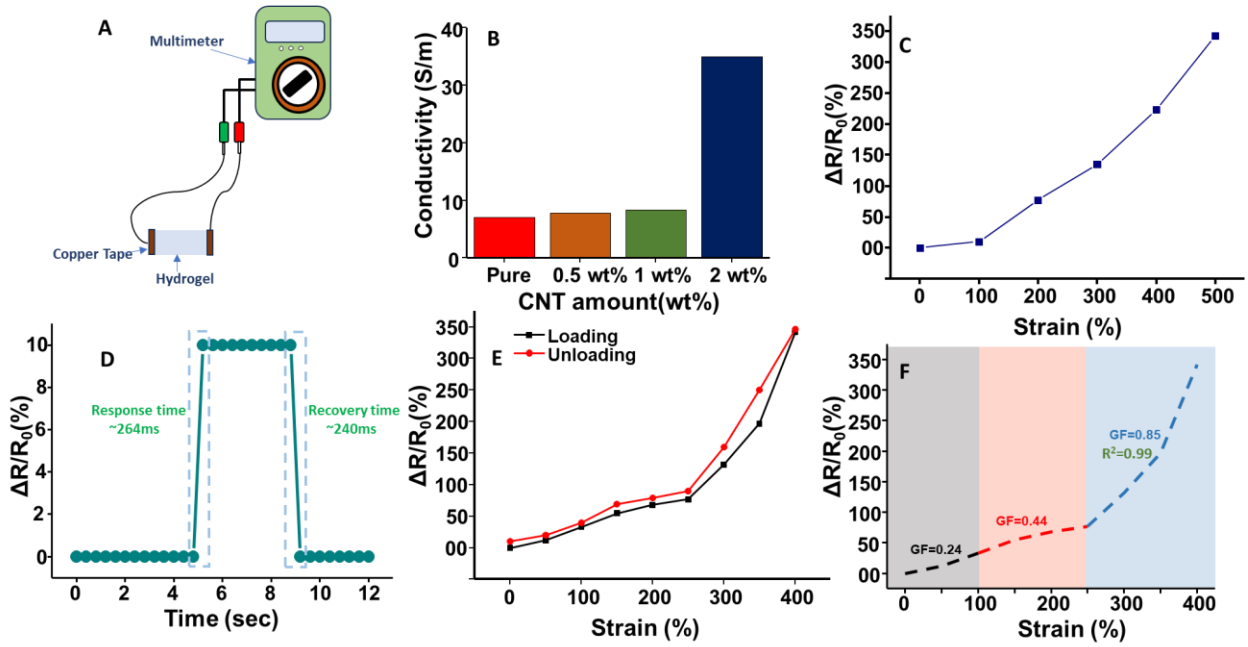

Figure 5.5: A) The schematics showing the experimental set-up utilised to monitor strain sensing data, B) The conductivity data of AAmCNH-n films measured at EIS study, C) the $\Delta R/R_0$ (%) values obtained at each extension, D) the response and recovery time of AAmCNH-2 film at each

extension and relaxation cycle, at a machine speed of 10mm/min, E) the $\Delta R/R_0$ (%) values obtained at each extension for forward and reverse extension cycle, F) plot of GF variation with change of extension.

The hydrogel samples were also tested for ionic conductivity from the EIS spectra by sandwiching the hydrogel between two copper plates. Based on the amount of CNT in the hydrogel matrix, the maximum conductivity obtained was 35 S/m with 2wt% CNT. The remaining hydrogel samples varied in the range of 17 S/m to 10 S/m with a changing amount of CNT from 1wt% to 0.5wt%. The sample with no CNT has the lowest conductivity of 7.5 S/m **(Figure 5.5 B)**. The strain-sensing ability of the AAmCNH-2 film was measured by recording the $\Delta R/R_0$ (%) values at different stretching conditions. The value of $\Delta R/R_0$ (%) increased with stretching extent. At 500% elongation, the value reached ~ 350, supporting their possibility to be used as a suitable material for strain-sensing applications **(Figure 5.5C).** Response time and recovery time[23],[24] were approximately ~264 ms, and ~240 ms, respectively, and showed correspondence with other systems previously reported in literature **(Figure 5.5D).** The loading-unloading of the hydrogel film was carried out, and the change in resistance was observed. The $\Delta R/R_0$ (%) value changes till 350 at ~500% elongation and is almost recoverable when the load is removed **(Figure 5.5E).** The change of gauge factor was also recorded with a change in elongation. The GF value was around 0.24 at around 100% elongation, and the maximum GF value was recorded around 0.85 at ~350% elongation[315]**(Figure 5.5F).**

The AAmCNH-2 hydrogel can detect conductive signals under different strains (50-250%), demonstrating excellent stability, which suggests the hydrogel sensor has reproducibility and sensitivity over a wide strain range. The $\Delta R/R_0$ (%) value observed was 15 at 50% elongation and ended up to 140 at an elongation % of 350% **(Figure 5.6A).** Repeated cycles of hydrogel film were

carried out at different elongation % to check the recyclability of the hydrogel film, which ensured the suitability of the hydrogel as a strain sensor. The maximum $\Delta R/R_0$ (%) value observed was 70 at elongation up to 200% **(Figure 5.6B).** Additionally, the stability and durability of strain sensors are critical parameters for long-term applications.

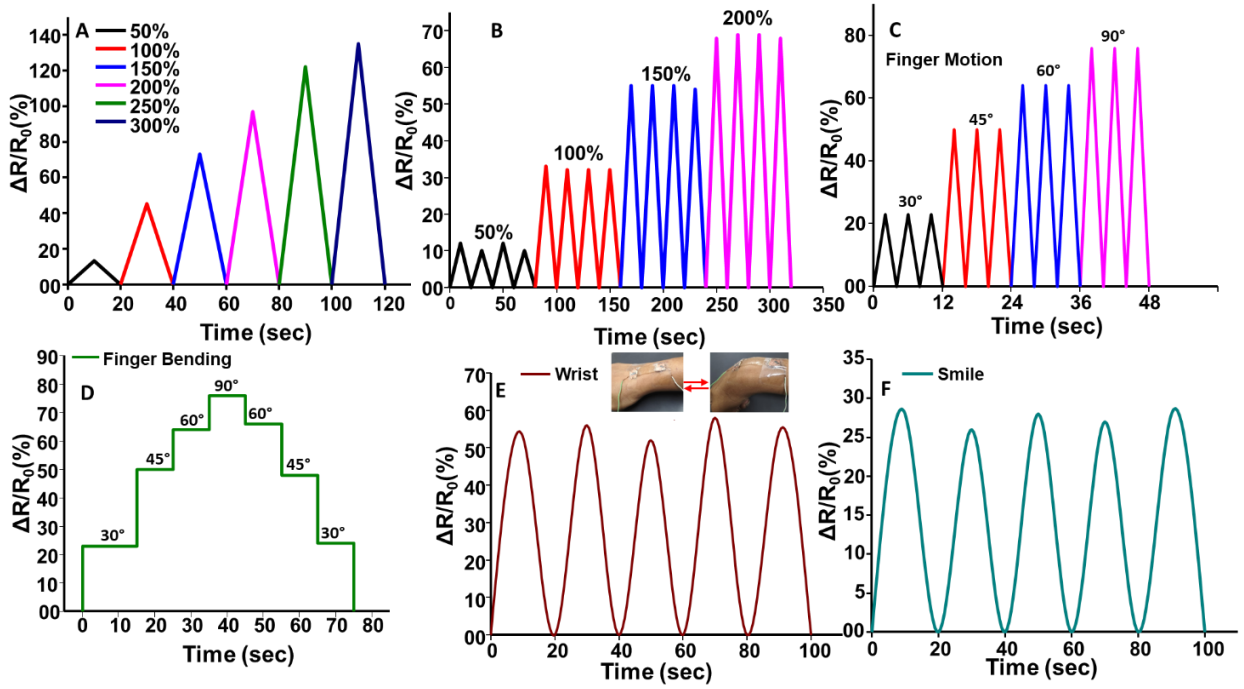

Figure 5.6: A) The $\Delta R/R_0$ (%) data of AAmCNH-2 film at different extensions, B) the $\Delta R/R_0$ (%) data of AAmCNH-2 film measured for three continuous cycles at a particular extension, C) the change in $\Delta R/R_0$ (%) values associated with the film of AAmCNH-2 measured for three continuous cycles at different bending angles of the index finger, D) the change in $\Delta R/R_0$ (%) at extension and relaxation of AAmCNH-2 at different bending angles of index finger, the change in $\Delta R/R_0$ (%) values associated with the film of AAmCNH-2 of five consecutive bending and relaxation cycles of (E) wrist and (F) smile.

Overall, the study supported the utility of hydrogel film for strain-sensing applications. A uniform AAmCNH-2 film was installed on various body parts, and the bodily motions were monitored.

The film attached to the index finger displayed a gradual increase in $\Delta R/R_0$ (%) from 20 to 80 for various bending angles of 30° to 90° of the finger, suggesting the utility of films to observe partial and full bending motion of the finger **(Figure 5.6D).** Subsequently, cycles of bending and relaxing of the index finger were performed at different bending angles, and the change in resistance $\Delta R/R_0$ (%) values was recorded from 25 to 80 **(Figure 5.6C).** Similarly, the film attached to the elbow showed $\Delta R/R_0$ (%) = 55 and smile $\Delta R/R_0$ (%) = 32 also effectively measured the bending motion of the part by displaying specific and repetitive $\Delta R/R_0$ (%) values supporting the viability of the systems for possible skin sensing applications **(Figure 6E-F).** The study supported that the AAmCNH-n films may be a possible candidate for sensing different body movements.

5.5 Conclusion

The work focused on the role of carbon nanotube (CNT) on the mechanical performance of the incorporated semi-network (SN) hydrogel designed for flexible strain sensing applications. The dual-monomer hydrogel systems were synthesised based on two key polymer segments: PAMPS (poly-2-acrylamide-2-methylpropane sulfonic acid) and PAAm (polyacrylamide). The PAMPs segment is responsible for the rigid and ionically charged network contributing to strength and toughness, whereas the PAAm is a soft and stretchable matrix that provides elasticity and flexibility to the hydrogel matrix. The semi-penetrating arrangement of the network showed effective stress transfer ability and mechanical reinforcement. Hydrogel incorporated with CNT have a crucial role in imparting electrical conductivity and strain sensing performance. The CNT formed a conductive network within the hydrogel matrix. Mechanical deformation of these hydrogels leads towards variations in electrical resistance, which allows their function as a reliable strain sensor. CNT-based hydrogel films exhibit a combined toughness, stretchability and adhesiveness along

with electronic conductivity, which are critical properties for wearable and soft electronic applications. The adhesive behaviour of the hydrogel made the conformal contact to substrates like skin, glass without any kind of binders. Overall, the synergistic combination of PAMPS-PAAm segments and CNT resulted in a multifunctional hydrogel with prominent mechanical toughness and stable electromechanical performance. Such CNT-introduced SN hydrogel showed potential for usefulness in wearable strain sensor device fabrication, motion monitoring devices, soft robotics and flexible electronics devices as they simultaneously required durability, sensitivity and comfort for device fabrication.

Summary &Future Recommendations

CHAPTER-VI

6.1 Summary and conclusion of the present work

Hydrogels have attracted considerable attention owing to their multifunctionality and outstanding mechanical properties, making them promising candidates for energy storage and conversion applications, including supercapacitors, batteries, and ion thermoelectric systems. Their unique characteristics, such as high toughness, controlled swelling behavior, and ionic or electronic conductivity, have positioned hydrogels as versatile materials for next-generation energy devices. Recent research has focused on optimizing these properties through various material design strategies, including the incorporation of nanomaterials, conductive polymers, and advanced network architectures.

Tough hydrogels are typically developed using double-network or topological designs, which effectively dissipate energy and enhance mechanical durability. Anti-swelling performance is achieved by increasing cross-linking density or introducing hydrophobic chains and inorganic nanoparticles to restrict excessive water uptake. Meanwhile, conductive hydrogels employ materials such as MXenes, carbon-based nanostructures, and conductive polymers to provide high flexibility, efficient ion transport, and suitability as solid-state electrolytes. These advancements enable hydrogels to function reliably in flexible and wearable energy devices while maintaining long-term operational stability.

Despite these advances, several key challenges remain. The electrochemical stability window of hydrogel-based systems, particularly in aqueous environments, is often limited, which constrains overall device performance. Achieving an optimal balance between ionic conductivity, mechanical robustness, and self-healing capability continues to be a significant challenge. Furthermore, the development of effective cross-linking strategies, the homogeneous integration of nanocomposite

components, and the maintenance of performance under extreme temperatures or mechanical deformation require further investigation. The significant results and conclusions of the thesis are summarized in the present chapter.

- The first major contribution of this thesis is to demonstrate a PEDOT: PSS-based, metal-free conducting system with significantly improved stretchability, mechanical robustness, and aqueous stability through polyelectrolyte complexation between poly(acryloyl hydrazide) triflate (PAHT) and PSS. The resulting printable conducting ink exhibits tunable viscosity and high PEDOT loading, enabling the fabrication of stretchable, self-healable solid electrolytes. Strong ionic interactions ensure film integrity in organic and aqueous media, delivering high stretchability (~1120%), adequate tensile strength (0.14 MPa), and high ionic conductivity (18 Sm^{-1}). The films show excellent electromechanical sensitivity ($\Delta R/R_0 \approx 26.2$ at 600% strain) and reliable strain-sensing performance under both ambient and submersible conditions, highlighting their suitability for wearable and flexible electronic applications.
- The second major contribution of the work is to the acrylamidomethyl-propanesulfonic acid (AMPS) and acrylamide (AAm) based dual monomer single network hydrogel.t he resulting hydrogel (PAMPSAAm-IP0.1) exhibit superior extensibility (ε, 1050%), tensile strength (UTS, 110 kPa) and adhesive strength (0.25 MPa) compared to that of the control synthesized in H_2O ($\varepsilon \approx 230\%$, UTS ≈ 70 kPa and adhesive strength ≈ 0.03 MPa) supporting the viability of the strategy. Importantly, these compositions having isopropyl alcohol (IPA) in the matrix retain their functional behaviour at low temperature application unlike the conventional hydrogels based on pure H_2O. Machine learning may be utilised to

predict the tensile behavior of compositions based on their precursor ratio and other experimental parameters.

- ❖ A final contribution of the thesis is to the utilisation of CNT-incorporated hydrogel for Ultra-stretchable and Adhesive for Fabrication of Highly Conductive Electrolytes in Sensors. CNT bundles embedded within the hydrogel, with no large agglomerates, indicating good mixing and physical compatibility, resulting hydrogel is ultra-stretchable, tough, adhesive, and highly conductive in nature.

The scope of work included Design and synthetic strategies of tough hydrogels, as well as the development of a one-pot synthetic strategy to improve the mechanical performance of hydrogels, which can further improve Functionalities like toughness, elasticity, self-healing, adhesive and strain-sensing properties.

Table 6.1 Comparison Table of Thesis Works

Chapter/ Hydrogel System	**Hydrogel Composition**	**Conductivity**	**Stretchability**	**Adhesion Strength**	**Gauge Factor**	**Sensing Range**	**Stability**
Chapter 3: PDTPS-PAHT-1.0 Conductive Hydrogel Film	PEDOT:PSS + Polyacryloyl hydrazide triflate (PAHT)	~18 S/m ionic conductivity	Maximum elongation~1120%	Not specifically quantify	4.4 (air) and 0.20 (underwater)	$\Delta R/R_0 \approx 26.2$ at 600% strain; underwater sensing up to 400%	Maintained reproducible response over 200 stretching/release cycles; retained UTS

						elongation; capable of sensing finger, wrist, elbow motion, temperature, and pressure	≈ 0.16 MPa underwater
Chapter 4: PAMPSAAm-IP0.1 Hydrogel	Dual monomer SN Hydrogel based on AMPS+ AAm prepared using Media Polatity Control (MPC) strategy with IPA-assisted phase mixing	Primarily machanically optimized hydrogel; conductivity not specifically reported	Maximum elongation~1050%	~0.25 MPa	Not reported	Designed for mechanically robust and adhesive soft-material applications	Retained functional performance at low-temperature conditions due to IPA incorporation

Chapter 5: AAmCNH -1 CNT	PAMPS/PAAm hydrogel incorporated with CNTs, forming conductive interconnected pathways	~35S/m conductivity	Maximum elongation ~ 500%	Strong adhesion towards skin, metal, glass, plastic, wood, and cardboard	~1.7 GF at 400% elongation	Reliable strain sensing over wide deformation range; response time ≈ 264 ms and recovery time ≈ 240 ms	xhibited reusable adhesion, long shelf-life, mechanical robustness, and stable conductivity under repeated deformation

6.2. Recommendations

Looking ahead, future research should focus on expanding the functional versatility of hydrogels to support next-generation device architectures, such as portable, fibre-shaped, and interdigitated energy systems. A deeper molecular-level understanding of ion–hydrogel interactions within the polymer matrix is essential for rational material design. Additionally, enhancing the integration of hydrogels with other advanced functional materials will be critical for enabling smart electronics and accelerating the development of sustainable and green energy technologies.

The findings of this thesis work would certainly provide a foundation for the following activities.

- Design and synthetic strategies of tough hydrogels and applications: An interdisciplinary approach

- Develop a one-pot synthetic strategy to improve the mechanical performance of the hydrogel. Also, Functionalities like toughness, elasticity, self-healability, adhesive and strain sensing properties.
- Integration of hydrogels in flexible sensors and personalised health care monitoring devices
- Novel supplementary networking strategy for high water content hydrogels
- Designing innovative techniques for device integrations, experimental setups for soft materials.

6.3. Future Perspectives

Future research will focus on addressing the existing challenges in the fabrication of flexible sensors, printed circuits, touch panels, soft robotics, and wearable electronic devices by further optimising the mechanical robustness, conductivity, and environmental stability of hydrogel-based systems. The synthesised hydrogels will be systematically explored as functional components in flexible energy storage devices, including batteries and supercapacitors, to evaluate their electrochemical performance and long-term durability.

Further improvement of the synthesis protocol will be pursued to enhance self-healing efficiency and anti-freezing properties, particularly for tough hydrogels with high water content, enabling reliable operation under extreme environmental conditions. Advanced in situ characterisation techniques such as in situ X-ray photoelectron spectroscopy (XPS), in situ Fourier-transform infrared spectroscopy (FTIR), will be employed to gain molecular- and nanoscale insights into hydrogel network evolution, morphology, and deformation mechanisms.

Also, some molecular dynamics simulations will be used to elucidate the fundamental structure-property relationships and provide a mechanistic understanding of ion transport, cross-linking dynamics, and self-healing behaviours. Beyond energy and sensing applications, tough hydrogels

will be extended to biomedical devices, point-of-care (POC) diagnostic tools, microfluidic platforms, electronic skin (e-skin), and related bio-integrated systems.

Overall, this work opens paths for interdisciplinary research spanning chemistry, materials science, chemical engineering, bioengineering, and allied fields, fostering the development of next-generation soft and intelligent functional materials.

References

1 Ahmed, E. M. (2013). Hydrogel: Preparation, characterization, and applications: A review. *Journal of Advanced Research*, *6*(2), 105–121. https://doi.org/10.1016/j.jare.2013.07.006.

2 Hasan, N., Bhuyan, M. M., & Jeong, J. (2024). Single/Multi-Network Conductive Hydrogels—A Review. *Polymers*, *16*(14), 2030. https://doi.org/10.3390/polym16142030.

3Van Bemmelen, J. M. (1894). Das Hydrogel und das krystallinische Hydrat des Kupferoxyds. *Zeitschrift Für Anorganische Und Allgemeine Chemie*, *5*(1), 466–483. https://doi.org/10.1002/zaac.18940050156.

4 HN, N., DO, Truong, Q. T., Le, P. K., & Ha, A. C. (2022). Recent developments in chitosan hydrogels carrying natural bioactive compounds. *Carbohydrate Polymers*, *294*, 119726. https://doi.org/10.1016/j.carbpol.2022.119726.

5 Bahram, M., Mohseni, N., & Moghtader, M. (2016). An introduction to hydrogels and some recent applications. In *InTech eBooks*. https://doi.org/10.5772/64301.

6 Wichterle, O., & Lím, D. (1960). Hydrophilic gels for biological use. *Nature*, *185*(4706), 117–118. https://doi.org/10.1038/185117a0.

7Haldon, R. A., & Lee, B. E. (1972). Structure and permeability of porous films of poly(hydroxy ethyl methacrylate). *British Polymer Journal*, *4*(6), 491–501. https://doi.org/10.1002/pi.4980040603.

8 Korsmeyer, R. W., & Peppas, N. A. (1981). Effect of the morphology of hydrophilic polymeric matrices on the diffusion and release of water soluble drugs. *Journal of Membrane Science*, *9*(3), 211–227. https://doi.org/10.1016/s0376-7388(00)80265-3.

9 Song, S., Cardinalx, J., Kim, S., & Kim, S. (1981). Progestin Permeation Through Polymer Membranes V: Progesterone Release from Monolithic Hydrogel Devices. *Journal of Pharmaceutical Sciences*, *70*(2), 216–219. https://doi.org/10.1002/jps.2600700226.

10Yean, L., Bunel, C., & Vairon, J. (1990). Reversible immobilization of drugs on a hydrogel matrix, 2. Diffusion of free chloramphenicol from poly(2-hydroxyethyl methacrylate) hydrogels. *Die Makromolekulare Chemie*, *191*(5), 1119–1129. https://doi.org/10.1002/macp.1990.021910514.

11Roorda, W., De Vries, M., De Leede, L., De Boer, A., Breimer, D., & Junginger, H. (1988). Zero-order release of oxprenolol-HCl, a new approach. *Journal of Controlled Release*, *7*(1), 45–52. https://doi.org/10.1016/0168-3659(88)90079-x.

12Rowley, J. A., Madlambayan, G., & Mooney, D. J. (1999). Alginate hydrogels as synthetic extracellular matrix materials. *Biomaterials*, *20*(1), 45–53. https://doi.org/10.1016/s0142-9612(98)00107-0.

13 Soon-Shiong, P., Heintz, R., Merideth, N., Yao, Q., Yao, Z., Zheng, T., Murphy, M., Moloney, M., Schmehl, M., Harris, M., Mendez, R., Mendez, R., & Sandford, P. (1994). Insulin independence in a type 1 diabetic patient after encapsulated islet transplantation. *The Lancet*, *343*(8903), 950–951. https://doi.org/10.1016/s0140-6736(94)90067-1.

14 Bellamkonda, R., Ranieri, J. P., Bouche, N., & Aebischer, P. (1995). Hydrogel-based three-dimensional matrix for neural cells. *Journal of Biomedical Materials Research*, *29*(5), 663–671. https://doi.org/10.1002/jbm.820290514.

15 Tabata, Y., Yamada, K., Miyamoto, S., Nagata, I., Kikuchi, H., Aoyama, I., Tamura, M., & Ikada, Y. (1998). Bone regeneration by basic fibroblast growth factor complexed with biodegradable hydrogels. *Biomaterials*, *19*(7–9), 807–815. https://doi.org/10.1016/s0142-9612(98)00233-6.

16 Zhang, Y., & Huang, Y. (2021). Rational design of smart hydrogels for biomedical applications. *Frontiers in Chemistry*, *8*, 615665. https://doi.org/10.3389/fchem.2020.615665.

17 Benwood, C., Chrenek, J., Kirsch, R. L., Masri, N. Z., Richards, H., Teetzen, K., & Willerth, S. M. (2021). Natural biomaterials and their use as bioinks for printing tissues. *Bioengineering*, *8*(2), 27. https://doi.org/10.3390/bioengineering8020027.

18 Eswaramma, S., & Rao, K. K. (2016). Synthesis of dual responsive carbohydrate polymer based IPN microbeads for controlled release of anti-HIV drug. *Carbohydrate Polymers*, *156*, 125–134. https://doi.org/10.1016/j.carbpol.2016.09.023.

19 Kougkolos, G., Golzio, M., Laudebat, L., Valdez-Nava, Z., & Flahaut, E. (2023). Hydrogels with electrically conductive nanomaterials for biomedical applications. *Journal of Materials Chemistry B*, *11*(10), 2036–2062. https://doi.org/10.1039/d2tb02019j.

20Chen, S., Feng, T., Wu, Z., & Bao, N. (2025). Recent applications and advancement of conductive hydrogels in biosensing, bioelectronics and bioengineering. *Microchimica Acta*, *192*(4), 263. https://doi.org/10.1007/s00604-025-07123-y.

21 Hu, C., He, Y., Wei, C., Tang, X., Peng, Y., & Zhang, M. (2025). A High-Strength Ionic Conductive Hydrogel with Antifreezing and Moisturizing Properties for Flexible Strain Sensors and Triboelectric Nanogenerator. *ACS Applied Polymer Materials*, *7*(13), 8653–8663. https://doi.org/10.1021/acsapm.5c01345.

22 Liu, X., Deng, Y., Wang, P., Tang, H., Li, S., & Xing, Z. (2025). Improved tough and conductive polyacrylamide/sodium alginate dual-network hydrogel by ionic liquid for flexible capacitor and multifunctional sensor. *Journal of Polymer Research*, *32*(9). https://doi.org/10.1007/s10965-025-04534-6.

23 Wang, S., Yu, L., Wang, S., Zhang, L., Chen, L., Xu, X., Song, Z., Liu, H., & Chen, C. (2022). Strong, tough, ionic conductive, and freezing-tolerant all-natural hydrogel enabled by cellulose-bentonite coordination interactions. *Nature Communications*, *13*(1), 3408. https://doi.org/10.1038/s41467-022-30224-8.

24Wang, Y., Gao, X., Wu, J., Jiang, M., Zhang, H., & Yan, C. (2024). Antifreezing/Antiswelling hydrogels: Synthesis Strategies and applications as flexible motion sensors. *ACS Applied Materials & Interfaces*, *16*(43), 58100–58120. https://doi.org/10.1021/acsami.4c13621.

25 Luo, F., Yang, S., Wu, Q., Li, Y., Zhang, J., Zhang, Y., Huang, J., Xie, H., & Chen, Y. (2024). Hydrogel electrolytes with an electron/ion dual regulation mechanism for highly reversible flexible zinc batteries. *Energy & Environmental Science*, *17*(22), 8570–8581. https://doi.org/10.1039/d4ee03067b.

26Ding, J., Yang, Y., Poisson, J., He, Y., Zhang, H., Zhang, Y., Bao, Y., Chen, S., Chen, Y. M., & Zhang, K. (2024). Recent advances in Biopolymer-Based hydrogel electrolytes for flexible supercapacitors. *ACS Energy Letters*, *9*(4), 1803–1825. https://doi.org/10.1021/acsenergylett.3c02567.

27 Wanyan, H., Li, Q., Huang, H., Li, J., Huang, L., Chen, L., Wei, J., Zhou, X., Tang, Z., & Wu, H. (2024). Flexible high electrochemical active hydrogel for wearable sensors and supercapacitor electrolytes. *International Journal of Biological Macromolecules*, *277*(Pt 2), 134356. https://doi.org/10.1016/j.ijbiomac.2024.134356.

28 Nguyen, T. K. L., & Pham-Truong, T. (2024). Recent advancements in gel polymer electrolytes for flexible energy storage applications. *Polymers*, *16*(17), 2506. https://doi.org/10.3390/polym16172506.

29 Chen, Y., Liu, L., Huang, Y., Cao, H., Liu, T., Qi, Z., Hu, J., Guo, Y., Sun, J., Liang, M., Wei, J., Zhang, H., Zhang, X., & Wang, H. (2024). Low-salt organohydrogel electrolytes for wide-potential-window flexible all-solid-state supercapacitors. *Applied Energy*, *363*, 123100. https://doi.org/10.1016/j.apenergy.2024.123100.

30 Chen, Y., & Zheng, C. (2025). Physically Cross-Linked Hydrogel Designed for Thermochromic Smart Windows: Balance between Thermal Stability and Processability. *ACS Sustainable Chemistry & Engineering*, *13*(6), 2574–2585. https://doi.org/10.1021/acssuschemeng.4c09950.

31 Kasprzak, D., Mayorga-Martinez, C. C., & Pumera, M. (2022). Sustainable and Flexible Energy Storage Devices: a review. *Energy & Fuels*, *37*(1), 74–97. https://doi.org/10.1021/acs.energyfuels.2c03217.

32 Nanda, D., Behera, D., Pattnaik, S. S., & Behera, A. K. (2025). Advances in natural polymer-based hydrogels: synthesis, applications, and future directions in biomedical and environmental fields. *Discover Polymers.*, *2*(1). https://doi.org/10.1007/s44347-025-00017-5.

33 Sheng, Z., Yan, S., Ma, J., Bai, J., Shen, Z., & Jia, Z. (2024). Mechanics of single-network hydrogels with network imperfection. *Giant*, *18*, 100287. https://doi.org/10.1016/j.giant.2024.100287.

34 Pruksawan, S., Loh, J. E. T., Chong, K. H. Z., Chua, Z. A., Chong, Y. T., Chia, Z. Y., Yew, K. S. A., & Wang, F. (2025b). Tough, self-healing and weldable hydrogel via thermal engineering optimized multi-scale structures. *Communications Materials*, *6*(1). https://doi.org/10.1038/s43246-025-00818-y.

35 Bashir, S., Hina, M., Iqbal, J., Rajpar, A. H., Mujtaba, M. A., Alghamdi, N. A., Wageh, S., Ramesh, K., & Ramesh, S. (2020). Fundamental concepts of hydrogels: synthesis, properties, and their applications. *Polymers*, *12*(11), 2702. https://doi.org/10.3390/polym12112702.

37 Zhu, R., Zhu, D., Zheng, Z., & Wang, X. (2024). Tough double network hydrogels with rapid self-reinforcement and low hysteresis based on highly entangled networks. *Nature Communications*, *15*(1), 1344. https://doi.org/10.1038/s41467-024-45485-8.

38 Li, L., Zhang, K., Wang, T., Wang, P., Xue, B., Cao, Y., Zhu, L., & Jiang, Q. (2020). Biofabrication of a biomimetic supramolecular-polymer double network hydrogel for cartilage regeneration. *Materials & Design*, *189*, 108492. https://doi.org/10.1016/j.matdes.2020.108492.

39 Yi, J., Nguyen, K. T., Wang, W., Yang, W., Pan, M., Lou, E., Major, P. W., Le, L. H., & Zeng, H. (2020). Polyacrylamide/Alginate double-network tough hydrogels for intraoral ultrasound imaging. *Journal of Colloid and Interface Science*, *578*, 598–607. https://doi.org/10.1016/j.jcis.2020.06.015.

40 Wang, F., Xu, Z., Deng, L., & Liu, J. (2025). A dual drug delivery system based on high toughness PAM/Gel hydrogels blended with chitosan microspheres. *New Journal of Chemistry*, *49*(30), 13199–13208. https://doi.org/10.1039/d5nj01811k.

41 Gad, Y. (2008). Preparation and characterization of poly(2-acrylamido-2-methylpropane-sulfonic acid)/Chitosan hydrogel using gamma irradiation and its application in wastewater treatment. *Radiation Physics and Chemistry*, *77*(9), 1101–1107. https://doi.org/10.1016/j.radphyschem.2008.05.002.

42 Gu, Z., Huang, K., Luo, Y., Zhang, L., Kuang, T., Chen, Z., & Liao, G. (2018). Double network hydrogel for tissue engineering. *Wiley Interdisciplinary Reviews Nanomedicine and Nanobiotechnology*, *10*(6), e1520. https://doi.org/10.1002/wnan.1520.

43 Li, T., Liu, T., Yu, Q., Li, Y., Liang, R., & Sun, G. (2025). Stretching-Orientation reinforced double network Solvent-Free eutectic gels for ultrarobust, flexible Human-Machine interaction devices. *Advanced Functional Materials*, *35*(46). https://doi.org/10.1002/adfm.202508233.

44 Zhang, Z., Luo, Y., Li, Y., Ding, S., Liu, K., & Luo, B. (2023). Flexible hybrid wearable sensors for pressure and thermal sensing based on a Double-Network hydrogel. *ACS Applied Bio Materials*, *6*(11), 5114–5123. https://doi.org/10.1021/acsabm.3c00867.

45Muddasar, M., Joyce, G., Pouzier, M., Serafin, A., & Collins, M. N. (2025). Engineering Lignin-Based tubular hydrogel scaffolds for Load-Bearing biomedical applications. *ChemSusChem*, *18*(20), e202501520. https://doi.org/10.1002/cssc.202501520.

46 Es-Haghi, S. S., & Weiss, R. A. (2023). Fabrication of Tough Double-Network Hydrogels from Highly Cross-Linked Brittle Neutral Networks Using Alkaline Hydrolysis. *Gels*, *10*(1), 29. https://doi.org/10.3390/gels10010029.

47 Choi, Y., Koh, H. Y., Han, J. Y., & Seo, S. (2025). Synthesis of Hydrogel-Based microgels and nanogels toward therapeutic and biomedical applications. *Applied Sciences*, *15*(3), 1368. https://doi.org/10.3390/app15031368.

48 Quazi, M. Z., & Park, N. (2022). Nanohydrogels: advanced polymeric nanomaterials in the era of nanotechnology for robust functionalization and cumulative applications. *International Journal of Molecular Sciences*, *23*(4), 1943. https://doi.org/10.3390/ijms23041943.

49 Wang, Z. J., Jiang, J., Mu, Q., Maeda, S., Nakajima, T., & Gong, J. P. (2022). Azo-Crosslinked Double-Network hydrogels enabling highly efficient mechanoradical generation. *Journal of the American Chemical Society*, *144*(7), 3154–3161. https://doi.org/10.1021/jacs.1c12539.

50 Lu, Y., Yue, Y., Ding, Q., Mei, C., Xu, X., Wu, Q., Xiao, H., & Han, J. (2021). Self-Recovery, Fatigue-Resistant, and multifunctional sensor assembled by a Nanocellulose/Carbon nanotube Nanocomplex-Mediated hydrogel. *ACS Applied Materials & Interfaces*, *13*(42), 50281–50297. https://doi.org/10.1021/acsami.1c16828.

51 Goswami, M., Dutta, A., Kulshreshtha, R., Vasilyev, G., Zussman, E., & Volokh, K. (2025). Mechanics of Physically Cross-Linked Hydrogels: Experiments and Theoretical Modeling. *Macromolecules*, *58*(9), 4478–4487. https://doi.org/10.1021/acs.macromol.5c00486.

52 Nonoyama, T., & Gong, J. P. (2021). Tough double network hydrogel and its biomedical applications. *Annual Review of Chemical and Biomolecular Engineering*, *12*(1), 393–410. https://doi.org/10.1146/annurev-chembioeng-101220-080338.

53 Liu, G., Jiao, P., Ma, Q., Li, D., Wu, W., Xue, M., & Zhang, X. (2025). Direct ink writing PEDOT:PSS-based interfaces with high stretchability and strong adhesion for flexible electronics. *Journal of Materials Science*. https://doi.org/10.1007/s10853-025-11470-9.

54 Xiang, M., Xiao, A., Rodrigue, D., Chen, X. Y., Wu, Y., Liu, Y., Ma, F., Kong, J., & Wang, Y. (2025). Controlled hydrogel surfaces adhesion via macrophase separation polymerization triggered by electrostatic interaction for wound dressing and Bio-Sensor. *Advanced Functional Materials*, *35*(35). https://doi.org/10.1002/adfm.202501708.

55 Cui, K., Ye, Y. N., Sun, T. L., Yu, C., Li, X., Kurokawa, T., & Gong, J. P. (2020). Phase separation behavior in tough and Self-Healing polyampholyte hydrogels. *Macromolecules*, *53*(13), 5116–5126. https://doi.org/10.1021/acs.macromol.0c00577.

56 Cui, K., Sun, T. L., Liang, X., Nakajima, K., Ye, Y. N., Chen, L., Kurokawa, T., & Gong, J. P. (2018). Multiscale energy dissipation mechanism in tough and Self-Healing hydrogels. *Physical Review Letters*, *121*(18), 185501. https://doi.org/10.1103/physrevlett.121.185501.

57 Wu, M., Han, L., Yan, B., & Zeng, H. (2023). Self-healing hydrogels based on reversible noncovalent and dynamic covalent interactions: A short review. *Supramolecular Materials*, *2*, 100045. https://doi.org/10.1016/j.supmat.2023.100045.

58 Kopač, T., Abrami, M., Grassi, M., Ručigaj, A., & Krajnc, M. (2021). Polysaccharide-based hydrogels crosslink density equation: A rheological and LF-NMR study of polymer-polymer interactions. *Carbohydrate Polymers*, *277*, 118895. https://doi.org/10.1016/j.carbpol.2021.118895.

59 Liu, X., Xu, H., Zhang, L., Zhong, M., & Xie, X. (2019). Homogeneous and Real Super Tough Multi-Bond Network Hydrogels Created through a Controllable Metal Ion Permeation Strategy. *ACS Applied Materials & Interfaces*, *11*(45), 42856–42864. https://doi.org/10.1021/acsami.9b18620.

60 Cui, K., Sun, T. L., Liang, X., Nakajima, K., Ye, Y. N., Chen, L., Kurokawa, T., & Gong, J. P. (2018b). Multiscale energy dissipation mechanism in tough and Self-Healing hydrogels. *Physical Review Letters*, *121*(18), 185501. https://doi.org/10.1103/physrevlett.121.185501.

61 Shi, J., Ouyang, J., Li, Q., Wang, L., Wu, J., Zhong, W., & Xing, M. M. Q. (2012). Cell-compatible hydrogels based on a multifunctional crosslinker with tunable stiffness for tissue engineering. *Journal of Materials Chemistry*, *22*(45), 23952. https://doi.org/10.1039/c2jm34862d.

62 Liu, Y., Zhang, Y., An, Z., Zhao, H., Zhang, L., Cao, Y., Mansoorianfar, M., Liu, X., & Pei, R. (2021). Slide-Ring Structure-Based Double-Network Hydrogel with Enhanced Stretchability and Toughness for 3D-Bio-Printing and Its Potential Application as Artificial Small-Diameter Blood Vessels. *ACS Applied Bio Materials*, *4*(12), 8597–8606. https://doi.org/10.1021/acsabm.1c01052.

63 Lu, N., Kang, H., Lu, Y., Li, Y., Li, J., Xue, Y., & Qiu, H. (2025). High-strength, conductive dual-network nanocomposite hydrogel for multi-substrate adhesion and enhanced wearable sensor performance. *Polymer*, *334*, 128743. https://doi.org/10.1016/j.polymer.2025.128743.

64Kunwar, P., Andrada, B. L., Poudel, A., Xiong, Z., Aryal, U., Geffert, Z. J., Poudel, S., Fougnier, D., Gitsov, I., & Soman, P. (2023). Printing Double-Network tough hydrogels using Temperature-Controlled Projection Stereolithography (TOPS). *ACS Applied Materials & Interfaces*, *15*(25), 30780–30792. https://doi.org/10.1021/acsami.3c04661.

65 Chen, F., Li, X., Yu, Y., Li, Q., Lin, H., Xu, L., & Shum, H. C. (2023). Phase-separation facilitated one-step fabrication of multiscale heterogeneous two-aqueous-phase gel. *Nature Communications*, *14*(1), 2793. https://doi.org/10.1038/s41467-023-38394-9.

66 Pumford, E. A., Hoffman, B. a. J., & Kasko, A. M. (2024). Nontoxic Initiator Alternatives to TEMED for Redox Hydrogel Polymerization. *ACS Applied Bio Materials*, *7*(4), 2264–2271. https://doi.org/10.1021/acsabm.3c01264.

67 Yuan, W., Wang, F., Qu, X., Wang, S., Lei, B., Shao, J., Wang, Q., Lin, J., Wang, W., & Dong, X. (2023). In situ rapid synthesis of hydrogels based on a redox initiator and persistent free radicals. *Nanoscale Advances*, *5*(7), 1999–2009. https://doi.org/10.1039/d3na00038a.

68 Panja, S., Dietrich, B., & Adams, D. J. (2021). Controlling syneresis of hydrogels using organic salts. *Angewandte Chemie International Edition*, *61*(4), e202115021. https://doi.org/10.1002/anie.202115021.

69 Simič, R., Mandal, J., Zhang, K., & Spencer, N. D. (2021). Oxygen inhibition of free-radical polymerization is the dominant mechanism behind the "mold effect" on hydrogels. *Soft Matter*, *17*(26), 6394–6403. https://doi.org/10.1039/d1sm00395j.

70 Wang, H., Zhang, B., Zhang, J., He, X., Liu, F., Cui, J., Lu, Z., Hu, G., Yang, J., Zhou, Z., Wang, R., Hou, X., Ma, L., Ren, P., Ge, Q., Li, P., & Huang, W. (2021). General One-Pot Method for Preparing Highly Water-Soluble and Biocompatible Photoinitiators for Digital Light Processing-Based 3D Printing of Hydrogels. *ACS Applied Materials & Interfaces*, *13*(46), 55507–55516. https://doi.org/10.1021/acsami.1c15636.

71 Wahid, F., Zhao, X., Jia, S., Bai, H., & Zhong, C. (2020). Nanocomposite hydrogels as multifunctional systems for biomedical applications: Current state and perspectives. *Composites Part B Engineering*, *200*, 108208. https://doi.org/10.1016/j.compositesb.2020.108208.

72 Montazerian, H., Mitra, S., Najafabadi, A. H., Seyedmahmoud, R., Zheng, Y., Dokmeci, M. R., Annabi, N., Khademhosseini, A., & Weiss, P. S. (2023). Catechol conjugation for bioadhesion in Photo-Cross-Linkable biomaterials. *ACS Materials Letters*, *5*(6), 1672–1683. https://doi.org/10.1021/acsmaterialslett.3c00193.

73 Quazi, M. Z., Quazi, A. S., Song, Y., & Park, N. (2025). Functional Hydrogels: a promising platform for biomedical and environmental applications. *International Journal of Molecular Sciences*, *26*(18), 9066. https://doi.org/10.3390/ijms26189066.

74 Rajaram, S., Dharmalingam, S. R., Natarajan, V., Ravi, K., & Shanmugam, N. (2022). An extensive review on hydrogels in pharmaceutical drug delivery applications. *International Journal of Pharmaceutical Investigation*, *12*(2), 102–112. https://doi.org/10.5530/ijpi.2022.2.20.

75Billah, S. M. R., Mondal, M. I. H., Somoal, S. H., & Pervez, M. N. (2019). Cellulose-Based hydrogel for industrial applications. In *Polymers and polymeric composites* (pp. 909–949). https://doi.org/10.1007/978-3-319-77830-3_63.

76 Trebunova, M., Cajkova, J., & Bacenkova, D. (2025). Hydrogels as bioactive scaffolds in biomedical engineering. *Acta Tecnología*, *11*(2), 75–79. https://doi.org/10.22306/atec.v11i2.272.

77Sun, S., & Chen, J. (2024). Recent advances in Hydrogel-Based biosensors for cancer detection. *ACS Applied Materials & Interfaces*, *16*(36), 46988–47002. https://doi.org/10.1021/acsami.4c02317.

78 Kulbay, M., Wu, K. Y., Truong, D., & Tran, S. D. (2024). Smart molecules in ophthalmology: Hydrogels as responsive systems for ophthalmic applications. *Smart Molecules*, *2*(1), e20230021. https://doi.org/10.1002/smo.20230021.

79 Li, J., & Mooney, D. J. (2016). Designing hydrogels for controlled drug delivery. *Nature Reviews Materials*, *1*(12). https://doi.org/10.1038/natrevmats.2016.71.

80 Sun, Y., Fei, J., Yan, S., Wang, X., An, D., & Zhu, X. (2024). Water Recovery from Wastewater by Hydrogels. *Environmental Science & Technology Letters*, *11*(4), 357–363. https://doi.org/10.1021/acs.estlett.4c00075.

81 Koushal, S., Vishnoi, M., Pj, R., Vishnoi, V., & Singh, K. (2025). Hydrogels as a key solution for sustainable agriculture: Exploring water retention and soil improvement. *International Journal of Research in Agronomy*, *8*(8S), 415–423. https://doi.org/10.33545/2618060x.2025.v8.i8sf.3604.

82 Yang, S., Sarkar, S., Xie, X., Li, D., & Chen, J. (2023). Application of optical hydrogels in environmental sensing. *Energy & Environment Materials*, *7*(3). https://doi.org/10.1002/eem2.12646.

83 López-Díaz, A., Vázquez, A. S., & Vázquez, E. (2024b). Hydrogels in Soft Robotics: past, present, and future. *ACS Nano*, *18*(32), 20817–20826. https://doi.org/10.1021/acsnano.3c12200.

84 Chung, T., Choi, J., Enomoto, T., Park, S., Kim, S., & Kim, Y. S. (2025). Self-Regulating Hydrogel actuators. *Chemical Reviews*, *125*(18), 9053–9088. https://doi.org/10.1021/acs.chemrev.5c00358.

85 Hull, S. M., Lou, J., Lindsay, C. D., Navarro, R. S., Cai, B., Brunel, L. G., Westerfield, A. D., Xia, Y., & Heilshorn, S. C. (2023). 3D bioprinting of dynamic hydrogel bioinks enabled by small molecule modulators. *Science Advances*, *9*(13), eade7880. https://doi.org/10.1126/sciadv.ade7880.

86 Chen, L., Liu, F., Abdiryim, T., & Liu, X. (2023). Stimuli-responsive hydrogels as promising platforms for soft actuators. *Materials Today Physics*, *40*, 101281. https://doi.org/10.1016/j.mtphys.2023.101281.

87 Wei, X., Xie, Y., Yuan, Z., Dong, T., Zhang, X., & Shao, W. (2025). Dynamic Bond-Constructed Hydrogel-Triboelectric Systems with Self-Healing, Strain Sensing, and Energy Harvesting Capabilities. *ACS Applied Polymer Materials*, *7*(21), 14096–14107. https://doi.org/10.1021/acsapm.5c01989.

88 He, H., Chen, Y., Pu, A., Wang, L., Li, W., Zhou, X., Tang, C. Y., Ban, K., Yang, M., & Xu, L. (2024). Strong and high-conductivity hydrogels with all-polymer nanofibrous networks for

applications as high-capacitance flexible electrodes. *Npj Flexible Electronics*, *8*(1). https://doi.org/10.1038/s41528-024-00346-8.

89 Ishikawa, S., & Sakai, T. (2023). One-Pot Approach to Synthesize Tough and Cell Adhesive Double-Network Hydrogels Consisting of Fully Synthetic Materials of Self-Assembling Peptide and Poly(ethylene glycol). *ACS Applied Bio Materials*, *6*(12), 5282–5289. https://doi.org/10.1021/acsabm.3c00562.

90 Moreno, J. M. C., Chelu, M., & Popa, M. (2025). Biocompatible Stimuli-Sensitive Natural Hydrogels: Recent advances in biomedical applications. *Gels*, *11*(12), 993. https://doi.org/10.3390/gels11120993.

91Shodmanov, J., Qin, G., Boymirzayev, A., Ibragimov, M., Ovodok, E., & Feng, Y. (2025). Design and evaluation of a Self-Healing, highly stretchable Double-Network gel polymer electrolyte for potential use in wearable supercapacitors. *ACS Omega*, *10*(29), 32476–32485. https://doi.org/10.1021/acsomega.5c05335.

92Lee, Y., So, J., & Koo, H. (2024). A Transparent Hydrogel-Ionic Conductor with High Water Retention and Self-Healing Ability. *Materials*, *17*(2), 288. https://doi.org/10.3390/ma17020288.

93 Hosseinzadeh, B., & Ahmadi, M. (2023). Degradable hydrogels: Design mechanisms and versatile applications. *Materials Today Sustainability*, *23*, 100468. https://doi.org/10.1016/j.mtsust.2023.100468.

94 Zhi, Z., Chen, Z., Xian, J., Xu, J., Zheng, J., Yu, Y., & Yang, P. (2025). Hydrogel electrolytes for zinc dendrite regulation: balancing conductivity and modulus. *Journal of Materials Chemistry A*, *13*(22), 16450–16455. https://doi.org/10.1039/d5ta03045e.

95 Zeng, Z., Liao, S., Ma, G., & Qu, J. (2024). High-Conductivity and ultrastretchable Self-Healing hydrogels for flexible Zinc-Ion batteries. *ACS Applied Materials & Interfaces*, *16*(43), 58961–58972. https://doi.org/10.1021/acsami.4c13058.

96 Tan, X., Chu, K., Chen, Z., Han, N., Zhang, X., Pan, H., Guo, W., Chen, G., Ni, B., Zhou, Z., & Song, H. (2024). Recent advances in self-healing hydrogel composites for flexible wearable electronic devices. *Nano Research Energy*, *3*(3), e9120123. https://doi.org/10.26599/nre.2024.9120123.

97 Shen, Z., Liu, Y., Li, Z., Tang, Z., Pu, J., Luo, L., Ji, Y., Xie, J., Shu, Z., Yao, Y., Zhang, N., & Hong, G. (2024). Highly-Entangled hydrogel electrolyte for fast Charging/Discharging properties in aqueous zinc ion batteries. *Advanced Functional Materials*, *35*(21). https://doi.org/10.1002/adfm.202406620..

98 Nadeem, A., Saqib, Z., Arif, A., Abid, L., Shahzadi, H., Saghir, A., Khan, E., Afzaal, T., Saadat, S., Rasheed, N., Mustafa, M. A., & Iqbal, M. Z. (2024). HYBRID HYDROGELS INCORPORATING NANOPARTICLES, THEIR TYPES, DEVELOPMENT, AND

APPLICATIONS: A COMPREHENSIVE REVIEW OF NANOGELS. *Universal Journal of Pharmaceutical Research*. https://doi.org/10.22270/ujpr.v9i5.1202.

99 Zhang, W., Ren, J., Zhang, M., Zhou, Z., Li, Y., & Yang, W. (2025). Preparation and Application of Ionic Liquid Improved Multifunctional Hydrogel with High Performance as Strain Sensors. *ACS Applied Polymer Materials*, *7*(12), 8081–8092. https://doi.org/10.1021/acsapm.5c01142.

100 Dou, L., Zhou, S., Ma, J., Zhao, C., Cui, P., Ye, S., Feng, P., Gu, X., Huang, S., & Tao, X. (2023). Organic redox additive incorporated PANI hydrogel electrodes for flexible high-energy-density supercapacitors. *Journal of Materials Chemistry C*, *12*(2), 521–532. https://doi.org/10.1039/d3tc03119e.

101 Mealy, J. E., Chung, J. J., Jeong, H., Issadore, D., Lee, D., Atluri, P., & Burdick, J. A. (2018). Injectable Granular Hydrogels with Multifunctional Properties for Biomedical Applications. *Advanced Materials*, *30*(20), e1705912. https://doi.org/10.1002/adma.201705912.

102 Zhang, Y., Lin, C., & Yeh, M. (2025). Tough, Wide-Temperature-Resistant, and Water-Retentive conductive hydrogel for human motion sensing. *ACS Applied Polymer Materials*, *7*(8), 4918–4930. https://doi.org/10.1021/acsapm.5c00035.

103 Morgan, F. L. C., Beeren, I. a. O., Moroni, L., & Baker, M. B. (2025). Designing dynamic hydrogels: the interplay of Cross-Linker length, valency, and reaction kinetics in Hydrazone-Based networks. *Chemistry of Materials*, *37*(8), 2709–2719. https://doi.org/10.1021/acs.chemmater.4c02573.

104 Zhang, C., Zhang, Y., Wang, Y., & Huang, Y. (2025). Advances in conductive filler-integrated hydrogels and derived aerogels: innovative strategies for electromagnetic interference shielding. *Materials Horizons*, *12*(18), 7066–7100. https://doi.org/10.1039/d5mh00577a.

105 Zhuang, Y., Kong, Y., Han, K., Hao, H., & Shi, B. (2017). A physically cross-linked self-healable double-network polymer hydrogel as a framework for nanomaterial. *New Journal of Chemistry*, *41*(24), 15127–15135. https://doi.org/10.1039/c7nj03392c.

106Zhu, J., Tao, J., Yan, W., & Song, W. (2023). Pathways toward wearable and high-performance sensors based on hydrogels: toughening networks and conductive networks. *National Science Review*, *10*(9), nwad180. https://doi.org/10.1093/nsr/nwad180.

107 Ulery, B. D.; Nair, L. S.; Laurencin, C. T. Biomedical applications of biodegradable polymers. *Journal of Polymer Science Part B Polymer Physics* **2011**, *49* (12), 832–864. https://doi.org/10.1002/polb.22259.

108 Trombino, S.; Cassano, R. *Designing hydrogels for controlled drug delivery*; 2020. https://doi.org/10.3390/books978-3-03928-357-6.

109 Sahu, N.; Gupta, D.; Nautiyal, U. Hydrogel: Preparation, characterization and applications. *Asian Pacific Journal of Nursing and Health Sciences* **2020**, *3* (1), 1–11. https://doi.org/10.46811/apjnh/3.1.2.

110 Fu, F.; Wang, J.; Zeng, H.; Yu, J. Functional conductive hydrogels for bioelectronics. *ACS Materials Letters* **2020**, *2* (10), 1287–1301. https://doi.org/10.1021/acsmaterialslett.0c00309.

111 Jang, K.-I.; Li, K.; Chung, H. U.; Xu, S.; Jung, H. N.; Yang, Y.; Kwak, J. W.; Jung, H. H.; Song, J.; Yang, C.; Wang, A.; Liu, Z.; Lee, J. Y.; Kim, B. H.; Kim, J.-H.; Lee, J.; Yu, Y.; Kim, B. J.; Jang, H.; Yu, K. J.; Kim, J.; Lee, J. W.; Jeong, J.-W.; Song, Y. M.; Huang, Y.; Zhang, Y.; Rogers, J. A. Self-assembled three dimensional network designs for soft electronics. *Nature Communications* **2017**, *8* (1), 15894. https://doi.org/10.1038/ncomms15894.

112 Sun, J.-Y.; Zhao, X.; Illeperuma, W. R. K.; Chaudhuri, O.; Oh, K. H.; Mooney, D. J.; Vlassak, J. J.; Suo, Z. Highly stretchable and tough hydrogels. *Nature* **2012**, *489* (7414), 133–136. https://doi.org/10.1038/nature11409.

113 Yin, S., Ding, Y., Zhang, Y., Zhou, C., Qian, C., Che, G., Zhao, C., & Jiang, L. (2025). Superstrong and Transparent Hydrogels with Homogeneous Multiple Networks. *Macromolecules*, *58*(9), 4357–4364. https://doi.org/10.1021/acs.macromol.4c03202.

114 Wang, G. K., Yang, Y. M., & Jia, D. (2024). Programming viscoelastic properties in a complexation gel composite by utilizing entropy-driven topologically frustrated dynamical state. Nature Communications, 15(1), 3569. https://doi.org/10.1038/s41467-024-47969-z.

115 Lv, H., Zong, S., Li, T., Zhao, Q., Xu, Z., & Duan, J. (2023). Room temperature CA2+-Initiated free radical polymerization for the preparation of conductive, adhesive, anti-freezing and UV-Blocking hydrogels for monitoring human movement. *ACS Omega*, *8*(10), 9434–9444. https://doi.org/10.1021/acsomega.2c08097.

116 Kowalski, G., Witczak, M., & Kuterasiński, Ł. (2024). Structure effects on swelling properties of hydrogels based on sodium alginate and acrylic polymers. *Molecules*, *29*(9), 1937. https://doi.org/10.3390/molecules29091937.

117 Zhang, L., Ma, W., Tang, N. H., Yu, Y., Wang, L., Li, T., Fang, Z., & Qiao, Z. (2023). Tough, low-friction and homogeneous physical hydrogel by a solvent-inducted strategy. *Chemical Engineering Journal*, *466*, 143195. https://doi.org/10.1016/j.cej.2023.143195.

118 Xu, Z., Lu, J., Lu, D., Li, Y., Lei, H., Chen, B., Li, W., Xue, B., Cao, Y., & Wang, W. (2024). Rapidly damping hydrogels engineered through molecular friction. *Nature Communications*, *15*(1), 4895. https://doi.org/10.1038/s41467-024-49239-4.

119 Nakajima, T. (2017). Generalization of the sacrificial bond principle for gel and elastomer toughening. *Polymer Journal*, *49*(6), 477–485. https://doi.org/10.1038/pj.2017.12.

120 Panja, S., Seddon, A., & Adams, D. J. (2021). Controlling hydrogel properties by tuning non-covalent interactions in a charge complementary multicomponent system. *Chemical Science*, *12*(33), 11197–11203. https://doi.org/10.1039/d1sc02854e.

121 Puza, F., Zheng, Y., Han, L., Xue, L., & Cui, J. (2020). Physical entanglement hydrogels: ultrahigh water content but good toughness and stretchability. *Polymer Chemistry*, *11*(13), 2339–2345. https://doi.org/10.1039/d0py00294a.

122 Ando, S., & Ito, K. (2025). Recent progress and future perspective in Slide-Ring based polymeric materials. *Macromolecules*, *58*(5), 2157–2177. https://doi.org/10.1021/acs.macromol.4c02021.

123 Li, Z., Li, T., Yang, H., Ding, M., Chen, L., Yu, S., Meng, X., Jin, J., Sun, S., Zhang, J., & Tian, H. (2024). Design and fabrication of viscoelastic hydrogels as extracellular matrix mimicry for cell engineering. *Chem & Bio Engineering*, *1*(11), 916–933. https://doi.org/10.1021/cbe.4c00129.

124 Xu, Z., Yue, P., & Feng, J. J. (2024). Hystereses in flow-induced compression of a poroelastic hydrogel. *Soft Matter*, *20*(35), 6940–6951. https://doi.org/10.1039/d4sm00678j.

125 Xie, X., Lu, M., Li, G., Gao, G., Kang, J., Zhang, Q., & Liu, X. (2024). Anti-impact electromagnetic shielding hydrogel with solvent-driven tunability. *Chemical Engineering Journal*, *505*, 159114. https://doi.org/10.1016/j.cej.2024.159114.

126 Wei, W., Ma, Y., Yao, X., Zhou, W., Wang, X., Li, C., Lin, J., He, Q., Leptihn, S., & Ouyang, H. (2020). Advanced hydrogels for the repair of cartilage defects and regeneration. *Bioactive Materials*, *6*(4), 998–1011. https://doi.org/10.1016/j.bioactmat.2020.09.030.

127 Hui, C., Cui, F., Zehnder, A., & Vernerey, F. J. (2021). Physically motivated models of polymer networks with dynamic cross-links: comparative study and future outlook. *Proceedings of the Royal Society a Mathematical Physical and Engineering Sciences*, *477*(2255). https://doi.org/10.1098/rspa.2021.0608.

128 Li, L., Sun, X., Guo, Y., Cheng, W., Shi, Y., & Pan, L. (2025). Recent Advances in Stimuli-Responsive Conductive Hydrogels for smart Sensing and Actuation: properties, design strategies, and applications. *Macromolecular Materials and Engineering*, *310*(9). https://doi.org/10.1002/mame.202500097.

129 One-step engineering dual-network reinforced hydrogel microspheres with excellent anti-coagulant and low-density lipoprotein removal.

130 Yammine, P., Safadi, A. E., Kassab, R., El-Nakat, H., Obeid, P. J., Nasr, Z., Tannous, T., Sari-Chmayssem, N., Mansour, A., & Chmayssem, A. (2025). Types of crosslinkers and their applications in biomaterials and biomembranes. *Chemistry*, *7*(2), 61. https://doi.org/10.3390/chemistry7020061.

131 Zhang, J., White, J. C., Lowry, G. V., He, J., Yu, X., Yan, C., Dong, L., Tao, S., & Wang, X. (2025). Advanced enzyme-assembled hydrogels for the remediation of contaminated water. *Nature Communications*, *16*(1), 3050. https://doi.org/10.1038/s41467-025-58338-9.

132Ahmad, Z., Salman, S., Khan, S. A., Amin, A., Rahman, Z. U., Al-Ghamdi, Y. O., Akhtar, K., Bakhsh, E. M., & Khan, S. B. (2022). Versatility of hydrogels: from synthetic strategies, classification, and properties to biomedical applications. *Gels*, *8*(3), 167. https://doi.org/10.3390/gels8030167.

133 Zhao, Y., Dai, Z., Huang, H., Tian, J., & Cai, H. (2024). Injectable Silver Nanoparticle-Based Hydrogel Dressings with Rapid Shape Adaptability and Antimicrobial Activity. *Applied Biochemistry and Biotechnology*, *197*(2), 821–836. https://doi.org/10.1007/s12010-024-05048-5.

134 Zhou, S.; Li, P.; Yin, S.; Lu, Y.; Wang, J.; Wang, J.; Hu, X.; Zhang, X.; Deng, L.; Liu, Y.; Luo, X.; Wang, J.; Wang, J.; Lou, L.; Qiu, J.; Zou, Z. Improved adhesion between glass fiber and PAAm / SA hydrogel via a synergy strategy. *Polymer Composites* **2025**, *46* (S2). https://doi.org/10.1002/pc.29877.

135 Sikdar, P.; Uddin, Md. M.; Dip, T. M.; Islam, S.; Hoque, Md. S.; Dhar, A. K.; Wu, S. Recent advances in the synthesis of smart hydrogels. *Materials Advances* **2021**, *2* (14), 4532–4573. https://doi.org/10.1039/d1ma00193k.

136 Gong, J. P.; Katsuyama, Y.; Kurokawa, T.; Osada, Y. Double-Network Hydrogels with Extremely High Mechanical Strength. *Advanced Materials* **2003**, *15* (14), 1155–1158. https://doi.org/10.1002/adma.200304907.

137 Sun, T. L.; Kurokawa, T.; Kuroda, S.; Ihsan, A. B.; Akasaki, T.; Sato, K.; Haque, Md. A.; Nakajima, T.; Gong, J. P. Physical hydrogels composed of polyampholytes demonstrate high toughness and viscoelasticity. *Nature Materials* **2013**, *12* (10), 932–937. https://doi.org/10.1038/nmat3713.

138 Wang, C.; Wang, M.; Xu, T.; Zhang, X.; Lin, C.; Gao, W.; Xu, H.; Lei, B.; Mao, C. Engineering bioactive Self-Healing antibacterial exosomes hydrogel for promoting chronic diabetic wound healing and complete skin regeneration. *Theranostics* **2018**, *9* (1), 65–76. https://doi.org/10.7150/thno.29766.

139 Rivnay, J.; Inal, S.; Collins, B. A.; Sessolo, M.; Stavrinidou, E.; Strakosas, X.; Tassone, C.; Delongchamp, D. M.; Malliaras, G. G. Structural control of mixed ionic and electronic transport in conducting polymers. *Nature Communications* **2016**, *7* (1), 11287. https://doi.org/10.1038/ncomms11287.

140 Yuk, H.; Zhang, T.; Parada, G. A.; Liu, X.; Zhao, X. Skin-inspired hydrogel–elastomer hybrids with robust interfaces and functional microstructures. *Nature Communications* **2016**, *7* (1), 12028. https://doi.org/10.1038/ncomms12028.

141 Choi, H. W.; Shin, D.-W.; Yang, J.; Lee, S.; Figueiredo, C.; Sinopoli, S.; Ullrich, K.; Jovančić, P.; Marrani, A.; Momentè, R.; Gomes, J.; Branquinho, R.; Emanuele, U.; Lee, H.; Bang, S. Y.; Jung, S.-M.; Han, S. D.; Zhan, S.; Harden-Chaters, W.; Suh, Y.-H.; Fan, X.-B.; Lee, T. H.; Chowdhury, M.; Choi, Y.; Nicotera, S.; Torchia, A.; Moncunill, F. M.; Candel, V. G.; Durães, N.; Chang, K.; Cho, S.; Kim, C.-H.; Lucassen, M.; Nejim, A.; Jiménez, D.; Springer, M.; Lee, Y.-W.; Cha, S.; Sohn, J. I.; Igreja, R.; Song, K.; Barquinha, P.; Martins, R.; Amaratunga, G. a. J.; Occhipinti, L. G.; Chhowalla, M.; Kim, J. M. Smart textile lighting/display system with multifunctional fibre devices for large scale smart home and IoT applications. *Nature Communications* **2022**, *13* (1), 814. https://doi.org/10.1038/s41467-022-28459-6.

142 Peng, Q.; Chen, J.; Wang, T.; Peng, X.; Liu, J.; Wang, X.; Wang, J.; Zeng, H. Recent advances in designing conductive hydrogels for flexible electronics. *InfoMat* **2020**, *2* (5), 843–865. https://doi.org/10.1002/inf2.12113.

143 Lu, Y.; Qu, X.; Zhao, W.; Ren, Y.; Si, W.; Wang, W.; Wang, Q.; Huang, W.; Dong, X. Highly stretchable, elastic, and sensitive MXENE-Based hydrogel for flexible strain and pressure sensors. *Research* **2020**, *2020*, 2038560. https://doi.org/10.34133/2020/2038560.

144 Iijima, S. Helical microtubules of graphitic carbon. *Nature* **1991**, *354* (6348), 56–58. https://doi.org/10.1038/354056a0.

145 Lau, A. K.-T.; Hui, D. The revolutionary creation of new advanced materials—carbon nanotube composites. *Composites Part B Engineering* **2002**, *33* (4), 263–277. https://doi.org/10.1016/s1359-8368(02)00012-4.

146 Zhang, P.; Li, J.; Yang, D.; Soomro, R. A.; Xu, B. Flexible Carbon Dots-Intercalated MXene Film Electrode with Outstanding Volumetric Performance for Supercapacitors. *Advanced Functional Materials* **2022**, *33* (1). https://doi.org/10.1002/adfm.202209918.

147 Xu, C.; Guan, S.; Wang, S.; Gong, W.; Liu, T.; Ma, X.; Sun, C. Biodegradable and electroconductive poly(3,4-ethylenedioxythiophene)/carboxymethyl chitosan hydrogels for neural tissue engineering. *Materials Science and Engineering C* **2017**, *84*, 32–43. https://doi.org/10.1016/j.msec.2017.11.032.

148 Kim, S.; Kim, S.; Baek, S.; Sluyter, R.; Konstantinov, K.; Kim, J. H.; Kim, S.; Kim, S.; Kim, Y. H. Wearable and implantable bioelectronics as eco-friendly and patient-friendly integrated nanoarchitectonics for next-generation smart healthcare technology. *EcoMat* **2023**, *5* (8). https://doi.org/10.1002/eom2.12356.

149 Haraguchi, K.; Takehisa, T. Nanocomposite Hydrogels: A Unique Organic–Inorganic Network Structure with Extraordinary Mechanical, Optical, and Swelling/De-swelling Properties. *Advanced Materials* **2002**, *14* (16), 1120. https://doi.org/10.1002/1521-4095(20020816)14:16.

150 Wei, Z.; Zhao, J.; Chen, Y. M.; Zhang, P.; Zhang, Q. Self-healing polysaccharide-based hydrogels as injectable carriers for neural stem cells. *Scientific Reports* **2016**, *6* (1), 37841. https://doi.org/10.1038/srep37841.

151 Xue, B.; Bashir, Z.; Guo, Y.; Yu, W.; Sun, W.; Li, Y.; Zhang, Y.; Qin, M.; Wang, W.; Cao, Y. Strong, tough, rapid-recovery, and fatigue-resistant hydrogels made of picot peptide fibres. *Nature Communications* **2023**, *14* (1), 2583. https://doi.org/10.1038/s41467-023-38280-4.

152 Okay, O. General properties of hydrogels. In *Springer series on chemical sensors and biosensors*; 2009; pp 1–14. https://doi.org/10.1007/978-3-540-75645-3_1.

153 Shi, Y.; Wang, R.; Bi, S.; Yang, M.; Liu, L.; Niu, Z. An Anti-Freezing hydrogel electrolyte for flexible Zinc-Ion batteries operating at −70 °C. *Advanced Functional Materials* **2023**, *33* (24). https://doi.org/10.1002/adfm.202214546.

154 Lin, K. A., Lin, T., Chen, Y., & Lin, Y. (2017). Ferrocene as an efficient and recyclable heterogeneous catalyst for catalytic ozonation in water. *Catalysis Communications*, *95*, 40–45. https://doi.org/10.1016/j.catcom.2017.03.004

155 Wu, J.; Gu, M.; Travaglini, L.; Lauto, A.; Ta, D.; Wagner, P.; Wagner, K.; Zeglio, E.; Savva, A.; Officer, D.; Mawad, D. Organic Mixed Ionic–Electronic Conductors Based on Tunable and Functional Poly(3,4-ethylenedioxythiophene) Copolymers. *ACS Appl. Mater. Interfaces* **2024**, *16*, 22, 28969–28979.

156 Luo, Y.; Abidian, M. R.; Ahn, J.-H.; Akinwande, D.; Andrews, A. M.; Antonietti, M.; Bao, Z.; Berggren, M.; Berkey, C. A.; Bettinger, C. J.; Chen, J.; Chen, P.; Cheng, W.; Cheng, X.; Choi, S.-J.; Chortos, A.; Dagdeviren, C.; Dauskardt, R. H.; Di, C.; Dickey, M. D.; Duan, X.; Facchetti, A.; Fan, Z.; Fang, Y.; Feng, J.; Feng, X.; Gao, H.; Gao, W.; Gong, X.; Guo, C. F.; Guo, X.; Hartel, M. C.; He, Z.; Ho, J. S.; Hu, Y.; Huang, Q.; Huang, Y.; Huo, F.; Hussain, M. M.; Javey, A.; Jeong, U.; Jiang, C.; Jiang, X.; Kang, J.; Karnaushenko, D.; Khademhosseini, A.; Kim, D.-H.; Kim, I.-D.; Kireev, D.; Kong, L.; Lee, C.; Lee, N.-E.; Lee, P. S.; Lee, T.-W.; Li, F.; Li, J.; Liang, C.; Lim, C. T.; Lin, Y.; Lipomi, D. J.; Liu, J.; Liu, K.; Liu, N.; Liu, R.; Liu, Y.; Liu, Y.; Liu, Z.; Liu, Z.; Loh, X. J.; Lu, N.; Lv, Z.; Magdassi, S.; Malliaras, G. G.; Matsuhisa, N.; Nathan, A.; Niu, S.; Pan, J.; Pang, C.; Pei, Q.; Peng, H.; Qi, D.; Ren, H.; Rogers, J. A.; Rowe, A.; Schmidt, O. G.; Sekitani, T.; Seo, D.-G.; Shen, G.; Sheng, X.; Shi, Q.; Someya, T.; Song, Y.; Stavrinidou, E.; Su, M.; Sun, X.; Takei, K.; Tao, X.-M.; Tee, B. C. K.; Thean, A. V.-Y.; Trung, T. Q.; Wan, C.; Wang, H.; Wang, J.; Wang, M.; Wang, S.; Wang, T.; Wang, Z. L.; Weiss, P. S.; Wen, H.; Xu, S.; Xu, T.; Yan, H.; Yan, X.; Yang, H.; Yang, L.; Yang, S.; Yin, L.; Yu, C.; Yu, G.; Yu, J.; Yu, S.-H.; Yu, X.; Zamburg, E.; Zhang, H.; Zhang, X.; Zhang, X.; Zhang, X.; Zhang, Y.; Zhang, Y.; Zhao, S.; Zhao, X.; Zheng, Y.; Zheng, Y.-Q.; Zheng, Z.; Zhou, T.; Zhu, B.; Zhu, M.; Zhu, R.; Zhu, Y.; Zhu, Y.; Zou, G.; Chen, X. Technology Roadmap for Flexible Sensors. *ACS Nano* **2023**, *17*, 5211 – 5295.

157 Vural, M.; Mohammadi, M.; Seufert, L.; Han, S.; Crispin, X.; Fridberger, A.; Berggren, M.; Tybrandt. K. Soft Electromagnetic Vibrotactile Actuators with Integrated Vibration Amplitude Sensing. *ACS Appl. Mater. Interfaces* **2023**, *15*, 30653–30662.

158 Martins, P.; Pereira, N.; Lima, A. C.; Ander García Díez; C. Mendes-Filipe; R. Policia; Correia, V.; Senentxu Lanceros-Méndez. Advances in Printing and Electronics: From Engagement to Commitment. *Adv. Funct. Mater*. **2023**, *33*, 2213744.

159 Kwon, J.; DelRe, C.; Kang, P.; Hall, A.; Arnold, D.; Jayapurna, I.; Ma, L.; Michalek, M.; Ritchie, R. O.; Xu, T. Conductive Ink with Circular Life Cycle for Printed Electronics. *Adv. Mater*. **2022**, *34*, 2202177.

160 Tavakoli, M.; Pedro Alhais Lopes; Abdollah Hajalilou; Silva, A.; Manuel Reis Carneiro; da, J.; Pereira, J.; A.T. de Almeida. 3R Electronics: Scalable Fabrication of Resilient, Repairable, and Recyclable Soft-Matter Electronics. *Adv. Mater*. **2022**, *34*, 2203266.

161 Yang, W.; List-Kratochvil, E. J. W.; Wang, C. Metal Particle-Free Inks for Printed Flexible Electronics. *J. Mater. Chem. C,* **2019**, *7*, 15098 – 15117.

162 Yuan, J.; Zhang, Y.; Li, G.; Liu, S.; Zhu, R. Printable and Stretchable Conductive Elastomers for Monitoring Dynamic Strain with High Fidelity. *Adv. Funct. Mater*. **2022**, *32*, 2204878.

163 Wang, H.; Zhao, Z.; Liu, P.; Guo, X. A Soft and Stretchable Electronics Using Laser-Induced Graphene on Polyimide/PDMS Composite Substrate. *npj Flex. Electron*., **2022**, *6*, 26.

164. Fan, X.; Nie, W.; Tsai, H.; Wang, N.; Huang, H.; Cheng, Y.; Wen, R.; Ma, L.; Yan, F.; Xia, Y. PEDOT:PSS for Flexible and Stretchable Electronics: Modifications, Strategies, and Applications. *Adv. Sci*. **2019**, *6*, 1900813.

165. Zhang, S.; Chen, Y.; Liu, H.; Wang, Z.; Ling, H.; Wang, C.; Ni, J.; Saltik, B. C.; Wang, X.; Meng, X.; Kim, H.; Baidya, A.; Ahadian, S.; Ashammakhi, N.; Dokmeci, M. R.; Travas-Sejdic, J.; Khademhosseini, A. Hydrogels: Room-Temperature-Formed PEDOT:PSS Hydrogels Enable Injectable, Soft, and Healable Organic Bioelectronics (Adv. Mater. 1/2020). *Adv. Mater.*, **2020**, *32*, 2070005.

166. Li, G.; Huang, K.; Deng, J.; Guo, M.; Cai, M.; Zhang, Y.; Guo, C. F. Highly Conducting and Stretchable Double-Network Hydrogel for Soft Bioelectronics. *Adv. Mater.*, **2022**, *34*, 2200261.

167. He, H.; Ouyang, J. Enhancements in the Mechanical Stretchability and Thermoelectric Properties of PEDOT:PSS for Flexible Electronics Applications. *Acc. Mater. Res*. **2020**, *1*, 146 – 157.

168. Li, Y.; Pang, Y.; Wang, L.; Li, Q.; Liu, B.; Li, J.; Liu, S.; Zhao, Q. Boosting the Performance of PEDOT:PSS Based Electronics via Ionic Liquids. *Adv. Mater*. **2024**, *36*, 2310973.

169. He, H.; Zhang, L.; Yue, S.; Yu, S.; Wei, J.; Ouyang, J. Enhancement in the Mechanical Stretchability of PEDOT:PSS Films by Compounds of Multiple Hydroxyl Groups for Their Application as Transparent Stretchable Conductors. *Macromolecules* **2021**, *54*, 1234 – 1242.

170. Miao, Q.; Yang, R.; Wang, Z.; Liu, Y.; Zhang, Q.; He, B.; Li, K.; Yang, Q.; Wei, L.; Pan, C.; Chen, M. Bioinspired Self-Healing Soft Electronics. *Adv. Funct. Mater*. **2023**, *33*, 2214479.

171. Khatib, M.; Zohar, O.; Haick, H. Self-Healing Soft Sensors: From Material Design to Implementation. *Adv. Mater.* **2021**, *33*, 2004190.

172. Shuai, L.; Guo, Z. H.; Zhang, P.; Wan, J.; Pu, X.; Wang, Z. L. Stretchable, Self-Healing, Conductive Hydrogel Fibers for Strain Sensing and Triboelectric Energy-Harvesting Smart Textiles. *Nano Energy*, **2020**, *78*, 105389.

173. Li, C.-H.; Wang, C.; Keplinger, C.; Zuo, J.-L.; Jin, L.; Sun, Y.; Zheng, P.; Cao, Y.; Lissel, F.; Linder, C.; You, X.-Z.; Bao, Z. A Highly Stretchable Autonomous Self-Healing Elastomer. *Nat. Chem*. **2016**, *8*, 618–624.

174. Wang, H.; Zhuang, T.; Wang, J.; Sun, X.; Wang, Y.; Li, K.; Dai, X.; Guo, Q.; Li, X.; Chong, D.; Chen, B.; Yan, J. Multifunctional Filler-Free PEDOT:PSS Hydrogels with Ultrahigh Electrical Conductivity Induced by Lewis-Acid-Promoted Ion Exchange. *Adv. Mater*. **2023**, *35*, 2302919.

175. Park, H.; Kang, T.; Kim, H.; Kim, J.-C.; Bao, Z.; Kang, J. Toughening Self-Healing Elastomer Crosslinked by Metal–Ligand Coordination through Mixed Counter Anion Dynamics. *Nat. Commun.* **2023**, *14*, 5026.

176. Kong, Z.; Boahen, E. K.; Kim, D. J.; Li, F.; Kim, J. S.; Kweon, H.; Kim, S. Y.; Choi, H.; Zhu, J.; Bin Ying, W.; Kim, D. H. Ultrafast Underwater Self-Healing Piezo-Ionic Elastomer via Dynamic Hydrophobic-Hydrolytic Domains. *Nat. Commun.* **2024**, 15, 2129.

177. Kim, Y. M.; Kwon, J. H.; Kim, S.; Choi, U. H.; Moon, H. C. Ion-Cluster-Mediated Ultrafast Self-Healable Ionoconductors for Reconfigurable Electronics. *Nat Commun*. **2022**, *13*, 3769.

178. Yin, J.; Pan, S.; Wu, L.; Tan, L.; Chen, D.; Huang, S.; Zhang, Y.; He, P. A Self-Adhesive Wearable Strain Sensor Based on a Highly Stretchable, Tough, Self-Healing and Ultra-Sensitive Ionic Hydrogel. *J. Mater. Chem. C*, **2020**, *8*, 17349 – 17364.

179. Hu, L.; Chee, P. L.; Sugiarto, S.; Yu, Y.; Shi, C.; Yan, R.; Yao, Z.; Shi, X.; Zhi, J.; Kai, D.; Yu, H.; Huang, W. Hydrogel-Based Flexible Electronics. *Adv. Mater*. **2023**, *35*, 2205326.

180. Clevenger, M.; Kim, H.; Song, H. W.; No, K.; Lee, S. Binder-Free Printed PEDOT Wearable Sensors on Everyday Fabrics Using Oxidative Chemical Vapor Deposition. *Sci. Adv*. **2021**, *7*, eabj8958.

181. Tirrell, M. Polyelectrolyte Complexes: Fluid or Solid? *ACS Cent. Sci.* **2018**, *4*, 532–533.

182. Ju, D.; Kim, D.; Yook, H.; Jeong Woo Han; Cho, K. Controlling Electrostatic Interaction in PEDOT:PSS to Overcome Thermoelectric Tradeoff Relation. *Adv. Funct. Mater*. **2019**, *29*, 1905590.

183. Roy, S.; Deo, K. A.; Hung Pang Lee; Soukar, J.; Namkoong, M.; Tian, L.; Jaiswal, A.; Gaharwar, A. K. 3D Printed Electronic Skin for Strain, Pressure and Temperature Sensing. *Adv. Funct. Mater*. **2024**, *34*, 2313575.

184. Saghafi, M. K.; Vasantham, S. K.; Hussain, N.; Mathew, G.; Colombo, F.; Schamberger, B.; Pohl, E.; Gabriel Cadilha Marques; Breitung, B.; Tanaka, M.; Bastmeyer, M.; Selhuber-Unkel, C.; Schepers, U.; Hirtz, M.; Aghassi-Hagmann, J. Printed Electronic Devices and Systems for Interfacing with Single Cells up to Organoids. *Adv. Funct. Mater*. **2023**, *34*, 2308613.

185. Su, Z.; Jin, Y.; Wang, H.; Li, Z.; Huang, L.; Wang, H. PEDOT:PSS and Its Composites for Flexible Supercapacitors. *ACS Appl. Energy Mater.*, **2022**, *5*, 11915-11932.

186. Sharma, N.; Aarju Mathew Koshy; Ganapathi Rao Kandregula; Ramanujam, K.; Ray, D.; Swaminathan, P. Printed Silver Nanowire-PEDOT:PSS Composite Electrodes for Flexible Transparent Microsupercapacitor Applications. *ACS Appl. Energy Mater*. **2024**, *7*, 363–372.

187. Kim, T. G.; Ha, S. R.; Choi, H.; Uh, K.; Kundapur, U.; Park, S.; Lee, C. W.; Lee, S. H.; Kim, J.; Kim, J. M. Polymerizable Supramolecular Approach to Highly Conductive PEDOT: PSS Patterns. *ACS Appl. Mater. Interface* **2017**, *9*, 19231-19237.

188. Kanwat, A.; Jang, J. High Work Function with Reduced Phase Separation of PSS in Metal Oxide Modified PEDOT:PSS Interlayers for Organic Photovoltaics. *RSC Adv*. **2016**, *6*, 114800 – 114807.

189. Casanova, N.; Shyam Shankar S; Gómez-Escalonilla, M. J.; Pilar; Singhal, R.; Sharma, G. D.; Langa, F. Improved Efficiency in Organic Solar Cells Based on A2-D-A1-D-A2 Nonfullerene Acceptors with a Benzoselenadiazole Core Induced by Higher Dipole Moment and Dielectric Constant. *ACS Appl. Energy Mater*. **2023**, *6*, 12052–12063.

190. Meisburger, S. P.; Case, D. A.; Ando, N. Diffuse X-Ray Scattering from Correlated Motions in a Protein Crystal. *Nat. Commun.* **2020***, 11*, 1271.

191. O'neill, S. J. K.; Huang, Z.; Chen, X.; Sala, R. L.; Mccune, J. A.; Malliaras, G. G.; Scherman, O. A. Highly stretchable dynamic hydrogels for soft multilayer electronics. Sci. Adv.2024, 10, eadn5142.

192 Shi, W.; Wang, Z.; Song, H.; Chang, Y.; Hou, W.; Li, Y.; Han, G. High-sensitivity and extreme environment-resistant sensors based on PEDOT:PSS@PVA hydrogel fibers for physiological monitoring. *ACS Appl. Mater. Interfaces* 2022, *14*, 35114– 35125.

193 Zhang, Z.; Chen, G.; Xue, Y.; Duan, Q.; Liang, X.; Lin, T.; Wu, Z.; Tan, Y.; Zhao, Q.; Zheng, W.; Wang, L.; Wang, F.; Luo, X.; Xu, J.; Liu, J.; Lu, B. Fatigue-Resistant Conducting Polymer Hydrogels as Strain Sensor for Underwater Robotics. *Adv. Funct. Mater.* **2023**, *33*, 2305705.

194 He, X.; Shi, J.; Hao, Y.; Wang, L.; Qin, X.; Yu, J. PEDOT:PSS/CNT composites based ultra-stretchable thermoelectrics and their application as strain sensors. *Compos. Commun.* **2021**, *27*, 100822.

195 Zhao, W.; Zhang, D.; Yang, Y.; Du, C.; Zhang, B. A Fast Self-Healing Multifunctional Polyvinyl Alcohol Nano-Organic Composite Hydrogel as a Building Block for Highly Sensitive Strain/Pressure Sensors. *J. Mater. Chem. A*, **2021**, *9*, 22082-22094.

196 Vahdani, M.; Razbin, M.; Moshizi, S. A.; Payne, D.; Huang, S.; Asadnia, M.; Peng, S.; Wu, S. Transient Piezoresistive Strain Sensors Based on Elastic Biopolymer Thin Films. *ACS Appl. Polym. Mater.* **2024**, *6*, 6530–6539.

197 A. Prameswati, S. A. N. Entifar, J. W. Han, A. F. Wibowo, J.H. Kim, Y. S. b. Sembiring, J. Park, J. Lee, A.Y Lee, M. H. Song, S. Kim, D. C. Lim, Y. Eom, S. Heo, M. W. Moon, M.S. Kim, Y. H. Kim. Self-Healable Conductive Hydrogels with High Stretchability and Ultralow Hysteresis for Soft Electronics. *ACS Appl. Mater. Interfaces* **2023**, *15*, 24648–24657.

198 Ji, H.; He, H.; Sun, J.; Lu, W.; Yu, H.; Zhu, J.; Liu, Y.; Chen, S.; Cao, H. Sensitive Wearable Strain Sensor Based on a Self-Doped Conductive Hydrogel. *ACS Appl. Electron. Mater*. **2024**, *6*, 4619–4629.

199 Li, P.; Wang, H.; Ju, Z.; Jin, Z.; Ma, J.; Yang, L.; Zhao, X.; Xu, H.; Liu, Y. Ti_3C_2Tx MXene- and Sulfuric Acid-Treated Double-Network Hydrogel with Ultralow Conductive Filler Content for Stretchable Electromagnetic Interference Shielding. *ACS Nano* **2024**, *18*, 2906– 2916.

200. Debnath, S.; Upadhyay, C.; Ojha, U. Healable, Recyclable, and Programmable Shape Memory Organogels Based on Highly Malleable Catalyst-Free Carboxylate Linkages. *ACS Appl. Mater. Interfaces* **2022**, *14*, 9618– 9631.

201. Kumar, A.; Rewati Raman Ujjwal; Mittal, A.; Bansal, A.; Ojha, U. Polyacryloyl Hydrazide: An Efficient, Simple, and Cost Effective Precursor to a Range of Functional Materials through Hydrazide Based Click Reactions. *ACS Appl. Mater. Interfaces* **2014**, *6*, 1855– 1865.

202 Wiita, E. G.; Toprakcioglu, Z.; Jayaram, A. K.; Knowles, T. P. J. Formation of nanofibrillar Self-Healing hydrogels using antimicrobial peptides. *ACS Applied Materials & Interfaces* **2024**, *16* (35), 46167–46176. https://doi.org/10.1021/acsami.4c11542.

203 Liang, C.; Dudko, V.; Khoruzhenko, O.; Hong, X.; Lv, Z.-P.; Tunn, I.; Umer, M.; Timonen, J. V. I.; Linder, M. B.; Breu, J.; Ikkala, O.; Zhang, H. Stiff and self-healing hydrogels by polymer entanglements in co-planar nanoconfinement. *Nature Materials* **2025**, *24* (4), 599–606. https://doi.org/10.1038/s41563-025-02146-5.

204 Tian, R.; Qiu, X.; Yuan, P.; Lei, K.; Wang, L.; Bai, Y.; Liu, S.; Chen, X. Fabrication of Self-Healing Hydrogels with On-Demand Antimicrobial Activity and Sustained Biomolecule Release for Infected Skin Regeneration. *ACS Applied Materials & Interfaces* **2018**, *10* (20), 17018–17027. https://doi.org/10.1021/acsami.8b01740.

205 Fang, Y.; Wang, C.-F.; Zhang, Z.-H.; Shao, H.; Chen, S. Robust Self-Healing hydrogels assisted by Cross-Linked nanofiber networks. *Scientific Reports* **2013**, *3* (1), 2811. https://doi.org/10.1038/srep02811.

206 Nandi, S. K.; Maji, K.; Haldar, D. Self-Healing Hydrogel from a Dipeptide and HCl Sensing. *ACS Omega* **2018**, *3* (4), 3744–3751. https://doi.org/10.1021/acsomega.8b00358.

207. Aguzin, A.; Dominguez-Alfaro, A.; Criado-Gonzalez, M.; Velasco-Bosom, S.; L. Picchio, M.; Casado, N.; Mitoudi-Vagourdi, E.; J. Minari, R.; G. Malliaras, G.; Mecerreyes, D. Direct Ink Writing of PEDOT Eutectogels as Substrate-Free Dry Electrodes for Electromyography. *Mater. Horiz*. **2023**, *10*, 2516-2524.

208. Lee, J. J.; Gandla, S.; Lim, B.; Kang, S.; Kim, S.; Lee, S.; Kim, S. Alcohol-Based Highly Conductive Polymer for Conformal Nanocoatings on Hydrophobic Surfaces toward a Highly Sensitive and Stable Pressure Sensor. *NPG Asia Mater*., **2020**, *12*, 65.

209. Dai, Z.; Ding, S.; Lei, M.; Li, S.; Xu, Y.; Zhou, Y.; Zhou, B. A Superhydrophobic and Anti-Corrosion Strain Sensor for Robust Underwater Applications. *J. Mater. Chem. A*, **2021**, *9*, 15282 – 15293.

210. Ren, J.; Liu, Y.; Wang, Z.; Chen, S.; Ma, Y.; Wei, H.; Shaoyu Lü. An Anti-Swellable Hydrogel Strain Sensor for Underwater Motion Detection. *Adv. Funct. Mater*. **2021**, *32*, 2107404.

211 Tybrandt, K.; A gentle nerve wrapper. *Nat. Mater.* **2024**, *23*, 878.

212 Correa, S.; Grosskopf, A.K.; Hernandez, H. L.; Chan, D.; Yu, A. C.; Stapleton, L. M.; and Appel, E. A.; Translational Applications of Hydrogels. *Chem. Rev.* **2021**, *121*, 11385–11457.

213 Tateyama, A.; Nagura, K.; Yamanaka, M.; Nakanishi, T.; Alkyl–π Functional Molecular Gels: Control of Elastic Modulus and Improvement of Electret Performance. *Angew. Chem. Int. Ed.* **2024**, *136*, e202402874.

214 Sidheekha, M. P.; Shabeeba, A.; Rajan, L.; Thayyil, M. S.; Ismail. Y. A.; Conducting Polymer/Hydrogel Hybrid Free-Standing Electrodes for Flexible Supercapacitors Capable of Self-Sensing Working Conditions: Large-Scale Fabrication Through Facile and Low-Cost. *Eng. Sci.* **2023**, *23*, 890.

215 Freedman, B.R.; Uzun, O.; Luna, N. M. M.; Rock, A.; Clifford, C.; Stoler, E.; Östlund-Sholars, G.; Johnson, C.; Mooney, D. J.; Degradable and Removable Tough Adhesive Hydrogels. *Adv. Mater.* **2021**, *33*, 2008553.

216 Shome, A.; Rather, A. M.; Manna, U.; Aloe vera mucilage derived highly tolerant underwater superoleophobic coatings. *J. Mater. Chem. A* **2018**, *6*, 22465-22471.

217 Zhang, L.; Ren, H.; Wu, L.; Liu, Z.; Xie, A.; Yao, X.; Ju, J.; Liu, M.; Recent advances in gel coatings: from lab to industry. *J. Mater. Chem. A* **2024**, *12*, 18901-18920.

218 Wang, M.; Yuan, N.; Wang, X.; Ning, X.; Chen, C.; Lin, D.; Thermal-induced Phase Transition Hydrogel Revealed with Photonic Crystal. *ES Energy Environ.* **2023**, *19*, 811.

219 Li, X.; Gong, J. P.; Design principles for strong and tough hydrogels. *Nat. Rev. Mater.* **2024**, *9*, 380-398.

220 Yao, X.; Liu, J.; Yang, C.; Yang, X.; Wei, J.; Xia,Y.; Gong, X.; Suo, Z.; Hydrogel Paint. *Adv. Mater.* **2019**, *31*,1903062.

221 Gong J.P.; Katsuyama, Y.; Kurokawa, T.; Osada, Y.; Double-Network Hydrogels with Extremely High Mechanical Strength. *Adv. Mater.* **2003**, *15*, 1155-1158.

222 Zhu, S.; Wang, S.; Huang, Y.; Tang, Q.; Fu, T.; Su, R.; Fan, C.; Xia, S.; Lee, P. S.; Lin ,Y.; Bioinspired structural hydrogels with highly ordered hierarchical orientations by flow-induced alignment of nanofibrils. *Nat. Commun.* **2024**, *15*, 118.

223 Sun, Xia.; Mao, Yimin.; Yu, Z.; Yang, P.; and Jiang, F.; A Biomimetic "Salting Out—Alignment—Locking" Tactic to Design Strong and Tough Hydrogel. *Adv. Mater.* **2024**, *36*, 2400084.

224 Sun, J. Y.; Zhao, X.; Illeperuma, W. R. K.; Chaudhuri, O.; Oh, K. H.; Mooney, D. J.; Vlassak, J. J.; Suo, Z.; Highly stretchable and tough hydrogels. *Nature* **2012**, *489*, 133–136.

225 Meng, X.; Qiao, Y.; Do, C.; Bras, W.; He, C.; Ke, Y.; Russell, T. P.; Qiu, D.; Hysteresis-Free Nanoparticle-Reinforced Hydrogels. *Adv. Mater.* **2022**, *34*, 2108243.

226 Liu, C.; Morimoto, N.; Jiang, L.; Kawahara, S.; Noritomi, T.; Yokoyama, H.; Mayumi, K.; Ito, K.; Tough hydrogels with rapid self-reinforcement. *Science* **2021**, *372*, 1078-1081.

227 Gong, J. P.; Why are double network hydrogels so tough?. *Soft Matter* **2010**, *6*, 2583-2590.

228 Hua, M.; Wu, S.; Ma, Y.; Zhao, Y.; Chen, Z.; Frenkel, I.; Strzalka, J.; Zhou, H.; Zhu, X.; He, X.; Strong tough hydrogels via the synergy of freeze-casting and salting out, *Nature* **2021**, *590*, 594-599.

229 Jiang, L.; Liu, C.; Mayumi, K.; Kato, K.; Yokoyama, H.; Ito, K. Highly Stretchable and Instantly Recoverable Slide-Ring Gels Consisting of Enzymatically Synthesised Polyrotaxane with Low Host Coverage. *Chem. Mater.* **2018**, *30*, 5013-5019.

230 Kim, J.; Zhang, G.; Shi, M.; Suo, Z. Fracture, Fatigue, and Friction of Polymers in which Entanglements Greatly Outnumber Cross-links. *Science* **2021**, *374*, 212-216.

231 Feng, Y.; Wang, S.; Li, Y.; Ma, W.; Zhang, G.; Yang, M.; Li, H.; Yang, Y.; Long, Y. Entanglement in Smart Hydrogels: Fast Response Time, Anti-Freezing and Anti-Drying. *Adv. Funct. Mater.* **2023**, *33*, 2211027.

232 Zhu, R.; Zhu, D.; Zheng, Z.; Wang, X. Tough Double Network Hydrogels with Rapid Self-Reinforcement and Low Hysteresis Based on Highly Entangled Networks. *Nat. Commun.* **2024**, *15*, 1344.

233 Mandal, S.; Vignesh, A.; Debnath, S.; Ojha, U. Mechanically Robust Anisotropic Hydrogel–Organogel Conjugates for Soft Actuators with Fast Response Time and Diverse Bi-Axial Programmable Folding Ability. *Chem. Mater.* **2022**, *34*, 5125–5137.

234 Frauenlob, M.; King, D. R.; Guo, H.; Ishihara, S.; Tsuda, M.; Kurokawa, T.; Haga, H.; Tanaka, S.; Gong, J. P. Modulation and Characterization of the Double Network Hydrogel Surface-Bulk Transition. *Macromolecules* **2019**, *52*, 6704–6713.

235 Wang, M.; Xiao, X.; Siddika, S.; Shamsi, M.; Frey, E.; Qian, W.; Bai, W.; O'Connor, B. T.; Dickey, M. D. Glassy Gels Toughened by Solvent. *Nature* **2024**, *631*, 313-318.

236 Cui, W.; Zhu, R.; Zheng, Y.; Mu, Q.; Pi, M.; Chen, Q.; Ran, R. Transforming Non-Adhesive Hydrogels to Reversible Tough Adhesives via Mixed-Solvent-Induced Phase Separation. *J. Mater. Chem. A* **2021**, *9*, 9706–9718.

237 Sato, K.; Nakajima, T.; Hisamatsu, T.; Nonoyama, T.; Kurokawa, T.; Gong, J. P. Phase-Separation-Induced Anomalous Stiffening, Toughening, and Self-Healing of Polyacrylamide Gels. *Adv. Mater.* **2015**, *27*, 6990–6998.

238 Li, M.; Lu, H.; Wang, X.; Wang, Z.; Pi, M.; Cui, W.; Ran, R. Regulable Mixed-Solvent-Induced Phase Separation in Hydrogels for Information Encryption. *Small* **2022**, *18*, 2205359.

239 Cui, W.; Zhu, R.; Zheng, Y.; Mu, Q.; Pi, M.; Chen, Q.; Ran, R. Transforming non-adhesive hydrogels to reversible tough adhesives via mixed-solvent-induced phase separation *J. Mater. Chem. A* **2021**, *9*, 9706.

240 Hu, L.; Luo, H.; Xie, J.; Li, M.; Lu, H.; Shen, H.; Cui, W.; Ran, R. Mixed-Solvent-Induced Phase Separation Enables Anisotropy and Strengthening of Hydrogels Composed of Flexible Network Chains. *Small*, 2025. DOI:10.1002/smll.202410734

241 Zhang, L.; Ma, W.; Tang, H.; Yu, Y.; Wang, L.; Li, T.; Fang, Z.; Qiao, Z. Tough, low-friction and homogeneous physical hydrogel by a solvent-inducted strategy. *Chem. Eng. J.* **2023**, *466*, 143195.

242 Li, F.; Han, J.; Cao, T.; Li, L. Design of Self-Assembly Dipeptide Hydrogels and Machine Learning via Their Chemical Features. *Proc. Nat. Ac. Sci.* **2019**, *116*, 11259.

243 Lavrentev, F. V.; Rumyantsev, I. S.; Ivanov, A. S.; Shilovskikh, V. V.; Orlova, O. Y.; Nikolaev, K. G.; Andreeva, D. V.; Skorb, E. V. Soft Hydrogel Actuator for Fast Machine-Learning-Assisted Bacteria Detection. *ACS Appl. Mater. Interfaces* **2022**, *14,* 7321–7328.

244 Meyer, T. A.; Ramirez, C.; Tamasi, M. J.; Gormley, A. J. A User's Guide to Machine Learning for Polymeric Biomaterials. *ACS Polym. Au* **2023**, *3*, 141–157.

245 Munson, B. P.; Chen, M.; Bogosian, A.; Kreisberg, J. F.; Licon, K.; Abagyan, R.; Kuenzi, B. M.; Ideker, T. De novo Generation of Multi-Target Compounds Using Deep Generative Chemistry. *Nat. Commun.* **2024**, *15,* 3636.

246 Bran, A. M.; Cox, S.; Schilter, O.; Baldassari, C.; White, A. D.; Schwaller, P. What is in Your LLM-based Framework?. *Nat. Machine Intelligence* **2024**, *6*, 525–535.

247 Roldán, E.; Reeves, N. D.; Cooper, G.; Andrews, K. Machine Learning to Predict Morphology, Topography and Mechanical Properties of Sustainable Gelatin-Based Electrospun Scaffolds. *Sci. Rep.* **2024**, *14*, 21017.

248 Yan, C.; Li, G. The Rise of Machine Learning in Polymer Discovery. *Adv. Intell. Syst.* **2023**, *5*, 2200243.

249 Zhu, J.; Jia, Y.; Lei, J.; Liu, Z. *Mathematics* **2021**, *9*, 2804.

250 Li, Z.; Song, P.; Li, G.; Han, Y.; Ren, X.; Bai, L.; Su, J.; AI Energized Hydrogel Design, Optimization and Application in Biomedicine. *Materials Today Bio.* **2024**, *25*, 101014.

251 Li, W.; Wen, Y.; Wang, K.; Ding, Z.; Wang, L.; Chen, Q.; Xie, L.; Xu, H.; Zhao, H.; Developing a machine learning model for accurate nucleoside hydrogels prediction based on descriptors. *Nat. Commun.* **2024**, *15*, 2603.

252 Xue, C.; Zhao, Y.; Liao, Y.; Zhang, H.; Bioinspired Super-Robust Conductive Hydrogels for Machine Learning-Assisted Tactile Perception System. *Adv. Mater.* **2025**, *37*, 2416275.

253 Fan, H.; Naohara, D.; Li, W.; Li, X.; Gong, J. P.; Tuning Network Structures of Hydrophobic Hydrogels by Controlling Polymerization Solvent. *Polym. Chem.* **2024**, *15,* 2104.

254 Gao, H.; Zhao, Z.; Cai, Y.; Zhou, J.; Hua, W.; Chen, L.; Wang, L.; Zhang, J.; Han, D.; Liu, M.; Jiang, L.; Adaptive and Freeze-Tolerant Heteronetwork Organohydrogels with Enhanced Mechanical Stability Over a Wide Temperature Range. *Nat. Commun.* **2017**, *8*, 15911.

255 Moreno, R. O.; Penott-Chang, E. K.; Gáscue, B. R.; Müller, A. J.; The Effect of the Solvent Employed in the Synthesis of Hydrogels of Poly (Acrylamide-Co-Methyl Methacrylate) on Their Structure, Properties and Possible Biomedical Applications. *Europ. Polym. J.* **2017**, *88*, 148-160.

256 Gilberta, J. B.; Rubnerb, M. F.; Cohen, R. E.; Depth-profiling X-ray Photoelectron Spectroscopy (XPS) Analysis of Interlayer Diffusion in Polyelectrolyte Multilayers. *Proc. Nat. Ac. Sci.* **2013**, *110*, 6651.

257 Sun, X.; Mao, Y.; Yu, Z.; Yang, P.; Jiang, F. A Biomimetic "Salting Out—Alignment—Locking" Tactic to Design Strong and Tough Hydrogel. *Adv. Mater*. **2024**, *36*, 2400084.

258 Mollart, C.; Trewin, A.; Rationalising the Influence of Solvent Choice on The Porosity of Conjugated Microporous Polymers. *Phys. Chem. Chem. Phys.* **2020**, *22*, 21642-21645.

259 Wang, M.; Zhang, P.; Shamsi, M.; Thelen, J. L.; Qian, W.; Truong, V. K.; Ma, J.; Hu, J.; Dickey, M. D.; Tough and Stretchable Ionogels by in situ Phase Separation. *Nat. Mater.* **2022**, *21*, 359.

260 Huang, Y.; Ming, X.; Tang, Z.; Chen, G.; Duan, X.; Zhu, H.; Zhu, S.; Zhang, Q.; Ultra-Strong Ionogel Adhesives via in situ Microphase Separation. *Adv. Funct. Mater.* **2024**, 2417011. DOI: 10.1002/adfm.202417011.

261 Liu, H.; Liu, C.; Shao, D.; Li, W.; Hu, X.; Tian, J.; Li, L.; Ding, S.; Zhou, C.; Lu, L. A Tough Janus Hydrogel Patch with Strong Wet Adhesion and Self-Debonding for Oral Ulcer Treatment. *Chem. Mater.* **2024**, *36*, 4976–4989.

262 He, X.; Liu, L.; Han, H.; Shi, W.; Yang, W.; Lu, X. Bioinspired and Microgel-Tackified Adhesive Hydrogel with Rapid Self-Healing and High Stretchability. *Macromolecules* **2019**, *52*, 72−80.

263 Jiang, Y.; Zhang, X.; Zhang, W.; Wang, M.; Yan, L.; Wang, K.; Han, L.; Lu, X. Infant Skin Friendly Adhesive Hydrogel Patch Activated at Body Temperature for Bioelectronics Securing and Diabetic Wound Healing. *ACS Nano* **2022**, *16*, 8662−8676.

264 Zhou, P.; Zhang, C.; Rao, Z.; Ma, X.; Hu, Y.; Chen, Y.; Wang, H.; Chen, J.; He, Y.; Tao G.; Cai, R. Bioinspired Adhesive Hydrogel Platform with Photothermal Antimicrobial, Antioxidant, and Angiogenic Properties for Whole-Process Management of Diabetic Wounds. *ACS Appl. Mater. Interfaces* **2025**, *17*, 5841−5865.

265 Zhu, J.; Li, Y.; Xie, W.; Yang, L.; Li, R.; Wang, Y.; Wan, Q.; Pei, X.; Chen, J.; Wang, J. Low-Swelling Adhesive Hydrogel with Rapid Hemostasis and Potent Anti-Inflammatory Capability for Full-Thickness Oral Mucosal Defect Repair. *ACS Appl. Mater. Interfaces* **2022**, *14*, 53575−53592.

266 Lee, J.; Choi, Y.; Song, J.; Seong, D.; Jin, S.; Ju, J.; Son, D.; Shin, M. Nerve-Mimetic Adhesive Hydrogel Electroceuticals: Tailoring In Situ Physically Entangled Domains in Singular Polymers. *ACS Nano* **2024**, *18*, 34949−34961.

267 Li, Y.; Liu, Y.; Liu, H.; Yu, S.; Ba, Z.; Liu, M.; Ma, S.; Xing, L. B. Design of Stretchable and Conductive Self-Adhesive Hydrogels as Flexible Sensors by Guar-Gum-Enabled Dynamic Interactions. *Langmuir* **2024**, *40*, 10305−10312.

268 Guo, H.; Huang, S.; Xu, A.; Xue, W. Injectable Adhesive Self-Healing Multiple-Dynamic-Bond Crosslinked Hydrogel with Photothermal Antibacterial Activity for Infected Wound Healing. *Chem. Mater.* **2022**, *34*, 2655−2671.

269 Zhang, Z.; Yao, A.; Raffa, P. Transparent, Highly Stretchable, Self-Healing, Adhesive, Freezing-Tolerant, and Swelling-Resistant Multifunctional Hydrogels for Underwater Motion Detection and Information Transmission. *Adv. Funct. Mater.* **2024**, *34*, 2407529.

270 Xue, B.; Gu, J.; Li, L.; Yu, W.; Yin, S.; Qin, M.; Jiang, Q.; Wang, W.; Cao, Y. Hydrogel Tapes for Fault-Tolerant Strong Wet Adhesion. *Nat. Commun.* **2021**, *12*, 7156.

271 Du, P.; Wang, J.; Hsu, Y. I.; Uyama, H. Hydrophobic Association Hydrogel Enabled by Multiple Noncovalent Interactions for Wearable Bioelectronics in Amphibious Environments. *Chem. Mater.* **2024**, *36*, 1318-1332.

272 Ling, Q.; Liu, W.; Liu, J.; Zhao, L.; Ren, Z.; Gu, H. Highly Sensitive and Robust Polysaccharide-Based Composite Hydrogel Sensor Integrated with Underwater Repeatable Self-Adhesion and Rapid Self-Healing for Human Motion Detection. *ACS Appl. Mater Interfaces* **2022**, *14*, 24741.

273 Yashima, S.; Takase, N.; Kurokawa, T.; Gong, J. P. Friction of hydrogels with controlled surface roughness on solid flat substrates. *Soft Matter* **2014**, *10*, 3192.

274 Li, M.; Lu, H.; Pi, M. Zhou, H.; Wang, Y.; Yan, B.; Cui, W.; Ran, R. Water-Induced Phase Separation for Anti-Swelling Hydrogel Adhesives in Underwater Soft Electronics. *Adv. Sci.* **2023**, *10*, 2304780.

275 Yang, J.; Bai, R.; Chen, B.; Suo, Z. Hydrogel Adhesion: A Supramolecular Synergy of Chemistry, Topology, and Mechanics. *Adv. Funct. Mater.* **2020**, *30*, 1901693.

276 Yi, B.; Li, T.; Yang, B.; Chen, S.; Zhao, J.; Zhao, P.; Zhang, K.; Wang, Y.; Wang, Z.; Bian, L. Surface hydrophobization of hydrogels via interface dynamics-induced network reconfiguration. *Nat. Commun.* **2024***, 15,* 239.

277 Li, K.; Rubungo, A. N.; Lei, X.; Persaud, D.; Choudhary, K.; DeCost, B.; Dieng, A. B.; Hattrick-Simpers, J. Probing out-of-distribution generalization in machine learning for materials. *Commun. Mater.* **2025**, *6*, 9.

278 Quiñonero-Candela, J.; Sugiyama, M.; Schwaighofer, A; Lawrence, N. D. Eds., 2009. Dataset shift in machine learning. MIT Press.

279 Chu, R.; Liu, W.; Liu, X.; Yu, D.; Song, Z.; Li, G.; Wang, H. Carbon Nanotube Aerogel-Based Composite Hydrogel for Strain Sensing. *ACS Appl. Nano Mater.* **2024**, *7* (16), 19355–19367. https://doi.org/10.1021/acsanm.4c03250.

280 Zhang, X.; Pint, C. L.; Lee, M. H.; Schubert, B. E.; Jamshidi, A.; Takei, K.; Ko, H.; Gillies, A.; Bardhan, R.; Urban, J. J.; Wu, M.; Fearing, R.; Javey, A. Optically- and Thermally-Responsive Programmable Materials Based on Carbon Nanotube-Hydrogel Polymer Composites. *Nano Lett.* **2011**, *11* (8), 3239–3244. https://doi.org/10.1021/nl201503e.

281 Lu, Y.; Yue, Y.; Ding, Q.; Mei, C.; Xu, X.; Wu, Q.; Xiao, H.; Han, J. Self-Recovery, Fatigue-Resistant, and Multifunctional Sensor Assembled by a Nanocellulose/Carbon Nanotube Nanocomplex-Mediated Hydrogel. *ACS Appl. Mater. Interfaces* **2021**, *13* (42), 50281–50297. https://doi.org/10.1021/acsami.1c16828.

282 Gilshteyn, E. P.; Lin, S.; Kondrashov, V. A.; Kopylova, D. S.; Tsapenko, A. P.; Anisimov, A. S.; Hart, A. J.; Zhao, X.; Nasibulin, A. G. A One-Step Method of Hydrogel Modification by Single-Walled Carbon Nanotubes for Highly Stretchable and Transparent Electronics. *ACS Appl. Mater. Interfaces* **2018**, *10* (33), 28069–28075. https://doi.org/10.1021/acsami.8b08409.

283 Li, Z.; Tang, M.; Bai, W.; Bai, R. Preparation of Hydrophilic Encapsulated Carbon Nanotubes with Polymer Brushes and Its Application in Composite Hydrogels. *Langmuir* **2017**, *33* (24), 6092–6101. https://doi.org/10.1021/acs.langmuir.7b00972.

284 Roy, S.; David-Pur, M.; Hanein, Y. Carbon Nanotube-Based Ion Selective Sensors for Wearable Applications. *ACS Appl. Mater. Interfaces* **2017**, *9* (40), 35169–35177. https://doi.org/10.1021/acsami.7b07346.

285 Peng, Z.; Zou, Y.; Xu, S.; Zhong, W.; Yang, W. High-Performance Biomass-Based Flexible Solid-State Supercapacitor Constructed of Pressure-Sensitive Lignin-Based and Cellulose Hydrogels. *ACS Appl. Mater. Interfaces* **2018**, *10* (26), 22190–22200. https://doi.org/10.1021/acsami.8b05171.

286 Deng, Z.; Hu, T.; Lei, Q.; He, J.; Ma, P. X.; Guo, B. Stimuli-Responsive Conductive Nanocomposite Hydrogels with High Stretchability, Self-Healing, Adhesiveness, and 3D Printability for Human Motion Sensing. *ACS Appl. Mater. Interfaces* **2019**, *11* (7), 6796–6808. https://doi.org/10.1021/acsami.8b20178.

287 Interfacial Welding of Sulfur-Containing CNTs for an Elastic and Conductive Hydrogel with High-Accuracy Motion Sensing and Electrophysiology Acquisition | *ACS Applied Electronic Materials.* https://pubs.acs.org/doi/10.1021/acsaelm.5c00368 (accessed 2025-12-29).

288 Fu, F.; Wang, J.; Zeng, H.; Yu, J. Functional Conductive Hydrogels for Bioelectronics. *ACS Materials Lett.* **2020**, *2* (10), 1287–1301. https://doi.org/10.1021/acsmaterialslett.0c00309.

289 Hughes, K. J.; Iyer, K. A.; Bird, R. E.; Ivanov, J.; Banerjee, S.; Georges, G.; Zhou, Q. A. Review of Carbon Nanotube Research and Development: Materials and Emerging Applications. *ACS Appl. Nano Mater.* **2024**, *7* (16), 18695–18713. https://doi.org/10.1021/acsanm.4c02721.

290 Zhang, J.; Zeng, L.; Qiao, Z.; Wang, J.; Jiang, X.; Zhang, Y. S.; Yang, H. Functionalizing Double-Network Hydrogels for Applications in Remote Actuation and in Low-Temperature Strain Sensing. *ACS Appl. Mater. Interfaces* **2020**, *12* (27), 30247–30258. https://doi.org/10.1021/acsami.0c10430.

291 Gu, Z.; Ma, R.; Chen, X.; Lin, Z.; Yang, Y.; Tan, B.; Sun, J.; Chen, T. Polyvinyl Alcohol Modified Plant Fiber Hydrogel Pressure and Strain Dual-Model Sensors for Biomedical Signal Detection. *Adv Compos Hybrid Mater* **2025**, *8* (2), 214. https://doi.org/10.1007/s42114-024-01165-1.

292 Zhang, X. Dry and Frost Resistance Conductive Hydrogels Based on Carbon Nanotubes Hybrids for Use as Flexible Strain Sensor. *Sensors and Actuators A: Physical* **2023**, *350*, 114143. https://doi.org/10.1016/j.sna.2022.114143.

293 Liu, C.; Zhang, R.; Li, P.; Qu, J.; Chao, P.; Mo, Z.; Yang, T.; Qing, N.; Tang, L. Conductive Hydrogels with Ultrastretchability and Adhesiveness for Flame- and Cold-Tolerant Strain Sensors. *ACS Appl. Mater. Interfaces* **2022**, *14* (22), 26088–26098. https://doi.org/10.1021/acsami.2c07501.

294 Deng, X. A Rapid Stretchable Hydrogel Strain Sensor Based on PVA/MXene and Graphene with Basketball Monitoring Function. *AIP Advances* **2024**, *14* (6), 065011. https://doi.org/10.1063/5.0207037.

295 Liu, X.-W.; Huang, Y.-X.; Sun, X.-F.; Sheng, G.-P.; Zhao, F.; Wang, S.-G.; Yu, H.-Q. Conductive Carbon Nanotube Hydrogel as a Bioanode for Enhanced Microbial Electrocatalysis. *ACS Appl. Mater. Interfaces* **2014**, *6* (11), 8158–8164. https://doi.org/10.1021/am500624k.

296 Kang, S. H.; Lee, G. Y.; Lim, J.; Kim, S. O. CNT–rGO Hydrogel-Integrated Fabric Composite Synthesized via an Interfacial Gelation Process for Wearable Supercapacitor Electrodes. *ACS Omega* **2021**, *6* (30), 19578–19585. https://doi.org/10.1021/acsomega.1c02091.

297 Khan, A.; Nichakornpong, N.; Wongsalam, T.; Prathumrat, P.; Likitaporn, C.; Kasemsiri, P.; Okhawilai, M. Development of Green Synthesised AgNPs Decorated on MWCNT Modified Guar Gum-Based Self-Healing Hydrogel for Strain Sensors. *Sci Rep* **2024**, *14* (1), 29715. https://doi.org/10.1038/s41598-024-81085-8.

298 Elyassi, M.; Rashidi, A.; Hantehzadeh, M.; Elahi, S. Hydrogen Storage Behaviors by Adsorption on Multi-Walled Carbon Nanotubes. *Journal of Inorganic and Organometallic Polymers and Materials* **2017**, *27*. https://doi.org/10.1007/s10904-016-0471-y.

299 Zhao, Y.; Zhang, J.; Wang, Y.; Chen, Z. A Highly Sensitive and Room Temperature CNTs/SnO2/CuO Sensor for H2S Gas Sensing Applications. *Nanoscale Research Letters* **2020**, *15*. https://doi.org/10.1186/s11671-020-3265-7.

300 Tamahkar Irmak, E. Carbon Nanotube Based Polyvinylalcohol-Polyvinylpyrolidone Nanocomposite Hydrogels for Controlled Drug Delivery Applications. *ANADOLU UNIVERSITY JOURNAL OF SCIENCE AND TECHNOLOGY A - Applied Sciences and Engineering* **2017**, *18*, 1–1. https://doi.org/10.18038/aubtda.322138.

301 Yang, X.; Zhang, H.; Wang, Z.; Sun, X.; Ren, H. Skin-Mountable and Self-Healable Hydrogel for Strain Sensing. *ACS Appl. Electron. Mater.* **2025**, *7* (9), 4371–4381. https://doi.org/10.1021/acsaelm.5c00554.

302 Huang, S.; Wang, W.; Yang, C.; Liu, J.; Li, K.; Zhou, L.; Zhang, H.; Zhang, D.; Huang, S.; Wang, W.; Yang, C.; Liu, J.; Li, K.; Zhou, L.; Zhang, H.; Zhang, D. Highly Stretchable Conductive Hydrogel-Based Flexible Triboelectric Nanogenerators for Ultrasensitive Tactile Sensing. *Polymers* **2025**, *17* (3). https://doi.org/10.3390/polym17030342.

303 Sun, X., Qin, Z., Ye, L., Zhang, H., Yu, Q., Wu, X., Li, J., & Yao, F. (2019). Carbon nanotubes reinforced hydrogel as flexible strain sensor with high stretchability and mechanically toughness. *Chemical Engineering Journal*, *382*, 122832. https://doi.org/10.1016/j.cej.2019.122832.

304 Yang, Y., Zhao, X., Yu, J., Chen, X., Chen, X., Cui, C., Zhang, J., Zhang, Q., Zhang, Y., Wang, S., & Cheng, Y. (2020). H-Bonding Supramolecular Hydrogels with Promising Mechanical Strength and Shape Memory Properties for Postoperative Antiadhesion Application. *ACS Applied Materials & Interfaces*, *12*(30), 34161–34169. https://doi.org/10.1021/acsami.0c07753.

305 Du, B., Yin, M., Yang, K., Wang, S., Pei, Y., Luo, R., Zhou, S., & Li, H. (2024). Ultrafast polymerization of a Self-Adhesive and strain sensitive Hydrogel-Based flexible sensor for human motion monitoring and handwriting recognition. *Polymers*, *16*(11), 1595. https://doi.org/10.3390/polym16111595.

306 Nie, X., Tang, Y., Wu, T., Zhao, X., Xu, Z., Yang, R., Sun, Y., Wu, B., Han, Q., Hui, J., & Liu, W. (2024). 3D printing sequentially strengthening high-strength natural polymer hydrogel bilayer scaffold for cornea regeneration. *Regenerative Biomaterials*, *11*, rbae012. https://doi.org/10.1093/rb/rbae012.

307 Sun, J., Zhao, X., Illeperuma, W. R. K., Chaudhuri, O., Oh, K. H., Mooney, D. J., Vlassak, J. J., & Suo, Z. (2012). Highly stretchable and tough hydrogels. *Nature*, *489*(7414), 133–136. https://doi.org/10.1038/nature11409.

308 Yang, X., Abe, K., Biswas, S. K., & Yano, H. (2018). Extremely stiff and strong nanocomposite hydrogels with stretchable cellulose nanofiber/poly(vinyl alcohol) networks. *Cellulose*, *25*(11), 6571–6580. https://doi.org/10.1007/s10570-018-2030-x.

309 Yang, J., Ma, M., Zhang, X., & Xu, F. (2016). Elucidating dynamics of precoordinated ionic bridges as sacrificial bonds in interpenetrating network hydrogels. *Macromolecules*, *49*(11), 4340–4348. https://doi.org/10.1021/acs.macromol.6b00874.

310 Mahamoud, M. M., Ketema, T. M., Kuwahara, Y., & Takafuji, M. (2024). Enhancement of mechanical properties of benign polyvinyl Alcohol/Agar hydrogel by crosslinking tannic acid and applying multiple Freeze/THAw cycles. *Gels*, *10*(8), 527. https://doi.org/10.3390/gels10080527.

311 Kim, H., Kim, G., Kim, T., Lee, S., Kang, D., Hwang, M., Chae, Y., Kang, S., Lee, H., Park, H., & Shim, W. (2018). Transparent, Flexible, Conformal Capacitive Pressure Sensors with Nanoparticles. *Small*, *14*(8). https://doi.org/10.1002/smll.201703432.

312 Yeo, J. C., Yap, H. K., Xi, W., Wang, Z., Yeow, C., & Lim, C. T. (2016). Flexible and stretchable strain sensing actuator for wearable soft robotic applications. *Advanced Materials Technologies*, *1*(3). https://doi.org/10.1002/admt.201600018.

313 Chen, S., Huang, J., Zhou, Z., Chen, Q., Hong, M., Yang, S., & Fu, N. H. (2021). Highly elastic anti-fatigue and anti-freezing conductive double network hydrogel for human body sensors. *Industrial & Engineering Chemistry Research*, *60*(17), 6162–6172. https://doi.org/10.1021/acs.iecr.1c00610.

List of Figures

Figure 1.1: Development of hydrogels over the years

Figure 1.2: Schematic of the classification of Single Network (SN) Hydrogel

Figure 1. 3: Schematics of the development of Hydrogel and its application

Figure 1.4: Schematic of the synthetic approach of Double Network (DN) Hydrogels

Figure 1.5: Schematic showing the synthetic strategy of tough hydrogel

Figure 1.6: Schematic of properties and applications of hydrogel in energy storage and conversion

Figure 1.7: Schematics showing the synthetic approach & application of tough hydrogel

Figure 2.1: Schematic diagram of the Universal tensile machine for mechanical performance testing

Figure 2.2: Schematic diagram of the Dynamic Mechanical Analyser for testing the strength of the hydrogel

Figure 2.3: Schematic diagram of the Thermal Gravimetric Analyser to test the thermal stability of the hydrogel

Figure 2.4: Schematic diagram of the Rheometer instrument for viscosity analysis of conductive ink

Figure 2.5: Schematic diagram of a Lyophiliser for freeze-drying the hydrogel

Figure 2.6: Schematic diagram of X-ray Powder Diffraction instrument to check the crystallinity of the hydrogel

Figure 2.7: Schematic diagram of the Small-angle X-ray Spectroscopy instrument for an insight study of the hydrogel matrix

Figure 2.8: Schematic diagram of X-ray Photoelectron Spectrometer for elemental analysis of hydrogel

Figure 2.9: Schematic diagram of FE-SEM instrument for morphological study of hydrogel surface

Figure 2.10: Schematic diagram of the AFM instrument for phase study of the hydrogel surface

Figure 2.11: Schematic diagram of a Fourier Transform Infra-red spectrometer for functional group analysis

Figure 2.12: Schematic diagram of a Confocal Raman Spectrometer for surface analysis

Figure 2.13: Schematic diagram of a Microscope for insight image capturing

Figure 2.14: Schematic diagram of a UV-Vis spectrometer to check the transparency of a hydrogel

Figure 2.15: Schematic diagram of Autolab potentiostat for electrochemical study of hydrogel

Figure 3.1: UV-Vis spectra of the synthesised PEDOT: PSS

Figure 3.2: CV data of the synthesised PEDOT: PSS

Figure 3.3: (A) The FTIR data of precursors and PDTPS-PAHT-1.0 films, (B) the Raman data of PEDOT: PSS and PDTPS-PAHT-1.0, (C) the XRD data of various PDTPS-PAHT-n compositions, (D) O 1s, (E) N 1s, (F) S 2p and (G) C 1s XPS traces of PDTPS-PAHT-1.0, (H) the solvent uptake ability of PDTPS-PAHT-1.0, demonstration of (I1) stretchability, (I2) twisting ability, (I3) rolling and (I4) foldability of the film and the folded film is pressed to show the mechanical resilience.

Figure 3.4: (A) The SAXS profile of PDTPS-PAHT-n films recorded under tensile mode, (B) the effect of stretching on the SAXS profile of PDTPS-PAHT-1.0, the AFM micrographs of (C & C1) PDTPS-PAHT-1.0, (D and D1) PDTPS-PAHT-1.4 and (E & E1) PDTPS-PAHT-2.4 at different magnification, the FESEM images of (F) PDTPS-PAHT-1.0, (G) PDTPS-PAHT-1.4 and (H) PDTPS-PAHT-2.4 films.

Figure 3.5: A, B) AFM and C) FE-SEM images of PDTPS-PAHT–0.5.

Figure 3.6: The water content in PDTPS-PAHT-n films.

Figure 3.7: (A) The tensile and (D) compressive traces of the PDTPS-PAHT-n films recorded under ambient conditions, (B) the comparative chart showing the ε and Gauze factor values of reported PEDOT:PSS based composites and PDTPS-PAHT-1.0, Ref S1 to S10 are available in SI, (C) the effect of PAHT:PSSNa molar ratio on the tensile properties of the PDTPS-PAHT-n. (E) tensile and (F) compressive hysteresis cycles of PDTPS-PAHT-1.0 film, (G) the TGA thermograms of the PDTPS-PAHT-n samples, (H) the frequency sweep data of the PDTPS-PAHT-n films, i, ii, iii, iv represents PDTPS-PAHT- 0.5, 2.4, 1.4, & 1.0 respectively (I) the viscosity versus shear rate data of the PDTPS-PAHT-n samples.

Figure 3.8: The (A) curved mesh and (C) honeycomb shape printed from the PDTPS-PAHT-1.0 conductive ink using a plastic nozzle, (B) the PDTPS-PAHT-1.0 mesh is folded manually, (D) 20 g weight is hanging from a folded honeycomb shape, (E) the FESEM image of the surface of 3D printed object, (F0) a thin rectangular film of PDTPS-PAHT-1.0, (F1) the film with a cut made using a blade, (F2) the partially healed F1, (F3) the healed F1 after 12 h, (G) the tensile traces of original and self-healed film, (H) the proposed mechanism of self-healing via reformation of the $CONHNH_3^+$---SO_3^- ionic linkage.

Figure 3.9A (1): EIS plots for the PDTPS-PAHT-n in 0.1 M NaCl electrolyte.

Figure 3.9B (1): EIS plots for the PDTPS-PAHT-1.0 with varying triflic acid (%) in 0.1 M NaCl + 6% Methanol electrolyte.

Figure 3.9A (2): EIS plots for the PDTPS-PAHT-n in 0.1 M NaCl + 6% Methanol electrolyte.

Figure 3.9C(1): EIS plots for the PDTPS-PAHT-1.0 in 0.1 M NaCl electrolyte with varying temperature.

Figure 3.9: (A) The conductivity data of the PDTPS-PAHT-n films measured in 0.1 M NaCl and 0.1 M NaCl + 6% methanol solutions, (B) the effect of triflic acid on the conductivity of PDTPS-

PAHT-1.0 film, (C) the effect of varying temperature on the conductivity of PDTPS-PAHT-1.0 film, in presence of 0.1M NaCl, (D) the $\Delta R/R_0$ data of PDTPS-PAHT-1.0 film measured for five continuous cycles at a particular extension, (E) the $\Delta R/R_0$ values obtained at each extension for forward and reverse extension cycle, (F) the $\Delta R/R_0$ values measured for 200 continuous extension (70 %) and release cycles, (G) denotes the change in $\Delta R/R_0$ values associated with the film of PDTPS-PAHT-1.0 for the bending of finger, $\Delta R/R_0$ values of five consecutive bending and relaxation cycles of a PDTPS-PAHT-1.0 film attached to (H) wrist and (I) elbow.

Figure 3.9J: $\Delta R/R_0$ values associated with the film of PDTPS-PAHT-1.0 for the neck and forehead movement.

Figure 3.9D(1): The $\Delta R/R_0$ data of PDTPS-PAHT-1.0 films possessing different thickness.

Figure 3.10: The (A) tensile traces and (B) water content of the PDTPS-PAHT-1.0 films possessing different thicknesses recorded under ambient conditions.

Figure 3.11: (A) The schematics showing the experimental set up utilized to monitor under-water strain sensing data, (B) the PDTPS-PAHT-1.0 film swellability under water, (C) the five repetitive cycles recorded at each elongation extent till 400%, (D) the $\Delta R/R_0$ values obtained at each extension for forward and reverse extension cycle, in under-water conditions, (E) the $\Delta R/R0$ value associated with the varying temperature (F) the $\Delta R/R_0$ value associated with changing pressure (G) finger, (H) wrist and (I) elbow motion under water, the change in $\Delta R/R_0$ value with temperature and pressure for under-water conditions.

Figure 3.12: The demonstration of the stretchability of PDTPS-PAHT-1.0 film recorded at 10 ℃.

Figure 4.1: FTIR Spectra of PAMSAAm and PAMSAAm-IP0.1 samples

Figure 4.2B": Tensile traces of as-synthesised PAMSAAm-IP-n samples while varying IPA amounts in the pre-gel formulation.

Figure 4.2G: Hysteresis plot of PAMSAAm-IP0.1 recorded under fixed strain (800%) mode for five consecutive loading-unloading cycles.

Figure 4.2I: Tensile trace of different PAAAAm, PAAAAm-IPn, PAMSAA, PAMSAA-IPn compositions

Figure 4.2: A) Tensile traces of PAMSAAm-IP0.1 (IPA:H_2O = 10:90, v:v), and PAMSAAm (IPA:H_2O = 00:100, v:v). B) Comparison of mechanical properties of PAMSAAm-IPn hydrogels with varying IPA amount in the pre-gel solution. C) Effect of PEGDA amount on the mechanical properties of a PAMSAAm-IP0.1 hydrogel. D) Plot depicting variation in stretchability of the resulting hydrogels when different solvents are used in the pre-gel formulations in 10 vol% along with the water. Demonstration of mechanical properties of the optimized PAMSAAm-IP0.1 hydrogel. E1-E2) Digital images of a hydrogel being twisted and stretched and F1-F2) knotting followed by stretching. Silicone oil coating is used to avoid stickiness while samples are being deformed. The scale bar is 1 cm for digital images.

Figure 4.3J: XPS elemental mapping for the freeze-dried hydrogel samples A) PAMSAAm and B) PAMSAAm-IP0.1 depicting O1s SnapMap.

Figure 4.3K: XPS survey spectra of PAMSAAm and PAMSAAm-IP0.1 samples.

Figure 4.3: XPS mapping of hydrogel surface- (A1) S 2p mapping of PAMSAAm, (A2) S 2p mapping of PAMSAAm-IP0.1, B1) N 1s mapping of PAMSAAm, B2) N 1s mapping of PAMSAAm-IP0.1, S 2p XPS depth profile data of C1) PAMSAAm & C2) PAMSAAm-IP0.1, C 1s XPS depth profile data of D1) PAMSAAm & D2) PAMSAAm-IP0.1, E) Schematics depicting *in situ* SAXS while the hydrogel is being stretched uniaxially, F) *In situ* SAXS scattering profile data of original and uniaxially stretched (200%) PAMSAAm film, G1-G2) corresponding 2D

scattering maps of original and stretched PAMSAAm, H) scattering profiles of original and stretched (200%) PAMSAAm-IP0.1 film and I1-I2) corresponding 2D scattering maps when PAMSAAm-IP0.1 sample stretched up to 0 and 200%, respectively.

Figure 4.4: A1-B1) Confocal Raman mapping of the surfaces of PAMSAAm at 1042 and 1224 cm^{-1} respectively and A2-B2) Confocal Raman mapping of the surfaces of PAMSAAm-IP0.1 at 1042 and 1224 cm^{-1} respectively. C1-C2) FESEM images of as synthesized followed by freeze dried PAMSAAm and PAMSAAm-IP0.1 films respectively, D1-D2) EDS elemental line scan data of C1 and C2, the overlaid plots showing intensity of elements along the line scan, E1-E2) AFM height profile images of freeze dried PAMSAAm and PAMSAAm-IP0.1 showing distinctive segregated microdomains for the latter and FESEM images of fully swelled in aqueous media followed by freeze dried (F1) PAMSAAm and (F2) PAMSAAm-IP0.1.

Figure 4.4G: Raman Spectra of A) PAMSAAm and B) PAMSAAm-IP0.1 hydrogels

Figure 4.5H: Adhesive performance of different PAMSAAm-IP-n samples when adhered to PAMSAAm hydrogel in lap shear mode. PAMSAAm hydrogel was adhered to glass slide and different PAMSAAm-IP-n samples were varied on the other glass substrate and sandwiched.

Figure 4.5: Demonstrations of adhesive properties of the PAMSAAm-IP0.1. Digital images of as-synthesized PAMSAAm-IP0.1 film adhered to different surfaces- A1) glass stopper, A2) human skin, A3) wood, A4) paper cup, A5) HDPE cap, A6) Stainless steel weight and A7) rubber stopper. B) Performance of PAMSAAm and PAMSAAm-IP0.1 under lap-shear adhesive test on glass surface. C) Self-adhesive performance of PAMSAAm film and other compositions under lap-shear test, when both glass substrates having similar hydrogel samples attached to it. D) Performance of PAMSAAm-IP0.1 under lap-shear adhesive test on PAMSAAm and PAMSAAm-IP-n hydrogel surfaces, when PAMSAAm-IP0.1 is attached to one glass substrate and the other one is varied. E)

Ashby plot of adhesive strength and elongation at break during tensile testing (in %) of PAMSAAM-IP0.1 with other reported hydrogel systems. F) Schematic illustration of the adhesion mechanism. G) Microscopic image of the interface between PAMSAAM-IP0.1 hydrogel and a glass substrate while the hydrogel is being peeled off. The scale bar for digital images is 1 cm.

Figure 4.6I: Water content of PAMSAAm-IP0.1 hydrogel after 12 hr of air exposure

Figure 4.6: Performance of PAMSAAm-IP0.1 hydrogel under sub-zero temperatures, A) digital images of PAMSAAm-IP0.1 film demonstrating stretchability at different subzero temperatures, digital images of a PAMSAAm-IP0.1 film subjected to different mechanical deformations such as B) folding, C) twisting and D) knotting at sub-zero temperature, adhesive performance of PAMSAAm-IP0.1 sample at sub-zero temperature when adhered to E) plastic cap, F) glass stopper and G) paper, (H1-H3) digital images of a PAMSAAm-IP0.1 film attached to a knee joint model kept at -15 ºC and subjected to repeated bending and relaxing cycles, the temperatures are visible in the sensor screens behind the scenes.

Figure 4.7I: Young's modulus of hydrogel samples utilised in the testing and training dataset.

Figure 4.7: Machine learning (ML) tool to predict pre—gel composition for a hydrogel with desired physicochemical properties. A-B) Plots illustrating UTS and elongation of all the hydrogel samples utilized as test and training data. The plots depicting ML model accuracy for different parameters: C) Solvent amount, D) Crosslinker PEGDA concentration and E) Solvent polarity index. RMSE, MAE, r values and distribution of test and training data along the 1:1 line visualise the accuracy of the ML model. F) Schematic illustration of a protocol to prepare a hydrogel with desired mechanical properties utilising the prediction from the trained MTRFR model. G) Comparison of UTS and elongation values of the model input and the experimental data recorded on the resulting hydrogel.

Figure 4.7J: Tensile traces of hydrogel samples prepared as per the machine learning predicted pre-gel formulation.

Figure 5.1: (A) Raman data of AAmCNH-n and AAmCNH-0 hydrogel film, (B) XRD spectra of CNT dispersion and AAmCNH-2 film, (C) HR-TEM images of CNT dispersion to check the structure of CNT particles, FE-SEM image of freeze-dried (D) AAmCNH-0 film, (E) AAmCNH-0.5 film, (F) AAmCNH-2 film, based on the concentration of CNT in hydrogel matrix

Figure 5.2: A) Tensile traces of AAmCNH-n hydrogel films. B) The cyclic tensile hysterisis plot of as-synthesised AAmCNH-2 hydrogel film. C1) Digital images of unstretched AAmCNH-2 hydrogel film, C2) Digital images of stretched AAmCNH-2 hydrogel film, D1) Digital images of AAmCNH-2 hydrogel film having a knot. D2) Digital image of knotted & stretched AAmCNH-2 hydrogel film. E1) Digital image of twisted AAmCNH-2 hydrogel film. E2) Digital image of twisted-stretched AAmCNH-2 hydrogel film. F) Hysterisis plot of AAmCNH-2 hydrogel film at different limiting strains. G) Percentage water content plot of AAmCNH-n hydrogel films.

Figure 5.3:A) Digital image of AAmCNH-2 hydrogel film pinched against the tip of the pen to check the toughness, B) Digital image of AAmCNH-2 hydrogel film to check the transparency of film, C) Digital image of AAmCNH-2 hydrogel film showing its load bearing ability, D) Radar plot showing the mechanical strain, stress, young's modulus and conductivity of AAmCNH-2 film, E) Ashby plot comparing the mechanical performance of AAmCNH-2 hydrogel with previously reported literature, F) DSC plot to check the thermal stability of AAmCNH-n films.

Figure 5.4: A) Schematic showing hydrogel tearing sandwiched between two glass slides & digital image of adhesion on human skin, B) Adhesion plot of the AAmCNH-n hydrogel film, C) Adhesion plot of the AAmCNH-n hydrogel film displaying the change of adhesive force with strain change, The macroscopic peeling test for AAmCNH-n hydrogels on human skin, D1)

Adhesion on the human skin, D2) Partial peeling on human skin, D3) complete peeling of human skin, D4) Human skin leaving no residue, Digital images of as-synthesized AAmCNH-2 film adhered to different surfaces- E1) metal, E2) human skin, E3) glass, E4) plastic cup, E5) wood, and E6) cardboard.

Figure 5.5: A) The schematics showing the experimental set-up utilised to monitor strain sensing data, B) The conductivity data of AAmCNH-n films measured at EIS study, C) the $\Delta R/R_0$ (%) values obtained at each extension, D) the response and recovery time of AAmCNH-2 film at each extension and relaxation cycle, E) the $\Delta R/R_0$ (%) values obtained at each extension for forward and reverse extension cycle, F) plot of GF variation with change of extension.

Figure 5.6: A) The $\Delta R/R_0$ (%) data of AAmCNH-2 film at different extensions, B) the $\Delta R/R_0$ (%) data of AAmCNH-2 film measured for three continuous cycles at a particular extension, C) the change in $\Delta R/R_0$ values associated with the film of AAmCNH-2 measured for three continuous cycles at different bending angles of the index finger, D) the change in $\Delta R/R_0$ (%) at extension and relaxation of AAmCNH-2 at different bending angles of index finger, the change in $\Delta R/R_0$ (%) values associated with the film of AAmCNH-2 of five consecutive bending and relaxation cycles of (E) wrist and (F) smile.

List of Tables

Table 1.1: Generational Development of hydrogel throughout the years

Table 1.2: Comparison table for Single Network and Double Network Hydrogel

Table 1.3: Application of Single Network and Double Network Hydrogel

Table 1.4: Common Single Network (SN) Hydrogel Systems used for Different Applications

Table 1.5: Common Double Network (DN) Hydrogel Systems in Flexible Electronic Devices

Table 1.6: Summary Comparing Single Network (SN) and Double Network (DN) Hydrogel Properties

Table 1.7: Future Potential of SN vs DN Hydrogels in Energy Storage Devices

Table 1.8 Tough Hydrogel Applications In Flexible Electronics

Table 1.9 : Comparison of Conductive Fillers In Tough Hydrogels

Table 3.1: Composition and mechanical property data of the PDTPS-PAHT-n compositions

Table 3.2: Table for the comparison of the Strain and Gauge factor values of the current material with the recent literature.

Table 3.3:Comparative Analysis of Previously Reported Self-Healing Hydrogels with PDTPS-PAHT-1.0

Table 4.1: Comparison table of adhesive strength (towards glass substrate) and elongation at break in a tensile test of PAMSAAm-IP0.1 hydrogel with reported hydrogel systems in literature.

Table 4.2: Table summarising mechanical properties of different hydrogel formulations

Table 4.3: Summary of the validation samples

Table 5.1: Comparison table of UTS, Stretchability and Young's Modulus of AAmCNH-2 and previously reported hydrogel systems

Table 6.1 Comparison Table of Thesis Works

List of Scheme

Scheme 3.1: The schematics showing the synthetic procedure of PDTPS-PAHT-n conductive ink and the possible ionic linkages present in the samples.

Scheme 4.1: A) Schematics of one-pot synthesis of the PAMSAAm-IP0.1 and PAMSAAm from the pre-gel solution containing monomers, crosslinker, photo initiator and solvent. Models demonstrating the unique morphology of PAMSAAm-IP0.1 and control along with enhanced physicochemical properties, such as adhesiveness and stretchability, B) Schematic illustration of machine learning tool to predict pre-gel formulation for a desired hydrogel with specific mechanical properties. The pre-gel formulations and hydrogel properties data are utilised in a machine learning model: random forest model (MTRFR) as test and training data to develop a predictive model for hydrogel formulations.

Schematic 5.1: The schematics showing the synthetic procedure of AAmCNH-0 and AAmCNH-n hydrogel film and possible morphological differences on CNT incorporation

List of Abbreviations

UV-vis	Ultraviolet Visible spectroscopy
CV	Cyclic Voltametry
UCS	Ultimate Compressive Stress
FTIR	Fourier-transform infrared spectroscopy
XPS	X-ray photoelectron spectroscopy
SAXS	Small-angle X-ray Scattering
MAE	Mean absolute error
RMSE	Root mean square error
PEGDA	Poly (ethylene glycol) diacrylate
MTRFR	Multi-target random forest regression
TOCNs	TEMPO oxidised cellulose nanofibers
XRD	X-ray powder diffraction
DSC	Differential Scanning Calorimeters
PEDOT:PSS	Poly (3,4-ethylenedioxythiophene) polystyrene sulfonate
PAHT	Polyacryloyl hydrazide triflate
AAm	Acrylamide
AMPS	2-Acrylamido-2-methyl-1-propanesulfonic acid
CNTs	Carbon Nanotubes
UTS	Ultimate Tensile Stress
UTM	Universal Tensile Machine
AFM	Atomic force microscopy

List of Publications

- **Anand, S**.; Tewary, A.; Upadhyay, C.; Sinha, A.S.K.; & Ojha, U.* "Polyelectrolyte Complexation Approach to Devise PEDOT:PSS Based Moldable, Self-Healable and Ultra-Stretchable Solid Electrolytes for Under-Water Electronics." ACS Appl. Electron. Mater. 2024, 6, 10, 7380–7391 **(Published)**
- Mandal, S.; **Anand, S**.; Mandal, D.; Sinha, A. S. K.; & Ojha, U.* "Media Polarity Control Strategy to Tailor the Mechanical Behaviour of Dual Monomer Single Network Hydrogels and Integrated Machine Learning Approach." Chem.Mater 2025,37,4085−4096. **(Published) equal contribution**
- **Anand, S**.; Ojha, U.* ; & Singh,O. "Ultra-stretchable and Adhesive Hydrogel Synthesis and Incorporation of Carbon Nanotube to Fabricate Highly Conductive Electrolytes for Sensors." **(Published).**

Conferences

1.Attended the "International Conference on Energy Conversion and Storage 2025"

2. Attended the "International Conference on 'Advanced Materials for Energy, Environment & Sustainability 2025" held on 16-18 May 2025, organised by IIT Bhubaneswar in association with Materials Research Society of India

3.Attended the "International Conference on Shaping the Energy Future: Challenges and Opportunities (SEFCO)" at CSIR-IIP, Dehradun (April 23-25, 2025).

Awards

Won Best Poster Award at AMEES 2025 in "International Conference on "Advanced Materials for Energy, Environment & Sustainability 2025" held on 16-18 May, 2025 Organised by IIT Bhubaneswar in association with Materials Research Society of India